Dissertation

submitted to the
Combined Faculties for the Natural Sciences and for Mathematics
of the Ruperto-Carola University of Heidelberg, Germany
for the degree of
Doctor of Natural Sciences

presented by

Frédérique Kok, MSc

born in Zoetermeer, the Netherlands

Oral examination: 23 February 2018

Disentangling mechanisms of positive and negative memory of interferon alpha signal transduction

Referees: Prof. Dr. Ursula Klingmüller

Prof. Dr. Ralf Bartenschlager

One, remember to look up at the stars and not down at your feet. Two, never give up work. Work gives you meaning and purpose and life is empty without it. Three, if you are lucky enough to find love, remember it is there and don't throw it away. – Stephen Hawking

Voor mijn ouders en verloofde Sebastiaan

Parts of this thesis are in preparation for submission:

Frédérique Kok[#], Marcus Rosenblatt[#], Tamar Nizharadze, Melissa Teusel, Christopher Dächert, Tim Maiwald, Georg Damm, Katrin Hoffmann, Marco Binder, Marcel Schilling, Jens Timmer, Ursula Klingmüller. Disentangling mechanism of positive and negative memory of interferon alpha signal transduction. In preparation**.** # shared first author

Contents

Abstract **1**

Zusammenfassung **2**

Acronyms **3**

1 Introduction **6**

1.1 Biological memory 6

1.2 Interferons 7

1.2.1 Characterization of interferons 7

1.2.2 Type I interferons 8

1.2.3 Type II interferon 9

1.2.4 Type III interferons 9

1.3 Induction and production of type I interferons 9

1.3.1 Sensing of intra- and extracellular pathogens 10

1.3.2 Pathogen-induced signaling pathways 11

1.3.2.1 Activation of transcription factors 11

1.3.2.2 Transcription factor network and IFN production 13

1.4 IFNα-induced signaling 13

1.4.1 Signal transduction by JAK/STAT 13

1.4.2 IFNα-induced JAK/STAT signaling 14

1.4.3 Regulators of IFNα-induced JAK/STAT signalling 15

1.4.3.1 Phosphatases 16

1.4.2.2 Suppressor of cytokine signalling: SOCS 16

1.4.2.3 Protein inhibitor of activated STAT: PIAS 16

1.4.2.4 Ubiquitin specific protease 18: USP18 17

1.4.2.5 Family of Interferon regulatory factors 17

1.4.4 Interferon stimulated genes 17

1.5 Role of IFNα in diseases 18

1.5.1 Viral persistence 18

1.5.2 Autoimmune disease 19

1.6 Systems biology to unravel signal transduction pathways 19

1.6.1 Mathematical modelling approaches 20

1.6.2 Mathematical modelling of signal transduction pathways 21

1.6.3 Mathematical models of IFNα-induced signaling 22

1.7 Objectives 23
2 Results 24
2.1 Dose-dependent memory of IFNα-induced signal transduction 24
2.2 Impact of dose-dependent memory of IFNα-induced signal transduction on expression of target genes 27
2.2 Unravelling the mechanisms of dose-dependent memory by combining quantitative data with mathematical modeling 30
2.2.1 Establishment of a mathematical model of IFNα-induced signalling transduction 30
2.2.2 Time-resolved measurements of IFNα-induced expression of proteins mediating feedback loops 33
2.2.3 Absolute quantification of IFNα-induced feedback proteins 35
2.2.4 IFNα-dose-dependent memory of IFNα 37
2.2.5 Pre-treatment with IFNα results in changes in complex formation 40
2.2.6 Model extension to the therapeutic interferon and HepG2-hNTCP cell line 41
2.2.7 Mechanism of IFNα-induced negative memory 44
2.2.8 Contribution of individual feedbacks to IFNα-induced positive and negative memory 49
2.3 Prediction of memory establishment in primary human hepatocytes 51
2.3.1 Impact of protein abundance of STAT1, STAT2, IRF9 in combination with USP18 abundance on establishment of positive memory of IFNα-induced signal transduction 51
2.3.2 Protein abundance in primary human hepatocytes 52
2.3.3 USP18 abundance as patient-specific indicator of dose-dependent memory of IFNα signal transduction 53
3 Discussion 57
3.1 Dose-dependent memory of IFNα-signal transduction 57
3.2 Mechanism of dose-dependent memory of IFNα-signaling 59
3.2.1 IFNα-induced signalling and feedback loops 59
3.2.2 Mechanism of positive and negative memory 60
3.3 Prediction of positive and negative memory establishment of IFNα-signaling in patients 63
3.4 Proposed further investigations 64
4 Materials and Methods 66
4.1 Molecular biology 66
4.1.1 Polymerase chain reaction 66
4.1.2 Molecular cloning 66
4.1.2.1 Gel purification 66
4.1.2.2 Digestion and purification 67
4.1.2.3 Ligation 67

4.1.3 Transformation of *Escherichia coli* cells 67
4.1.3.1 Transformation of E.coli DH5α 67
4.1.3.2 Transformation of E.coli BL21-CodonPlus(DE3)-RIL 67
4.1.4 Purification of plasmid DNA and sequencing 67
4.1.5 Sequencing 68
4.1.6 Construction of plasmids 68
4.1.6.1 pMOWSIN-TRE-t-USP18 68
4.1.6.2 pGEX-2T-USP18 68
4.2 Cell biology 68
4.2.1 Cultivation of Huh7.5 cell line 68
4.2.2 Cultivation of primary human hepatocytes 69
4.2.3 Transient transfection of Phoenix ampho cells for retroviral transduction 69
4.2.4 Retroviral transduction 69
4.2.5 Transient siRNA transfection 69
4.2.6 Titration of interferon concentration 70
4.2.7 Cell stimulation 70
4.3 Protein biochemistry 70
4.3.1 Cell lysis 70
4.3.1.1 Cellular fractionation 70
4.3.1.2 Total cell lysis 71
4.3.2 Sample processing and immunoprecipitation 71
4.3.3 SDS-PAGE and quantitative immunoblotting 71
4.3.3.1 SDS-PAGE 71
4.3.3.2 Immunoblotting 72
4.3.3.3 Quantitative immunoblot detection and quantification 72
4.3.3.4 Reprobing of immunoblots 72
4.3.5 Determination of molecules per cell by quantitative immunoblotting 73
4.3.5.1 Production of recombinant proteins 73
4.3.5.2 Determination of amount of molecules per cell 73
4.4 RNA Analysis 73
4.4.1 Isolation of total RNA and production of cDNA 73
4.4.2 Quantitative RT-PCR 74
4.5 Transcription factor binding site analysis 74
4.6 Data processing and Mathematical modeling 75
4.6.1 Conversion of interferon concentrations 75

4.6.2 Normalization of quantitative immunoblot data 75
4.6.3 Data scaling and error estimation by blotIt 75
4.6.4 Mathematical modeling 75
5 Appendix 77
5.1 Model analysis 77
5.1.1 List of observables 77
5.1.2 Model equations 78
5.1.3 Estimated parameter values 80
5.1.4 Profiles of estimated parameter values 83
5.1.5 Likelihood waterfall plot 87
5.2 Additional experimental data belonging to the complete Huh7.5-IFNα dataset 87
5.2.1 Dose- and time- resolved IFNα-induced signal transduction 87
5.2.2 IFNα-induced expression of feedback genes 88
5.2.3 IFNα-induced stimulation in Huh7.5 cells pre-treated with different doses of IFNα 90
5.2.4 IFNα-induced signalling in USP18 siRNA transfected cells 90
5.2.5 IFNα-induced signal transduction in Huh7.5-TetON-USP18 91
5.3 Complete dataset of Roferon-induced signal transduction in Huh7.5 and HepG2-hNTCP 92
5.4 Complete dataset of IFNα-induced signal transduction in primary human hepatocytes 95
Bibliography 99

Abstract

The anti-viral cytokine interferon alpha (IFNα) is used for the treatment of chronic Hepatitis B and C and various types of cancers. Often patients do not respond to the treatment which has been correlated to pre-activation of IFNα-induced signaling, as assessed by enhanced expression of IFNα target genes. IFNα activates the JAK/STAT signal transduction pathway, which involves negative feedback loops mediated by SOCS1, SOCS3 and USP18 and positive feedback loops mediated by IRF9, STAT1 and STAT2. The objective of this study was to investigate if the dynamic behavior of IFNα-induced signal transduction is affected in IFNα pre-treated cells and to dissect the mechanism contributing to a possible memory effect of pre-activation of IFNα-induced signal transduction. These aims were approached by combining quantitative time- and dose-resolved data of IFNα-induced signaling in hepatoma cell lines and primary human hepatocytes with mathematical modeling.

To examine the effect of pre-activation of the IFNα-induced signaling transduction, cells were pre-treated with different doses of IFNα, were stimulated with a high dose of IFNα and the dynamical behavior of IFNα-induced signaling was analyzed by quantitative immunoblotting. The obtained results revealed that pre-treatment with a low dose of IFNα resulted in enhanced IFNα-induced phosphorylation of STAT1 and STAT2 observed in the nucleus, while pre-treatment with a high dose of IFNα resulted in much reduced IFNα-induced phosphorylation of STAT1 and STAT2 in the cytoplasm and in the nucleus, indicating a positive and negative memory of IFNα-induced signal transduction, respectively. The analysis of IFNα-induced gene expression showed that negative memory of IFNα-induced signal transduction prevented no further induction of IFNα-induced gene expression, while positive memory resulted in faster gene expression of IFNα-target genes.

To unravel the mechanisms contributing to positive and negative memory of IFNα-induced signal transduction, a mathematical model was established and calibrated with time- and dose-resolved data comprising pre-treatment with different doses of IFNα and subsequent IFNα stimulation to characterize the induction of the positive and the negative feedback loops. Experiments showed that IRF9, STAT1 and STAT2 are induced at lower IFNα doses compared to USP18, SOCS1 and SOCS3. To analyze the specific role of USP18, USP18 expression was induced to the same amount as present in cells pre-treated with a high dose of IFNα, IFNα-induced phosphorylation of STAT1 and STAT2 was lower compared to wildtype cells, but much higher compared to cells pre-treated with a high dose of IFNα, indicating that USP18 abundance alone is not sufficient to explain the negative memory of IFNα-induced signal transduction. Mathematical model analysis revealed that SOCS1 and USP18 together synergistically enhance degradation of active receptor complexes and thereby much reduced the IFNα-induced phosphorylation of STAT1 and STAT2. Model analysis of the positive memory identified STAT2 and IRF9 as key contributors. Model simulations predicted that the abundance of STAT2 and USP18 together, but not of SOCS1, is sufficient to predict the direction and extent of the memory of IFNα-induced signal transduction. Quantification of the amount of STAT2 and USP18 in primary human hepatocytes from three different patients identified high patient-to-patient-variability in the amount of USP18, but not of STAT2. Therefore, USP18 abundance was identified and experimentally validated as patient-specific indicator of memory of IFNα signal transduction, providing new perspectives for optimal dosing of IFNα that would prevent non-responsiveness to IFNα treatment in individual patients.

Zusammenfassung

Das antivirale Zytokin Interferon alpha (IFNα) wird zur Behandlung von chronischer Hepatitis B und C und verschiedenen Krebsarten eingesetzt. Oftmals reagieren Patienten nicht auf die Behandlung. Dies wurde, basierend auf einer verstärkte Expression von IFNα-Zielgenen, mit der Voraktivierung der IFNα-induzierten Signaltransduktion korreliert. IFNα aktiviert den JAK/STAT-Signaltransduktionsweg, der negative, durch SOCS1, SOCS3 und USP18 vermittelte Rückkopplungsmechanismen und positive, durch IRF9, STAT1 und STAT2 vermittelte Rückkopplungs-mechanismen beinhaltet. Ziel der vorgelegten Doktorarbeit war die Untersuchung der Dynamik der IFNα-induzierten Signaltransduktion in IFNα-vorbehandelten Zellen und die Entschlüsselung des Mechanismus, der zu einem möglichen Memory-Effekt der Voraktivierung der IFNα-induzierten Signaltransduktion beiträgt. Dafür wurden quantitative Zeit- und Dosis-aufgelöste Daten der IFNα-induzierten Signaltransduktion in Hepatomzelllinien und primären humanen Hepatozyten mit mathematischer Modellierung kombiniert.

Um den Effekt der Voraktivierung der IFNα-induzierten Signaltransduktion zu untersuchen, wurden die Zellen mit unterschiedlichen IFNα Dosen vorbehandelt, mit einer hohen IFNα-Dosis stimuliert und die Dynamik der IFNα-induzierten Signaltransduktion durch quantitatives Immunoblotting analysiert. Die Ergebnisse zeigten, dass die Vorbehandlung mit einer geringen IFNα Dosis zu einer verstärkten IFNα-induzierten Phosphorylierung von STAT1 und STAT2 im Zellkern führt, während eine Vorbehandlung mit einer hohen IFNα Dosis zu einer stark reduzierten IFNα-induzierten STAT1 und STAT2 Phosphorylierung im Zytoplasma und im Zellkern führt, was auf einen positiven bzw. negativen Memory-Effekt der IFNα-induzierten Signaltransduktion hinweist. Die Analyse der IFNα-induzierten Genexpression zeigte, dass ein negativer Memory-Effekt der IFNα-induzierten Signaltransduktion eine weitere Induktion der IFNα-induzierten Genexpression unterbindet, während ein positiver Memory-Effekt zu einer schnelleren Genexpression von IFNα-Zielgenen führt.

Um die zugrundeliegenden Mechanismen zu entschlüsseln, wurde ein mathematisches Modell etabliert und mit Zeit- und Dosis-aufgelösten Daten kalibriert, die eine Vorbehandlung mit verschiedenen IFNα Dosen und Charakterisierung der Induktion der positiven und negativen Rückkopplungsmechanismen umfassen. Die Experimente zeigten, dass IRF9, STAT1 und STAT2 bereits bei geringeren IFNα-Dosen als USP18, SOCS1 und SOCS3 induziert werden. Um die spezifische Rolle von USP18 zu analysieren, wurde die USP18-Expression gleich stark induziert, wie sie in Zellen vorliegt, die mit einer hohen IFNα-Dosis vorbehandelt wurden. In diesen Zellen war die IFNα-induzierte STAT1 und STAT2 Phosphorylierung deutlich höher als in Zellen, die mit einer hohen IFNα-Dosis vorbehandelt wurden. Dies zeigte, dass die Expression von USP18 alleine nicht ausreicht, um den negativen Memory-Effekt der IFNα-induzierten Signaltransduktion zu erklären. Die Modellanalyse zeigte, dass SOCS1 und USP18 zusammen den Abbau aktiver Rezeptorkomplexe verstärken und dadurch die IFNα-induzierte STAT1 und STAT2 Phosphorylierung stark reduzieren. Die Modellanalyse identifizierte STAT2 und IRF9 als Hauptkomponenten des positiven Memory-Effekts. Modellsimulationen sagten voraus, dass die Expression von STAT2 und USP18 zusammen, aber nicht von SOCS1, ausreicht, um die Richtung und das Ausmaß des Memory-Effekts vorherzusagen. Die Quantifizierung der Menge an USP18 und STAT2 in primären menschlichen Hepatozyten von drei Patienten zeigte eine starke Variabilität in der Menge an USP18, jedoch nicht an STAT2. Daher wurde die USP18-Expression als entscheidender Patienten spezifischer Indikator zur Vorhersage des Memory-Effekts der IFNα-Signaltransduktion identifiziert und dieser Befund konnte experimentell validiert werden, was neue Perspektiven für eine optimale Dosierung von IFNα liefert, die das Ansprechen auf die IFNα-Behandlung bei einzelnen Patienten erhöhen könnte.

Acronyms

a.u.	Arbitrary units
ADAR	Adenosine deaminase acting on RNA
AEBSF	4-(2-aminoethyl)benzenesulfonyl fluoride hydrochloride
AP	Aprotinin Protease Inhibitor
AP1	Activated protein 1
aRecIFN	Active receptor in complex with IFN
aRecIFNSTAT1c	Active receptor in complex with IFN and cytoplasmic STAT1 protein
aRecIFNSTAT2c	Active receptor in complex with IFN and cytoplasmic STAT2 protein
BIC	Bayesian information criterion
BSA	Bovine serum albumin
CARD	Caspase activation and recruitment domain
CARDIF	CARD adaptor inducing interferon beta
CXCL10	Chemokine (C-X-C motif) ligand 10
CXCL11	Chemokine (C-X-C motif) ligand 11
DAMP	Damage-associated molecules pattern
DDX3	DEAD-box helicase 3 X-linked
DHX9	DExH box helicase 9
DMEM	Dulbecco's Modified Eagle Medium
DMSO	Dimethyl sulfoxide
DNA	Deoxyribonucleic acid
Dox	Doxycyclin
E. coli	Escherichia coli
EIF2AK2	Eukaryotic translation initiation 2 alpha kinase 2
ERIS	Endoplasmatic Reticulum interferon stimulator
FCS	Fetal calf serum
GAPD	Glyceraldehyde-3-phosphate dehydrogenase
GAS	Gamma activated sequence
GFP	Green fluorescent protein
GST	Glutathione S-transferase
HBV	Hepatitis B virus
HCV	Hepatitis C virus
HPRT	Hypoxanthine-guanine phosphoribosyltransferase
Huh7.5	Human hepatocarcinoma cell line 7, clone 5
IFI6	Interferon alpha-inducible protein 6
IFIT	Interferon induced protein with tetratricopeptide repeats
IFITM	Interferon induced transmembrane protein
IFN	Interferon
IFNα	Interferon alpha
IFNβ	Interferon beta
IFNγ	Interferon gamma
IFNλ	Interferon lambda
IFNAR	Interferon alpha receptor

IFNλR1	Interferon lambda receptor 1
IL	Interleukin
IL10R2	Interleukin 10 receptor 2
IL28Rα	Interleukin 28 receptor alpha
IκB	Inhibitor of kappa B
IKK	I kappa B kinase
IPS-1	Interferon beta promoter stimulator
IRF	Interferon responsive factor
IRF9c	Cytoplasmic IRF9 protein
IRF9n	Nuclear IRF9 protein
IRG	Interferon regulated gene
ISG	Interferon stimulated gene
ISG15	Interferon stimulated gene 15
ISGF3	Interferon-stimulated gene factor 3
ISGF3c	Cytoplasmic ISGF3
ISGF3n	Nuclear ISGF3
ISRE	Interferon stimulated response element
IRF-E	Interferon regulatory element
JAK	Janus kinase
LC	Linear chain
LGP2	Laboratory of Genetics and Physiology 2 protein
MAPK	Mitogen-activated protein kinease
MAVS	Mitochondrial Antiviral Signaling protein
MDA5	Melanoma Differentiation-Associated protein 5
mDC	Myeloid dendritic cell
mRNA	Messenger RNA
Mx1	Interferon-induced GTP-binding protein
MyD88	Myeloid differentiation primary response gene 88
NEMO	NF-kappaB essential modulator
NF-κB	Nuclear factor kappa-light-chain-enhancer of activated B cells
NK cell	Natural killer cell
NLS	Nuclear localization signal
NMI	NMYC interactor
NS	Non structural
NT siRNA	Non-targeting siRNA
occISREbs	Occupied ISRE-binding sites
PAMP	Pathogen-associated molecular pattern
pDC	Plasmacytoid dendritic cell
PEG	Polyethylene glycol
pegIFNα	Pegylated interferon alpha
PHH	Primary human hepatocytes
PIAS	Protein inhibitor of activated STAT
PKR	Protein kinase R
PRR	Pattern recognition receptor
PTP	Protein tyrosine phosphatase

PTPN	Phosphatase non-receptor
PVDF	Polyvinylidene difluoride
qRT-PCR	Quantitative real time polymerase chain reaction
Rec	Receptor
RFP	Red fluorescent protein
RLU	Relative luciferase units
RIG-I	Retinoic acid inducible gene I
RLR	RIG-I like receptor
RNA	Ribonucleic acid
SDS	Sodium dodecyl sulfate
SDS-PAGE	Sodium dodecyl sulfate polyacrylamide gel electrophoresis
siRNA	Short interfering RNA
SOCS	Suppressor of cytokine signaling
STAT	Signal transducer and activator of transcription
STAT1c	Cytoplasmic STAT1 protein
STAT1dimc	Cytoplasmic STAT1 protein dimer
STAT1dimn	Nuclear STAT1 protein dimer
STAT1n	Nuclear STAT1 protein
STAT2c	Cytoplasmic STAT2 protein
STAT2n	Nuclear STAT2 protein
STING	Stimulator of interferon genes
TANK	TRAF family member associated NF-kappa B activator
TBK1	TANK binding kinase 1
TBP	TATA box binding protein
TC-PTP	T-cell protein tyrosine phosphatase
TLR	Toll-like receptor
TMEM173	Transmembrane protein 173
TRAF	TNF receptor associated factor 6
tRNA	Transfer RNA
TRIM	Tripartite motif containing protein
TYK2	Tyrosine kinase 2
USP18	Ubiquitin Specific Peptidase 18
VISA	Virus-induced signaling adaptor
ZNFX1	Zinc FNX1-type containing 1

1 Introduction

1.1 Biological memory

Biological memory is defined as a sustained cellular response as consequence of a transient stimulus (Burrill & Silver, 2010). Cells can accomplish a sustained cellular response by induction of transcriptional states that define cellular phenotypes. Transcriptional states can be bi-stable and are regulated by signal transduction cascade which are triggered by internal and external stimuli. Activated transcription factors, co-activators and co-repressors form a network that determines the speed and sustainability of the transcriptional state (Alon, 2006). Biological memory depends on positive feedback mechanisms, which can be established by three different networks: autoregulatory positive feedback networks whereby the activated transcription factor induces expression of its own gene, double negative feedback networks involving two transcription factors that inhibit each other or double positive feedback networks whereby two transcription factors induce each other's expression (Ferrell, 2002). If the concentrations of the transcription factors exceed a certain threshold, a switch from the previous to the next steady state is reached. The stability of the new steady state depends on the protein production relative to the protein degradation and the dilution by cell division of the transcription factor (Burrill & Silver, 2010).

Classical examples of biological bi-stable systems include the two-states of bacteriophage lambda, and the lactose operon that regulates lactose transport and metabolism. The bacteriophage lambda can switch between the latent and lytic stage of infection, the switch is achieved between mutual repression of the two transcriptional regulators lambda repressor and Cro (Eisen *et al*, 1970; Ptashne, 2006). Another classic example involved in metabolism is regulation of the lac operon by means of a positive feedback loop combined with double negative feedback loops. Glucose is the preferable energy source of bacteria, but bacteria can grow on lactose in absence of glucose. The lac operon encodes for three proteins involved in lactose uptake and metabolism in bacteria, in presence of glucose and absence of lactose expression of the lac operon is inhibited. Lactose binding inhibits the lac repressor, while glucose binding inhibits the transcriptional activator of the Lac operon and the lactose transporter (Benno Müller-Hill, 1996).

Chromatin modifications, such as histone modification and DNA methylation affect the chromatin structure and thereby alter gene expression. Chromatin structure can be studied as a bi-stable system that can switch between an active state where transcription can take place and an inactive, silenced state. Chromatin modifications can establish during development, cell differentiation and upon environmental stimuli and are maintained by positive autoregulatory feedback mechanism whereby the modified nucleosome recruits modifying enzymes that modify neighbouring nucleosomes, resulting in a more stable and heritable memory (Zhu & Reinberg, 2011).

Interferon alpha (IFNα) is a stimulus involved in establishment of an anti-viral state in cells. IFNα has been used to treat chronic infections of hepatitis B or hepatitis C viruses (HBV, HCV), however, many patients do not respond to the therapy (Fried, 2002). The non-responsive state has been correlated to pre-activation of the endogenous IFNα-induced signaling cascade (Chen *et al*, 2005; Zhu *et al*, 2012; Li *et al*, 2014) as determined by elevated levels of IFNα target genes in liver biopsies of patients with chronic HCV (Sarasin-Filipowicz, 2008) and in hepatocytes isolated from patients with chronic HBV infection (Zhu *et al*, 2012). Cell culture and *in vivo* experiments in mice confirmed a potentially negative memory established by IFNα, also called refractoriness or desensitization, which has been originally characterized as "a return to pretreatment levels of transcription and the inability of

further IFN treatment to re-induce the transcription of these (two interferon induced) genes (IFN-IND-1 and IFN-IND-2)" (Larner *et al*, 1986). This possible negative memory required IFN-induced protein synthesis (Larner *et al*, 1986), and the IFNα-induced negative regulator USP18 has been identified as a factor contributing to a negative memory (Sarasin-Filipowicz *et al*, 2009a; Makowska *et al*, 2011; François-Newton *et al*, 2011). IFNα-induced signaling involves positive and negative feedback loops, but how biological memory is established is unclear and will be addressed in this study. Understanding what determines the establishment of the non-responsive state, referred to as negative memory of the IFNα signal transduction pathway, will identify possible drug targets and provide perspectives for patient-tailored treatment.

1.2 Interferons

1.2.1 Characterization of interferons

In 1957, interferon was discovered, then characterized as a substance named after its capacity to interfere with viral infection (Isaacs, A. and Lindenmann, 1957). Interferon is a small signaling protein belonging to the cytokine family. Cytokines are produced by many cell types and act in an autocrine or paracrine fashion. A cytokine can result in pleiotropic responses depending on their target cell (Crow & Manel, 2015). In the case of interferon, anti-viral activities, anti-proliferative activities and immunomodulatory activities have been reported (Haque & Sharma, 2006; Stark *et al*, 1998).

Cytokines exert their function by the activation of cytokine receptors. Cytokine receptors are transmembrane glycoproteins containing a single membrane spanning region, an extracellular domain and a cytoplasmic domain. All cytokine receptors are classified as class I or class II based on the amount of cysteine residues and the characteristic WSXWS motif in the extracellular domain present in class I receptors, but not in class II receptors (Bazan, 1990b). Interferon receptors are classified as class II cytokine receptors (Bazan, 1990a) and interferons themselves can be classified in three types based on the interferon receptor they bind. The characteristics of the three types of interferons are summarized in Table 1. The different interferon types induce partially subtype-specific and partially overlapping sets of genes (Der *et al*, 1998).

Table 1. Classification of different types of interferon. Subtypes, characteristics of the signaling cascade they activate, from receptors, transcription factor complex to transcription factor binding sites of target genes. IFNδ is specifically found in swine (Lefèvre *et al*), IFNτ in ruminant species (Roberts, 2007) and IFN-ζ is found in mice (Hardy *et al*, 2004).

	Type I	**Type II**	**Type III**
Subtypes	IFNα IFNβ IFNε IFNκ IFNω IFNδ IFNτ IFN-ζ (limitin)	IFNγ	IFNλ1 (IL-29) IFNλ2 (IL-28A) IFNλ3 (IL-28B) IFNλ4
Receptors	Interferon alpha receptor 1 Interferon alpha receptor 2	Interferon gamma receptor 1 Interferon gamma receptor 2	Interleukin 10 receptor 2 Interferon lambda receptor (IL28Rα)
Transcription factor complex	Interferon stimulated gene factor 3	STAT1 homodimer	Interferon stimulated gene factor 3
Promoter element of target genes	AGTTTCNNTTTCNC/T	TTNCNNNAA	AGTTTCNNTTTCNC/T

1.2.2 Type I interferons

Type I interferons is the largest class of interferons. In human there are 13 subtypes of IFNα, and single subtypes of IFNβ, IFNω and the less well defined IFNε, IFNκ (Pestka *et al*, 2004). The most studied interferons are IFNα and IFNβ, both were discovered as factors secreted by different cell types and were named leukocyte interferon and fibroblast interferon, respectively.

IFNα is a multi-gene family consisting of partially homologues genes clustered on chromosome nine (Díaz *et al*, 1994). Each IFNα subtype exhibits a unique activity profile based on anti-viral activity and anti-proliferative activity (Lavoie *et al*, 2011). Even though low sequence similarity is present between the type I interferons, all type I interferons consist of five alpha helici that form a four-helix bundled protein and differ in a loop involved in receptor binding (reviewed in Pestka et al., 2004).

Plasmacytoid dendritic cells produce high amounts of type I interferon in response to antigens (Siegal *et al*, 1999; Colonna *et al*, 1999), however, any infected cell type is able to produce type I interferons upon viral infection. Type I interferons can act on cells expressing the interferon alpha receptor 1 and interferon alpha receptor 2 (IFNAR1, IFNAR2). IFNAR1 and IFNAR2 are expressed by different cell types including liver cells, lung cells, kerotinocytes and immune cells (reviewed in De Weerd & Nguyen, 2012).

Recombinant human IFNα-2a and human IFNα-2b are used in the clinic for the treatment of various cancers and viral diseases (reviewed in (Friedman, 2008)). The pharamokinetic properties such as distribution, reduced renal clearance and overall circulation in the blood of IFNα were improved by conjugation of IFNα to polyethylene glycol (PEG). Pegylated IFNα (pegIFNα) showed a hundred-fold reduced clearance from the body with a half-life of 160 hours compared to 5.1 hours for unpegylated interferon, as shown for Pegasys and Roferon respectively (Roche). Consequently, patients require weekly injections of Pegasys, instead of three-weekly injection of Roferon. Therefore, pegIFNα has increased patient compliance. However, pegylation of IFNα results in reduced *in vitro* activity caused

by a reduced binding affinity to the receptor due to steric hindrance of the PEGylated groups (Dhalluin *et al*, 2005).

Recombinant IFNα has been approved for the treatment of chronic hepatitis C virus (HCV) and chronic hepatitis B virus (HBV), treatment with pegIFNα is combined with a nucleoside or nucleotide analogue, respectively (Hoofnagle & Seeff, 2006; Marcellin *et al*, 2004). In addition recombinant interferon has been applied for cancers originating from virus infection, for example human herpes virus 8-relatad Kaposi's sarcoma (Tur & Brenner, 1998) and human papillomatosis virus-induced cancer such as respiratory papillomatosis (Gerein *et al*, 2005) and genital warts (Scheinfeld & Lehman, 2006). Furthermore, recombinant IFNα can be applied as anti-tumor drug both in the haematological cancers hairy-cell leukaemia and chronic myelogenous leukaemia, and in the metastasised solid tumours renal-cell carcinoma and cutaneous melanoma which has spread to the lymph nodes (Quesada *et al*, 1984; Talpaz *et al*, 1983; Cohen & McGovern, 2005; Tsao *et al*, 2004). The development of targeted drugs for chronic HCV, haematological cancers and solid tumours have replaced the IFNα as standard of care (Friedman, 2008).

Recombinant IFNα2a was used in this study to investigate how pre-treatment with IFNα shapes the response to subsequent stimulations and establishes an IFNα-induced memory. Findings were validated with the unpegylated therapeutically relevant IFNα2a named Roferon (Roche).

1.2.3 Type II interferon

Type II interferons are represented by only one subtype, IFNgamma (IFNγ). IFNγ is produced by natural killer cells and T-cells and therefore also referred to as immune interferon (Schoenborn & Wilson, 2007). In contrast to IFN type I and type III, IFNγ does not utilize the signal transducer and activator of transcription (STAT) 2, but instead IFNγ signaling activates homodimers of STAT1 to regulate gene expression of target genes. Interferon gamma receptors 1 and interferon gamma receptor 2 are expressed on most cell types (reviewed in De Weerd & Nguyen, 2012).

1.2.4 Type III interferons

Four subtypes of type III interferons, IFNλ1 (IL-29), IFNλ2 (IL-28A), IFNλ3 (IL-28B) and IFNλ4, were identified based on sequence similarities with type I interferon genes (Prokunina-Olsson *et al*, 2013; Kotenko *et al*, 2003). These interferons are induced upon viral infection in different cell types, and display anti-viral activity (Kotenko *et al*, 2003). In contrast to IFN type I, they signal through a different receptor pair: interleukin 10 receptor 2 (IL10R2) and interferon lambda receptor 1 (IFNλR1, also called interleukin 28 receptor alpha: IL28Rα) (Schoenborn & Wilson, 2007). While IL10R2 is expressed on many cell types, expression of IFNλR1 is more restricted to epithelial cells, hepatocytes and the gastro intestinal tract (reviewed in De Weerd & Nguyen, 2012).

1.3 Induction and production of type I interferons

In healthy conditions no or minor amounts of IFNα circulate in the blood, with concentrations up to 2 U/ml to be considered healthy (Lebon *et al*, 2002). In contrast, at pathological conditions, at for instance rotavirus infection, the IFNα concentration can increase up to 5000 U/ml under acute viral infection (De Boissieu *et al*, 1993). The balance between low levels of IFNα at healthy conditions, but high levels of IFNα at pathological conditions requires tight regulation of IFNα production and secretion. Three transcription factor complexes are involved in the induction of type I interferons. These transcription factors are regulated via multiple pathogen-induced signal transduction pathways, as discussed in more detail below and summarized in Figure 1.

1.3.1 Sensing of intra- and extracellular pathogens

Pattern recognition receptors (PRRs) sense pathogens present both inside and outside the cells. Ligands for the PRRs receptors are referred to as pathogen-associated molecular patterns (PAMPs) which include proteins, cell wall components and nucleic acids. Toll-like receptors (TLRs) are responsible for sensing PAMPs in the extracellular space and in endosomes (Nishiya & DeFranco, 2004). Ten different TLRs have been identified in human, specialized in detection of different types of PAMPs. The different receptors differ in their expression among cell types (Muzio *et al*, 2000). Upon ligand binding the TLRs dimerize, either forming homo-or heterodimers, establishing docking sites for adaptor proteins that interact with additional adaptor proteins and with kinases (Lester & Li, 2014; Jensen & Thomsen, 2012; Randall & Goodbourn, 2008). The adaptor proteins recruit TNF receptor associated factor 6 (TRAF6) or TRAF3, two proteins functioning as central nodes for activation of either mitogen-activated protein kinase (MAPK) signaling, canonical IκB kinase (IKK) signaling or a non-canonical IKK signalling pathway involving IKK-related kinases IKKε and TANK-binding kinase 1 (TBK1), respectively.

In addition to sensing pathogen associated molecular patterns in the extracellular space and in endosomes, other pattern recognition receptors are specialized in detecting PAMPs in the cytosol.

Three RNA helicases belonging to the RIG-I-like receptors (RLRs) have been described: the protein retinoic acid-inducible gene I (RIG-I), the protein melanoma differentiation factor 5 (MDA5), and the protein laboratory of genetics and physiology 2 (LGP2). The different RLRs show different specificity for specific viruses. While some viruses like for instance Influenza and Zaire Ebola virus only recognition by RIG-I has been reported, while for other viruses like for instance norovirus only recognition by MDA5 has been reported, while for multiple viruses like for instance HCV, dengue virus, West Nile virus, rotavirus and herpes simplex virus-2 (Goubau *et al*, 2013b). The RLR discriminate foreign RNAs from host RNAs with high specificity based on specific primary, secondary and tertiary RNA structures combined with virus or host specific modifications. LGP2 can bind dsRNA as well, but lacks downstream signaling domains (Bruns *et al*, 2014). The role of LGP2 in RLR-induced signaling is not fully understood and LGP2 might function in a virus-specific manner, since it has been reported to improve substrate recognition of MDA5, thereby increasing MDA5 induced antiviral signaling (Bruns *et al*, 2014) but impairing RIG-I mediated anti-viral response in the context of paramyxovirus Sendai infection, functioning as a negative regulator (Rothenfusser *et al*, 2005)

Both RIG-I and MDA5 utilize caspase activation and recruitment domains (CARDs) for downstream signaling. Upon ligand binding, RIG-I undergoes a conformational change from an auto-inhibitory conformation to an active conformation exposing the CARDs. K63-linked-polyubiquitilation of the CARD2 domain by tripartite motif-containing protein 25 (TRIM25) triggers the formation of a multimeric complex that activates downstream signaling. Structural studies on MDA5 with dsRNA ligands revealed that multiple copies of MDA5 bind one RNA ligand, forming filaments with stacked CAR domains that enable downstream signaling (Wu *et al*, 2013; Berke *et al*, 2012; Berke & Modis, 2012). Both the CAR domains from MDA5 and RIG-I are able to interact with the CAR domains from mitochondrial antiviral-signaling protein (MAVS, also known as IFN-β promoter stimulator 1:IPS-1, CARD-adaptor-inducing IFN-β: CARDIF and virus-induced signaling adaptor: VISA) located at the mitochondria, peroxisomes and mitochondrial-associated endoplasmic reticulum membrane. This interaction leads to a conformation change of the MAVS protein that induces the formation of large aggregates involved in recruiting the kinases TBK1 and IKKε, and IKKα and IKKβ that can activate the transcription factors IRF3 and IRF7 and NF-κB, respectively (Hou *et al*, 2011).

RLRs are present at low level at healthy conditions and are upregulated upon IFNα treatment. In addition, RNA helicase family member outside the RLRs like the DEAD-Box helicase 3 X-linked (DDX3) and the DExH-Box helicase 9 (DHX9) have been implicated in IFNα and IFNβ production upon viral infection. DDX3 and DHX9 are constitutively expressed and have been linked to MAVS mediated IFN induction, thereby supplementing the RLRs in the early phase of infection before RLR expression is enhanced by the autocrine signaling of type I interferon (Zhang *et al*, 2011; Oshiumi *et al*, 2010).
While the RIG-I like and Toll-like receptors specifically recognize PAMPs, cytosolic DNA receptors cannot discriminate between pathogen-associated DNA and self-DNA from the host, which can reside in the cytosol as a consequence of incomplete degradation of apoptotic bodies by DNAses in the lysosomes (Okabe *et al*, 2009) or as a consequence of functional loss DNAses, such as DNAse II or T-REX involved in degradation of transposon DNA (Crow & Manel, 2015). Type I IFN induction has been shown for the DNA recognizing receptors DAI, RNA polymerase III, AIM2-like proteins including IFI6, c-GAS, other DEXD-box helicases and proteins previously described in the DNA damage response like DNA-PK and MREII (Paludan & Bowie, 2013) and stimulator of interferon genes (STING, also known as MITA, Endoplasmic Reticulum interferon stimulator: ERIS, Transmembrane protein 173: TMEM173 AND MPYS) has been identified as key mediator of TLR-independent DNA induced activation of IRF3 and NF-κB and subsequently type I interferon production (Ishikawa & Barber, 2008; Zhong *et al*, 2008; Sun *et al*, 2009; Jin *et al*, 2008).

1.3.2 Pathogen-induced signaling pathways

Pathogens can be sensed by Toll-like receptors, RIG-I like receptors or other RNA and DNA sensing pattern recognition receptors. Pathogen-induced activation of the different pattern recognition receptors results in recruitment of adaptor proteins and regulators, with TRIF and MyD88 as important scaffold proteins in TLR-signaling, MAVS in RLR-signaling and STING in DNA-activated PRR.

1.3.2.1 Activation of transcription factors

As has been described in the context of TLR3-signaling, the adaptor protein TRIF recruits the E3-ligase TRAF6 and the kinase RIP1. This results in the poly-ubiquitination of both TRAF6 and RIP1 and the subsequent recruitment of the TAK1 kinase with the TAB2 and TAB3 scaffolding proteins. TAK1 recruits IKKγ (also known as the NF-κB essential modulator: NEMO) together with IKKα and IKKβ and TAK1 phosphorylates and thereby activates IKKβ. IKKβ phosphorylates inhibitor of κB (IκB), resulting in degradation of IκB and subsequent release of the NF-κB complex (Wullaert *et al*, 2006). The NLS of the NF-κB complex is no longer shielded by IκB and therefore NF-κB can translocate to the nucleus to regulate gene expression (Jacobs & Harrison, 1998). This pathway is also referred to the canonical IKK signalling cascade. In addition, TAK1 activates MAPK-signaling leading to phosphorylation of the transcription factors c-JUN and ATF2 which together form the transcription factor complex activated protein 1 (AP1) (Dérijard *et al*, 1994; Gupta *et al*, 1995).
Furthermore, TRIF can also activate a non-canonical IKK signaling cascade by recruiting TRAF3, by forming a complex with TRAF family member associated the NF-κB activator (TANK), which recruits TBK1 and IKKε, the two kinases responsible for phosphorylation of IRF3 and IRF7 (Fitzgerald *et al*, 2003; Sharma *et al*, 2003). Phosphorylation of serine residues at the C-terminus of the transcription factors IRF3 and IRF7 leads to a conformational change that enables dimerization and nuclear localisation by exposing a nuclear localization sequence (NLS) (Sato *et al*, 1998; Lin *et al*, 1998; Dragan *et al*, 2007). Most cell types express only IRF3, but not IRF7 at healthy conditions (Jensen & Thomsen, 2012; Marie *et al*, 1998). In contrast, plasmacytoid dendritic cells do express high levels of IRF7 (Izaguirre *et al*, 2003), which explains why these cells are such potent type I interferon

producers. Interestingly, the kinase TANK also interacts with IKKγ, resulting in the activation of the NF-κB complex (Chariot *et al*, 2002).

In response to RLR-signaling via the adaptor protein MAVS, both the canonical and non-canonical IKK signalling cascade is activated (Zhao *et al*, 2007; Paz *et al*, 2011).

For DNA-activated PRR signalling through STING, STING has been proposed to function as a scaffold, bringing IRF3 and TBK1 in close proximity to allow phosphorylation of IRF3 (Tanaka & Chen, 2012).

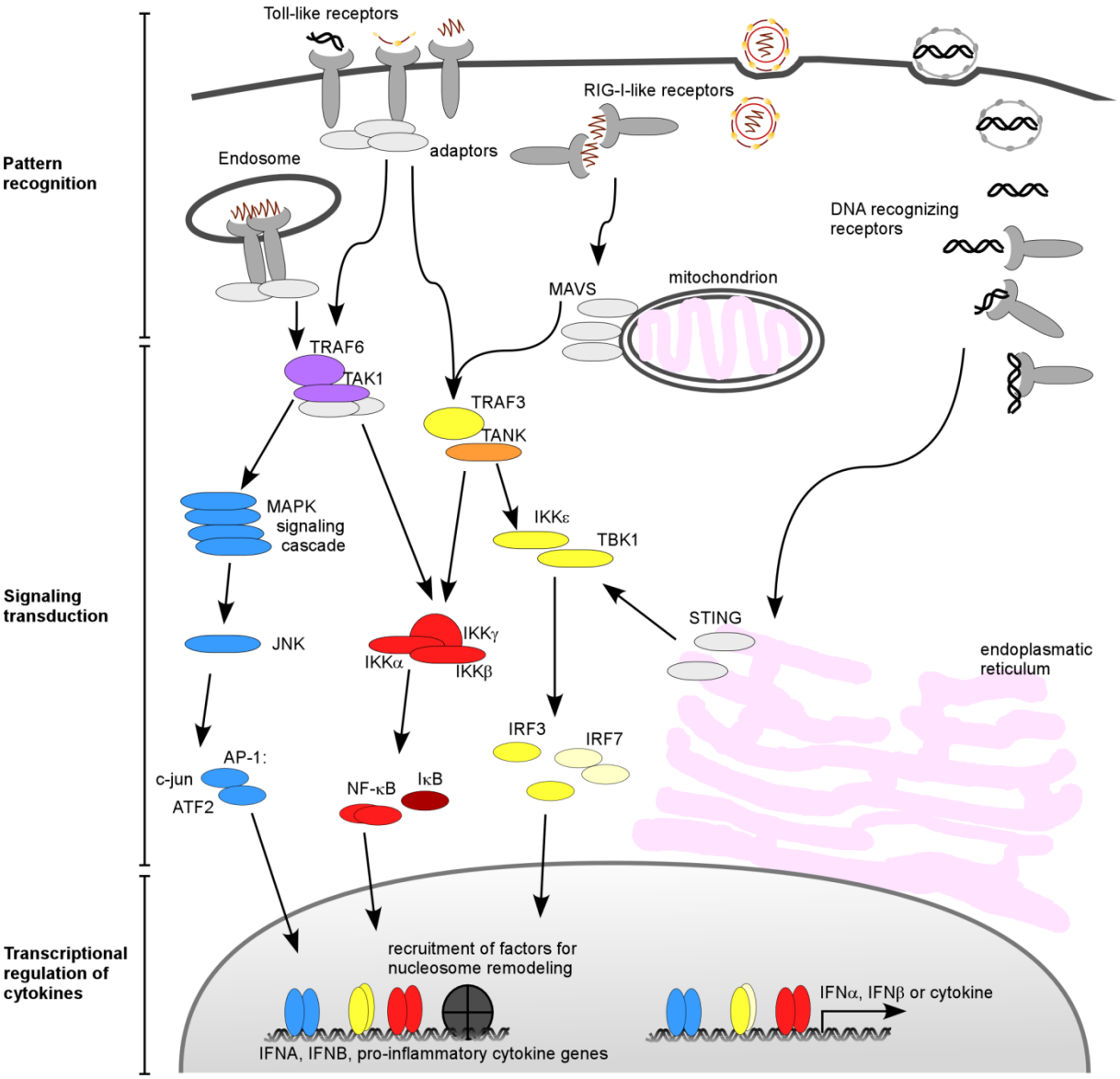

Figure 1. Pathogen-induced production of interferon and pro-inflammatory cytokine genes.

Non-self RNA, DNA or pathogen-specific glycoproteins activate signal transduction pathways leading to the activation of transcription factors and production of interferons and pro-inflammatory cytokines. Three types of receptors are activated upon binding of pathogen-associated molecular patterns, either extracellularly (Toll-like receptors) and intracellularly (RIG-I-like receptors and DNA recognizing receptors). Upon activation, each receptor type forms homo- or heterodimers, thereby generating docking sites for adaptors and enabling signal transduction. Via different adaptor proteins, either at the cellular membrane, at the mitochondrial membrane or at the endoplasmatic reticulum, the MAPK signaling cascade and IKKγ become activated. MAPK signaling cascade leads to the activation of the kinase JNK, which phosphorylates and thereby activates the transcription factor complex AP-1 consisting of c-jun and ATF2. IKKγ either associates with TBK1, leading to phosphorylation and activation of the transcription factors IRF3 and IRF7, or IKKγ activates IKKα and IKKβ which mediate degradation of IκB by phosphorylation, thereby releasing NF-κB. The activated transcription factor translocate to the

nucleus and bind pro-inflammatory genes including interferon alpha and interferon beta genes (IFNA, IFNB). All three factors are required for nucleosome remodeling, and contribute to transcription of target genes.

1.3.2.2 Transcription factor network and IFN production

Three types of transcription factors complexes are involved in induction of type I interferons: NF-κB, AP1 and IRF3 and IRF7 complexes. Studies suggest a crucial role of the IRF3 and IRF7 and a minor role for NF-κB and AP1 (Peters *et al*, 2002; Ellis & Goodbourn, 1994; Reis *et al*, 1989). The enhanceasome model proposes that each of the three transcription factor complexes bind the promoter with limited affinity and whereby cooperativity of binding of the different transcription factor complexes is required for optimal induction as has been validated for IFNβ (reviewed in (Honda *et al*, 2006; Ford & Thanos, 2010).

Studies in mice have shown that infected cells produce type I interferons in two rounds: first IFNβ and IFNα4 are induced, these interferons feedback via autocrine signaling and induce expression of the interferon stimulated gene and transcription factor IRF7 (Sato *et al*, 1998; Marie *et al*, 1998; Erlandsson *et al*, 1998). This first round is also referred as the priming phase, since cells primed with IFN showed higher production of type I interferons, as demonstrated for IFNβ in HeLa cells (King & Goodbourn, 1994). Upon activation, IRF7 can, together with other transcription factors, then enhance expression of the "primary" interferons β and α4 and further induce other IFNα genes, leading to the second round of IFN production. Induction of the IFNβ and the IFNα4 requires IRF3 and can take place in absence of IRF7, while induction of the remaining IFNα genes requires IRF7 (Marie *et al*, 1998).

1.4 IFNα-induced signaling

1.4.1 Signal transduction by JAK/STAT

Interferons activate a branch of the janus kinase/signal transducer and activator of transcription (JAK/STAT) signaling pathway. Cytokine receptors lack intrinsic kinase activity and therefore depend on the associated janus kinases for signal transduction. Four janus kinases: JAK1, JAK2, JAK3 and TYK2 have been described in human and different receptors utilize one or two JAK members. With exception of JAK3, the JAKs are expressed in most cell types (Schindler & Plumlee, 2008). JAKs are cytosolic tyrosine kinases that associate with cytokine receptors. As shown in Figure 2A, structural organization of JAKs reveals seven JAK-homology (JH1-7) domains, comprised of a FERM domain, SH2 domain, kinase domain and pseudokinase domain (reviewed in (Schindler & Plumlee, 2008)). Only the kinase domain has catalytic activity, whose activity requires phosphorylation for displacement of an inactivation loop. The FERM domain and SH2 domains are involved in protein-protein interaction, with the FERM domain involved in receptor binding. In addition, the SH2 domain has been indicated in stabilizing the activated state of kinases (Filippakopoulos *et al*, 2009). Upon ligand binding, the janus kinases get in close proximity, transphosphorylate and thereby transactivate each other. Activated JAKs phosphorylate the intracellular domain of cytokine receptors to generate docking sites for STAT proteins that are subsequently phosphorylated. STAT proteins are latent transcription factors both involved in signal transduction and activation of transcription and form dimeric or trimeric complexes. The STAT family consists of seven family members: STAT1, STAT2, STAT3, STAT4, STAT5a, STAT5b and STAT6 that have originated from a single gene, as has been proposed based on the chromosomal distribution and homologues identified between species (Miyoshi *et al*, 2001). As displayed in Figure 2B, structural analysis reveals seven conserved domains: NH2-domain, coiled-coil domain, DNA binding domain, linker domains, SH2 domain, tyrosine activation motif and

transcriptional activation domain (Schindler & Plumlee, 2008)). In the inactive anti-parallel dimer formation protein-protein interaction is mediated via the DNA-binding domains, coiled-coil domains and the N-terminal domains. In this conformation, the SH2 domains and tyrosine activation motives are exposed and therefore available for binding to the receptor and phosphorylation by JAKs (Zhong *et al*, 2005; Mertens *et al*, 2006). Upon phosphorylation of the tyrosine activation motif, STAT form dimers in the parallel conformation by binding of the SH2 domain to the phosphorylated tyrosine residues. In this conformation the nuclear localization signals (NLS) are exposed and STATs can therefore translocate to the nucleus mediated by importinα5 (McBride *et al*, 2002; Fagerlund *et al*, 2002; Sekimoto *et al*, 1997), DNA-binding, nuclear retention (Wenta *et al*, 2008) and consequently, regulation of expression of target genes involved in regulation of inflammation, proliferation, apoptosis, differentiation and maturation (Gao *et al*, 2012). The transcriptional activation domain is localized at the C-terminus and differs among the different STAT members, leading to STAT specific association with transcriptional regulators and chromatin remodellers required for activation of transcription (Schindler & Plumlee, 2008). In addition to tyrosine phosphorylation, STATs can be acetylated, serine phosphorylated, O-glycosylated and SUMOylated. While serine phosphorylation, acetylation and O-glycosylation increase transcriptional activity as a consequence of increased affinity for transcriptional regulators (reviewed in (Schindler & Plumlee, 2008), SUMOylation has been reported to inhibit transcriptional activity (Zimnik *et al*, 2009; Maarifi *et al*, 2015). Lastly, contradictory results have been reported for arginine methylation of STAT1 and STAT3 (Mowen *et al*, 2001; Komyod *et al*, 2005).

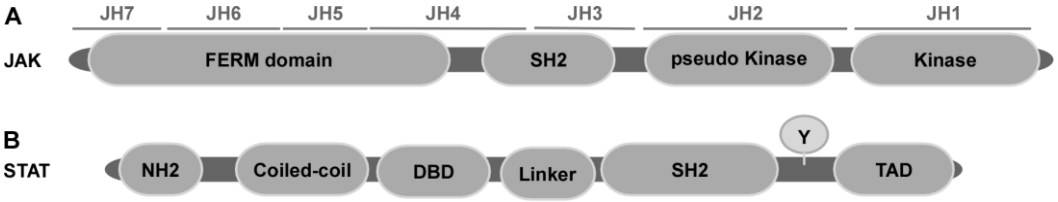

Figure 2. Functional protein domains of JAK (A) and STAT (B) protein. FERM domain: F for 4.1 protein, E for ezrin, R for radixin and M for moesin; SH2: Src Homology; NH2: amino-terminal; DBD: DNA Binding Domain; Y: tyrosine activation motif TAD: transcriptional activation domain. Figure was adapted from (Schindler & Plumlee, 2008).

1.4.2 IFNα-induced JAK/STAT signaling

As depicted in Figure 3, type I interferons signal via IFNAR1 and IFNAR2 (Lutfalla *et al*, 1995; Domanski *et al*, 1995; Uzé *et al*, 1990; Novick *et al*, 1994). Upon binding of IFNα, IFNAR1 and IFNAR2 dimerize, leading to activation of JAK1 and TYK2 and subsequent activation of STAT1 and STAT2 (Platanias *et al*, 1994). STAT1 can form homodimers, also referred to as Gamma-activated factor (GAF) or Alpha-activated factor (AAF) (Decker *et al*, 1991). In presence of STAT2, STAT1 forms a heterodimer with STAT2 (Li *et al*, 1996) and can bind the interferon response factor 9 (IRF9). This trimeric complex is defined as interferon stimulated gene factor 3 (ISGF3) and translocates to the nucleus regulating expression of target genes (Schindler *et al*, 1992b, 1992a; Veals & et al., 1992). ISGF3 binds promoters containing the interferon stimulated response element (ISRE), while STAT1 homodimers bind promoters containing the gamma-activated sequence (GAS), which displays partial overlap with the ISRE element. STAT1 and IRF9 are involved in promoter recognition, while STAT2 stabilizes the complex bound to the DNA (Qureshi & Salditt-Georgieff, 1995; Bluyssen & Levy, 1997). Signal termination at the receptor level is mediated by transcriptional feedback loops mediated by SOCS1, SOCS3 and USP18 (Song & Shuai, 1998; Malakhova *et al*, 2006). It is unclear if the different negative feedback loops regulate signal termination under the same conditions, or whether there is a

division of labor depending on IFNα dose or time after IFNα stimulation and will be addressed in this study. In addition, phosphatases and proteins of inhibitor of activated STAT modulate the response, while IRF2 represses transcription of target genes (Harada *et al*, 1994), as will be discussed in more detail below.

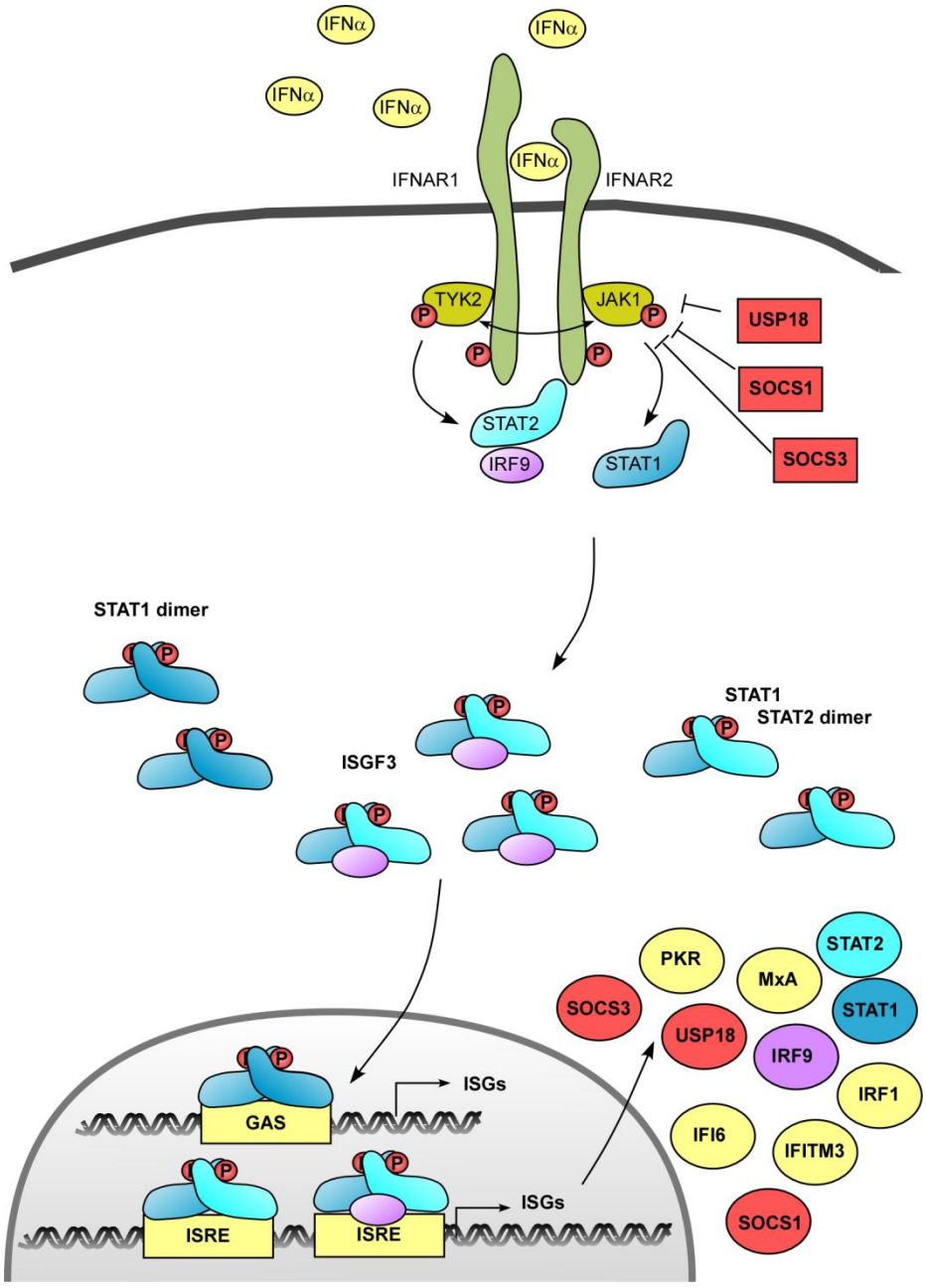

Figure 3. IFNα-induced JAK/STAT signal transduction pathway. Binding of IFNα results in dimerization of IFNAR1 and IFNAR2, and cross phosphorylation of their associated kinases JAK1 and TYK2. Phosphorylated JAK1 and TYK2 phosphorylate IFNAR1 and IFNAR2. Phosphorylated receptor chains function as docking sites for STAT1 and STAT2, which become phosphorylated and form dimers. Either STAT1 homodimers, STAT1-STAT2 heterodimer or the STAT1-STAT2 heterodimer bound to ISGF3, yielding the trimeric complex termed ISG3. All three complexes translocate to the nucleus and induce expression of interferon stimulated genes (ISGs) including the negative feedback proteins SOCS1, SOCS3 and USP18, which act at the activated receptor. Figure adapted from (Schneider, 2011).

1.4.3 Regulators of IFNα-induced JAK/STAT signalling

Signaling dynamics of IFNα-induced signaling is shaped by both positive and negative regulators. While higher levels of positive regulators can accelerate and increase the overall response, negative regulators can promote signal attenuation and decrease the overall response. The balance between positive and negative regulators determines the extent of the overall response.

1.4.3.1 Phosphatases

In contrast to kinases, protein phosphatases modify proteins by removing phosphorylation, returning the signaling proteins to their inactive conformation. JAK/STAT signaling is regulated by phosphatases that act on the receptor, janus kinases and STATs. The Tyrosine-protein phosphatase non-receptor type 11 (PTPN11, also known as SHP-2) (You *et al*, 1999), and T-Cell Protein Tyrosine Phosphatase (TC-PTP) (Hoeve, 2002) have been reported to regulate IFNα-and IFNγ-induced STAT1 phosphorylation IFNα-induced signaling. While PTPN1 (also known as protein-tyrosine phosphatase 1B: PTP1B) regulates TYK2, but not JAK1 phosphorylation (Myers *et al*, 2001).

1.4.2.2 Suppressor of cytokine signalling: SOCS

Suppressor of cytokine signaling (SOCS) proteins are negative regulators of JAK/STAT signalling. Eight SOCS family members have been described in mammals (SOCS1-7 and cytokine inducible SH2-containing protein CISH). SOCS1, SOCS2, SOCS3 and CISH primarily act on cytokine induced signalling, while SOCS4-7 primarily act on growth factor induced signalling (Trengove & Ward, 2013). In cytokine-induced signalling, SOCS proteins function as a negative feedback by inhibiting signaling from the receptor. SOCS1 and SOCS3 act by directly binding to JAK and thereby inhibiting kinase activity, while CISH, SOCS2 and SOCS3 bind the receptor and thereby block access for STAT proteins binding (Trengove & Ward, 2013). Binding is mediated by the SH2-domain on the SOCS protein to the phosphorylated tyrosine residues of the binding partner. SOCS1 and SOCS3 in addition contain a kinase inhibitory region in their N-terminus which inhibits JAK kinase activity possibly by functioning as pseudo substrate (Yoshimura *et al*, 2007; Yasukawa *et al*, 1999; Sekimoto *et al*, 1997; Endo *et al*, 1997).

In addition to inhibition of signal transduction by kinas inhibition, SOCS proteins contain E3 ligase ubiquitination activity mediating degradation of target proteins. The SOCS-box domain includes a BC box involved in binding to Elongin B and C (Zhang *et al*, 1999) and a Cul box involved in binding to Cullin5 (Kamura *et al*, 2004), which are co-regulators of the E3- ubiquitin ligase complex and are involved in recruitment of additional co-regulators and E2 ubiquitination enzymes. In the context of type I interferon-induced signalling, TYK2 has been identified as target of SOCS1-mediated ubiquitination and proteasomal degradation (Piganis *et al*, 2011). Degradation of TYK2 destabilizes IFNAR1 and results in lower receptor levels at the cell surface (Ragimbeau *et al*, 2003; Piganis *et al*, 2011).

1.4.2.3 Protein inhibitor of activated STAT: PIAS

PIAS proteins are E3 SUMO protein ligases that regulate transcription factors including activated STAT dimers (Shuai, 2006; Liao *et al*, 2000). Four PIAS genes have been described in mammals with each two isoforms for PIAS3, PIASx (PIAS2), PIASy (PIAS4) and a single isoform for PIAS1 (Rytinki *et al*, 2009). SUMOylation affects protein-protein interactions and it has been described to affect protein localization, signal transduction, protein stability or modulate activity of transcription factors (reviewed in (Johnson, 2004)). Besides SUMOylation, PIAS can regulate transcription by blocking DNA binding of transcription factors as it has been described for PIAS1 and PIAS3 (Liu *et al*, 1998; Chung *et al*, 1997) or by recruiting transcriptional repressors or activators as has been described for PIASx and PIASy (Arora *et al*, 2003; Liu *et al*, 2001).

PIAS1 knockout mice show increased protection against bacterial or viral infection, and macrophages isolated from these mice show increased levels of a subset of interferon stimulated genes (so called PIAS1 sensitive genes) upon stimulation with IFNβ or IFNγ, suggesting a minor role for PIAS1 as negative regulator of interferon-induced JAK/STAT signaling (Liu *et al*, 2004).

1.4.2.4 Ubiquitin specific protease 18: USP18

USP18 (UBP43) functions as a negative feedback loop involved in downregulation of IFNα-induced JAK/STAT signaling. USP18 is named ubiquitin-specific protease 18 contributed to its function in removing ubiquitin-like chains formed by ISG15 from target proteins (Malakhov *et al*, 2002). In addition, independent from its protease function, USP18 functions as negative regulator in IFN-induced JAK/STAT-pathway by competing with JAK1 for binding to IFNAR2 (Malakhova *et al*, 2006). By employing $USP18^{-/-}$ mice and USP18 siRNA in cell lines, expression of USP18 has been described to cause non-responsiveness to IFNα-induced signaling (François-Newton *et al*, 2011; Makowska *et al*, 2011; Sarasin-Filipowicz *et al*, 2009b). Non-responsiveness, also named refractoriness and desensitization, is characterized by the inability to induce phosphorylation of STAT1 and STAT2 and of target genes, upon IFNα treatment of cells previously exposed to type I IFN.

Surprisingly, IFNβ establishes refractoriness to IFNα stimulation, but not to IFNβ stimulation(François-Newton *et al*, 2011), which might be explained by more stable IFN-receptor complexes as a consequence of higher binding affinity between IFNβ and IFNAR2, (Wilmes *et al*, 2015). Furthermore, USP18 is proposed as the discriminating factor of IFNα vs IFNβ giving rise to ligand specific phenotypes (Francois-Newton *et al*, 2012)

Two isoforms of USP18 exist of 34 and 38 kDa. Both isoforms are functional and originate from the same gene and mRNA (Burkart *et al*, 2012). The smaller isoform of 34 kDa is truncated at the N-terminus and is synthesized from an internal ribosome entry site on the mRNA. The importance of signal attenuation of IFNα-induced signal is highlighted by the evolution of the short isoform of USP18, which can still be synthesized when 5' cap-dependent translation is impaired by activity from protein kinase R (PKR) (Burkart *et al*, 2012).

1.4.2.5 Family of Interferon regulatory factors

Nine interferon regulatory factors (IRFs) have been identified. The IRF proteins are transcriptional regulators, first identified in the context of IFNβ gene (Miyamoto *et al*, 1988). Via their N-terminal domain they either positively or negatively regulate gene expression by binding to IFN regulatory elements (IRF-Es) and the ISRE in promoters of target genes. As described previously at section 1.3.1.3, IRF9 is part of the trimeric transcription factor complex ISGF3 involved in IFNα-induced expression of ISGs (Veals & et al., 1992) and functions as a positive feedback loop. IRF1 and IRF2 are target genes of ISGF3. Both IRF1 and IRF2 bind the same regulatory elements, IRF1 functions a transcriptional activator, while IRF2 functions as a transcriptional repressor (Harada *et al*, 1989).

1.4.4 Interferon stimulated genes

IFNα activated JAK/STAT signaling regulates expression of interferon stimulated genes (ISGs), also referred to as interferon-regulated genes. ISGs include over 300 genes contributing to limit virus replication and spread (de Veer *et al*, 2001; Der *et al*, 1998). Currently, the interferon regulated gene database Interferome contains about 2000 genes, with ISGs classified based on IFN subtype, IFN dose and cell type specificity (Samarajiwa *et al*, 2009). Upon treatment with IFN, the induced ISGs show different dynamic expression profiles, more specifically the genes differ in time of induction, time of maximal activation and duration of expression (Bolen *et al*, 2014; Robichon, 2015)

It is unclear how all ISGs act together over time, or how each ISG contributes in the context of different viruses. Overexpression of individual ISGs identified that most ISGs display antiviral activity, but with different anti-viral potencies, even specific ISGs have been identified to favour virus replication when overexpressed individually (Schoggins *et al*, 2011). ISGs can have a direct or indirect effect on limiting viral replication and viral spread.

ISGs with indirect anti-viral functions are involved in regulation and signal transduction. Regulatory proteins, as for instance IRF1, belong to the most potent anti-viral proteins against a wide spectrum of viruses like HCV, human immunodeficiency virus, yellow fever virus and west Nile virus (Schoggins *et al*, 2011c). IFNα-induced expression of ISGs leads to increased sensing of pathogens by inducing expression of the Toll-like receptors TLR3, TLR4, TLR7, the RIG-I-like receptors RIG-I, MDA5 and LGP2, as well as TRIM25, the E3 ligase required for signal transduction (Sirén *et al*, 2005). Furthermore, the transcription factor IRF7 involved in transcription of type I IFN genes is induced by IFN, providing an additional positive feedback loop (Marie *et al*, 1998). Besides positive feedback genes, also many negative feedback genes are induced involved in targeting proteins for degradation, target proteins include MDA5, RIG-I, MAVS, TRIF, TBK1, IKKb, IRF3, IRF7 and NF-κB, as reviewed in (Porritt & Hertzog, 2015). Furthermore, as discussed in section 1.4.2 and 1.4.3, the many regulators of IFNα-induced signaling are ISGs. Lastly, other ISGs with indirect anti-viral functions are involved in regulation of proliferation, apoptosis and the immune response (de Veer *et al*, 2001), for instance by upregulation of MHC-class I and class II responsible for antigen presentation (Keskinen *et al*, 1997).
For a subset of ISGs direct anti-viral functions have been identified. These ISGs act at different steps of the viral infection cycle, starting from inhibition of viral entry (TRIM5α and IFITM proteins), interference of viral replication by degradation of RNA genome (RNase L) or mutagenesis of the RNA genome (ADAR-1, APOBEC3), inhibition of production of viral proteins (PKR, also known as EIF2AK2) and inhibition of assembly and release of viral particles (Viperin, Tetherin) (reviewed in (Goubau *et al*, 2013a)). Different viruses are targeted by unique sets of ISGs and some ISGs act more virus specific while others exert anti-viral activity against many different viruses (Schoggins & Rice, 2011). For instance IFITM2 displayed a virus-specific activity, while IFITM3 displayed anti-viral activity towards many viruses (Schoggins *et al*, 2011b). Furthermore, ISGs that act on many viruses, can also affect the host. As for instance illustrated by the anti-viral protein dsRNA dependent kinase PKR phosphorylates the alpha subunit of the eukaryotic initiation factor 2 (eIF2α). The ternary complex of eIF2α, GTP and ^{Met}tRNA, is required for the correct position of the ^{Met}tRNA on the ribosome. Phosphorylation of eIF2α prevents the regeneration of GTP in the ternary complex leading to arrest of translation of both cellular and viral mRNAs (García *et al*, 2007). Other examples include enzymes involved in RNA editing (ADAR1) and nucleases (RNAse L) that cleave nucleotides unspecific, thereby generating damage and pathogen associated molecular patterns that function as substrate for innate immunity and adaptive immunity (Mannion *et al*, 2014; Malathi *et al*, 2007; Goubau *et al*, 2013b). ISGs that act aspecific are potent inhibitors of virus spread, but requiring tight regulation.

1.5 Role of IFNα in diseases

The many positive and negative feedback loops induced by IFN signaling provide a buffering system to reduce noise (Hancock *et al*, 2017) and lead to a tailored response depended on the amount of pathogen. Implementation of positive feedback loops result in buffering and high sensitivity (Hornung & Barkai, 2008). As illustrated for this system by the requirement of two rounds of pathogen detection: first cells sense pathogens with low sensitivity leading to production of IFNα4 and IFNβ which act as positive feedback loop by upregulation of the pattern recognition receptors. Consequently cells can sense pathogens with higher sensitivity and produce a tailored response to the pathogen load to balance the anti-viral response and the collateral damage to the host.

1.5.1 Viral persistence

Despite of the well-regulated interferon response, viruses have been able to adapt and survive. Viruses mutate with higher frequency than the host which give them opportunities to develop strategies to persists (Elena SF, 2005).
In case of hepatitis C viral infection, often the virus persists and causes chronic inflammation. Chronic inflammation induces tissue damage with increasing risk of fibrosis, cirrhosis and hepatocellular carcinoma over time (Bartosch, 2010; Campos Appel-Da-Silva *et al*, 2016; Jacobson *et al*, 2010; Cabibbo & Craxì, 2010). Mechanism that could contribute to HCV persistence include low induction of IFNs, and inhibition of IFN-induced signaling. Specifically, the viral protein NS3/4A cleaves the critical adaptor protein TRIF and MAVS involved in TLR3 and RLR signaling, respectively (Ferreon *et al*, 2005; Li *et al*, 2005; Lin *et al*, 2006; Bellecave & Sarasin-Filipowicz, 2010), while the viral proteins NS5 and core have been associated with reduced levels of STAT1 (Lin *et al*, 2005), reduced phosphorylation of STAT1 (Kumthip *et al*, 2012) and impaired nuclear trafficking of STAT1 (Melén *et al*, 2004).
Different viruses have developed multiple strategies to circumvent the interferon response, these strategies act on different levels, either preventing recognition by pattern recognition receptors, inhibiting signal transduction pathways of either pathogen-induced or IFNα-induced signaling or directly inhibiting anti-viral proteins (García-Sastre, 2017; Randall & Goodbourn, 2008). Controversially, some anti-viral proteins can favour virus replication, for instance the global inhibition of translation by PKR can be circumvented either by viral PKR inhibitors or eIF2α independent translation as a consequence of cleavage of other initiation of translation factors or use of hairpin loop RNA structure of the viral genome (Dabo & Meurs, 2012).

1.5.2 Autoimmune disease

In contrast to viral persistence, uncontrolled IFNα-induced signaling results in autoimmunity. Overproduction of interferons is a hallmark of type I interferonopathies, a collection of mendelian disorders similar to Aicardi-Goutieres syndrome, a disease characterized as an inflammatory disorder affecting the brain or skin (Crow & Manel, 2015). Type I interferonopathies covers monogenic diseases originating from different mutated genes (Crow & Manel, 2015). Most mutated genes are involved in nucleic acid regulation and detection, thereby either favouring IFN production due to increased substrate exposure, increased signaling or increased sensitivity of detection. Examples include the loss of function of DNA 3‘ repair exonuclease 1 (TREX1) (Crow *et al*, 2006a), adenosine deaminase acting on RNA (ADAR) (Rice *et al*, 2012), or the three subunits of the ribonuclease H2 endonuclease complex (RNase H2A, RNase H2B and RNase H2C) (Crow *et al*, 2006b), or the gain-of-function of STING (Liu *et al*, 2014; Jeremiah *et al*, 2014) or mutations changing the sensitivity of MDA5 (Rice *et al*, 2014) or RIG-I (Jang *et al*, 2015). Furthermore, loss of USP18-mediated negative regulation results in disease as well (Zhang *et al*, 2014).
Diseases can be understood as perturbations of biological systems. By studying how all components in a cell or signal transduction cascade act together, emerging properties of the system can be understood (Marks *et al*, 2017).

1.6 Systems biology to unravel signal transduction pathways

A biological system can be defined along different scales: from a molecular complex or organelle in a cell, the cell itself, a population of cells, an organ up to the body. Biological systems can be very complex, with for instance 2-4 million proteins per femtoliter of cell volume (Milo, 2013). A reductionism approach does not suffice to capture the emerging properties of a biological system.

Systems biology takes an holistic approach by combining mathematical modelling with experimental data (Kitano, 2002).
Mathematical models are based on assumptions and simplification, but still provide insight to specific research questions (Klipp *et al*, 2009). To arrive at the answer of the research question, an iterative cycle between mathematical modelling and data generation is required (Figure 4), starting with formulation of the research question based on literature and experimental data, followed by establishment of a model structure, model calibration based on experimental data, evaluation of parameter estimation, design of new experiments to improve model performance, *in silico* experiments to generate model-derived hypotheses, and experimental validation (Kitano, 2002).

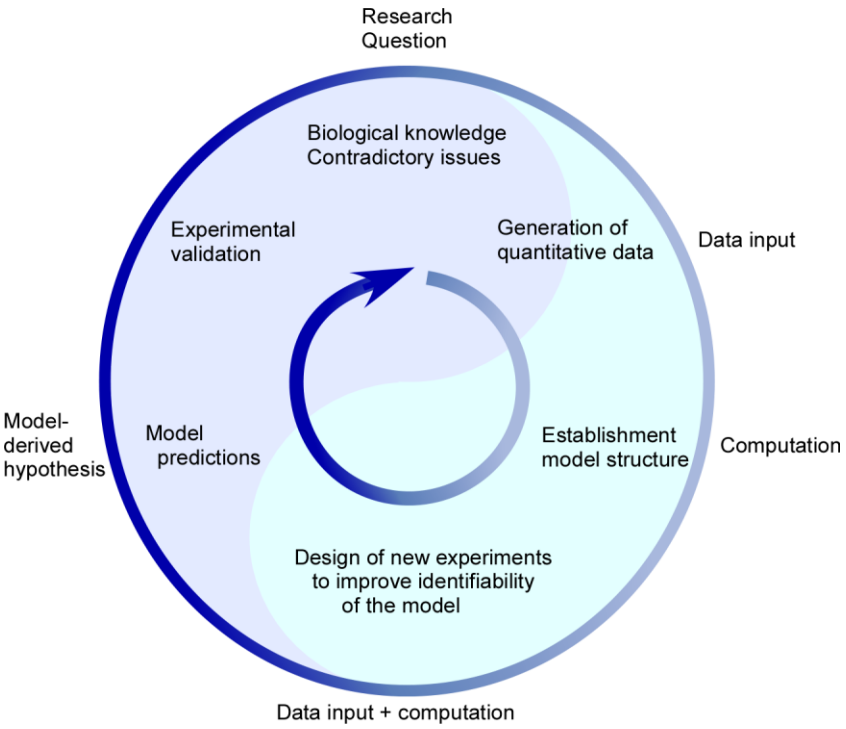

Figure 4. Hypotheses-driven research in systems biology. An iterative cycle between mathematical modeling and quantitative data generation is applied to address contradictory issues in biological knowledge, whereby data is generated and applied for model calibration. The model prediction generates hypothesis which require experimental validation. Figure adapted from (Kitano, 2002).

1.6.1 Mathematical modelling approaches

Different types of modelling approaches can be used depending on the research question, available data and prior knowledge of the system. To understand emerging properties of a system a bottom-up or a top-down approach can be used. A bottom-up approach is applied when prior knowledge of subsystems and molecular networks can be employed to deduce emerging properties from systems. In contrast, when little or no prior knowledge is available, a data-driven approach is required to identify molecular mechanisms between components that contribute to the emerging properties of the system (Marks *et al*, 2017). A data-driven approach relies on statistical models to interpret large amount of data when limited prior knowledge is available. It is often applied to analyze static data obtained by genomics, transcriptomics, proteomics or epigenomics. Statistical models can be used to identify relationships between components in a biological system. Methods include linear regression to determine correlations between components, clustering analysis to identify groups with similar characteristics and multivariate analysis like the principal components analysis to reduce dimensionality while preserving variability in the data, and help to interpret large amount of data (Jolliffe & Cadima, 2016).

Network models consist of nodes connected by edges, specifically in biological systems the interactions represent the edges and proteins or genes represent nodes. Biological systems comprise scale-free networks with nodes surrounded by many edges, called hubs, and nodes with fewer edges. (Marks *et al*, 2017). The identification of hubs provides insight for drug targets. Examples of network models include Boolean, Bayesian, stoichiometric, stochastic and deterministic models, which are applied to study different types of networks. In Boolean networks, interactions between components are directed and binary (Kauffman, 1969). Boolean networks are often used for the development of gene regulatory networks were genes can either be on or off. Whereas Boolean networks involves discrete values, Bayesian networks involve continuous values. Values of output nodes are described by a probability function that depends on the values of the input nodes, and edges represent conditional dependencies (Machado *et al*, 2011). Constraint-based stoichiometric models are applied to perform stoichiometric analysis or flux balance analysis of metabolic networks (Maarleveld *et al*, 2013). When fewer than 100 to 1000 copies of a protein are present in the cell, stochastic fluctuations need to be taken into account. Therefore stochastic models are applied to study noise and variability of biological systems (Chen *et al*, 2010). In contrast to stochastic models, deterministic models assume that reactants are abundant and that states can be predicted from knowledge of the previous state (Wilkinson, 2009). The velocity of each reaction is specified using a rate equation based on the law of mass-action or based on enzyme kinetics as Michaelis–Menten or Hill kinetics (Wilkinson, 2009). Under the assumption that the system consists as a well-stirred reactor, each reaction can be represented by ordinary differential equations (ODEs). When spatial dynamics need to be taken into account as well, partial differential equations are utilized, which comes at high computational cost (Cowan *et al*, 2012).

1.6.2 Mathematical modelling of signal transduction pathways

Cells respond to external signals via signal transduction pathways involving interactions between proteins, RNA, DNA or lipid components. Signaling components are abundant, but their concentration can change over time as a consequence of regulated production, degradation and localization. Furthermore their activity can change due to post-translational modifications. The wiring of the signaling network determines the phenotypic response of the cell. Deterministic mathematical models are often used to study signaling cascades (Klipp *et al*, 2009). To gain mechanistic insight in signal transduction cascades, ODE-derived mathematical models are calibrated with quantitative time- and dose-resolved measurements of signaling components. High quality of quantitative data is ensured by following standard operating procedures (Schilling *et al*, 2005a, 2005b). Cell lines are a valuable tool to generate data, since they are available in high amounts and easy to handle and manipulate, however, cell lines either originate from cancer or are immortalized. Therefore findings found in cell lines require validation using primary cells directly obtained from an animal or patient.
To study interferon-induced signaling, a human hepatocellular carcinoma cell line Huh7.5 is used. The Huh7.5 cell line carries a mutation in RIG-I and therefore does not produce interferon upon viral infection (Sumpter Jr. *et al*, 2005). Furthermore, Huh7.5 displays comparable dynamic behaviour of IFNα-induced signal transduction as primary human hepatocytes (Schneider, 2011). Consequently, Huh7.5 is a suitable system to study IFNα-signaling in a controlled manner and with high amount of materials. In addition Huh7.5 cells are susceptible to HCV infection (Blight *et al*, 2002), providing opportunities to study the interplay between interferon-induced signaling and viral persistence of HCV.

Quantitative time- and dose-resoled data is applied for model calibration. The change in concentration of each pathway component over time is modelled by ordinary differential equations (ODEs), also referred to as rate equations which equal a rate constant multiplied with the concentrations of reactants (Chen *et al*, 2010). Rate equations are derived from the law-of-mass-action according to chemical reaction network theory and include Michaelis-Menten kinetics to describe enzymatic reactions. A typical rate equation comprises consumption and production terms, each with a specific rate constant. Rate constants, also further referred to as parameters, are estimated from the data in a iterative numerical approach. Optimal parameters values are estimated in an n-parameter hyper-dimensional space. Different algorithms, belonging to stochastic, deterministic or hybrid optimization can be employed to identify parameter values best describing the data. For this study, a deterministic approach with randomly chosen initial values was employed, based on previous experience (Raue *et al*, 2013). How well the estimated parameters describe the data is scored by the objective function, also called cost function or loss function. The objective function is defined as the distance between model trajectory and data: the smaller the objective function, the better the model is able to describe the data.

While the objective function provides insights how well the identified parameters describe the data, profile likelihood estimation, a statistical test, can be used to analyze if the parameters can be accurately identified (Raue *et al*, 2009). By varying the parameter of interest while refitting all other parameters 95% confidence interval of the parameter of interest can be determined. An increase of 3.84 in the likelihood corresponds to 95% confidence interval of the profiled parameter. If the threshold of 3.84 is exceeded in one of the both directions, the parameter is classified as not identifiable. Such a parameter can be structurally or practically non-identifiable. Structural non-identifiability requires adjustment of the model structure, while practical non-identifiability is related to the amount and quality of the data (Raue *et al*, 2009).

When parameter values are identifiable, the model is more likely to converge to the best set of parameter values. Convergence of parameter estimation to a possible global optimum can be investigated by performing multiple rounds of parameter estimation starting from independent initial starting values and sorting them according to their objective values (Raue *et al*, 2013). If the parameter estimation converges, multiple steps forming a stairs are visible in the corresponding waterfall likelihood plot. If the local optimum with the lowest objective value is found repeatedly, this is very likely the global optimum.

Bayesian information criterion (BIC, also referred to as Schwarz criterion) is a statistical test related to the likelihood ratio test that compares different model structures (Schwarz, 1978). BIC incorporates penalties related to the amount of parameters and the amount of data points, thereby compensating for overfitting (Ghosh & Samanta, 2001).

1.6.3 Mathematical models of IFNα-induced signaling

Two ODE-models of IFNα-induced JAK/STAT signaling have been described previously. While Schneider and Maiwald et al developed a mathematical model addressing the early dynamics of IFNα-signaling dynamics (Schneider, 2011; Maiwald *et al*, 2010), Robichon and Maiwald et al developed a mathematical model to address dynamic expression profiles of target genes (Robichon, 2015). Schneider and Mawaild et al identified that the positive regulator IRF9 functions as crucial regulator by acceleration of IFNα-induced signalling. Robichon and Maiwald et al identified IRF2 as negative regulator for gene expression, resulting in transient expression profiles of IRF2 target genes.

1.7 Objectives

IFN-induced signal transduction is tightly regulated by both positive and negative feedback loops mediated by different proteins. Stable expression of feedback regulators can establish biological memory, defined as a sustained response after a transient stimulus (Burrill & Silver, 2010). The extent of the overall response depends on the balance of the induced feedback loops. Pre-exposure to a ligand could result in higher activation, equal activation or lower activation of the pathway upon stimulation that can be referred to as positive memory, no memory, or negative memory, respectively. Whether IFNα-induced feedback loops are sustained and are able to establish a positive memory is unclear. Based on non-responsiveness to IFNα treatment in patient chronically infected with HBV or HCV (Chen *et al*, 2005; Zhu *et al*, 2012; Li *et al*, 2014; Sarasin-Filipowicz, 2008) combined with cell culture and *in vivo* experiments (Sarasin-Filipowicz *et al*, 2009a; Makowska *et al*, 2011; François-Newton *et al*, 2011; Larner *et al*, 1986) indicate the establishment of a non-responsive state, referred to as negative memory. Despite the reported evidence of a negative memory modulating the activation of the IFNα-signaling cascade, it remained unclear under which conditions a negative memory establishes.

To unravel the effect of pre-activation of the IFNα-induced signaling pathway, the presented work addresses the following major aims:

1. Under which conditions is a negative memory established and can a positive memory be established as well?

2. What is the mechanism behind negative memory?

3. Can the establishment of a negative memory be predicted?

This work addressed these aims by combining quantitative data with mathematical modelling to gain mechanistic insights how the different feedbacks shape the response to multiple rounds of ligand exposure. Understanding the mechanisms behind IFN-induced memory provides new perspectives for patient-tailored treatment by identification of biomarkers, possible drug targets or patient-tailored dosing scheme.

2 Results

2.1 Dose-dependent memory of IFNα-induced signal transduction

There has been evidence that pre-activation of the IFNα-induced signaling pathway changes the dynamic behavior of the IFNα-induced signaling transduction, but the underlying mechanism is unknown. To examine the impact of IFNα pre-treatment on the dynamics of IFNα-induced signal transduction in a cell culture system, Huh7.5 cells were growth-factor-depleted and pre-treated with a low dose of 2.8 pM IFNα, a high dose of 1400 pM IFNα or were left untreated. After 24 hours the cells were stimulated by adding a high dose of 1400 pM IFNα (Figure 5A) and cytoplasmic as well as nuclear lysates were analyzed by quantitative immunoblotting. The dynamics of the activation of the IFNα-signaling cascade in the first hour was investigated by detecting tyrosine phosphorylated STAT1 and STAT2 (pSTAT1, pSTAT2) (Figure 5B, Figure 5C). The quantitative analysis shown in Figure 5D revealed that upon stimulation with IFNα, the amount of pSTAT1 and pSTAT2 in the cytoplasm and the nucleus was maximally increased at ten minutes after stimulus addition and remained elevated over one hour in cells without pre-treatment (Figure 5C). A 25 fold change was observed for cytoplasmic pSTAT1, while a 75 fold change was observed for nuclear pSTAT1, indicating an enrichment of pSTAT1 in the nucleus. This enrichment in the nucleus was less visible for pSTAT2. In contrast to cells without pre-treatment, in cells pre-treated with a high dose of IFNα the addition of 1400 pM IFNα did not trigger the phosphorylation of STAT1 and STAT2 in the cytoplasm or the nucleus (Figure 5B, 5C, 5D) indicating an inability to respond to stimulation. Interestingly, in cells pre-treated with a low dose of IFNα the phosphorylation of nuclear STAT1 and STAT2 was elevated compared to the phosphorylation levels observed in the nucleus of IFNα treated cells that were not pre-treated. Stimulation with IFNα resulted in nuclear pSTAT1 levels that were 1.5 fold higher in cells pre-treated with a low dose, compared to cells that were not pre-treated. Interestingly, For STAT2, stimulation with IFNα resulted in nuclear pSTAT2 levels that were 2-3 fold higher in cells pre-treated with a low dose compared to cells that were not pre-treated. Analyzes of the cytoplasmic lysates for IRF9 and USP18, functioning as positive and as negative feedback loop, revealed that the IRF9 protein was highly induced both in cells pre-treated with a low dose as in cells pre-treated with a high dose (Figure 5B). In contrast, the expression of USP18 was only induced to a minor extent in cells pre-treated with a low dose for 24 hours, but highly induced in cells pre-treated with a high dose for 24 hours (Figure 5B). Furthermore pre-treatment with a high dose showed elevated levels of STAT1 and STAT2 both in the cytoplasm and in the nucleus.

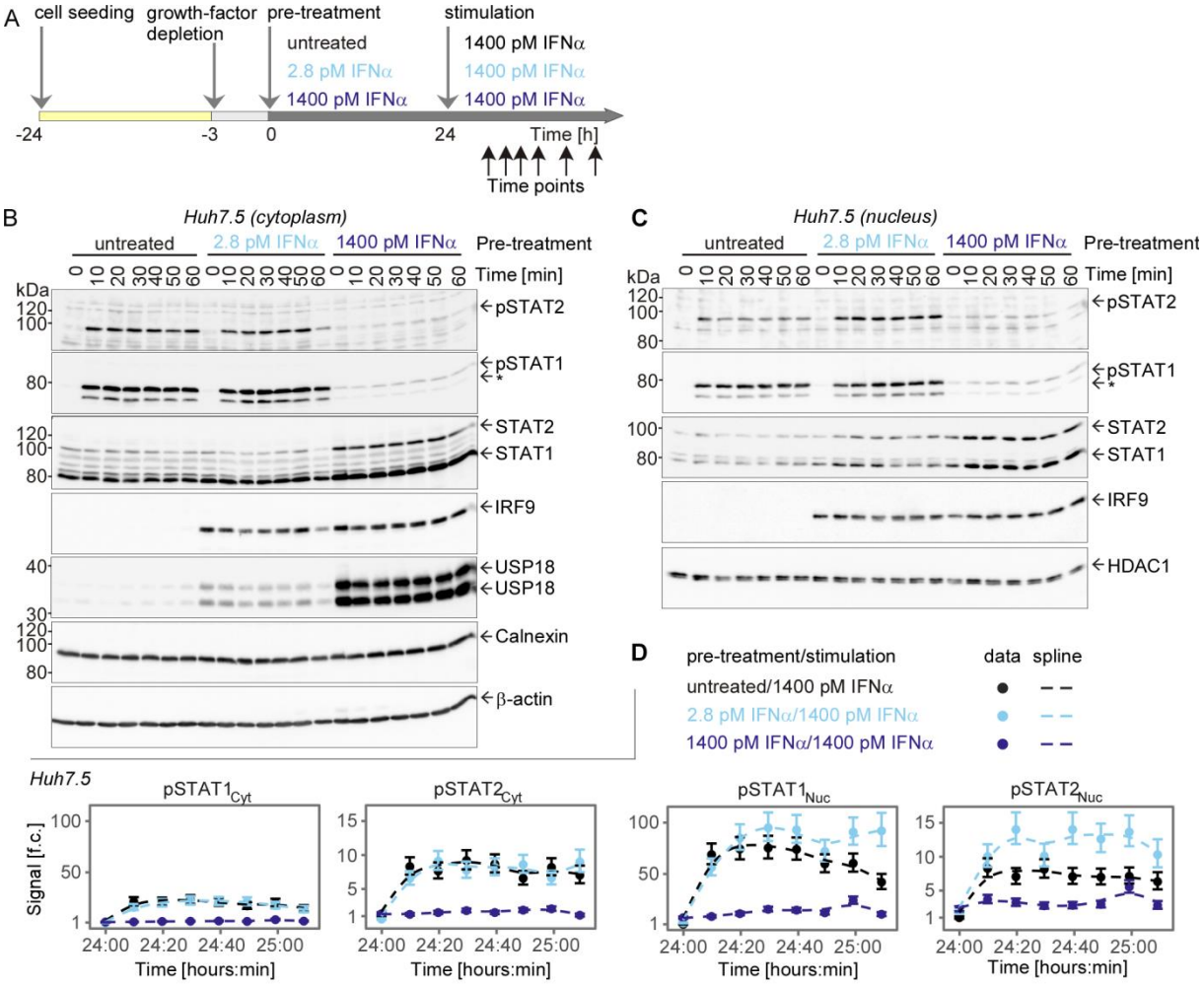

Figure 5. Effect of pre-treatment with IFNα on the dynamic behaviour of IFNα-induced signalling. A) Experimental design of experiments of IFNα pre-treatment combined with IFNα stimulation in Huh7.5 cells. Cells were seeded 24 hours prior to the start of the experiment. Three hours before pre-treatment, cells were growth-factor-depleted and subsequently, were pre-treated with 2.8 pM IFNα, 1400 pM IFNα or were left untreated. After 24 hours, cells were stimulated with 1400 pM IFNα. Cytoplasmic and nuclear protein lysates were collected at indicated time points. B and C) Representative immunoblot of IFNα-induced phosphorylation of STAT1 and STAT2 upon stimulation of Huh7.5 cells pre-treated for 24 hours with 2.8 pM IFNα, 1400 pM IFNα or without pre-treatment. Time points are indicated starting at the time of stimulation. 20 µg of cytoplasmic lysates (B) or 10 µg of nuclear lysates (C) were analysed using antibodies for the indicated protein targets. Phosphorylation of STAT1 and STAT2 was detected by immunoblot utilizing antibodies recognizing STAT1 phosphorylated on tyrosine residue 701, or STAT2 phosphorylated on tyrosine residue 690. * indicates pSTAT1β. Calnexin, β-actin or HDAC1 served as loading controls. Molecular weights are indicated on the left. Immunoblot detection was performed with chemoluminescence employing a CCD camera device (Imagequant).D) Quantification of immunoblots of IFNα-induced phosphorylation of cytoplasmic and nuclear STAT1 and STAT2 in Huh7.5 cells pre-treated with 2.8 pM IFNα, 1400 pM IFNα or without pre-treatment. Time points are displayed starting from the time of pre-treatment of 24 hours. Data is displayed with errors estimated by the error model, comprising 1σ confidence interval estimated from biological replicates (N=3). Dashed lines indicate splines. f.c.: fold change.

To test whether the observed changes in the dynamical behavior of IFNα-induced signaling depended on the presence of IFNα, a low and high dose of IFNα was added to the cells and removed by washing at one or 20.5 hours post pre-treatment. Subsequently, 24 hours after pre-treatment, the ligand was reapplied and the dynamics of IFNα-induced signal transduction was monitored by quantitative immunoblotting (Figure 7). A time-frame of two hours of stimulation was investigated to observe the induction of IFNα-induced phosphorylation of STAT1 and STAT2 combined with the effect of signal termination.

Removing the ligand after 20.5 hours after pre-treatment showed comparable IFNα-induced phosphorylation of STAT1 and STAT2 to pre-treated cells that still contained the ligand in the medium, as shown by higher nuclear pSTAT1 and pSTAT2 signals in cells pre-treated with a low dose of IFNα and lower cytoplasmic and nuclear pSTAT1 and pSTAT2 signals in cells pre-treated with a high dose of IFNα (Figure 7A). Quantitative analysis of the induced feedback proteins IRF9, USP18, total STAT1 and total STAT2 protein did not indicate an effect from ligand removal as visible for both cells pre-treated with a low dose and cells pre-treated with high dose.

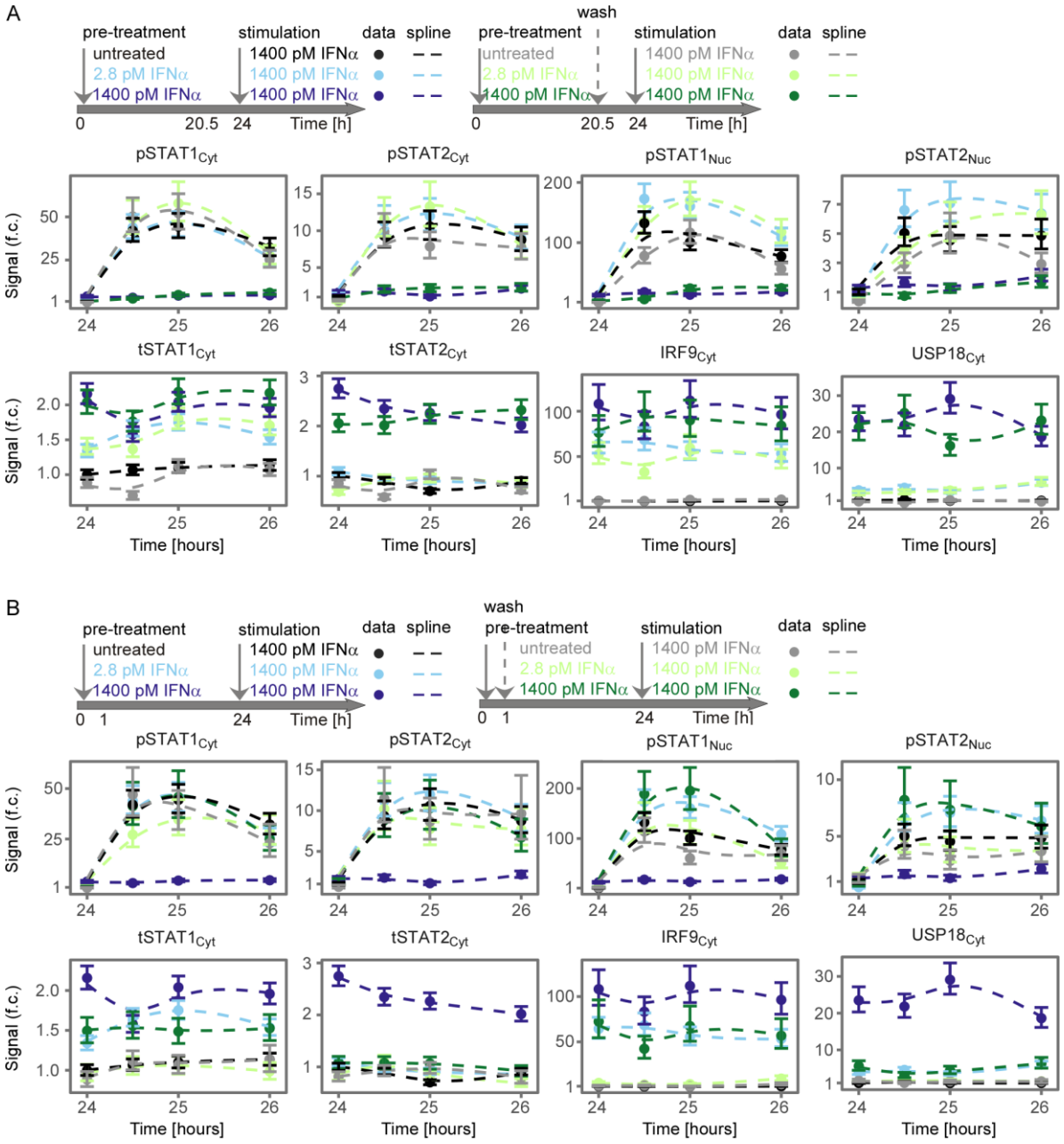

Figure 6. Effect of ligand removal on IFNα-induced dynamical behaviors in cells pre-treated with a low or high dose of IFNα. Huh7.5 cells were growth-factor depleted for three hours and received pre-treatment with 2.8 pM IFNα, 1400 pM IFNα or no pre-treatment. Cells were washed at 20.5 hours after pre-treatment and starved for another three hours (A) or were washed and kept in starvation medium after one hour of pre-treatment (B) before cells were stimulated with 1400 pM IFNα 24 hours after pre-treatment. Cytoplasmic and nuclear lysates were subjected to quantitative immunoblotting. IFNα-induced phosphorylation of STAT1 and STAT2 and induction of feedback proteins was detected with chemoluminescence utilizing a CCD camera device (Imagequant). Data is represented by filed circle with 1σ confidence-interval estimated from biological replicates (N=2 to N=3) using an error model. Dashed line represents smoothing spline.

In contrast, ligand-removal one hour after pre-treatment with a low dose of IFNα did not result in elevated IFNα-induced phosphorylated STAT1 and STAT2 observed in the nucleus, but showed comparable nuclear pSTAT1 and pSTAT2 levels to cells that did not receive pre-treatment. The similar dynamic behavior of IFNα-induced phosphorylation of STAT1 and STAT2 correlated with comparable expression of the feedback proteins STAT1, STAT2, IRF9 and USP18.
In line with the previous findings, cells pre-treated with a high dose of IFNα showed a much reduced IFNα-induced phosphorylation of cytoplasmic and nuclear STAT1 and STAT2. Interestingly, ligand removal after one hour and stimulation 23 hours later did not show the much reduced IFNα-induced phosphorylation of STAT1 and STAT2, but instead showed elevated pSTAT1 and pSTAT2 signals in the nucleus, which might be a consequence of either residual intrinsic signaling caused by phosphorylation of STAT1 and STAT2 that did not return to basal after one hour or it might be a possible artifact from incomplete washing responsible for triggering additional phosphorylation of STAT1 and STAT2. The observed elevated levels of nuclear pSTAT1 and pSTAT2 correlated with elevated expression of IRF9 and STAT1 to levels comparable in cells pre-treated with a low dose of IFNα.
To conclude, IFNα-induced phosphorylation of STAT1 and STAT2 is much reduced in cells pre-treated with a high dose of IFNα, while IFNα-induced phosphorylated STAT1 and STAT2 is increased in cells pre-treated with a low dose of IFNα. These effects correlated with elevated expression of STAT1, STAT2, IRF9 and USP18 at the time of stimulation and were independent from ligand removal after 20.5 hours, suggesting that pre-treatment with a low dose of IFNα establishes a positive memory of IFNα-induced signal transduction, while pre-treatment with a high dose of IFNα establishes a negative memory of IFNα-induced signal transduction.

2.2 Impact of dose-dependent memory of IFNα-induced signal transduction on expression of target genes

To investigate how the negative memory observed at the level of IFNα-induced signal transduction in Huh7.5 affected the dynamics of target gene expression, interferon stimulated genes (ISGs) with different expression profiles were selected for analysis by quantitative RT-PCR. ISGs with different expression dynamics were selected based on a time-resolved microarray analysis performed with Huh7.5 stimulated with IFNα (Maiwald *et al*, 2010). Katharine Robichon (DKFZ) and Clemens Kreutz (University of Freiburg) performed cluster analysis of the gene expression profiles and identified three classes (Robichon, 2015) which were used as input for this study. Specifically, in this study the genes were grouped based on their expression levels after 24 hours, resulting in the three classes: (1) genes with early and transient dynamics with expression close to basal level after 24 hours, (2) genes with sustained dynamics either reaching maximal expression after 24 hours, or increasing expression in the investigated time span of 48 hours, and (3) genes with an intermediate expression profile, whose expression is transient, but does not return to the basal expression level after 24 hours. Representative genes selected for each class included genes coding for feedback mediators and anti-viral genes. Huh7.5 cells were pre-treated for 24 hours with a high dose of IFNα and were subsequently stimulated with a high dose of IFNα or were left untreated. IFNα-induced gene expression was assessed for 48 hours comprising the time period of the pre-treatment and of the stimulation. Pre-treatment with a high dose of IFNα-induced a strong activation of all 20 genes during the first 24 hours (Figure 7). The intermediate genes (Figure 7B) showed a peak of maximal expression at eight hours after pre-treatment with IFNα, interestingly the early genes (Figure 7A) showed a peak of maximal expression either at eight hours, for example CXCL10, or earlier for

example IRF1 displayed maximal expression at one hour after stimulation with IFNα, while IFIT2 reached maximal expression at four hours after stimulation. The sustained genes reached maximal expression at 8 hours after pretreatment or did not reach saturation in the investigated timeframe (Figure 7C).

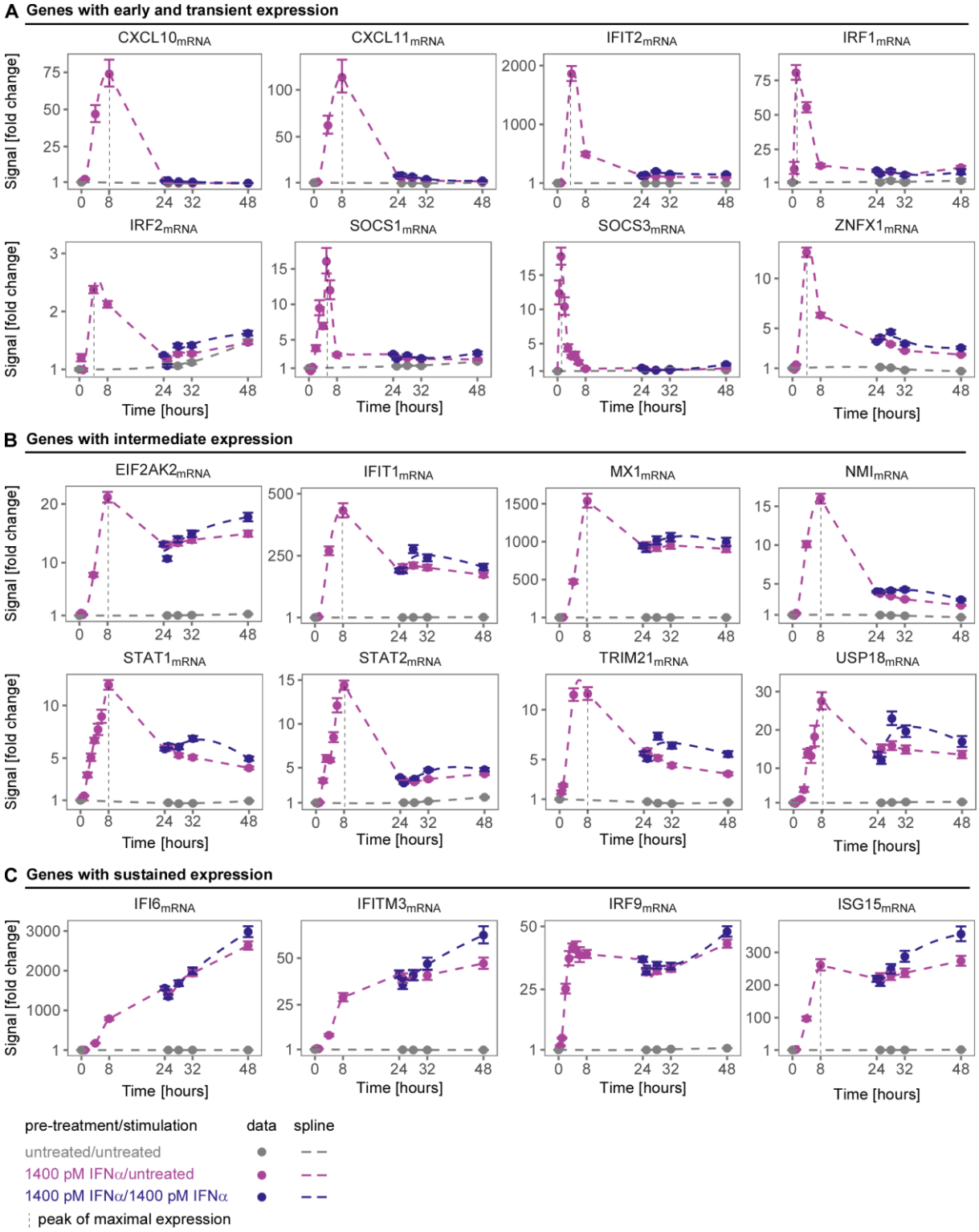

Figure 7. Expression of interferon-stimulated genes upon pre-treatment with 1400 pM IFNα and stimulation with 1400 pM IFNα in Huh7.5 cells was assessed by quantitative RT-PCR. RNA levels were normalized to the geometric mean of reference genes GAPDH, HPRT and TBP and were displayed as fold change. Peak of maximal gene expression upon pre-

treatment is indicated. Data points are displayed as dots with 1σ confidence-interval estimated from biological replicates (N=4 to N=14) using an error model, dashed lines indicate spline.

Stimulation with IFNα at 24 hours did not trigger induction of genes with early and transient dynamics showing that the negative memory on the signaling level propagated to the level of gene expression (Figure 7A). Surprisingly, the genes with the intermediate and sustained expression profiles showed a minor further induction upon stimulation with IFNα in comparison to the induction upon pre-treatment.

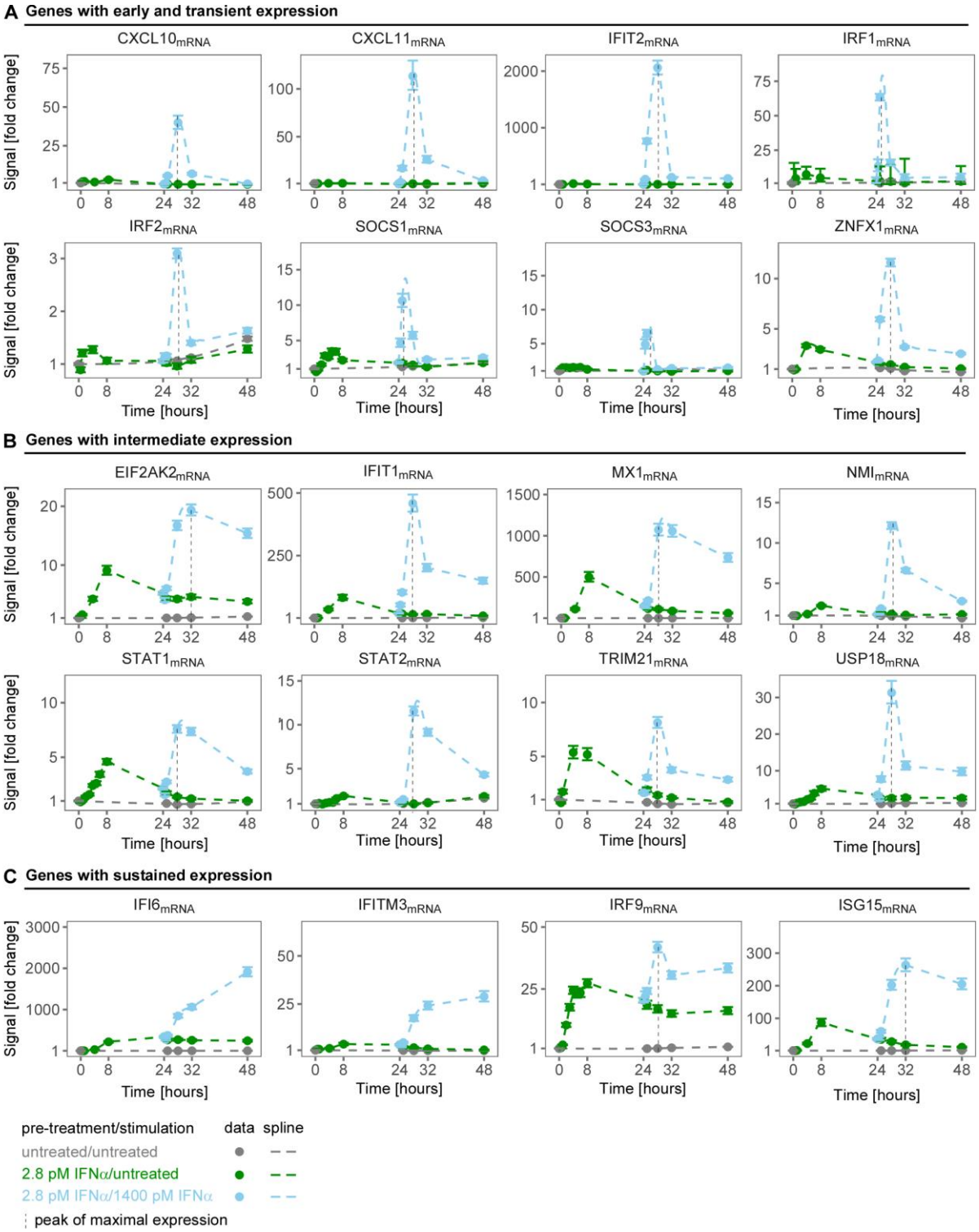

Figure 8: Expression of interferon-stimulated genes upon pre-treatment with 2.8 pM IFNα and stimulation with 1400 pM IFNα in Huh7.5 cells was assessed by quantitative RT-PCR. RNA levels were normalized to the geometric mean of reference genes GAPDH, HPRT and TBP and are displayed as fold change. Peak of maximal gene expression upon re-stimulation is indicated. Data points are displayed as dots with 1σ confidence-interval estimated from biological replicates (N=4 to N=6) using an error model, dashed lines indicate spline.

To investigate how the positive memory observed at the level of IFNα-induced signal transduction in Huh7.5 affected the dynamics of target gene expression, gene expression of the selected genes was investigated by quantitative RT-PCR in cells pre-treated for 24 hours with 2.8 pM IFNα and were subsequently stimulated with 1400 pM IFNα or were left untreated. As in the previous experiment, IFNα-induced gene expression was assessed for 48 hours comprising the time period of the pre-treatment and of the stimulation. As shown in Figure 8, pre-treatment with the low dose of IFNα-induced lower gene expression of all the genes compared to pre-treatment with the high dose of IFNα, however, pre-treated cells did respond after 24 hours to stimulation with IFNα and responded faster compared to cells that had not been pre-treated with IFNα, as illustrated by an earlier peak of maximal expression at four hours instead of eight hours for instance for CXCL10, CXCL11, STAT1, STAT2, USP18. The genes EIF2AK2 and ISG15 showed a peak of maximal expression at eight hours comparable to the peak of maximal activation in cells without pre-treatment (first 24 hours of Figure 7B and 7C), however expression levels at four hours were already more elevated compared to cells without pre-treatment, thereby indicating the same tendency of faster activation.
To conclude, the positive and negative memory observed at the level of signaling is propagated to the regulation of target genes.

2.2 Unravelling the mechanisms of dose-dependent memory by combining quantitative data with mathematical modeling

2.2.1 Establishment of a mathematical model of IFNα-induced signalling transduction

Pre-treatment with IFNα established a positive or negative memory of IFNα-induced signaling transduction which correlated with the expression of positive and negative feedback proteins such as IRF9 and USP18. To unravel mechanisms how the pre-treatment with a low dose of IFNα generates a positive memory, while the pre-treatment with a high dose of IFNα generates a negative memory of IFNα-induced signal, an ordinary differential equation (ODE)-based model was established by Marcus Rosenblatt (University of Freiburg) (University of Freiburg). The model structure was developed in collaboration with Marcus Rosenblatt (University of Freiburg) and Dr. Tim Maiwald (University of Freiburg), and model calibration and model analysis was performed by Marcus Rosenblatt (University of Freiburg). Rate equations were derived from the law of mass-action according to chemical reaction network theory, including Michaelis-Menten kinetics. As visualized in Figure 9, the ODE model incorporates IFNα-induced signal transduction starting with activation of the receptors IFNAR1 and IFNAR2, followed by the phosphorylation and complex formation of STAT1 and STAT2, their translocation to the nucleus and transcriptional regulation resulting in the induction of feedback genes. The model integrates the pre-treatment and the stimulation with different IFNα doses over time. A list of all model equations, list of observables and estimated parameter values can be found in the Appendix section 5.1.
In brief, IFNAR1 and IFNAR2 in complex with JAK1 and TYK2 are summarized as one species termed Receptor (Rec). Upon binding of IFNα, the receptor is phosphorylated and therefore activated (aRecIFN), recruits cytoplasmic STAT1 (STAT1c) or STAT2 (STAT2c) thereby giving rise to the

intermediate species aRecIFNSTAT1c and aRecIFNSTAT2c, which can phosphorylate STAT1 either leading to release of phosphorylated STAT1 homodimers (pSTAT1dimc) or pSTAT1pSTAT2 heterodimers, respectively, that are released from the active receptor complex. Binding of cytoplasmic IRF9 (IRF9c) to pSTAT1pSTAT2c heterodimers produces ISGF3c. The three complexes pSTAT1dimc, pSTAT1pSTAT2c and ISGF3c translocate to the nucleus and regulate expression of target genes. In the nucleus, pSTAT1 homodimers (pSTAT1dimn) regulate the expression of SOCS3 by binding to STAT1 transcription factor binding sites named occupied Gamma-activated-sequence binding sites (OccGASbs), while pSTAT1pSTAT2n and ISGF3n regulate expression of the genes coding for the feedback proteins STAT1, STAT2, IRF9, USP18, SOCS1 and IRF2 mediated by the occupied interferon-stimulated-response-element (ISRE) binding sites (OccISREbs). By means of the model, the induction by ISGF3n was estimated to be stronger than for pSTAT1pSTAT2n, which is in agreement with literature showing that IRF9, STAT1 and STAT2 all contribute to binding to the ISRE (Qureshi & Salditt-Georgieff, 1995). All transcription factor complexes can dissociate into their individual components STAT1, STAT2 and IRF9, which have freedom to shuttle between cytoplasm and nucleus (Banninger & Reich, 2004; Meyer *et al*, 2002). The induced feedback mRNAs are translated into proteins by taking into account gene-specific time-delays for the translation that were incorporated via linear chains between mRNA and protein (MacDonald, 1976). One linear chain was incorporated for SOCS1, two for IRF9 and USP18, three for STAT1 and five for STAT2, while SOCS3 translation was estimated to be very fast and therefore did not require incorporation of linear chains. To capture the different dose-sensitivities between the genes, gene-specific saturation levels were incorporated for IRF9 and STAT1. Additionally, a STAT1-specific saturation level of mRNA into protein was incorporated to capture the observed mRNA fold change and the amount of molecules per cell in cells stimulated with different doses of IFNα.

Signal termination involves three negative feedback mechanisms. 1) SOCS1 and SOCS3 act at the receptor level by directly inhibiting formation of the active receptor-IFN-bound complex (aRecIFN) (Chen *et al*, 2000). 2) SOCS1 mediates degradation of the activated receptor complexes bound to IFNα and STAT1, IFNα and STAT2 or only bound to IFNα (aRecIFN, aRecIFNSTAT1c and aRecIFNSTAT2c) (Piganis *et al*, 2011). Testing different model structures by means of Bayesian Information Criterion (BIC) revealed that SOCS1 and USP18 act synergistically on reducing the active receptor complexes (Figure 17D). 3) USP18 inhibits signaling transduction of the activated receptor complex (Malakhova *et al*, 2006).

The mathematical model estimated a higher degradation rate of the STAT2-bound active receptor complex (aRecIFNSTAT2c) compared to the degradation rate of the active receptor complex (aRecIFN) or the STAT1-bound active receptor complex (aRecIFNSTAT1c), which is in agreement with STAT2-mediated recruitment of USP18 to IFNAR2 (Arimoto *et al*, 2017a).

Additionally, the transcriptional modulator IRF2 was incorporated to capture transient dynamics of SOCS1 mRNA (Harada *et al*, 1994; Robichon, 2015). Turnover of all species include basal production and degradation.

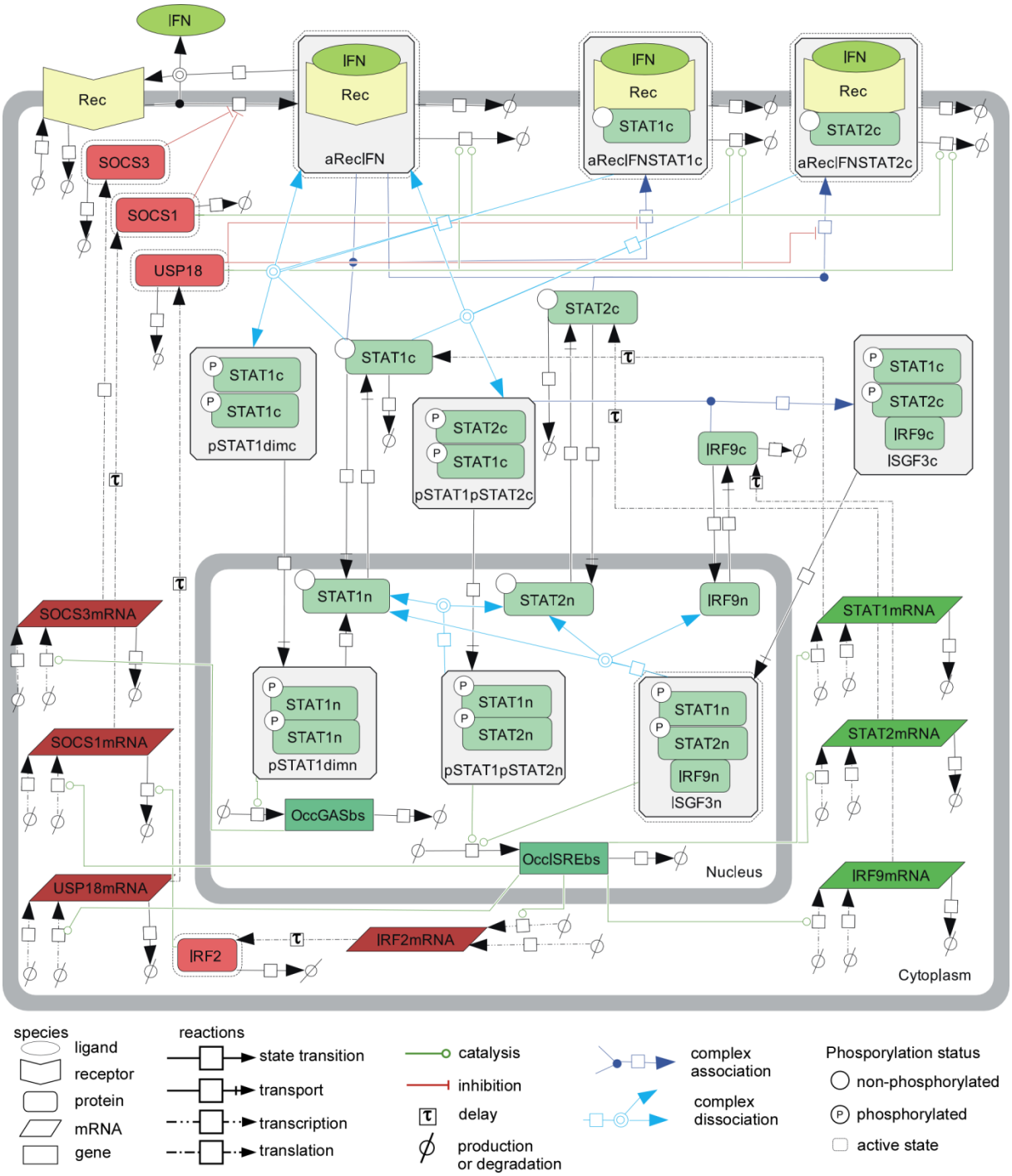

Figure 9. Mathematical model structure of IFNα-induced JAK/STAT signaling cascade.
The model structure is represented by a process diagram displayed according to Systems Biology Graphical Notation (Le Novere *et al*, 2009). Negative regulators are depicted in red. c: cytoplasm, n: nucleus, dim: dimer, rec: receptor, a: active, occGASbs: occupied binding sites containing Gamma-activated sequence, occISREbs: occupied binding sites containing Interferon Stimulated Response Element.

To capture dynamic properties of the system, the IFNα-signaling model was calibrated with the complete dataset of IFNα-induced signaling in Huh7.5 consisting of 1918 data points corresponding to 25 conditions, comprising quantitative time-resolved data obtained at the protein and RNA level. (visualized in Appendix section 5.2) Profile likelihood analysis revealed that out of 84 model parameters, 79 parameters were identifiable (Appendix section 5.1.4). The remaining five

parameters include formation of pSTAT1pSTAT2 heterodimer, formation of pSTAT1 homodimer, translocation of pSTAT1 homodimer to the nucleus, degradation of SOCS3 protein and SOCS1-and-USP18-mediated degradation of the STAT2-active receptor complex. These parameters were practically non-identifiable with confidence intervals open to plus infinity; no model reduction was applied due to the biological relevance of the parameters.
Furthermore, reliable convergence of parameter estimation was assessed by likelihood waterfall analysis, as displayed by ranked objective values of 500 rounds of parameter estimations, each starting from randomly selected initial values (Appendix section 5.1.5). This likelihood waterfall plot showed several steps corresponding to local optima and the global optimum was found in 20 of the 500 cases.
In summary, a calibrated ODE model consisting of seven feedbacks was established. 79 out of 84 parameters were identifiable and parameter estimation converged repeatedly to the global optimum. This model was used to investigate the mechanisms constituting establishment of IFNα-dose dependent memory. Model fits will be described in the sections below.

2.2.2 Time-resolved measurements of IFNα-induced expression of proteins mediating feedback loops

To analyze the dynamic behavior of IFNα-induced phosphorylation of STAT1 and STAT2 and subsequent transcriptional regulation of genes encoding feedback loops during the 24 hours timeframe of pre-treatment, Huh7.5 cells were treated with 0, 0.028 pM, 0.28 pM, 0.84 pM. 2.8 pM, 8.4 pM, 14 pM, 28 pM, 140 pM, 280 pM, 700 pM, 1400 pM or 14 000 pM IFNα and signaling proteins and mRNA were monitored at different time points for up to 24 hours by quantitative immunoblotting and quantitative RT-PCR. The experimental data was employed for model calibration together with the remaining conditions of the complete dataset. For simplification, only 0, 2.8 pM, 28 pM and 1400 pM IFNα are displayed combined with only cytoplasmic targets, the remaining dose-resolved time-courses and dose-response measurement are visualized in Appendix section 5.2.1 and 5.2.2, together with protein targets measured in the nucleus. As visualized in Figure 10A, treatment with 2.8 pM, 28 pM or 1400 pM IFNα resulted in transient phosphorylation of both STAT1 and STAT2 with a maximal amplitude observed between 15 minutes and one hour for all investigated doses. The maximal amplitude of cytoplasmic pSTAT1 showed 5-fold, 20-fold and 40 fold increase upon treatment with 2.8 pM, 28 pM and 1400 pM IFNα, respectively, while the maximal amplitude of cytoplasmic pSTAT2 showed 2-fold, 6-fold and 8-fold increase upon treatment with 2.8 pM, 28 pM and 1400 pM IFNα, respectively. Cells treated with 2.8 pM or 28 pM IFNα displayed pSTAT1 and pSTAT2 levels that returned to basal level after 8 hours, while cells treated with 1400 pM IFNα displayed pSTAT1 and pSTAT2 levels that were close to basal level after 24 hours. Interestingly, treatment with 1400 pM IFNα showed in addition a dampened second peak in pSTAT1 and pSTAT2 levels at 14 hours, both visible for cytoplasmic and nuclear pSTAT1 and pSTAT2. Analysis of the proteins mediating positive and negative feedback loops revealed different kinetic profiles for IRF9, USP18 and STAT1 and STAT2. While IRF9 reached saturation at six hours after stimulation, USP18 reached saturation at eight hours after stimulation, while STAT1 and STAT2 reached saturation only at 14 after stimulation. Subsequently, the expression of IRF9, USP18, STAT1 and STAT2 remained sustained.

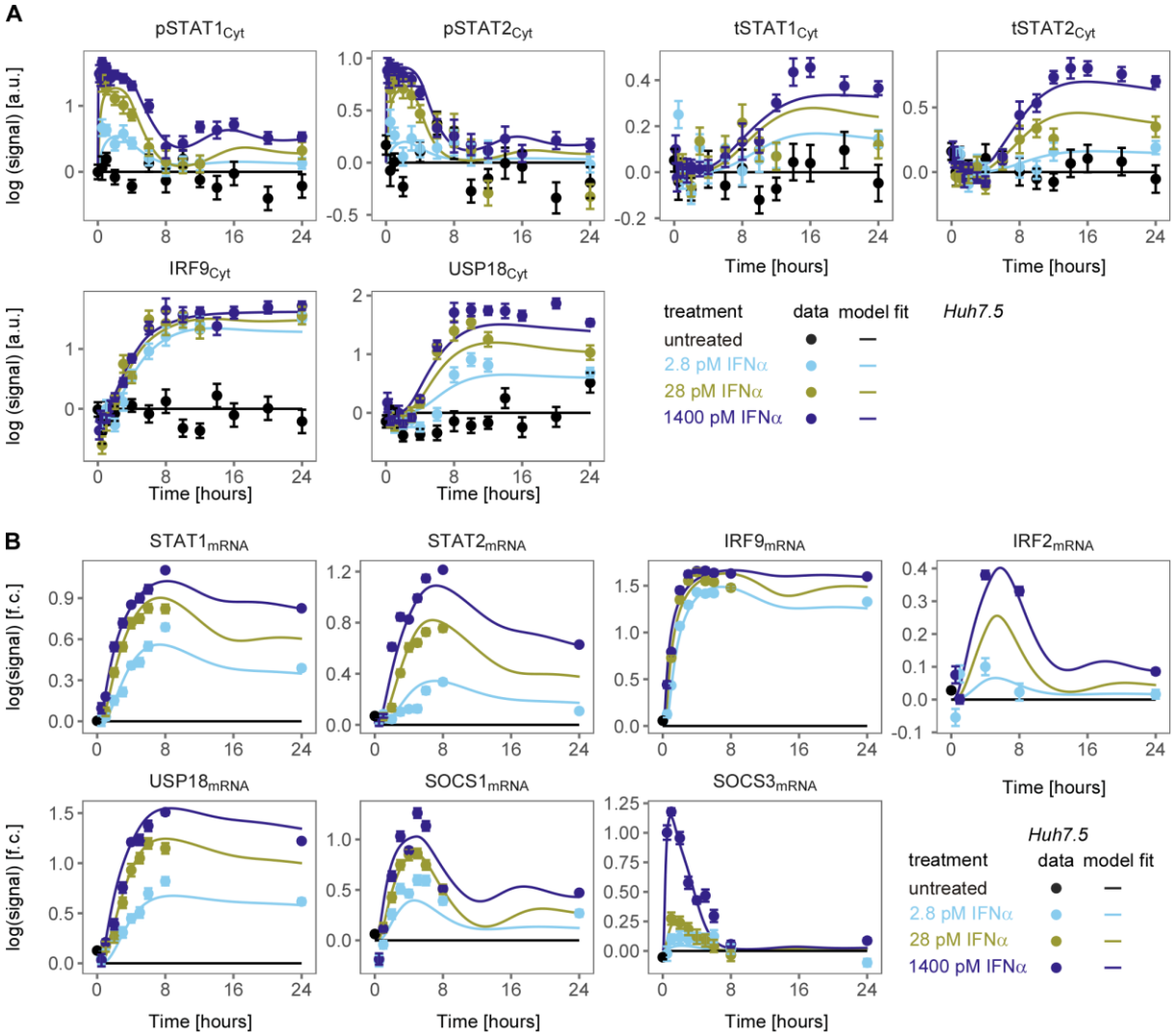

Figure 10. IFNα-induced phosphorylation of STAT1 and STAT2 and expression genes and proteins functioning as feedback loop. A) Growth-factor-depleted Huh7.5 cells were treated with 2.8 pM, 28 pM, 1400 pM IFNα or left untreated and IFNα-induced signaling was measured by time-resolved quantitative immunoblotting, detected with chemoluminescence using CCD-based camera. Data was normalized to reference proteins Calnexin or HDAC1 and represented by filled circles with errors representing 1σ confidence-interval estimated from biological replicates (N=3 to N=23) using an error model. Model trajectories are represented by the line. B) Growth-factor-depleted Huh7.5 cells were treated with 2.8 pM, 28 pM, 1400 pM IFNα or left untreated and IFNα-induced expression of feedback genes was analyzed by quantitative RT-PCR. RNA levels were normalized to the geometric mean of reference genes GAPDH, HPRT and TBP and were displayed as fold change. Experimental data is represented by filled circles with errors representing 1σ confidence-interval estimated from biological replicates (N=3 to N=14) using an error model. Model trajectories are represented by the line.

The quantitative analysis at the RNA level shown in Figure 10B, revealed sustained expression profile for IRF9, close to sustained expression of USP18 but less sustained expression of STAT1 and STAT2 over 24 hours, in agreement with the kinetic behavior observed previously (Figure 7). While IRF9 protein levels increased starting from four hours and reached maximal expression at six hours after treatment with the different doses of IFNα, IRF9 mRNA levels increased starting from two hours and reached maximal expression at four hours after treatment, indicating a delay between mRNA and protein. The time delay between USP18 mRNA and USP18 protein could be observed in the data as well, with an increase in USP18 protein levels starting from four to five hours and reaching maximal expression at eight hours after treatment and an increase in USP18 mRNA levels starting from four hours and reaching saturation at six hours after treatment. Time-resolved measurements on SOCS1,

SOCS3 and IRF2 mRNA revealed transient dynamics, with SOCS1 and IRF2 showing mRNA levels above basal expression at 24 hours after pre-treatment, while SOCS3 mRNA levels returned to basal levels at 8 hours after treatment (Figure 10B). IRF2 mRNA showed maximal expression at 4 after treatment with 1400 pM IFNα, with an amplitude of 2.5 fold, while treatment with 2.8 pM IFNα resulted in expression levels just above background. Interestingly, SOCS1 and SOCS3 mRNA showed very different dynamical behavior. While SOCS3 mRNA reached maximal expression already at one hour after treatment, SOCS1 mRNA reached maximal expression only at five hours after treatment, as visible for all observed doses.

In addition to the difference in timing of induction of the investigated proteins and mRNA targets, a difference in IFNα dose-sensitivities was observed which was consistent between the mRNA and protein. USP18, STAT1, STAT2 and SOCS1 displayed dose-dependent induction within the range of investigated doses. In contrast, IRF9 expression was already close to saturation after treatment with a low dose of 2.8 pM of IFNα. Interestingly, SOCS3 mRNA displayed a strong upregulation upon treatment with 1400 pM IFNα, but only a minor upregulation upon treatment with 2.8 or 28 pM IFNα.

The model trajectories showed the model was able to describe the different dynamical behaviors of all the investigated targets across the different IFNα doses.

Taken together, the obtained results showed that the feedback components of IFNα-signaling had different kinetics and IFNα dose sensitivities.

2.2.3 Absolute quantification of IFNα-induced feedback proteins

The absolute abundance of pathway components determines complex formation and dynamic behavior of signaling networks (Adlung *et al*, 2017; Lucarelli *et al*, 2017). To calibrate the mathematical model with the different protein abundances established after IFNα pre-treatment, the amount of molecules per cell of STAT1, STAT2, IRF9 and USP18 protein were determined experimentally in Huh7.5 treated with 0 pM, 2.8 pM, 28 pM or 1400 pM IFNα for 24 hours (Figure 11). For absolute quantification recombinant proteins with known concentrations is required, therefore protein calibrators consisting of the protein of interest fused to an affinity tag for purification were spiked into total cell lysates prior to quantitative immunoblotting. In case of IRF9 and USP18 full length proteins fused to the GST-tag were utilized, while for STAT1 and STAT2 N-terminally truncated proteins fused to the SBP-tag were utilized and antibodies raised against the C-termini were employed for detection. The calibration curves were fitted by linear regression thereby fixing the offset to the measured background intensities (Figure 11B). Drag lines indicate the interpolated amount of nanogram protein corresponding to the signal intensities of the samples and the amount of protein expressed in nanogram was converted to number of molecules by taking into account the molecular weight of the respective calibrator and the Avogadro constant. Finally the total amount of molecules per cell were determined by taking into account the total amount of protein in the lysate expressed in gram and the number of cells, counted for each condition just before cell lysis (Figure 11A and 11B). The quantitative analysis visualized in Figure 11C, showed that the amount of STAT1 protein per is 900 000 molecules per cell in untreated cells and increased upon treatment with IFNα in a dose-dependent manner, with 1 200 000 molecules per cell, 1 400 000 molecules per cell and 1 900 000 molecules per cell in cells treated with 2.8 pM, 28 pM and 1400 pM IFNα, respectively. In contrast, the amount of STAT2 protein of 55 000 molecules in untreated cells was one order of magnitude lower compared to STAT1 and showed with 57 000 molecules per cell in cells treated with 2.8 pM IFNα, 83 000 molecules per cell on cells treated with 28 pM IFNα, and

185 000 molecules per cell in cells treated with 1400 pM IFNα a higher fold change compared to STAT1 upon treatment with IFNα. Furthermore, consistent with the dose-resolved time course measurements (Figure 10), only a minor increase of STAT2 protein was observed in cells treated with 2.8 pM IFNα. The feedback proteins IRF9 and USP18 were present at very low levels at basal conditions with 15 000 ± 13 000 molecules per cell of IRF9 and 2600 ± 2200 molecules per cell of USP18. Upon treatment with IFNα, IRF9 protein levels increased starting from treatment with 2.8 pM IFNα, while USP18 protein levels showed only a minor increase after treatment with 2.8 pM and 28 pM IFNα, in agreement with the previously observations of the dose-resolved time course measurements (Figure 10). IRF9 protein abundance increased to 43 000 molecules per cell, 46 000 molecules per cell and 80 000 molecules per cell upon treatment with 2.8 pM, 28 pM and 1400 pM IFNα, respectively. While USP18 protein abundance increased to 7 000 molecules per cell, 9 000 molecules per cell and 55 000 molecules per cell upon treatment with 2.8 pM, 28 pM and 1400 pM IFNα, respectively.

Taken together, treatment with different IFNα doses increased the molecules per cell of STAT1, STAT2, IRF9 and USP18 for each target and at each IFNα dose to a different, resulting in different ratios of abundance between STAT1, STAT2 and IRF9 in cells treated with different doses of IFNα. While untreated cells expressed relatively high amounts of STAT1 and relatively low amount of IRF9, cells pretreated with 2.8 pM IFNα expressed comparable amounts of IRF9 and STAT2, but one order of magnitude higher amounts of STAT1. Furthermore, treatment with a higher dose of IFNα increased STAT2 abundance and increased with a smaller fold change STAT1 abundance, resulting a different ratio of between STAT1 and STAT2 abundance compared to untreated cells.

The absolute protein abundances were included in the complete dataset used for model calibration. Model fits in Figure 11C revealed that the model was able to describe the absolute abundance of STAT1, STAT2, IRF9 and USP18 within the error range derived from four biological replicates and the mathematical could capture different IFNα dose sensitivities of STAT1, STAT2, IRF9 and USP18.

In summary, STAT1, STAT2, IRF9 and USP18 were present at different abundance and showed different IFNα dose-dependent inductions as visible in the data and captured by the model.

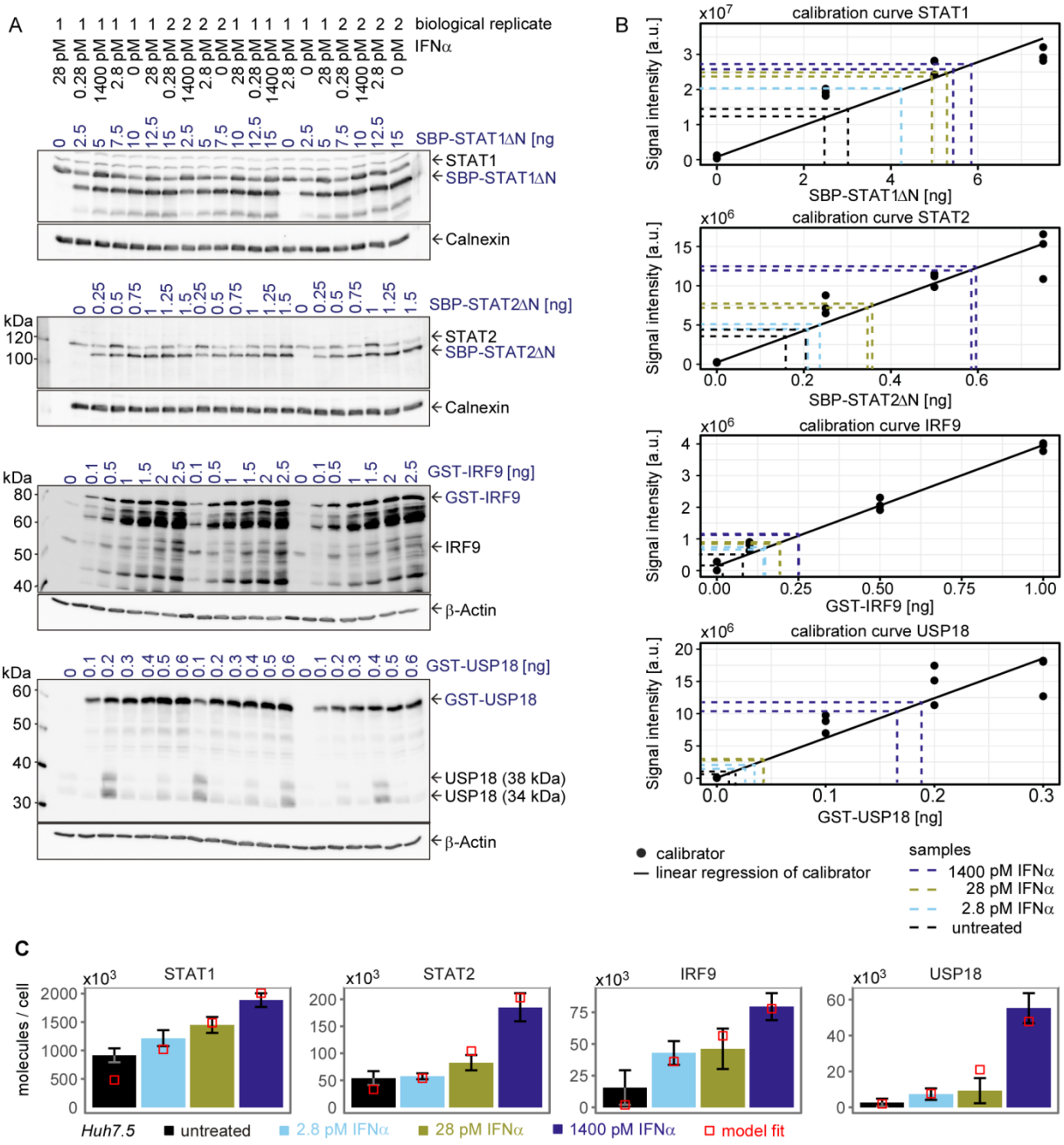

Figure 11. Determination of amount of STAT1, STAT2, IRF9 and USP18 molecules per cell in Huh7.5 after treatment with different doses of IFNα for 24 hours. Calibrator proteins were spiked in 10 µg of total protein lysate and subjected to quantitative immunoblotting. Immunoblot detection was performed by chemiluminescense using a CCD-camera based device. A) representative quantitative immunoblots from one independent experiment, containing two biological replicates N=2. B) representative linear calibration curves with indicated interpolated intensities of samples. Technical replicates were averaged. C) Amount of molecules per cell of STAT1, STAT2, IRF9 and USP18. Average displayed with standard deviation (N=4) and model fit (red squares).

2.2.4 IFNα-dose-dependent memory of IFNα

The signaling components STAT1, STAT2 and IRF9 showed different absolute abundances at basal condition and IFNα treatment induced different fold changes for STAT1, STAT2 and IRF9 for each IFNα dose, resulting in different ratios between the transcription factors STAT1, STAT2 and IRF9 across different doses of IFNα. To examine the impact of different IFNα pre-treatment doses on the dynamics of IFNα-induced signal transduction, Huh7.5 cells were growth-factor-depleted and pre-treated with a variety of doses of IFNα, including 2.8 pM, 28 pM and 1400 pM IFNα, or were left

untreated. After 24 hours the cells were stimulated with 1400 pM IFNα for up to six hours to capture both the rise and the decline in IFNα-induced phosphorylation of STAT1 and STAT2 for model calibration. Cytoplasmic and nuclear lysates were analyzed by quantitative immunoblotting and the data was included in the complete Huh7.5-IFNα dataset used for model calibration. To analysis IFNα-induced phosphorylation, nuclear pSTAT1 and pSTAT2 are displayed, while cytoplasmic IRF9, USP18, STAT1 and STAT2 are displayed to investigate the expression levels of IRF9, USP18, STAT1 and STAT2. Remaining targets are displayed in Appendix section 5.2.3.

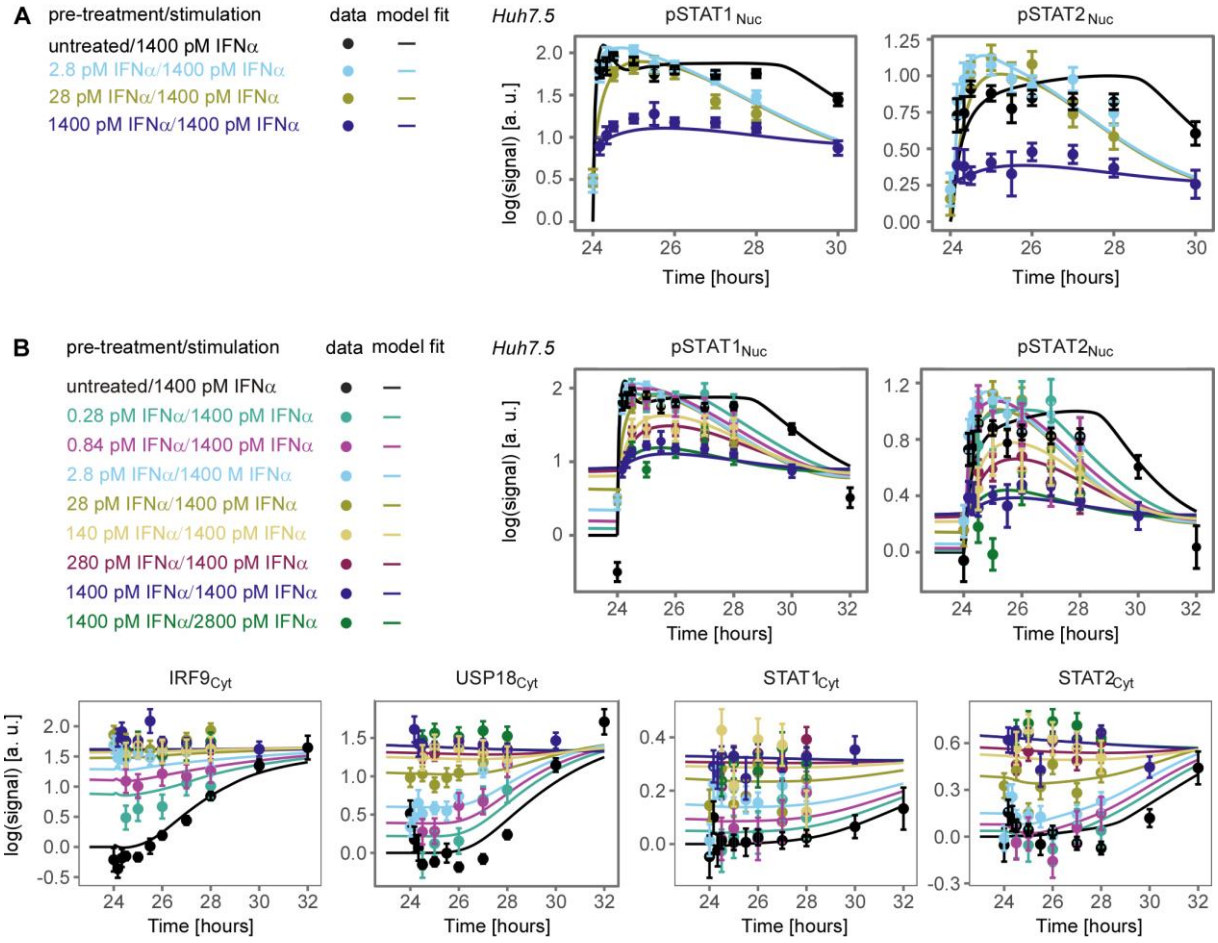

Figure 12. Effect of pre-treatment with a wide range of IFNα doses on the dynamic behaviour of IFNα-induced signal transduction. Growth-factor-depleted Huh7.5 were pre-treated with a range of 0.28 pM to 1400 pM IFNα for 24 hours and stimulated with 1400 or 2800 pM IFNα. IFNα-induced phosphorylation of nuclear STAT1 and STAT2 and expression of feedback proteins were analyzed by quantitative immunoblotting. Data was normalized to reference proteins Calnexin or HDAC1 and represented by filled circles with errors representing 1σ confidence-interval estimated from biological replicates A) (N=4 to N=19) and B) (N=1 to N=19) using an error model. Model trajectories are represented by the line.

In cells without pre-treatment stimulation with 1400 pM IFNα showed maximal levels of nuclear pSTAT1 and pSTAT2 starting from the first time point of 0.5 hour after stimulation (displayed as 24.5 hours) and nuclear pSTAT1 and pSTAT2 levels stayed high until six hours after stimulation (displayed as 30 hours) (Figure 12A and 12B). Interestingly, stimulation with 1400 pM IFNα of cells pre-treated with 2.8 or 28 pM IFNα resulted in a sharper and higher peak of maximal nuclear pSTAT1 and pSTAT2 levels visible at one hour (displayed as 25 hours) after stimulation. IFNα nuclear pSTAT1 displayed a maximal amplitude of 80-fold, 100-fold and 70-fold in cells pre-treated with 0 pM, 2.8 pM and 28 pM

IFNα, respectively. While nuclear pSTAT2 displayed maximal amplitudes of 7.5-fold, 11.5-fold and 13-fold in cells pre-treated with 0 pM, 2.8 pM and 28 pM IFNα, respectively, which is in agreement with previous findings showing lower fold increases of pSTAT2 than of pSTAT1 (Figure 5, and Figure 10). Interestingly, pre-treatment with 28 pM IFNα resulted in higher IFNα-induced pSTAT2 signals at one hour after stimulation compared to cells without pre-treatment, whereas pre-treatment with 28 pM IFNα resulted in lower IFNα-induced pSTAT1 signals at one hour after stimulation compared to cells without pre-treatment. Furthermore, nuclear pSTAT1 and pSTAT2 levels displayed more transient behaviour illustrated by reduced pSTAT1 and pSTAT2 levels starting from three hours after stimulation (displayed as 27 hours). Pre-treatment with 1400 pM IFNα resulted in much reduced IFNα-induced phosphorylation, as illustrated by a fold change of 16-fold for pSTAT1 and of 2.5-fold for pSTAT2 compared to cells that never received IFNα, and a 1.8 fold-change for pSTAT1 and 1.4-fold change for pSTAT2 relative to cells pre-treated with 1400 pM IFNα for 24 hours that did not receive stimulation, suggesting a negative memory of IFNα-induced signal transduction.

To gain more insights in dose-dependent effects established by IFNα pre-treatment, Huh7.5 cells were pre-treated with doses ranging from 0.28 pM to 1400 pM IFNα and stimulated with 1400 pM IFNα 24 hours later. Quantitative analysis showed (Figure 12B) that pre-treatment with increasing IFNα doses up to 28 pM IFNα generated elevated nuclear pSTAT1 and pSTAT2 at one hour of stimulation compared to cells without pre-treatment, indicating a positive memory, while pre-treatment with increasing IFNα doses higher than 28 pM IFNα generated gradual lower levels of nuclear pSTAT1 and pSTAT2, indicating a gradual negative memory. Furthermore, stimulation with 2800 pM IFNα of cells pre-treated with 1400 pM IFNα showed much reduced nuclear pSTAT1 and pSTAT2 levels, indicating that stimulation with the higher dose could not overcome the established negative memory.

In agreement with the observations from the analysis of the number of molecules per cell, different IFNα dose-sensitivities were observed for STAT1, STAT2, IRF9 and USP18 in cells pre-treated with different doses of IFNα. IFNα-stimulation further enhanced expression of IRF9 in cells pre-treated with doses up to 0.84 pM IFNα, while higher doses did not further induce IRF9 expression, indicating that saturation of IRF9 was reached. In contrast, IFNα-stimulation further enhanced expression of USP18 in cells pre-treated with doses up to 28 pM IFNα, indicating once more that USP18 expression saturated at higher doses of IFNα compared to IRF9. No increase in STAT1 or STAT2 protein levels was observed in the investigated time frame of up to six hours after stimulation.

The dynamic behavior of pSTAT1 and pSTAT2, and IRF9, USP18, STAT1 and STAT2 was used for model calibration as part of the complete dataset. The model trajectories could describe the earlier and more transient dynamics of pSTAT1 and pSTAT2 observed in IFNα pre-treated cells, together with the elevated expression of IRF9, USP18, STAT1, STAT2 established by pre-treatment with different doses of IFNα. Furthermore, the model was able to describe the different IFNα-induced dynamic behaviors of nuclear pSTAT1 and pSTAT2 in cells pre-treated with 28 pM IFNα.

In conclusion, pre-treatment with doses below 28 pM IFNα established a positive memory, characterized by faster IFNα-induced phosphorylation of pSTAT1 and pSTAT2, resulting in an earlier time to peak with a higher amplitude and faster signal termination compared to cells without pre-treatment. IFNα doses above 28 pM IFNα established a gradual negative memory of IFNα-induced signaling transduction, characterized by much reduced IFNα-induced phosphorylation of STAT1 and STAT2. Interestingly, pSTAT1 and pSTAT2 displayed different dynamic behavior in cells pre-treated with 28 pM IFNα. All three observed effects could be described by the calibrated mathematical model.

2.2.5 Pre-treatment with IFNα results in changes in complex formation

Pre-treatment with 28 pM IFNα resulted in enhanced IFNα-induced phosphorylation of pSTAT2, but not of STAT1. The mathematical model of IFNα-signaling was employed to unravel mechanisms explaining the discrepancy in the dynamic behavior of nuclear pSTAT1 and pSTAT2 in cells pre-treated with 28 pM IFNα. Model simulations performed by Marcus Rosenblatt (University of Freiburg) revealed different dynamical behavior of nuclear pSTAT1 homodimers, pSTAT1pSTAT2 heterodimers and ISGF3 contributing to the experimentally observed pSTAT1 signal (Figure 13A). Stimulation with 1400 pM IFNα in cells without pre-treatment first showed a sharp increase of pSTAT1 homodimers with a peak at 7000 arbitrary units within the first 30 minutes after stimulation, after which the signal steeply declined with a residual plateau returning to basal level four hours after IFNα stimulation (displayed as 28 hours). pSTAT1pSTAT2 heterodimer gradually increased with a maximal amplitude of 4000 arbitrary units at the broad peak between one and three hours after IFNα stimulation (displayed as 25 and 27 hours). ISGF3 levels gradually increased after two hours of IFNα stimulation and peaked five hours after stimulation (displayed as 29 hours) with a peak height of 3500 arbitrary units. IFNα stimulation of cells pre-treated with 2.8 pM IFNα resulted in lower amounts of pSTAT1 homodimer, with a peak height of 3000 arbitrary units, much reduced pSTAT1pSTAT2 heterodimer amounts, but high amounts of ISGF3. ISGF3 showed a steep increase, with peak height of 7500 at one hour after stimulation (displayed as 25 hours) followed by a slow decline over six hours. Interestingly, IFNα stimulation of cells pre-treated with 28 pM IFNα resulted in much reduced amounts of pSTAT1 homodimer, no pSTAT1pSTAT2 heterodimers, but high amounts of ISGF3. Comparable to cells pre-treated with 2.8 pM IFNα, ISGF3 showed a steep increase followed by a slow decline over six hours; however the peak height at one hour after stimulation (displayed as 25 hours) was with 5500 lower. Lastly, IFNα stimulation of cells pre-treated with 1400 pM IFNα resulted in much reduced amounts of ISGF3 and no pSTAT1 homodimer and no pSTAT1pSTAT2 heterodimers, indicating the negative memory.

In summary, the model predicted that pre-treatment with increasing doses resulted in decreased levels of IFNα-induced pSTAT1 homodimer formation. To test this model-derived hypothesis, the expression of a target gene of pSTAT1 homodimers was investigated. pSTAT1 homodimers bind to Gamma-activated-sequences (GAS) to induce target gene expression, while ISGF3 bind to interferon-stimulated-response-elements (ISREs). To investigate whether SOCS3 is a target of pSTAT1 homodimers, but not of ISGF3, a transcription factor binding site analysis was performed. The obtained results revealed GAS binding sites upstream and at the beginning of the SOCS3 gene, whereas no ISRE binding sites were found identifying SOCS3 as a unique target of pSTAT1 homodimers, but not of ISGF3 (Figure 13B).

The model predicted that lower pSTAT1 homodimers would result in lower SOCS3 expression. To test this model-derived hypothesis, Huh7.5 cells were pre-treated with 0 pM, 2.8 pM or 28 pM IFNα and 24 hours later stimulated with 1400 pM IFNα. Cytoplasmic lysates were subjected to immunoprecipitation and SOCS3 protein was investigated by quantitative immunoblotting. IFNα-induced SOCS3 protein expression increased after 30 minutes and showed with 12.5 fold increase a maximal induction at 1.5 hours after IFNα stimulation in cells without pre-treatment (displayed as 25.5 hours) after which levels slowly declined. IFNα-induced expression of SOCS3 in cells pre-treated with 2.8 pM IFNα showed comparable dynamic behavior with a lower amplitude of 9 fold, in contrast IFNα-induced expression of SOCS3 in cells pre-treated with 28 pM IFNα showed a much reduced expression of SOCS3 protein with an amplitude of 3.5 fold relative to untreated. The model

trajectories displayed with 66% confidence intervals, derived independent from the data, revealed the same trend as the data.

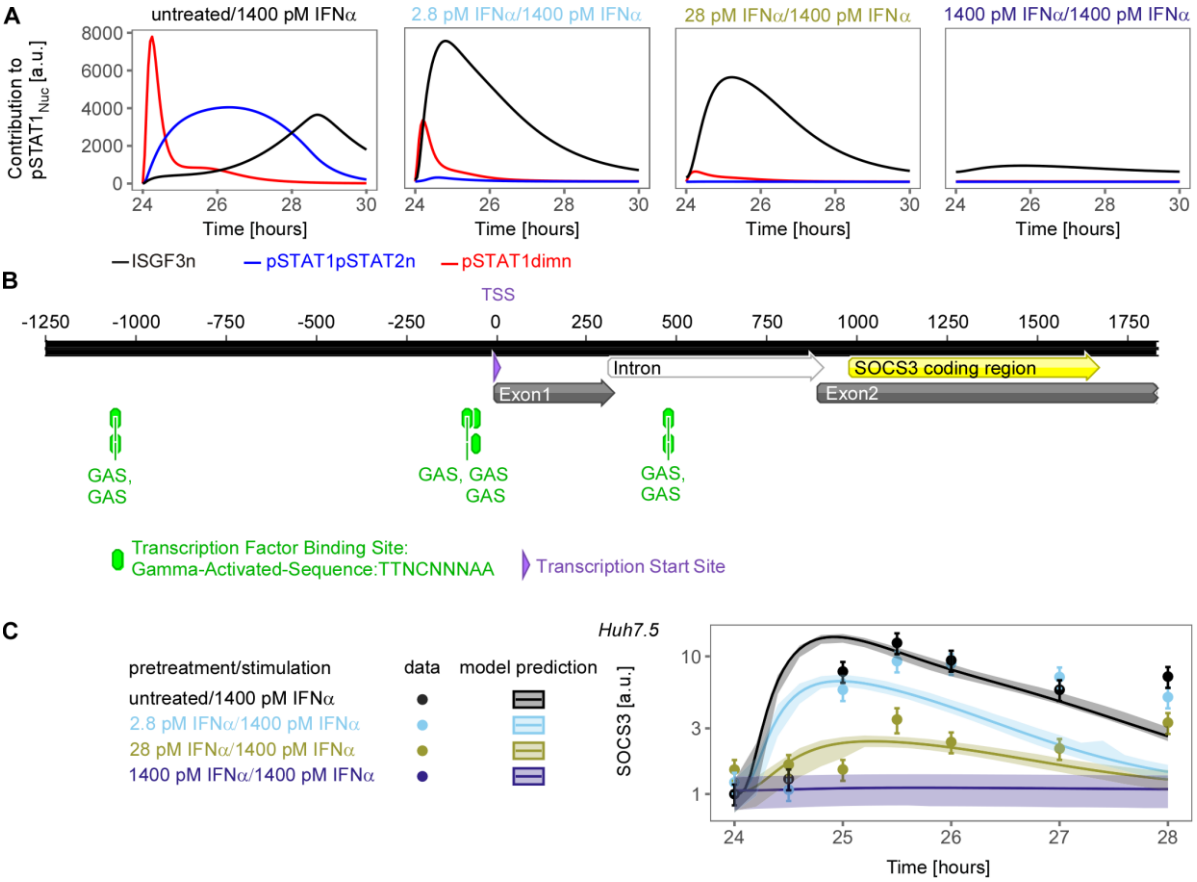

Figure 13. Model prediction and experimental validation of IFNα-induced signalling in memory conditions. A) Model simulations of nuclear ISGF3 (ISGF3n), nuclear pSTAT1pSTAT2 heterodimer (pSTAT1pSTAT2n) and nuclear pSTAT1 homodimer (pSTAT1dimn) contributing to the observable nuclear pSTAT1 signal of cells stimulated with 1400 pM IFNα after 24 hours pre-treatment with 0, 2.8 pM, 28 pM or 1400 pM IFNα. B) Promoter analysis of the human SOCS3 gene. C) Model prediction overlaid with experimental validation of IFNα-induced protein expression of SOCS3 in Huh7.5 pre-treated with 0, 2.8 pM, 28 pM or 1400 pM IFNα. Line with shadow represents model prediction with 66% confidence interval calculated utilizing prediction profile likelihood method. Experimental data is represented by filled circles with errors representing 1σ confidence-interval estimated from biological replicates (N=3) using an error model.

To conclude, model simulations revealed that IFNα pre-treatment resulted in different dynamical behavior of pSTAT1 homodimers, pSTAT1pSTAT2 heterodimer and ISGF3. Pre-treatment with an increasing IFNα doses correlated with decreasing amounts of pSTAT1 homodimers. SOCS3 was identified as unique target of pSTAT1 homodimers and used for experimental validation of the model predictions. Thereby validating the predictive power of the mathematical model.

2.2.6 Model extension to the therapeutic interferon and HepG2-hNTCP cell line

Roferon is a recombinant human IFNα-2a used for treatment of various cancer and viral diseases. To study the dynamics of IFNα-induced phosphorylation of STAT1 and STAT2 in Huh7.5 and HepG2-hNTCP cells pre-treated with different doses of Roferon, equipotent doses of Roferon and IFNα utilized in this study were determined by a viral titration assay performed by Christopher Dächert (Figure 14). In brief, the activity of Roferon (Roche) and IFNα-2a (PBL) were titrated to the interferon standard from The National Institute for Biological Standards and Control (NIBSC) using the Huh7-

Lunet: a cell line carrying a stable replicating subgenomic HCV replicon with a firefly luciferase reporter. Cells were treated with two-fold serial dilutions of the interferons for 48 hours and the amount of viral replication was determined by luciferase activity (Figure 14A). Four-parameter Hill kinetics were fitted to the data to determine the concentration where 50% of viral replication is inhibited (IC_{50}). As shown in Figure 14B, IC_{50} values of Roferon were comparable to the NIBSC standard, in contrast IC_{50} values of the IFNα used in this study were two- to four-fold higher, indicating a lower activity of IFNα compared to the NIBSC standard or to Roferon. 1 unit of IFNα of the NIBSC standard corresponded to a range of 0.33 and 1 pM of IFNα used in this study (Figure 14C) and equipotent doses of the low and high dose of 2.8 pM and 1400 pM IFNα used in this study corresponded to 6.3 U/ml and 3150 U/ml Roferon, respectively (Figure 14D).

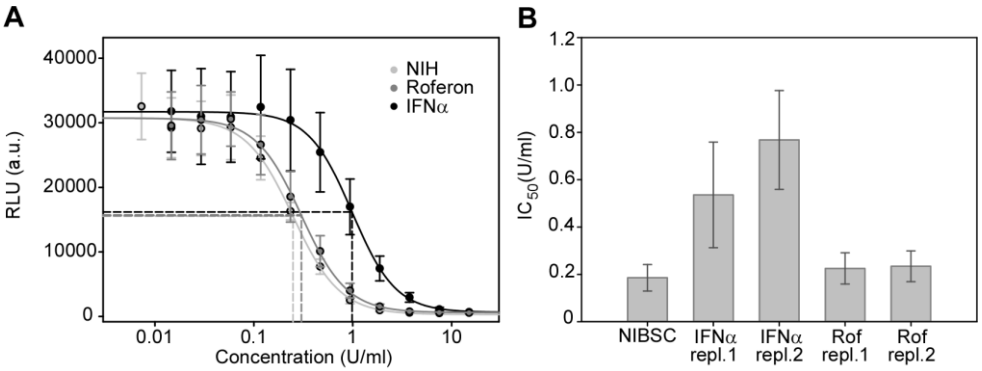

C

Calibration to NIBSC standard
1 U IFNα NIBSC
3.6 U ± 1.8 U IFNα
0.67 pM ± 0.34 pM IFNα
1.3 U ± 0.55 U Roferon

D

Equipotent doses
low dose
15 U/ml IFNα (=2.8 pM)
6.3 U/ml Roferon
high dose
7500 U/ml IFNα (=1400 pM)
3150 U/ml Roferon

Figure 14, Determination of equipotent doses of IFNα (PBL) and Roferon (Roche). Huh7 LucUbiNeo cells harboring HCV replicon were treated with serial dilution of IFNα (PBL), Roferon or NIBSC standard and luciferase units were determined. A) Luciferase intensities of one representative experiment RLU: relative luciferase units. droplines indicate IC50 values eight biological replicates of one independent experiment B) IC50 values for NIBSC standard, IFNα and Roferon displayed as average with standard deviation of n=24 from three independent experiments. repl indicates replicates of three independent experiments. C) IC50 values from replicates 1 were used to determine equipotent doses of IFNα and Roferon employed for the memory experiments. D) calibration of IFNα and Roferon to NIBSC standard. All replicates were used incorporated and errors are derived from Gaussian error propagation. Data generated by Christopher Dächert (DKFZ).

To examine the impact of Roferon pre-treatment on the dynamics of Roferon-induced signal transduction, Huh7.5 cells were pre-treated with 6.3 U/ml or 3150 U/ml Roferon corresponding to the low and high doses of IFNα respectively, or were left untreated. After 24 hours the cells were stimulated with 3150 U/ml Roferon and IFNα-induced phosphorylation of nuclear STAT1 and STAT2 was investigated over time by quantitative immunoblotting. Data was generated by Tamar Nizharadze (DFKZ). The quantitative analysis displayed in Figure 14A, revealed that Huh7.5 cells without pre-treatment displayed maximal levels of Roferon-induced phosphorylation of STAT1 and STAT2 starting from 30 minutes after stimulation (displayed as 24.5 hours) that sustained at high levels in the observed time frame of four hours after stimulation. Interestingly, Roferon-induced phosphorylation in cells pre-treated with a low dose of Roferon, showed elevated pSTAT2 levels in the nucleus characterized by higher amplitude and faster signal termination relative to Roferon-

induced pSTAT2 levels in cells without pre-treatment, suggesting a positive memory. In contrast to pSTAT2, nuclear pSTAT1 only showed minor elevated levels upon stimulation with Roferon of cells pre-treated with a low dose of Roferon relative to Roferon-induced pSTAT1 levels in cells without pre-treatment, as visible in the data. In contrast, Roferon-induced phosphorylation of STAT1 and STAT2 was much reduced in cells pre-treated with a high dose of Roferon relative to Roferon-induced phosphorylation of STAT1 and STAT2 in cells without pre-treatment, suggesting a negative memory.

To examine whether the effect of Roferon pre-treatments on Roferon-induced signaling dynamics is cell-context specific or a more general property of the IFNα signal transduction pathway, HepG2-hNTCP cells were left untreated or were pre-treated for 24 hours with the equipotent amounts of Roferon corresponding to a 9.3 U/ml and 4600 U/ml Roferon, due to technical reasons. Cells were subsequently stimulated with 4600 U/ml Roferon. Data was generated by Melissa Teusel (DKFZ). The results (Figure 15B) revealed that pre-treatment with a high Roferon dose strongly decreased the Roferon induced presence of pSTAT1 and pSTAT2 in the nucleus of HepG2-hNTCP cells confirming a negative memory effect. Furthermore, pre-treatment with a low dose resulted in elevated levels of pSTAT1 and pSTAT2 in response to Roferon stimulation suggesting a positive memory.

The mathematical model was extended by Marcus Rosenblatt (University of Freiburg) with incorporation of cell line-specific protein synthesis rates of STAT1, STAT2, IRF9 and USP18, and cell line-specific receptor abundance. Parameter estimation of these additional parameters was performed based on 626 data points belonging to 35 conditions generated by Tamar Nizharadze (DKFZ) and Melissa Teusel (DKFZ) constituting dose- and time-resolved quantitative data of Roferon-induced signalling in Huh7.5 and HepG2-hNTCP and numbers of molecule per cell of STAT1, STAT2, IRF9 and USP18 in HepG2-hNTCP (see Appendix section 5.3). Dose- and –time-resolved measurements revealed that Roferon and IFNα-induced signalling showed comparable dynamical behaviour, while analysis of HepG2-hNTCP revealed higher abundance of USP18 protein compared to Huh7.5.

The model trajectories are able to capture the dynamics of Roferon-induced signalling in cells pre-treated with a low or a high dose both in Huh7.5 and HepG2-hNTCP, confirming that incorporation of cell line specific protein synthesis rates of STAT1, STAT2, IRF9 and USP18, and cell-line specific receptor abundance is sufficient to capture the positive and negative memory of Roferon-induced IFNα signal transduction.

In conclusion, pre-treatment with a low dose of Roferon established a positive memory of Roferon-induced signal transduction both in Huh7.5 and in HepG2-hNTCP cells, while both cell lines established a negative memory of Roferon-induced signal transduction when pre-treated with a high dose of Roferon . By incorporating STAT1, STAT2, IRF9 and USP18 cell line specific synthesis rates together with cell line specific receptor abundances, the mathematical model is able to describe Roferon-induced signal transduction in different cell lines.

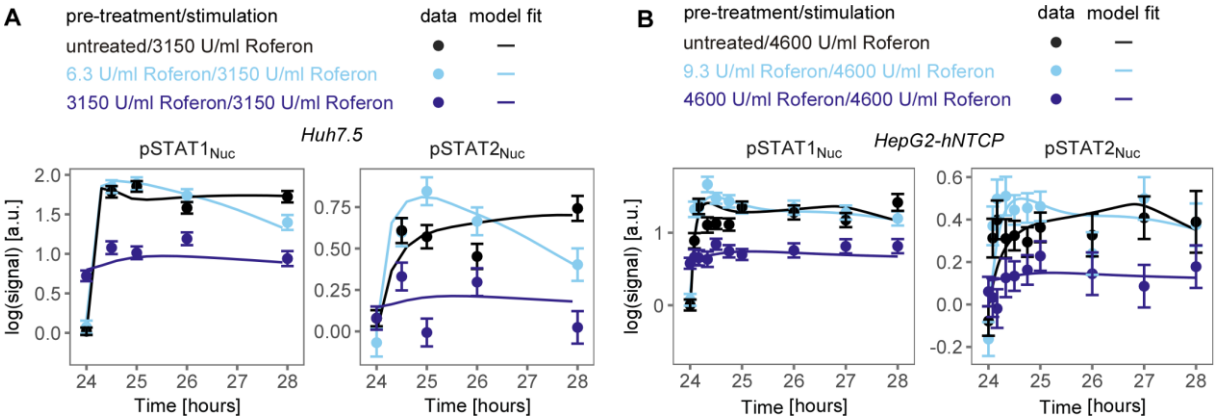

Figure 15. Effect of pre-treatment with Roferon on the dynamic behaviour of Roferon-induced signalling in Huh7.5 and HepG2-hNTCP. A) Dose-dependent memory of the therapeutic interferon Roferon. Growth-factor-depleted Huh7.5 were pre-treated with 0, 6.3 or 3150 U/ml Roferon and stimulated with 3150 U/ml Roferon 24 hours later. Nuclear lysates were subjected to quantitative immunoblotting and Roferon-induced phosphorylation of STAT1 and STAT2 was detected by chemoluminescence utilizing a CCD-based camera device (Imagequant). Dots represent scaled data with errors representing 1σ confidence-interval estimated from biological replicates (N=3 to N=5) using an error model. Model trajectories are represented by the line. B) Dose-dependent memory of the therapeutic interferon Roferon in HepG2-hNTCP. Growth-factor-depleted HepG2-hNTCP were pre-treated with 0, 9.3 or 4600 U/ml Roferon and stimulated with 4600 U/ml Roferon 24 hours later. Nuclear lysates were subjected to quantitative immunoblotting and Roferon-induced phosphorylation of STAT1 and STAT2 was detected by chemoluminescence utilizing a CCD-based camera device (Imagequant). Dots represent scaled data with errors representing 1σ confidence-interval estimated from biological replicates (N=3) using an error model. Model trajectories are represented by the line. Data generated by Tamar Nizharadze (DKFZ) and Melissa Teusel (DKFZ).

2.2.7 Mechanism of IFNα-induced negative memory

To investigate if USP18 abundance is sufficient to cause negative memory of IFNα-induced signal transduction, knockdown and overexpression studies of USP18 were performed in Huh7.5 cells and the data incorporated for model calibration as part of the complete Huh7.5-IFNα dataset, additional targets measured at the condition USP18 siRNA transfection are displayed in the Appendix section 5.2.4.

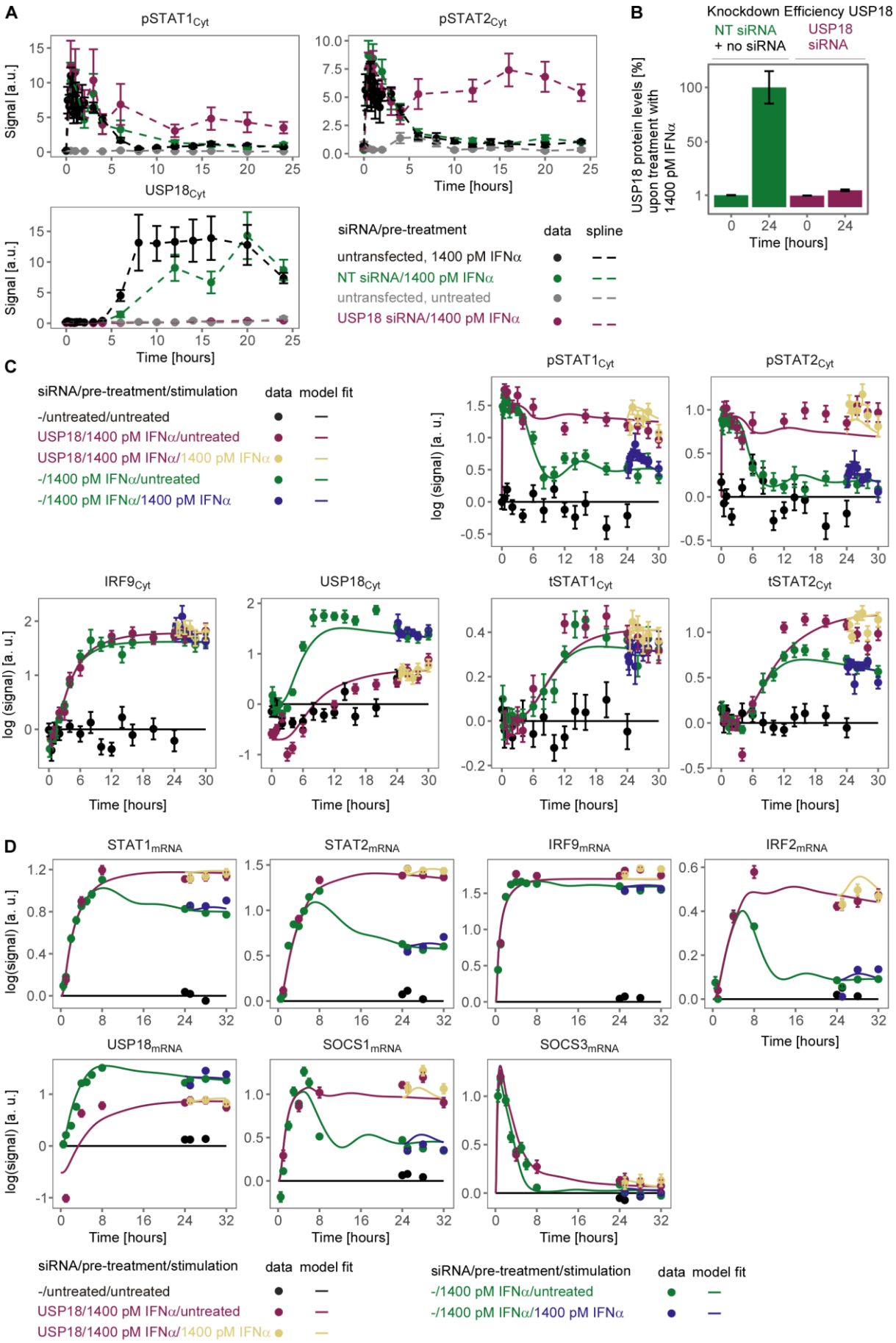
A
pSTAT1Cyt
pSTAT2Cyt
USP18Cyt
Signal [a.u.]
Time [hours]
siRNA/pre-treatment
data
spline
untransfected, 1400 pM IFNα
NT siRNA/1400 pM IFNα
untransfected, untreated
USP18 siRNA/1400 pM IFNα
B
Knockdown Efficiency USP18
NT siRNA + no siRNA
USP18 siRNA
USP18 protein levels [%] upon treatment with 1400 pM IFNα
Time [hours]
C
siRNA/pre-treatment/stimulation
data
model fit
-/untreated/untreated
USP18/1400 pM IFNα/untreated
USP18/1400 pM IFNα/1400 pM IFNα
-/1400 pM IFNα/untreated
-/1400 pM IFNα/1400 pM IFNα
pSTAT1Cyt
pSTAT2Cyt
IRF9Cyt
USP18Cyt
tSTAT1Cyt
tSTAT2Cyt
log (signal) [a. u.]
Time [hours]
D
STAT1mRNA
STAT2mRNA
IRF9mRNA
IRF2mRNA
USP18mRNA
SOCS1mRNA
SOCS3mRNA
log(signal) [a. u.]
Time [hours]
siRNA/pre-treatment/stimulation
data
model fit
-/untreated/untreated
USP18/1400 pM IFNα/untreated
USP18/1400 pM IFNα/1400 pM IFNα
siRNA/pre-treatment/stimulation
data
model fit
-/1400 pM IFNα/untreated
-/1400 pM IFNα/1400 pM IFNα

Figure 16, IFNα-induced signaling in USP18 siRNA transfected Huh7.5 cells. A) Huh7.5 transfected with non-targeting (NT) control siRNA triggers IFNα-induced phosphorylation comparable to Huh7.5 wild type cells. Huh7.5 were incubated with non-targeting siRNA or USP18 siRNA for 20 hours, growth-factor-depleted and stimulated with 1400 pM IFNα. IFNα-induced phosphorylation of cytoplasmic STAT1 and STAT2, and USP18 expression was analyzed by quantitative immunoblotting utilizing chemoluminescence detected by a CCD-based camera device (Imagequant). Dashed line indicates spline. B) USP18 knockdown efficiency determined by quantitative immunoblotting of cytoplasmic lysates of Huh7.5 transfected with USP18 siRNA relative to Huh7.5 wildtype and Huh7.5 transfected with non-targeting siRNA. Cells were stimulated with 1400 pM IFNα for 24 hours. C) Knockdown of USP18 results in sustained signaling. Model fit and experimental data of Huh7.5 cells transfected with control or USP18 siRNA, growth-factor-depleted and pre-treated with 1400 pM IFNα, stimulated with 1400 PM IFNα or unstimulated. Experimental data of IFNα-induced phosphorylation of STAT1 and STAT2 and expression of STAT1, STAT2, IRF9 and USP18 were analyzed by quantitative immunoblotting using chemoluminescence and a CCD camera device (Imagequant). For model purposes data in control siRNA and untransfected Huh7.5 are combined to one condition. Data from multiple partially overlapping time courses scaled together is displayed as filled circles with errors representing 1σ confidence-interval estimated from biological replicates (N=3) using an error model. Line represents model trajectory.
D) Analysis of expression of IFNα-feedback genes in Huh7.5 transfected with USP18 siRNA, control siRNA or untransfected. Cells were pre-treated with 1400 pM IFNα and 24 hours later stimulated with 1400 pM IFNα and gene expression was analyzed by quantitative RT-PCR. Data from untransfected Huh7.5 was merged with Huh7.5 transfected with control siRNA. Filled circles represent scaled data with errors representing 1σ confidence-interval estimated from biological replicates (N=2 to N= 16) and model trajectories represented by lines.

To investigate the impact of knockdown of USP18 on the effect of pre-treatment with IFNα and the establishment of a negative memory of IFNα signal transduction, Huh7.5 cells were transfected with siRNAs targeting USP18 one day prior to pre-treatment with a high dose of 1400 pM IFNα for 24 hours. Pre-treated cells were stimulated with 1400 pM IFNα or were left untreated, and IFNα-induced phosphorylation of STAT1 and STAT2 and expression of feedback proteins was investigated by quantitative immunoblotting and quantitative RT-PCR (Figure 16). Huh7.5 cells transfected with the non-targeting control siRNA showed comparable dynamics of IFNα-induced phosphorylation of STAT1 and STAT2 relative to IFNα-induced phosphorylation of STAT1 and STAT2 observed in untransfected Huh7.5 cells, as characterized for pSTAT1 and pSTAT2 with a peak time within the first hour of treatment combined with transient expression with levels close to basal levels 8 hours after stimulation with IFNα (Figure 16A), indicating that the method did not interfere with activation of the signalling pathway. Therefore, the data obtained in cells transfected with control siRNA was scaled together with data obtained in untransfected Huh7.5 cells. The quantitative analysis shown in Figure 16B identified an average knockdown efficiency of 94.5% ±2% on USP18 protein level at 24 hours after pre-treatment with 1400 pM IFNα. Time-resolved experiments revealed that IFNα pre-treatment of cells transfected with USP18 siRNA resulted in sustained levels of cytoplasmic pSTAT1 and pSTAT2 in the investigated time frame of 30 hours, confirming the role of USP18 as negative regulator. Stimulation of cells transfected with USP18 siRNA showed the same peak time in the first hour of treatment and peak height. Additional IFNα stimulation at 24 hours did not trigger a further increase in pSTAT1 and pSTAT2 detectable above the biological and technical noise of the data.
In both IFNα pre-treated USP18 siRNA transfected and IFNα pre-treated control cells IRF9 was maximally induced after 6 hours of treatment, with a 68-fold increase in USP18 siRNA transfected cells and 65-fold increase in control cells, showing comparable dynamic behavior of IRF9. Interestingly, STAT1 and STAT2 protein showed similar kinetic profiles upon IFNα stimulation of USP18 siRNA transfected cells and control cells, however STAT2 expression levels reached a higher plateau in USP18 siRNA transfected cells, with a 10-fold increase after 24 hours of IFNα stimulation, compared to 4.5 fold increase after 24 hours of IFNα pre-treatment in control cells. While STAT1 displayed comparable increased expression after 24 hours of IFNα pre-treatment, with 2.3 fold and 2.5 fold elevated in control and USP18 siRNA transfected cells ,respectively. IFNα-induced expression

of STAT1 mRNA, STAT2 mRNA, IRF2 mRNA and SOCS1 mRNA showed sustained expression in USP18 siRNA transfected cells (Figure 16D). While SOCS1 mRNA reached the same level of maximal expression, STAT1 mRNA, STAT2 mRNA and IRF2 mRNA showed higher levels of maximal expression.
Interestingly, SOCS3 mRNA expression still showed transient dynamics upon IFNα treatment with slower signal termination in USP18 siRNA transfected cells compared to control cells. suggesting transient dynamics of pSTAT1 homodimers (Figure 13B). Furthermore, stimulation with 1400 pM IFNα at 24 hours did not increase the expression of any of the investigated genes.
The data was incorporated in the complete Huh7.5-IFNα dataset used for model calibration and the model was able to capture the changed dynamic behaviour of all investigated targets in IFNα-treated cells transfected with USP18 siRNA. Interestingly, IFNα stimulation at 24 hours of USP18 siRNA transfected cells that were pre-treated with IFNα, did not trigger a further increase in pSTAT1 and pSTAT2 detectable above the biological and technical noise of the data, while the model estimated a minor increase of pSTAT1 and pSTAT2 after stimulation with IFNα at 24 hours.
In summary, USP18 siRNA transfection resulted in sustained IFNα-induced phosphorylation of STAT1 and STAT2 and sustained IFNα induced expression of STAT1 mRNA, STAT2 mRNA, IRF2 mRNA and SOCS1 mRNA. Stimulation with IFNα in USP18 siRNA transfected cells pre-treated with IFNα did not show a further increase in pSTAT1 or pSTAT2 or an increase in the expression of target genes, suggesting saturation of the pathway, combined with an inability to respond further.
To analyse if the elevated abundance of USP18 protein alone is sufficient to establish the negative memory of the IFNα signaling pathway, a stable cell line with inducible USP18 under the control of the TetON promoter was established by retroviral transduction (Huh7.5-TetON-USP18). To induce USP18 expression cells were pre-treated with doxycyclin for 24 hours. Quantitative immunoblotting of Huh7.5-TetON-USP18 cells and Huh7.5-TetON control pre-treated with doxycycline for 24 hours showed dynamics of pSTAT1 and pSTAT2 comparable to Huh7.5 wild type cells (Figure 17A). Furthermore also the expression levels of USP18 was comparable between both cell lines and therefore the data obtained in both cell lines was scaled together. In the Huh7.5-TetON-USP18 cell line, USP18 protein was induced to similar expression levels as observed in Huh7.5 wild type cells pre-treated with 1400 pM IFNα for 24 hours (Figure 17B). Interestingly, stimulation of the USP18 overexpressing cell line with IFNα resulted in slightly lower activation of pSTAT1 and pSTAT2 relative to cells that had not been pre-treated with IFNα (Figure 17C, Appendix 5.2.5). However, compared to cells pre-treated with 1400 pM IFNα, the USP18 overexpressing cell line showed a significantly higher response, suggesting that USP18 alone is not sufficient to cause the negative memory.
The calibrated mathematical model was able to describe the data and was employed to test different model structures based on hypotheses of mechanisms explaining the negative memory.

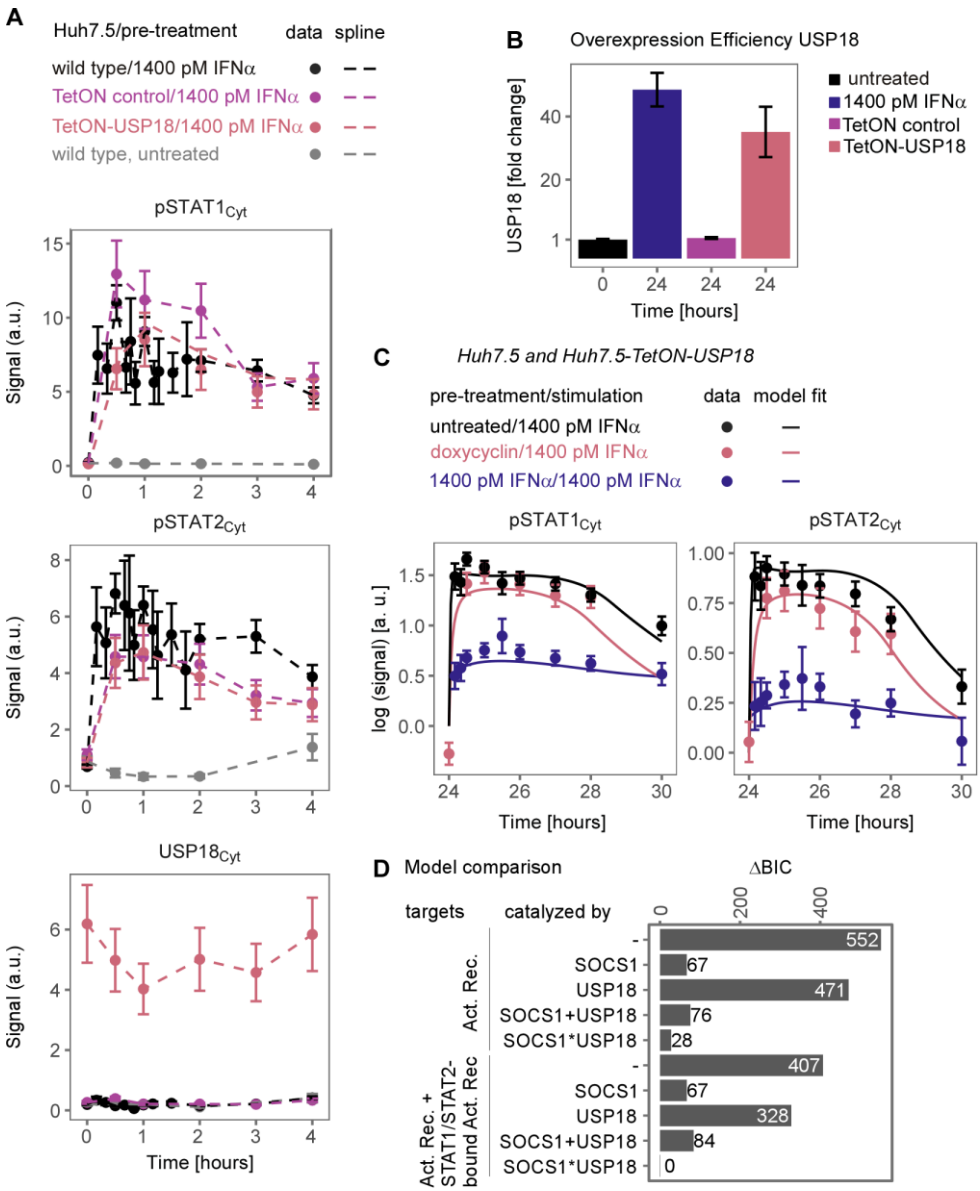

Figure 17. USP18 protein abundance alone is not sufficient to cause negative memory. A) Huh7.5 wild type, or Huh7.5 stable cell lines transduced with the TetON inducible system of either TetON empty vector control or TetON-USP18 were stimulated with 1400 pM IFNα and cytoplasmic lysates were analysed for pSTAT1, pSTAT2 and USP18 by quantitative immunoblotting. Filled circles indicate experimental data with errors representing 1σ confidence-interval estimated from biological replicates (N=3) using an error model. Dashed lines indicates splines. B) Induced expression of USP18 after treatment for doxycycline for 24 hours of Huh7.5-TetONUSP18 and Huh7.5-TetON control in comparison with Huh7.5 wild type cells treated with 1400 pM IFNα for 24 hours. Analysis by quantitative immunoblotting. C) Model fit and experimental data of IFNα-induced phosphorylation in Huh7.5-TetON-USP18 treated with doxycyclin for 24 hours and stimulated with 1400 pM IFNα or Huh7.5 wildtype cells pre-treated with 0 or 1400 pM IFNα and stimulated with 1400 pM IFNα after 24 hours. Experimental data was obtained by quantitative immunoblotting using chemoluminescence and CCD camera device (Imagequant). For model purposes data Huh7.5-TetON empty vector control and untransduced Huh7.5 are combined to one condition. Data is displayed as filled circles with errors representing 1σ confidence-interval estimated from biological replicates (N=3) using an error model. Line represent model trajectory. D) Model-driven hypothesis testing revealed synergy of SOCS1 and USP18 on reducing active receptor complexes. Different model structures concerning SOCS1 and USP18 catalyzed degradation of the active receptor complexes were tested by Bayesian Information Criterion (BIC). Degradation rates of either the active receptor (Act. Rec) alone or combined with degradation rates of STAT1- or STAT2-bound active receptor complexes (Act. Rec + STAT1/STAT2-bound Act. Rec). The same kinetic rates for active receptor and STAT1-bound active receptor were estimated, while different kinetic rates were estimated for STAT2-bound active receptor.

To identify possible mechanisms that could explain the negative memory as well as the USP18 overexpression data, ten different model structures were tested by Marcus Rosenblatt (University of Freiburg) (Figure 17D). The model structures contained different mechanisms for degradation of the activate receptor in complex with IFNα (the active receptor complex: Act. Rec.). Degradation of the active receptor complex included either only basal degradation rates or additional degradation rates catalyzed by SOCS1 alone, USP18 alone, or SOCS1 and USP18 together. SOCS1 and USP18 contributions could be additive (SOCS1+USP18) with a rate for SOCS1-catalyzed degradation and a rate for USP18 catalyzed degradation, or a SOCS1 and USP18 contributions could be synergistic (SOCS1*USP18) implemented by one rate that depends on the concentration of both USP18 and SOCS1. These five modes of degradation could either act on just the active receptor complex (Act. Rec) or in addition on the active receptor in complex with STAT1 or STAT2 (STAT1/STAT2-bound Act. Rec). Based on literature knowledge, different rates for the STAT2-bound active receptor were estimated, while the same rates were estimated for STAT1-bound active receptor and active receptor (Arimoto *et al*, 2017b). These ten models were calibrated on the complete Huh7.5-IFNα dataset and model performance of the individual models was evaluated by means of Bayesian Information Criterion (BIC). The BIC analysis indicated that the model best describing the experimental data contained an additional degradation term of both the active receptor complex and the active receptor complex bound to STAT1 and STAT2 (Figure 17D). This degradation term depended both on SOCS1 and USP18 and the best model performance was obtained when synergy between SOCS1 and USP18 was assumed rather than additive contributions of SOCS1 and USP18.
In conclusion, USP18 acted as a negative regulator and impacts signal attenuation. Knockdown of USP18 resulted in sustained signalling in IFNα pre-treated cells and USP18 overexpression alone was not sufficient to induce the negative memory, but rather USP18 and SOCS1 have a synergistic effect on reducing the active IFNα receptor complexes by enhancing their degradation.

2.2.8 Contribution of individual feedbacks to IFNα-induced positive and negative memory

Marcus Rosenblatt (University of Freiburg) performed model simulations to dissect the mechanisms contributing to the dose-dependent memory observed for IFNα signaling. To this aim, the response in the nucleus, defined by ISRE promoter bindings sites occupied by ISGF3, was simulated for different expression levels of the individual feedback proteins STAT1, STAT2, IRF9, USP18, SOCS1 and SOCS3, and of the receptor. For each component the expression levels were increased or reduced to levels comparable after 24 hours pre-treatment with 2.8 pM or 1400 pM IFNα (Figure 18A). The model simulations revealed an IFNα dose-dependent increase in the fold-change of the levels of STAT1, STAT2, IRF9, USP18 and SOCS1, while the number of available receptor copies at the cell surface was reduced for the high IFNα dose and SOCS3 levels remained low for all conditions.

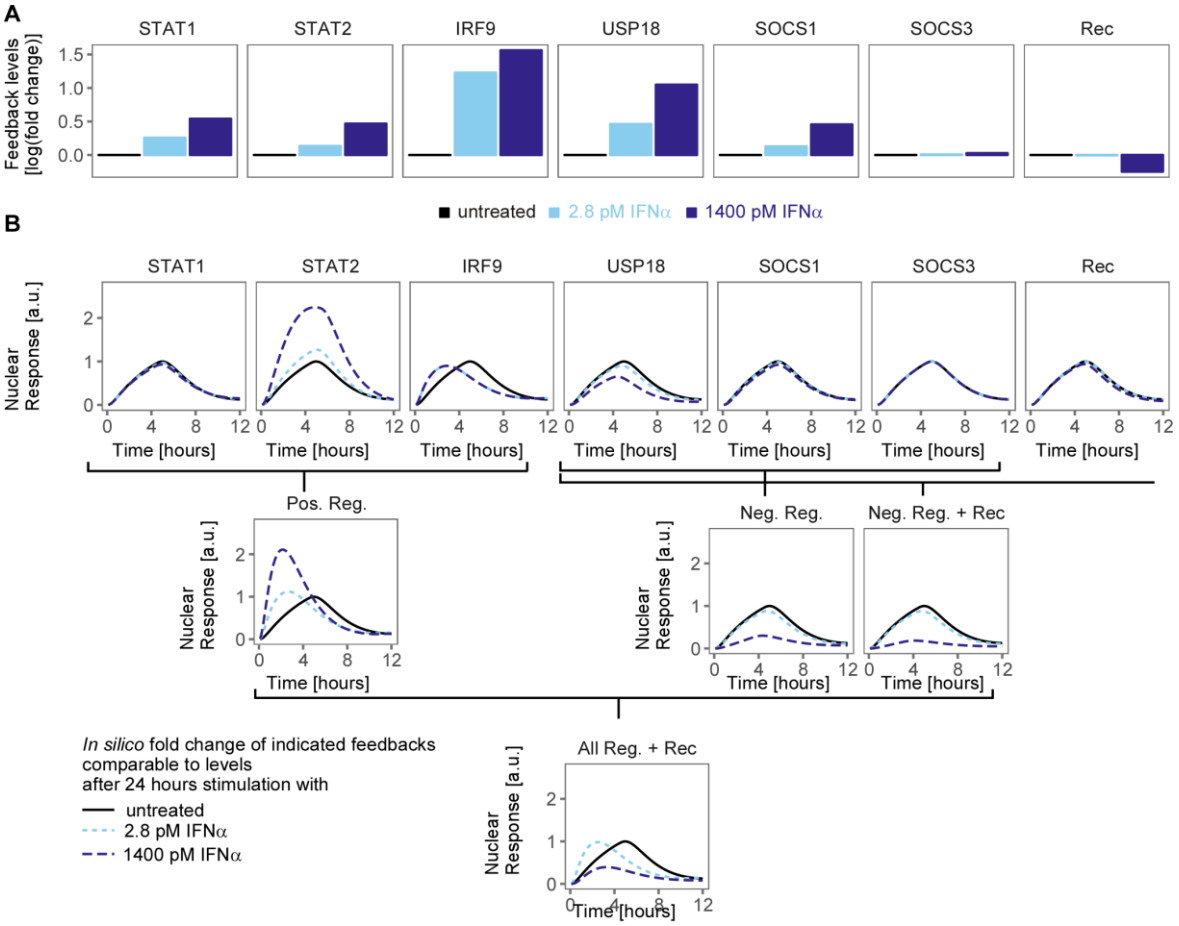

Figure 18. Model simulations reveal contribution of individual feedbacks to positive and negative memory. A) Model fit of fold changes in STAT1, STAT2, IRF9, USP18, SOCS1 and SOCS3 proteins and receptor abundance upon pre-treatment of Huh7.5 with 0, 2.8 pM or 1400 pM IFNα for 24 hours. Fold changes were expressed relative to untreated cells. Rec: receptor. B) Contributions of each feedback component to the nuclear response upon stimulation with 1400 pM IFNα. The occupancy of promoter binding sites containing interferon stimulated response elements (species OccISREbs in the model) was utilized as readout for nuclear response. Contribution of individual feedbacks (upper panel), combination of positive regulators (Pos. Reg.), negative regulators (Neg. Reg.), negative regulators combined with receptor levels (Neg.Reg. + Rec), and all feedbacks combined (All Reg. + Rec).

For each of the obtained fold changes, *in silico* experiments were performed to investigate the impact on the dynamic behaviour of the occupied binding sites of the promoters containing the interferon-stimulated-response-element (OccISREbs). As shown in Figure 18B, the model simulations revealed that the different expression levels of STAT1 established in response to the different pre-treatment conditions did not affect the dynamic behaviour induced upon stimulation with 1400 pM IFNα, as visualized by a similar time to peak, amplitude of the peak and the overall area under the curve (AUC) from 0 to 12 hours. Interestingly, STAT2 and IRF9 both accelerated the IFNα-induced response as indicated by a reduced time to peak. Furthermore, the increase of STAT2 upon prestimulation with 2.8 pM IFNα and 1400 pM IFNα increased the amplitude and the AUC in the investigated time-frame in a STAT2-dose-dependent manner, while IRF9 had no major influence on the amplitude and AUC over 12 hours. Combining the increase in the expression of the positive regulators STAT1, STAT2, IRF9 (Pos. Reg.) revealed an earlier time to peak, higher amplitude and higher AUC over 4 or 12 hours of stimulation. This dynamic behaviour was observed with both fold changes established by pretreatment with 2.8 pM and 1400 pM IFNα indicating that these

components contribute to a positive memory. Investigating the role of the negative regulator USP18 showed that pre-treatment with 2.8 pM IFNα and stimulation 1400 pM IFNα resulted in a dose-dependent decrease of the IFNα-induced response as visualized by a reduced AUC over 12 hours. In contrast, the increase in SOCS1 upon pre-treatment with 2.8 pM IFNα and 1400 pM IFNα only had a minor effect on the AUC of the IFNα-induced response, while SOCS3 did not have an effect. Combining the enhanced expression of the negative regulators USP18, SOCS1 and SOCS3 (Neg. Reg.) showed that this resulted in a further decrease of the response. These model-based insights revealed that both USP18 and SOCS1 decrease the AUC of the IFNα-induced response, indicating that these components contribute to a negative memory. Downregulation of receptor abundance at the cell surface in response to pre-treatment with the high IFNα dose also dampened the nuclear response and resulted in a lower AUC. Combining the impact of the negative regulators with the downregulation of the receptor generated an even lower nuclear response, indicating an even stronger negative memory. Finally, the combination of all positive and negative feedbacks including the receptor (All Reg. + Rec) revealed that after pre-treatment with 2.8 pM IFNα, the influence of the positive regulators was stronger than of the negative regulators with STAT2 and IRF9 shaping the response. In contrast, after pre-treatment with 1400 pM IFNα, the negative regulators determined the response by counteracting the effect from IRF9 and STAT2 and thereby reducing the area under the curve. Thus, the model-based analysis revealed that the positive and negative feedbacks balance each other and thereby generate dose-dependent memory-effects.

2.3 Prediction of memory establishment in primary human hepatocytes

2.3.1 Impact of protein abundance of STAT1, STAT2, IRF9 in combination with USP18 abundance on establishment of positive memory of IFNα-induced signal transduction

The mathematical model indicated that the abundance of the feedback proteins and of the receptor determined the establishement of the positive and the negative memory in IFNα signaling. When only an increase of the positive feedback components was simulated, the extent of the positive memory was increased, indicating the role of abundance of the feedback proteins mediating the feedback loops. Furthermore, positive and negative memories of IFNα-induced signal transduction established in Roferon pre-treated HepG2-hNTCP cells could be described by the mathematical model of IFNα signalling by incorporating cell line specific synthesis rates of STAT1, STAT2, IRF9 and USP18 together with a cell line specific receptor abundance. To gain deeper insight into how the abundance of the feedback regulators impact the memory effect, the mathematical model of IFNα signalling calibrated on the complete IFNα-Huh7.5 dataset was employed to examine how the pairwise combination of differences in the abundance of STAT1 and USP18, STAT2 and USP18, or IRF9 and USP18 at steady state conditions impacted the establishment of a positive or negative memory. Model simulations focussed on components that could be measured experimentally and were performed by Marcus Rosenblatt (University of Freiburg). As a quantitative measure for the established memory, the area under the curves (AUCs) of the model simulations for the occupied ISRE promoter binding sites (occISREbs) were compared between cells that were pre-treated with 2.8 pM IFNα for 24 hours or were left untreated, and that were, in line with previous experiments, stimulated for four hours with 1400 pM IFNα. Pre-treatment with the low, non-saturating dose of IFNα would provide insights for establishment of both the positive and the negative memory in relation to protein abundance of the feedback components. Furthermore, the memory was displayed as the logarithm of the ratio of the different AUCs indicating with positive values a positive memory,

with negative values a negative memory and zero indicates no memory. In summary, the quantitative measure for the memory was defined as:

$$Memory = \log \frac{AUC\ of\ occISREbs\ (24\ h\ pretreatment\ with\ 2.8\ pM\ IFN\alpha\ ,\ \ stimulation\ with\ 1400\ pM\ IFN\alpha\ for\ 4\ \ hours)}{AUC\ of\ occISREbs\ (no\ pretreatment,\ \ stimulation\ with\ 1400\ pM\ IFN\alpha\ for\ 4\ \ hours)}$$

Formula (1)

The simulations of the memory in response to increasing amounts of USP18 and STAT1 (Figure 11A) revealed that below 10 000 molecules per cell of USP18 a positive memory was observed, while above 10 000 molecules per cell of USP18 no memory was observed. Upon higher amounts of molecules per cell of USP18 a negative memory was observed. On the contrary for a wide range of STAT1 molecules per cell an increase in the abundance of STAT1 had no effect on the establishment of a memory. Interestingly, varying the abundance of STAT2 together with the abundance of USP18 showed that high amounts of either STAT2 or USP18 or of both promoted the establishment of a negative memory. The combination of an increase of USP18 with different amounts of IRF9 showed that IRF9 only promoted the establishment of a positive memory at amounts below 5000 IRF9 molecules per cell, but did not promote the establishment of a negative memory or have an impact on the memory at higher molecules per cell.

In conclusion, model predictions performed under steady-state conditions showed that the abundance of STAT2 and USP18 predicted the threshold between positive and negative memory of IFNα-induced signal transduction.

2.3.2 Protein abundance in primary human hepatocytes

To investigate the range of physiologically relevant abundance of STAT1, STAT2, IRF9 and USP18 and to assess patient-to-patient variability, the amount of molecules per cell was determined in primary human hepatocytes (PHH) that were isolated from tumor-free tissue of three patients. The cells were either left untreated or were stimulated with 1400 pM IFNα for 24 hours and the amount of molecules per cell for both conditions was determined by quantitative immunoblotting (Figure 11B). At basal conditions, for patient one 250 000 molecules per cell STAT1, for patient two 150 000 molecules per cell STAT1 and for patient three 400 000 molecules per cell STAT1 were detected. Upon stimulation with IFNα a 2.5 to 5 fold increase in STAT1 was observed corresponding to 1 200 000 STAT1 molecules per cell in patient one, 400 000 STAT1 molecules per cell in patient two and 1 050 000 STAT1 molecules per cell in patient three. On the contrary for STAT2, very comparable values in the PHHs derived from the three patients were observed, indicating low patient-to-patient variability, with at basal conditions approximately 50 000 molecules per cell and upon stimulation with IFNα an increase to approximately 200 000 molecules per cell. For IRF9, again high patient-to-patient variability was observed. At basal conditions 75 000 molecules per cell of IRF9 were detected in PHHs from patient one, whereas PHHs from patient two and three harboured about 30 000 IRF9 molecules per cell. These values increased two- to three-fold upon IFNα stimulation and reached 200 000 IRF9 molecules per cell in PHHs from patient one, 100 000 IRF9 molecules per cell in PHHs from patient two and 75 000 IRF9 molecules per cell in PHHs from patient three. Similarly, the expression of USP18 protein showed a strong patient-to-patient variability. For USP18 already at basal conditions a two- to five fold difference in the amount of USP18 was detectable in the PHHs from the three patients. Untreated PHH contained 7900 molecules per cell USP18 for patient one, 17 400 molecules per cell USP18 for patient two and 4 500 molecules USP18 per cell for patient three. In IFNα-treated PHH 120 000, 170 000 and 75 000 molecules USP18 per cell were detected for

patients one, two and three, respectively. These results demonstrate that except for STAT2 the expression of the feedback regulators of the IFNα signaling pathway is highly variable between patients and that there is no correlation between the respective levels of the feedback regulators, suggesting that the particular expression levels are characteristic for the individual patient.
Comparison of the amounts of molecules per cell determined in the three patients to the amount of molecules per cell determined in the hepatoma cell line Huh7.5 (Figure 11) and HepG2-hNTCP (Appendix section 5.3) revealed that all three patients displayed two- to four-fold lower levels of STAT1 before and after stimulation with IFNα in Huh7.5, while STAT2 molecules per cell were comparable between Huh7.5 and the PHH derived from the three patients, both before and after treatment with IFNα. PHH from patient two and patient three showed an IRF9 abundance in the same range as Huh7.5, both in untreated cells and cells treated with IFNα, whereas PHH from patient one displayed a two- to three-fold higher abundance of IRF9 both in untreated cells and in IFNα-treated cells. Untreated HepG2-hNTCP cells displayed comparable molecules per cell as Huh7.5 for both STAT1, STAT2 and IRF9, indicating that the higher abundance of STAT1 is characteristic for both these hepatoma cell lines. Lastly, the comparison of the amount of molecules per cell of USP18 revealed that the PHH derived from the three patients displayed a higher abundance of USP18 than Huh7.5, which contained 2600 molecules per cell in untreated cells and 55 000 molecules per cell in IFNα-treated cells. In contrast, HepG2-hNTCP cells displayed with 38 000 at basal conditions a high abundance of USP18, indicating both high variability among patients and hepatoma cell lines.
To summarize, primary human hepatocytes isolated from three different patients revealed heterogeneity in STAT1, IRF9 and USP18 abundances, while STAT2 abundances were very comparable between the three patients, as well as to the hepatoma cell lines Huh7.5 and HepG2-hNTCP.

2.3.3 USP18 abundance as patient-specific indicator of dose-dependent memory of IFNα signal transduction

Having identified STAT2 and USP18 abundance as determinants for the memory combined with high patient-to-patient-to-hepatoma cell line variability in USP18 but not in STAT2, suggested that USP18 abundance would be most informative for memory predictions. Therefore, the establishment of the memory was investigated in relation to different pre-treatment doses of IFNα and different initial abundances of USP18 protein (Figure 11C). Relative to Formula (1) the only variable changed was the pre-treatment dose, whereas the time frame of 4 hours stimulation with 1400 pM IFNα after 24 hours pre-treatment was kept unchanged. Model simulations performed by Marcus Rosenblatt (University of Freiburg) revealed a positive memory upon pre-treatment with a dose up to 280 pM IFNα in cells expressing below 1000 molecules per cell of USP18 and a dose up to 2.8 pM in cells expressing 10 000 molecules per cell of USP18. At IFNα doses above 2.8 pM a linear relationship between IFNα dose and USP18 abundance was observed for the threshold of positive to negative memory. To compare the model predictions with the USP18 abundance at basal conditions of the different patients and the hepatoma cell lines, the corresponding abundances were indicated at the low pre-treatment dose of 2.8 pM IFNα and the high pre-treatment dose of 1400 pM IFNα in Figure 11C. USP18 molecules per cell in the range of 2600 to 38 000 seen in the patients (filled symbols) and hepatoma cell lines (open symbols) combined with a low pre-treatment dose of IFNα predicted a positive memory for Huh7.5 and PHH from patient one and three. Interestingly, for patient two and HepG2-hNTCP the model predicted a minor positive memory to no memory. Pre-treatment with the high dose of IFNα predicted a negative memory for both the patients and the cell lines.

To validate this model prediction, the prediction was compared with memory experiments performed using the same cells from the three patients as used for the molecules per cell experiments. Cells were growth-factor-depleted and pre-treated with 2.8 pM IFNα, 1400 pM IFNα or were left untreated. 24 hours later cells were stimulated with 1400 pM IFNα and IFNα-induced phosphorylation of cytoplasmic STAT1 and STAT2 was investigated over time by quantitative immunoblotting. Due to technical reasons involving limited material only cytoplasmic lysates were obtained. The error range of 30% observed from the quantitative immunoblot data of the Huh7.5 was assumed for the single replicates of PHH from the different patients. Subsequently, the data was used for model calibration (Figure 19D) together with time-resolved measurements for STAT1, STAT2, IRF9 and USP18 (Appendix section 5.4) in the three patients and combined with the measured amounts of molecules per cell of STAT1, STAT2, IRF9 and USP18 (Figure 19A) comprising 382 data points belonging to 9 conditions in total. Similar as for the HepG2-hNTCP, the previously established Huh7.5 calibrated model was extended by incorporating patient-specific protein synthesis rates of STAT1, STAT2, IRF9 and USP18 as well as patient-specific receptor abundances. The model required in addition patient-specific basal mRNA synthesis rates for STAT1, STAT2, IRF9 and USP18 to be able to capture patient-specific fold changes in protein abundance, while HepG2-hNTCP showed comparable fold changes to Huh7.5 and therefore did not require these HepG2-hNTCP specific basal mRNA synthesis rates. The model was able to simultaneously fit patient-specific abundances of IRF9, STAT1, STAT2 and USP18 protein (Figure 19B), while capturing the patient-specific dynamics observed in the time-resolved measurements (Figure 19D, Appendix section 5.4). Most interestingly, the model described the trend whether a patient established a positive memory after pre-treatment with 2.8 pM IFNα for 24 hours, as visualized with a positive memory for pSTAT1 and pSTAT2 in PHH from patient one and patient three, while no memory was visible for pSTAT1 and pSTAT2 in PHH from patient two. In agreement with the model predictions, all three patients established a strong negative memory upon pre-treatment with a high dose of IFNα.

To conclude, USP18 abundance was identified as patient-specific indicator of positive or negative memory of IFNα-induced signal transduction and was experimentally validated in primary human hepatocytes from the three different patients.

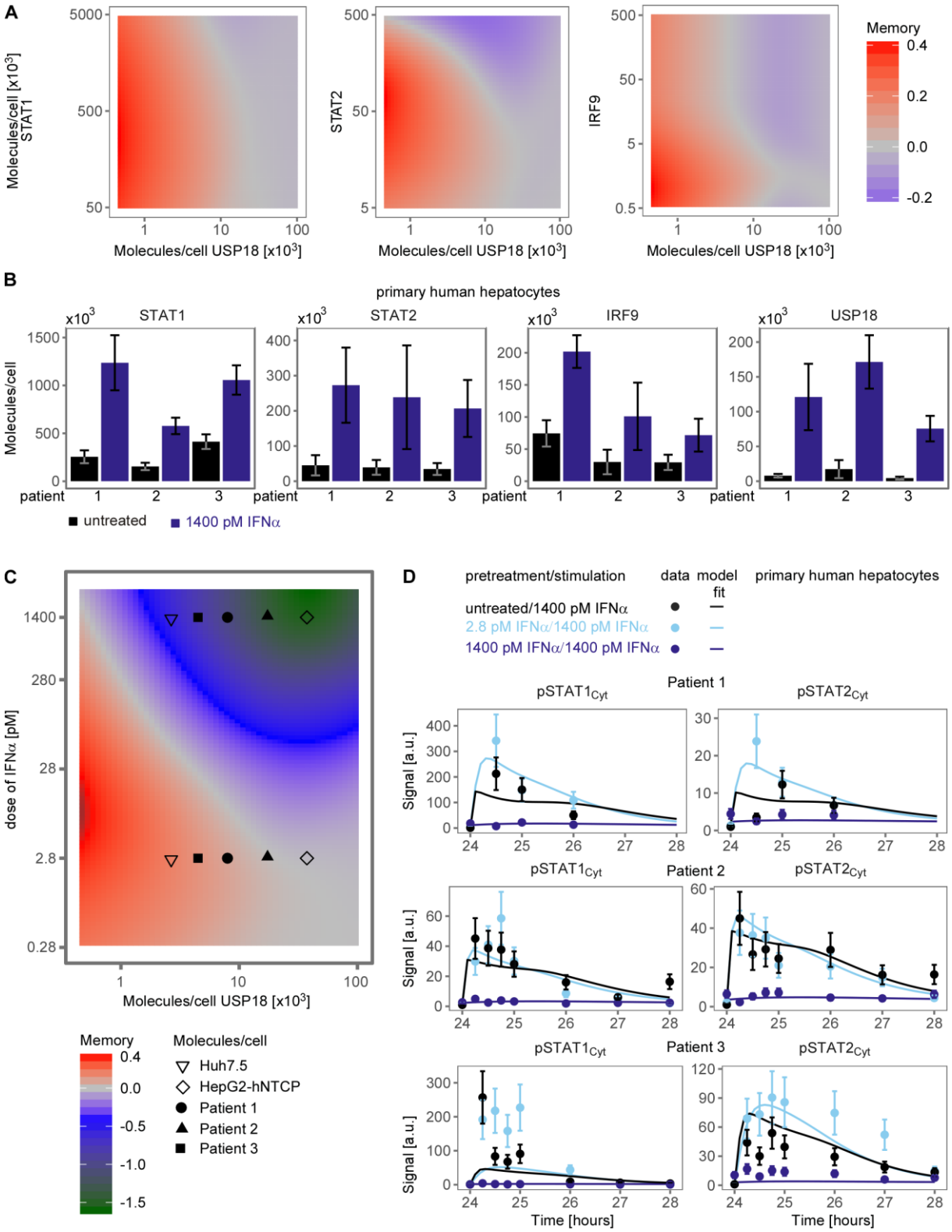

Figure 19, USP18 abundance predicts dose-dependent memory in primary human hepatocytes from different patients. A) Model simulations of IFNα-induced memory of IFNα-induced signal transduction of cells pretreated with 2.8 pM IFNα for different protein abundance of STAT1, STAT2, IRF9 and USP18. Memory is defined as the log ratio of the area under curve of response upon re-stimulation for four hours in cells pretreated with 2.8 pM IFNα over cells without pretreatment (see text). Response is defined as occupancy of promoter binding sites containing interferon stimulated response elements (species occISREbs in the model). B) The amount of molecules per cell for STAT1, STAT2, IRF9 and USP18 were determined experimentally in primary human hepatocytes from three different patients. Cells were harvested after 24 hours pretreatment with 1400 pM IFNα or without pretreatment, and total cell lysates were spiked in with different amounts of protein calibrators and subjected to immunoblotting. Detection was performed with antibodies specific to STAT1, STAT2, IRF9 or USP18 using chemiluminescence on a CCD camera based device (Imagequant). Average of at least N=3 displayed

with standard deviation. Quantitative immunoblotting was performed by Tamar Nizharadze. C) Model predictions of IFNα-induced memory of IFNα induced signal transduction upon stimulation of cells pretreated with different doses of IFNα doses over USP18 abundance. Memory is defined as the log ratio of the area under curve of response upon stimulation for four hours in cells pretreated with 2.8 pM IFNα over cells without pretreatment (see text). Response is defined as occupancy of promoter binding sites containing interferon stimulated response elements (species occISREbs in the model). D) Experimental data and model fit of IFNα-induced phosphorylation of cytoplasmic STAT1 and STAT2 in growth-factor depleted primary human hepatocytes pretreated with 0, 2.8 pM or 1400 pM IFNα. Primary human hepatocytes from the same patients 1-3 as in panel B were used. Experimental data is represented by filled circles, per patient N=1. 30% errors were assumed. Lines indicate model fits.

3 Discussion

IFNα is used to treat chronic HBV and HCV infections and various cancers, but often patients do not respond to the treatment as a consequence of prior activation of the IFNα-induced signaling cascade (Chen *et al*, 2005; Zhu *et al*, 2012; Li *et al*, 2014; Sarasin-Filipowicz, 2008). This negative memory of the IFNα signal transduction has been observed in cell culture and *in vivo* studies (Sarasin-Filipowicz *et al*, 2009a; Makowska *et al*, 2011; François-Newton *et al*, 2011; Larner *et al*, 1986), but conditions that determine establishment of negative memory were unknown. Quantitative experimental data performed in this study revealed that IFNα signal transduction establishes, depending on the pre-treatment dose of IFNα, a positive or negative memory of IFNα-induced signal transduction. Pre-treatment with a low dose of IFNα established a positive memory characterized by increased IFNα-induced phosphorylation of STAT1 and STAT2 observable in the nucleus and faster gene-expression of target genes. In contrast, pre-treatment with a high dose of IFNα established a negative memory characterized by a decreased IFNα-induced phosphorylation of STAT1 and STAT2 detectable in the cytoplasm and the nucleus and resulting in much reduced gene expression.

By combining quantitative time- and dose-resolved measurement of IFNα-induced signal transduction with mathematical modelling, the mechanisms of dose-dependent memory were unravelled. At positive memory conditions the proteins IRF9 and STAT2 shaped the response, while at negative memory conditions USP18 and SOCS1 together reduce the available receptor copies at the cell surface.

By analyzing the protein abundance of USP18 in patients, establishment of a positive or negative memory over a wide range of IFNα concentrations can be predicted by the mathematical model, thereby providing new perspectives for patient-tailored treatment with optimized IFNα dosing to prevent establishment of a negative memory.

3.1 Dose-dependent memory of IFNα-signal transduction

Pre-treatment of Huh7.5, HepG2-hNTCP and primary human hepatocytes with a low dose of IFNα resulted in elevated pSTAT1 and pSTAT2 levels upon stimulation with IFNα indicating a positive memory of IFNα-induced signal transduction, while pre-treatment with a high dose of IFNα resulted in much reduced pSTAT1 and pSTAT2 levels upon stimulation with IFNα indicating a negative memory of IFNα-induced signal transduction This dose-dependent memory of IFNα-induced signal transduction provides new insights for optimal dosing in IFNα-based therapy to prevent establishment of a negative memory in the treatment of patients suffering for instance from chronic HBV infection.

A positive memory of IFNγ-induced signal transduction has been reported for monocytes primed with IFNγ produced by PBMC during macrophage development by electro mobility shift assay (EMSA) and immunoblotting of pSTAT1 and target proteins (Hu *et al*, 2002). Priming of monocytes with IFNγ enhanced pSTAT1 levels upon stimulation with IFNα as well, as shown in monocytes by immunoblotting (Hu *et al*, 2002) and in macrophages by EMSA (Lehtonen *et al*, 1997).

The IFNα-induced negative memory has been studied in more detail, also referred to as ligand desensitization or refractoriness. By treating fibroblasts with multiple rounds of IFNα, long term ligand desensitization has been observed for up to three days as assessed by transcription of target genes (Larnerl & Chaudhuri, 1986). This desensitization was dependent on protein synthesis, since treatment with cyclohexamide did not lead to long-term desensitization (Larnerl & Chaudhuri, 1986). Interestingly, while Lehtonen and colleagues observed a positive memory for IFNα signal

transduction in IFNγ pre-treated macrophages, macrophages pre-treated with IFNα showed a reduced ISGF3 and STAT1 homodimer formation as assessed by EMSA, indicating and IFN type specific effect (Lehtonen *et al*, 1997). Furthermore, liver cells isolated from mice receiving multiple injections of IFNα over time showed only a weak induction of pSTAT1 and reduced amount of ISGF3 upon the second stimulation, as demonstrated by immunoblot and EMSA, respectively (Sarasin-Filipowicz *et al*, 2009b).

In addition, it has been observed that negative memory for IFNα-induced signaling can be established by pre-treatment with IFNβ, IFNλ1 or IFNλ4 (François-Newton *et al*, 2011; Sun *et al*, 2016; Sung *et al*, 2017; Makowska *et al*, 2011) or other stimuli such as TNFα and LPS (MacParland *et al*, 2016). Negative memory established by IFNα, IFNβ or IFNλ1 was shown by reduced IFNα-induced phosphorylation of STAT1, STAT2, TYK2 and JAK1 assessed by immunoblotting and IFNα-triggered induction of target genes in HLLR1-1.4 cells (François-Newton *et al*, 2011). Furthermore, IFNα treatment of IFNλ4 pre-treated Huh7 cells (Sun *et al*, 2016; Sung *et al*, 2017) and primary human hepatocytes producing IFNλ4 upon infection with HCV (Sung *et al*, 2017) showed upon stimulation with IFNα a reduced pSTAT1 and pSTAT2 induction assessed by immunoblot and target gene induction. Additional immunoblot data showed reduced induction of pSTAT1 upon stimulation with IFNα2 in U5A cells primed with IFNβ (Wilmes *et al*, 2015). Liver cells isolated from mice injected first with IFNβ, and later with IFNα showed reduced pSTAT1 levels by immunoblot and ISGF3 DNA binding by EMSA, but mice injected first with IFNλ2, and later with IFNα only showed a very minor effect on pSTAT1 induction and ISGF3 DNA binding upon exposure to IFNα (Makowska *et al*, 2011). Lastly, pre-treatment with LPS or TNFα prevented the IFNα-induced transcription of the target gene Mx1 in Huh7.5 cells and primary murine hepatocytes (MacParland *et al*, 2016).

Results from this study indicated that negative memory of IFNα-induced signal transduction level propagates to expression of target genes. In line with previous results by Larnerl and colleagues (Larnerl & Chaudhuri, 1986), pre-treatment with a high dose of IFNα did not enhance IFNα-induced gene expression. IFNα-induced mRNA expression was much suppressed to different extents for the different gene clusters in cells pre-treated with a high dose of IFNα, which might be caused by other transcriptional regulators resulting from cross-talk with different signaling pathways that might be less sensitive to the negative memory. For instance it has been reported that IFNα-2b can activate the p38 MAPK signaling cascade and ERK1 and ERK2, but not AKT in human liver cancer cells (Hep3B, HLF, Huh6, and PLC/PRF/5) suggesting possible regulation by the transcription factors c-Myc, c-Jun or c-Fos (Matsumoto *et al*, 2005). Based on the observation that gene expression is still present after phosphorylated STAT1 and STAT2 were detectable, Cheon and colleagues proposed that unphosphorylated STAT1 and STAT2 form a non-canonical unphosphorylated ISGF3 (named U-ISGF3) that drives a subset of ISGs. Promoter analysis of ISGs revealed that STAT1, STAT2 and IRF9 were bound to a subset of genes in absence of IFN stimulation of hTERT-HME1 cells lentivirally transduced with unphosphorylated STAT1, STAT2 and IRF9. Target genes of this proposed U-ISGF3 included STAT1, MX1 and IFIT1. (Cheon & Stark, 2009; Cheon *et al*, 2013). These genes were part of this study and showed a partial upregulation upon treatment with IFNα in Huh7.5 cells pre-treated with a high dose of IFNα. It is unclear if unphosphorylated ISGF3 complexes can form under physiological conditions. Lastly, the observations in this study are correlated with IFNα-induced expression, making it more plausible that a minor amount of phosphorylated STAT1 and STAT2 drives this expression together with co-factors previously assembled on the actively transcribed genes. ISGs that were not expressed upon stimulation with IFNα in Huh7.5 pre-treated with a high dose, might have a different chromatin structure and consequently would no longer be accessible for ISGF3.

Experiments performed in this study at positive memory conditions showed that IFNα-induced phosphorylation and nuclear translocation of STAT1 and STAT2 was faster. Furthermore, target genes showed different kinetics with an earlier time to peak, and a faster signal termination was observed for target genes with transient expression profiles. Presence of chromatin marks established upon pre-treatment with a low dose of IFNα might also contribute to the accelerated induced gene-expression, and IFNα pre-treatment induced expression of co-regulators such as IRF1 and IRF2 might also contribute to the different dynamical behaviour of the target gene expression (Harada *et al*, 1989).

3.2 Mechanism of dose-dependent memory of IFNα-signaling

3.2.1 IFNα-induced signalling and feedback loops

To unravel the mechanism of IFNα-dose-dependent memory an ODE-based model that comprises multiple positive and negative feedbacks was established. Maiwald and colleagues developed a model on IFNα-signaling that focused on the early antiviral response (up to four hours) and identified IRF9 as a crucial positive feedback (Maiwald *et al*, 2010). Time-resolved quantitative experiments within this study revealed that the positive feedbacks mediated by STAT1 and STAT2 become relevant after approximately 14 to 16 hours, therefore in the ODE-based model developed in this study two additional positive feedback loops mediated by STAT1 and STAT2 were incorporated. Furthermore, dose- and time-resolved quantitative measurements within this study identified three instead of one negative feedback loop mediated by SOCS1, SOCS3 and USP18. Lastly, a transcriptional regulator was incorporated based on the model developed in the study by Maiwald colleagues (Robichon, 2015). For instance IL6-induced JAK/STAT signaling incorporates only the negative feedback loop of SOCS3, while Epo-induced JAK2/STAT5 signaling incorporates two negative feedback loops: SOCS3 and CIS (Sobotta *et al*, 2017; Bachmann *et al*, 2011), while IFNα-induced JAK/STAT signaling incorporates multiple positive and negative feedback loops indicating a tight regulation of IFNα-signaling with possible redundancy. In case of IFNα-signaling activation one might hypothesize that strong regulation is required, since the expression of target genes could a negative impact on the host, as it has been illustrated by unspecific cleavage of RNAs by RNAse L and global translation inhibition by PKR (García *et al*, 2006; Malathi *et al*, 2007). Furthermore, immune-modulatory effects of IFNα have been described, such as cytokine release leading to recruitment of other immune cells, as for example shown by the recruitment of monocytes to the side of infection upon release of the chemokine CCL2 in mice infected with HSV-1 (Conrady *et al*, 2013). Additional immune-modulatory effects include modulation of cellular state and activity, as shown for interferon induced cytotoxicity of Natural killer cells (Biron *et al*, 1999), interferon induced partial activation ofB-cells that lowers the threshold required for B-cell activation (Braun *et al*, 2002) and interferon modulation of T-cell survival, proliferation and differentiation (Tough, 2012). Furthermore, IFNα modulates the maturation of dendritic cells and leads to increased antigen presentation by upregulation of MHC-class II receptors and co-stimulatory factors (Simmons *et al*, 2012). Thus, uncontrolled IFNα-signalling does not solely effect the phenotype of the cell itself, but it results in paracrine effects

The requirement for positive feedbacks serves as noise filter, requiring stimuli above a threshold before the system is activated (Hornung & Barkai, 2008). Furthermore positive feedbacks can serve to accelerate the signal transduction. While IL-6-induced signal transduction and Epo-induced signal transduction act much earlier and more transient, for instance in CFU-E cells showed a sharp peak of

maximal Epo-induced phosphorylation of STAT5 10 minutes after stimulation, followed by gradual decline of pSTAT5 signals (Bachmann *et al*, 2011), while IFNα-induced signal transduction displayed sustained pSTAT1 and pSTAT2 levels for multiple hours, returning only to basal level at 8 hours of stimulation. To prevent hyper activation of the signal transduction pathway negative regulators are transcriptionally induced. For Epo-induced signaling a division of labor between SOCS3 and CIS was identified, with CIS acting dominantly at low doses of Epo, and SOCS3 acting dominantly at high doses of Epo (Bachmann *et al*, 2011). Incorporation of multiple feedback mechanisms can provide robustness (Iwanami *et al*, 2005; Kitano, 2007) in signal transduction pathways as well as division of labor, with feedbacks acting on different time frames and activated upon different ligand doses. In this study, the contributions of three negative feedbacks at the receptor level were established. The negative feedback loop mediated by SOCS3 showed transient expression, was only induced at high doses of IFNα and acted first in time with maximal protein expression around 1.5 hours after stimulation. The second feedback mechanism was mediated by USP18, which was induced later and at lower doses of IFNα compared to SOCS3 with protein levels increasing starting from four hours after stimulation up to eight hours followed by sustained expression. Lastly, the third negative regulator SOCS1 was induced at lower doses of IFNα compared to USP18 and SOCS3 and SOCS1 mRNA reached maximal expression at five hours after stimulation after which expression decreased to lower levels slightly above basal expression. The three negative feedbacks show partial redundant mechanism, with both SOCS3 and SOCS1 inhibiting kinase activity of the activated associated janus kinases at the receptor. SOCS1 additionally mediated the degradation of the associated kinases TYK2, which result in decreased expression of the receptor at the cell surface (Ragimbeau *et al*, 2003; Piganis *et al*, 2011). Lastly, USP18 acts by competing with JAK1 for IFNAR2 binding, thereby inhibiting the catalytic activity of the activated receptor complex. Furthermore, USP18 has been reported to destabilize the receptor complex (Wilmes *et al*, 2015).

In contrast to the proteins mediating the negative feedback loops, the proteins mediating the positive feedback loops are components from the transcription factor complex ISGF3 (Lehtonen *et al*, 1997). Quantitative analysis of molecules per cell of STAT1, STAT2 and IRF9 protein performed in this study, revealed 900 000 molecules per cell of STAT1 at basal conditions in Huh7.5. In contrast 50 000 molecules per cell of STAT2 and 5000 to 20 000 molecules per cell of IRF9 indicate that these proteins are an order of magnitude lower compared to STAT1 abundance. Model simulations of the nuclear transcription factor complexes pSTAT1 homodimer, pSTAT1pSTAT2 heterodimer and the trimeric complex ISGF3 revealed different dynamic behaviour over time. Upon stimulation with IFNα, a fast and strong, but transient induction of pSTAT1 homodimers was observed, while pSTAT1pSTAT2 heterodimer and ISGF3 showed delayed and less transient dynamics. Transient dynamics of pSTAT1 homodimers might be explained by shorter half-lives, which would be in agreement with reported phosphatases acting on STAT1, but not STAT2 (Hoeve, 2002; Wu *et al*, 2002). Furthermore, by employing ODE-based modelling Maiwald and colleagues identified an important role of IRF9 in complex stability by phosphatase protection of DNA-bound ISGF3 (Maiwald *et al*, 2010).

3.2.2 Mechanism of positive and negative memory

Analysis with the mathematical model of quantitative data in cells perturbed with either USP18 knockdown or USP18 overexpression in this study, revealed that USP18 abundance is not sufficient to establish a negative memory of IFNα-induced signal transduction, instead USP18 synergizes with SOCS1 on reducing the active receptor by SOCS1 and USP18 catalyzed degradation. By investigating the specific role of USP18 on establishment of the negative memory of IFNα-induced signal

transduction, knockdown of USP18 by siRNA transfection in combination with pre-treatment with 1400 pM IFNα performed in this study showed sustained phosphorylation levels of STAT1 and STAT2 as well as sustained expression of target genes over 24 hours in Huh7.5 cells. The maximum amplitude of pSTAT1 and pSTAT2 was comparable between the USP18 knockdown setting and Huh7.5 wild type and Huh7.5 transfected with control siRNAs and additional stimulation with IFNα resulted did not elevate phosphorylated STAT1 and STAT2 protein levels further. Other studies performed in different cell lines and primary cells with different doses of IFNα observed less sustained signalling in context of USP18 and a larger fold increase upon an additional stimulation with IFNα. For instance, François-Newton and colleagues stimulated HLLR1-1.4 cells with 50 pM IFNα or 50 pM IFNβ and observed more transient dynamics compared to Huh7.5 wildtype cells treated with 1400 pM IFNα (François-Newton *et al*, 2011). USP18 knockdown combined with pre-treatment with 50 pM IFNβ, showed lower pSTAT1 and pSTAT2 levels at time of the additional stimulation (after 24 hours) and consequently higher fold increase of pSTAT1 and pSTAT2 upon stimulation with IFNα, as assessed by immunoblot (François-Newton *et al*, 2011). While USP18$^{-/-}$mice injected with IFNα displayed higher amplitude in liver cells isolated from USP18 knockout mice, compared to control mice, these cells also displayed partial sustained signal transduction at the time of stimulation (8 hours) and responded only with a minor increase in pSTAT1 levels upon stimulation with IFNα, as shown by immunoblot (Sarasin-Filipowicz *et al*, 2009b). Furthermore, within this study the role of USP18 in negative memory by ectopic expression of USP18 was addressed by means of a Huh7.5 cell line under the control of Tet-inducible promoter and induced overexpression of USP18 to levels comparable to pre-treatment with 1400 pM IFNα for 24 hours. Ectopic expression of USP18 resulted in a lower amplitude of pSTAT1 and pSTAT2 compared to wild type or uninduced Huh7.5 cells. However, both quantification of the data and mathematical modeling revealed that this reduction in activation was weaker than the negative memory. Other studies performed in different cell lines and with different extent of overexpression showed a larger effect on IFNα-induced signalling. François-Newton colleagues employed HU13 cells, a HLLR1-1.4 cell clone overexpressing USP18, which showed a large reduction of pTYK2, pSTAT1 and pSTAT2 upon stimulation with IFNα compared to HLLR1-1.4 parental cells as assessed by immunoblot (François-Newton *et al*, 2011). Furthermore, Wilmes et al overexpressed EGFP-USP18 under control of the CMV promoter, which resulted in reduced co-locomotion of HaloTag-IFNAR1 and SNAPf-IFNAR2c in U5A cells upon treatment with 50 nM IFNα as assessed by single-molecule co-locomotion analysis (Wilmes *et al*, 2015). Thus, USP18 overexpression can generate a partial negative memory, but is not sufficient to explain the negative memory established by pre-treatment with IFNα. Within this study, a mechanism whereby USP18 and SOCS1 synergistically mediate the degradation of active receptor copies was proposed by testing different model structures based on assumptions that either SOCS1 catalyses the degradation of the activated receptor, USP18 catalyses the degradation of the activated receptor, or USP18 and SOCS1 catalyse the degradation of the activated receptor with additive contributions or by synergism between USP18 and SOCS1. The synergistic effect between USP18 and SOCS1 on reducing receptor levels at the cell surface is most likely indirect, with SOCS1 destabilizing the receptor by removing TYK2 and USP18 further destabilizing the receptor by removing JAK1. It has been reported for IFNAR1 that turnover from the cellular membrane is enhanced in TYK2 -/- cell (Piganis *et al*, 2011), furthermore USP18 has been proposed to destabilize the complex of IFN, IFNAR1 and IFNAR2 as demonstrated with lower binding affinities of IFN in the presence of USP18 overexpression (Wilmes *et al*, 2015). A synergistic effect between USP18 and SOCS1 could be explained by both destabilizing the receptor complex and thereby increasing the receptor turnover, resulting in lower receptor

copies available for an additional stimulation. The number of receptor copies at the cell surface were previously shown to have a crucial impact on TGFβ signaling (Vizán *et al*, 2013) and EGF/HGF signaling (Lyashenko *et al*, 2017). In case of TGFβ, however, the authors observed that negative memory is already established one hour after stimulation and the time span of the negative memory coincides with the time span of ligand depletion, while experiments performed in this study indicated no direct correlation with IFNα presence. In case of EGF/HGF-signaling, it was shown that cells sense relative concentrations. This "gradual" negative memory could be fully attributed to receptor abundance at the cell surface, since stimulation with EGF or with HGF established a negative memory for an additional EGF or HGF stimulation, respectively, but no negative memory was observed upon pre-treatment with EGF and stimulation with HGF or vice versa. Since both growth factors activate the same signal transduction pathway, negative memory had to be established at the receptors.

In contrast to the negative memory, the positive memory is established downstream of the receptor. In silico experiments within this study revealed STAT2 as the main component responsible for the positive memory, and a smaller contribution of IRF9 both on the overall response and as an accelerator, which is in agreement with Maiwald and colleagues who identified IRF9 as early regulator and accelerator of IFNα-signaling by means of sensitivity analysis of an ODE-based model and experimental validation (Maiwald *et al*, 2010). Results in this study further indicate that STAT1 does not strongly contribute to the positive memory in Huh7.5, which is in contrast to IFNγ-induced positive memory (Hu *et al*, 2002), where STAT1 was shown to be the key component. However, in Huh7.5 employed in this study STAT1 abundance is an order of magnitude higher than STAT2 abundance, while in the monocytes used to investigate IFNγ-induced positive memory STAT1 protein levels were close to detection limit, revealing cell type-specific protein abundances of STAT1. In addition, IFNγ signal transduction relies on STAT1 homodimer as transcription factor complex, indicating STAT1 as a crucial factor.

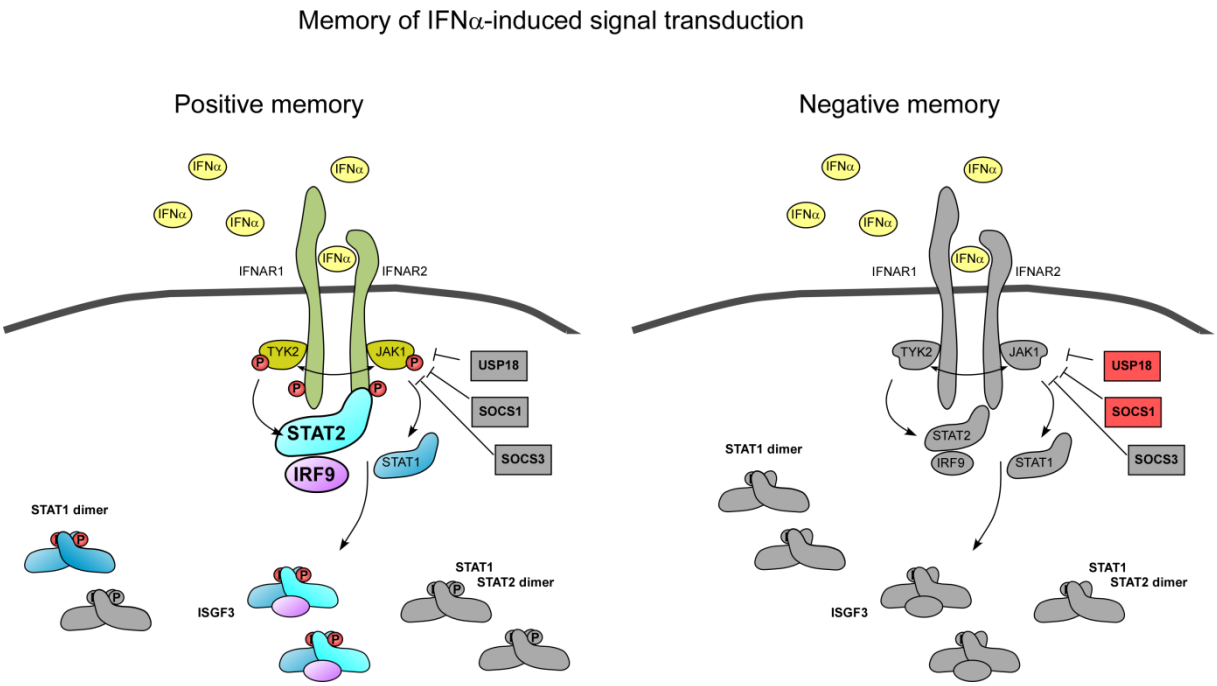

Figure 20. Graphical cartoon displaying memory of IFNα-induced signal transduction established pre-treatment with IFNα. IRF9 and STAT2 determine the positive memory, while USP18 and SOCS1 determine the negative memory.

3.3 Prediction of positive and negative memory establishment of IFNα-signaling in patients

Experiments performed in this study highlighted that the therapeutically relevant IFNα Roferon can establish positive and negative memory in the two hepatoma cell lines Huh7.5 and HepG2-hNTCP. Furthermore IFNα was able to establish a positive and a negative memory in primary human hepatocytes isolated from different patients. By employing the mathematical model, the protein abundance of STAT1, STAT2, IRF9, USP18 and receptor copies was identified as key requirement to describe positive and negative memories established in the different cell line and primary cells from the different patients, while SOCS1 abundance was not required. Interestingly, USP18 requires SOCS1 to establish a negative memory, however SOCS1 abundance was found not to be predictive for the extent of the memory. Model analysis identified that negative regulation by SOCS1 is independent from SOCS1 concentration, as a consequence of the double role of SOCS1: SOCS1-mediated inhibition of the active receptor and degradation of the active receptor. Abundance of pathway components determines the wiring of signalling networks, as demonstrated in the context of Epo-induced activation of the AKT and ERK pathway by the combination of quantitative experiments and mathematical modelling (Adlung *et al*, 2017). Furthermore, different abundances of pathway components required for IFNα-induced signaling have been reported in different cell types within the same organ, as illustrated with higher basal expression of IFNβ mRNA in cardiac myocytes, but inversely higher basal expression of IFNAR1 and JAK1, TYK2, STAT1, STAT2 and IRF9 in adjacent cardiac fibroblasts (Zurney *et al*, 2007). The authors proposed that cardiac fibroblasts are more responsive to IFN which prevent chronic infection and possible spread to the non-replenishable cardiac myocytes (Zurney *et al*, 2007).

Furthermore, viruses have been reported to degrade signaling components. Examples include downregulation of IFNAR1 in Huh7.5 cells persistently infected with HCV (Chandra *et al*, 2014), downregulation of STAT1 protein upon overexpression of the HCV protein NS5 (Lin *et al*, 2005), while for instance Dengue virus has been reported to degrade STAT2 involving the viral protein NS5 and the host protein UBR4 (Ashour *et al*, 2009; Morrison *et al*, 2013).

Thus, in summary, protein abundances are important for wiring of cellular networks and can be cell type specific or can be affected by viral infections.

By means of *in silico* experiments performed in this study, STAT2 and USP18 abundance was identified as predictor establishment of positive memory of IFNα-induced signal transduction. Primary human hepatocytes from different patients showed high patient-variability in USP18 abundance, but not in STAT2 abundance, therefore USP18 abundance was identified and experimentally validated as predictor for the direction and extend of the established memory. Studies focused on the classification of responders versus non-responders to pegIFNα in patients suffering from chronic HCV identified that upregulated ISG expression including USP18 gene expression as classifier for response. Specifically, Chen and colleagues showed that patients with chronic HCV can be classified as non-responders to PegIFNα if they showed elevated interferon stimulated genes prior to treatment (Chen *et al*, 2005), and the expression status of the ISGs Viperin, Mda5/helicard, OAS1 and USP18 prior to treatment was further validated as low for responders, and high for non-responders to PegIFNα treatment (Sarasin-filipowicz *et al*, 2008).

In conclusion, monitoring USP18 abundance provides insights in which dose a patient should receive to avoid the establishment of negative memory, thereby generating new perspectives toward patient-tailored treatment.

3.4 Proposed further investigations

This work presents novel mechanisms of IFNα-induced positive and negative memory of the IFNα-signal transduction pathway, providing possible drug targets and biomarkers of IFNα non-responsiveness together with a possible IFNα dosing range to prevent IFNα-induced negative memory.

Future work includes the validation of the role of SOCS1 combined with USP18 in the establishment of the negative memory of IFNα-induced signal transduction. To this aim, IFNα dose-dependent induction of both SOCS1 and USP18 would be optimal to establish overexpression levels comparable to the established negative memory. Challenges would lie in the detection of the SOCS1 protein due to the lack of good antibodies combined with a putative low abundance. Furthermore, expression of SOCS1 has been correlated with anti-proliferative effects in gastric cancer cells (Souma *et al*, 2012), indicating the requirement of a tightly regulated expression system for the establishment of a stable cell line or cell clone.

The model-derived hypothesis identified within this work proposes that SOCS1 and USP18 synergistically reduce the amount of receptor at the cell surface, therefore it would be interesting to investigate receptor dynamics upon stimulation with IFNα and assess the role of receptor downregulation in the establishment of a negative memory. To increase the resolution of the description of the receptor activation in the mathematical model, quantifying IFNAR1, IFNAR2, JAK1 and TYK2, would allow identifying which component is downregulated during establishment of the negative memory of IFNα-induced signal transduction. Upon stimulation, IFNα forms a trimeric complex with IFNAR1 and IFNAR2, this trimeric complex is internalized and IFNAR1 is targeted for lysosomal degradation, IFNAR2 however can be recycled and returned to the cellular membrane (Chmiest *et al*, 2016), suggesting a different ratio between IFNAR1 and IFNAR2 after IFNα-induced signal transduction. IFNAR1 and IFNAR2 molecules per cell have been reported in reviews in the order of magnitude of 100 to 1000 copies per cell (Piehler *et al*, 2012; Wilmes *et al*, 2015; You *et al*, 2016; Cohen *et al*, 1995) and the sensitivity of reported antibodies is limited. Therefore tagging of the receptors would be a possible solution. For endogenous expression, homology directed repair with CRISPR-Cas9 could be applied, requiring efficient homology directed repair of Huh7.5, while overexpression of tagged receptors will affect the wiring of the system, and most likely will shift the range of IFNα pre-treatment doses establishing positive, no or negative memory of IFNα-induced signal transduction as a function of the relative abundance to the other signaling components and negative regulators of the system, but would provide insight in potential receptor downregulation upon establishment of negative memory of IFNα-induced signal transduction.

By incorporating RNA and protein half-lives of the feedback components the model could be employed to investigate the time-frame of the established memory. Furthermore, the model could be expanded to incorporate virus-mediated degradation of protein signalling components, to investigate the interplay between virus-mediation reduction of for instance STAT1 and pre-treatment induced expression of STAT1.

This study was performed at cell population levels. It would be informative to investigate if the observed gradual negative memory induced by increasing doses of IFNα pre-treatment is a consequence of switch-like behaviour of cells or gradual negative memory established in individual cells. While using a BAC reporter construct in NIH3T3 cells, Rand et al observed a bimodal response of cells to IFN stimulation, suggesting a possible switch-like behaviour (Rand *et al*, 2012). Furthermore, a biological memory often involves switch-like behaviour (Burrill & Silver, 2010). If establishment of a negative memory would indeed be switch-like, identification what determines a

cell to switch to a negative memory would strengthen the findings in this study and provide further perspectives for patient-tailored response.

4 Materials and Methods

4.1 Molecular biology

4.1.1 Polymerase chain reaction

Polymerase chain reaction was the method employed to amplify a construct and modify at the same time the 5' and 3' ends by incorporating restriction recognition sites in the forward and reverse primers. Reaction mixes were prepared according to Table 2 and incubated with a denaturation phase, an amplification phase of 35 cycles with denaturation of the DNA, primer annealing and primer extension, and a final extension phase (Table 3).

Table 2. PCR reaction mix.

Reagents	**Volume**
5x Phusion HF buffer (ThermoFisher Scientific)	10 µl
10 mM dNTPs (Roche)	1 µl
forward primer (10 pmol/µl) (Eurofins)	0.5 µl
reverse primer (10 pmol/µl) (Eurofins)	0.5 µl
Plasmid (10 ng/µl)	1 µl
Phusion Hot Start II DNA Polymerase (2 U/µl) (ThermoFisher Scientific)	0.5 µl
Autoclaved ddH_2O	36.5 µl
Total volume	50 µl

Table 3. PCR treatment scheme.

Phase	**Temperature**	**Time**	**Number of cycles**
Denaturation	98°C	30s	1
Amplification cycles:			35
-Denaturation	98°C	10s	
-Annealing	65°C	30s	
-Extension	72°C	60s	
Extension	72°C	10 min	1
Storage	4°C	∞	1

4.1.2 Molecular cloning

4.1.2.1 Gel purification

The PCR products were mixed with 5x loading dye (Qiagen) and loaded on 1% agarose gels (Agarose (Biozym) + Midori green advanced DNA stain (Nippon Genetics) dissolved in 0.5x TAE buffer (0.022 M Tris-AcOH pH8.0, 0.5 mM EDTA) and fragments were separated by size by means of gel

electrophoresis. Gels were run in 0.5x TAE buffer for 40 minutes at 80 V. Bands of interest were excised and isolated from the gel according to manufacturer's instruction using the QIAEX II Gel Extraction kit (Qiagen).

4.1.2.2 Digestion and purification

Vectors and inserts were digested for two hours at 37°C using restriction enzymes from New England Biolabs (NEB) in recommended buffers supplied by NEB. After digestion, digested vectors were purified by gel electrophoresis and gel extraction, as described above, while the inserts were purified using the QIAquick PCR purification kit (Qiagen) according to manufacturer's protocol.

4.1.2.3 Ligation

Digested vectors and inserts were ligated using 100 ng vector combined with different molar excesses ranging from 1 to 6 of the insert. For ligation, vector and insert DNA were supplemented with 10 µl 2x Quick Ligase Reaction Buffer (NEB), 1 µl DNA quick ligase (NEB) and autoclaved ddH_2O to a final volume of 20 µl and incubated for 5-20 minutes at room temperature. A control without insert was always included. 5 µl of the ligation mixes were used for bacterial transformation.

4.1.3 Transformation of *Escherichia coli* cells

Competent cells of *E.coli* strain DH5α (Invitrogen) were used for plasmid amplification, while competent cells of *E.coli* strain BL21-CodonPlus(DE3)-RIL (Agilent) were used for production of mammalian proteins.

4.1.3.1 Transformation of *E.coli* DH5α

Competent cells of the *E.coli* strain DH5α (Invitrogen) were thawn on ice, aliquoted in 50 µl per transformation and supplemented with 5 µl ligation mix or 10 ng plasmid DNA. After 20-30 minutes incubation on ice, bacteria were heat-shocked for 5 minutes at 37 °C, left on ice for 10 minutes and supplemented with 1 ml pre-warmed S.O.C. medium (Invitrogen). After 30 minutes incubation at 37 °C, while shaking at 225 rpm, bacteria were pellet by centrifugation of 1 minute at 5000 rpm. The volume of the supernatant was reduced to 100 µl, the bacterial pellet resuspended and plated on LB-agar plates containing 100 µg/ml of the selective marker ampicillin (Sigma-Aldrich). Bacteria were grown at 37 °C overnight. The next day, single colonies were picked and grown in mini-cultures of 2.5 ml ampicillin-containing LB medium.

4.1.3.2 Transformation of *E.coli* BL21-CodonPlus(DE3)-RIL

100 µl aliquots of the frozen competent *E.coli* strain BL21-CodonPlus(DE3)-RIL (Agilent) were thawed on ice and supplemented with 50 ng plasmid. After 30 minutes of incubation on ice, cells were heat-pulsed at 42 °C for 20 seconds and kept on ice for 2 minutes. Next 900 µl pre-warmed S.O.C. medium (Invitrogen) was added and bacteria were shaked at 225 rpm at 37 °C for 1 hour. 100 µl of cell suspension was plated on pre-warmed selective TB-agar plates ((Sigma-Aldrich) containing 100 µg/ml ampicillin (Sigma-Aldrich) and bacteria were grown at 37 °C overnight.

4.1.4 Purification of plasmid DNA and sequencing

For cloning purposes, plasmids were isolated from 2 ml bacterial cultures using the QIAprep Spin Miniprep Kit (Qiagen) according to the manufacturer's protocol.

For cell culture purposes, plasmids were isolated from a 100 ml bacterial culture and isolated using the JetStar maxiprep kit (Genomed). Isolation was performed according to manufacturer's

instruction. DNA pellet was dissolved in TE overnight and concentration determined by measuring absorbance at 260nm with NanoDrop 2000 (ThermoFisher Scientific).

4.1.5 Sequencing

Sequences of the plasmids were confirmed by Sanger Sequencing performed at Eurofins. 20 µl samples were prepared containing 1 µg plasmid DNA, 2 µl primer (10 pmol/µl) and autoclaved ddH_2O.

4.1.6 Construction of plasmids

cDNA of USP18 (AL136690) was kindly provided by the Vector and Clone Repository of the Genomics and Proteomics Core Facility of the DKFZ.

4.1.6.1 pMOWSIN-TRE-t-USP18

To establish a cell line with inducible USP18, human USP18 was cloned in the retroviral vector containing the tight Tet-responsive element: pMOWSIN-TRE-t (Pfeifer *et al*, 2010). USP18 was amplified and enriched with BamHI and MfeI restriction sites by PCR using the 5'-GCAGGATCCATGAGCAAGGCGTTTGGGCTCCT-3' as forward primer and 5'-CAGCAATTGTTAGCACTCCATCTTCATGTAAACCAGAAGATATG-3' as reverse primer. pMOWSIN-TRE-t was digested with BamHI-HF and EcoRI-HF (NEB), generating compatible sticky ends to the digested insert.

4.1.6.2 pGEX-2T-USP18

To generate a recombinant protein of USP18, USP18 sequence was fused to an affinity tag for purification by cloning USP18 into the glutathione S-transferase (GST)-containing vector pGEX-2T (GE Healthcare). USP18 was amplified and enriched with MfeI and BamHI restriction sites by PCR using the 5'-GCACAATTGATGAGCAAGGCGTTTGGGCTCCT-3' as forward primer and 5'-CAGGGATCCTTAGCACTCCATCTTCATGTAAACCAGAAGATATG-3' as reverse primer. pGEX-2T was digested with EcoRI-HF and BamHI-HF (NEB), generating compatible sticky ends to the digested insert.

4.2 Cell biology

4.2.1 Cultivation of Huh7.5 cell line

The human hepatocellular carcinoma cell line Huh7.5 (Blight *et al*, 2002) was kindly provided by Ralf Bartenschlager (University of Heidelberg). Huh7.5 cells were cultivated in 15 cm cell culture dishes in growth medium consisting of Dulbecco's Modified Eagle Medium #31053 (Gibco), 10% FCS (Gibco), 1% GlutaMAX (Gibco), 1 mM sodium pyruvate (Gibco), 100 U/ml penicillin⁄streptomycin (Gibco). Cells were cultivated for 10 passages. For passaging, cells were washed two times with DPBS (Pan Biotech) and incubated with 0.25% Trypsin without phenolred priorly diluted in PBS (Gibco) for 5 minutes at 37 ^{o}C. Cells were resuspended in cultivation medium and counted using the Neubauer counting chamber.

Cells were stored in liquid nitrogen in a mixture of 90% FCS and 10% DMSO. For freezing of cells, cells were pelleted by centrifugation for 2 min at 1000 rpm at room temperature and resuspended in 90%FCS and 10%DMSO with a concentration of 2 million cells/ml. Cells were frozen slowly using isoproponal freezing chambers in a -80 ^{o}C freezer and cells were then stored in liquid nitrogen.

To take in cells in culture, cells were thawed at 37 °C, diluted 1:10 in growth medium, centrifugated for 2 min at 1000 rpm at room temperature and resuspended in growth medium and cultivated in TPP cell culture plates.
Cell line authentication was performed using Multiplex Cell Authentication by Multiplexion (Heidelberg, Germany) as described recently (Castro *et al*, 2013). The SNP profiles matched known profiles or were unique. Purity of cell lines was validated using the Multiplex cell Contamination Test by Multiplexion (Heidelberg, Germany) as described recently (Schmitt & Pawlita, 2009). No Mycoplasma, SMRV or interspecies contamination was detected.

4.2.2 Cultivation of primary human hepatocytes

Primary human hepatocytes were kindly provided by Dr. Georg Damm (University of Leipzig) and Prof. Dr. med. Katrin Hoffmann (University Hospital Heidelberg). Informed consent of the patients for the use of tissue for research purposes was obtained according to the ethical guidelines of University of Leipzig and University Hospital Heidelberg, respectively. Tissue samples were collected by partial hepatectomy and originate from healthy sections of resected liver tissue. Hepatocytes were isolated as described in (Kegel *et al*, 2016) and were cultivated in adhesion medium (Williams' Medium E (Biochrom F1115), 10 % FCS (Gibco), 0.1 µM dexamethasone, 0.1 % insulin, 2 mM L-glutamine (Gibco), 1% penicillin⁄streptomycin (Gibco)) overnight.

4.2.3 Transient transfection of Phoenix ampho cells for retroviral transduction

For transient transfection, 800 000 Phoenix ampho cells were seeded in 2 ml growth medium (Dulbecco's Modified Eagle Medium #31885 (Gibco), 10% FCS (Gibco), 1% GlutaMAX (Gibco), 1 mM 100 U/ml penicillin⁄streptomycin (Gibco)) in 6 well plates (TPP) and cultivated for 24 hours. Subsequently, co-transfected with 8 µg pMOWS-TRE-t-USP18-puro or pMOWS-TreT and 2 µg pMOWS-TAM2 (Pfeifer *et al*, 2010) using calcium phosphate transfection method. Calcium precipitation was performed by mixing 10 µg plasmid DNA with 12.5 µl of 2.5 M $CaCl_2$ precipitated by dropwise adding 125 µl 2x HBS (560 mM NaCl, 100 mM HEPES, 1.5 mM Na_2HPO_4 pH 7.05), while vortexing the solution. The cells were incubated with the transfection mic for eight hours, after which the medium was replaced with fresh growth medium and incubated overnight. The retroviral supernatant was collected, filtered through a 0.45 µm filter (Millipore) and used for retroviral transduction.

4.2.4 Retroviral transduction

200 000 Huh7.5 cells were seeded in 6-well plates (TPP) 24 hours prior to retroviral transduction. For retroviral transduction, supernatants produced by phoenix ampho cells were supplemented with 8 µg/ml polybrene and added to the Huh7.5 cells. Cells were transduced by centrifugation for three hours at 340 *x g* at 37 °C. 48 hours after transduction, cells were cultured in growth medium containing 0.75 µg/ml puromycin (Sigma). Cells were kept under selection for passaging, while the antibiotic was removed during experiments.

4.2.5 Transient siRNA transfection

For knockdown studies Huh7.5 cells were transfected with 50 nM siRNA using Lipofectamine RNAiMax (Invitrogen) according to manufacturer's protocol. Cells were incubated with the siRNA complexes for 20 hours. The following siRNAs of Dharmacon (GE healthcare) were used: ON-TARGETplus Human USP18 (11274) siRNA - SMARTpool and ON-TARGETplus Non-targeting pool.

4.2.6 Titration of interferon concentration

The activity of Roferon (Roche), Pegasys (Roche), and IFNα-2a (PBL) were titrated to the NIBSC standard using the LucUbiNeo-ET cell line (Lohmann et al., 2003), a Huh7-Lunet cell line with a stably replicating HCV genotype 1b (Con1) subgenomic replicon under the selective pressure of G418 (0.5 mg/ml). The replicon contains a neomycin phosphatase as well as a firefly luciferase reporter gene instead of the viral structural genes and harbors replication-enhancing mutations in the nonstructural genes (Con1-ET). The following standard was used: WHO International Standard interferon alpha, (human leukocyte-derived), NIBSC code 94/784 (National Institute for Biological Standards and Control, Potters Bar, Hertfordshire, EN6 3QG, United Kingdom) which was reconstituted in sterile H_2O, aliquoted and frozen at -80 before use. To perform the titration, 75 000 cells were seeded in 96 well plate format in the absence of G418 and the next day IFN was added in two-step serial dilutions. After 48 hours, cells were lysed in Luciferase Lysis buffer (1% Triton-X 100, 25 mM glycyl-glycine pH 7.8, 15 mM $MgSO_4$, 4 mM EGTA pH 7.8, 10% glycerol, 1 mM DTT) and stored at -80°C. Luciferase activity was measured on a Mithras^2 LB 943 Monochromator Multimode Microplate Reader (Berthold Technologies). Signal intensities were normalized to untreated cells and were fitted by four-parameter Hill kinetics to determine the IC50s. 1 nM of IFNα (PBL) is within the range of 750 to 2250 U/ml (1482 ± 738 U/ml) relative to NIBSC standard (Figure 14).

4.2.7 Cell stimulation

1 million Huh7.5 cells were seeded in 6 well plate format (TPP) 24 hours in advance. Before stimulation, cells were washed three times with DPBS (Pan Biotech) and growth-factor-depleted in starvation medium (Dulbecco's Modified Eagle Medium #31053 (Gibco), 1% GlutaMAX (Gibco), 1 mM Sodium pyruvate (Gibco)) supplemented with 1 mg/ml BSA and 25 mM HEPES (Gibco) for three hours (or overnight for HepG2-hNTCP). After growth-factor-depletion, cells were stimulated on a 37^{o}C heating block by addition of interferon alpha 2a (PBL 11000-1) or Roferon (Roche, PZN 08543409) and harvested at different time points. For memory experiments comprising two days, 600 000 cells were seeded prior to the stimulation. After growth-factor-depletion, cells were pretreated with interferon and stimulated with IFNα 24 hours later by addition of interferon.

1 or 1.5 million viable primary human hepatocytes were seeded in 6 well collagen coated plates (Bio Coat, Corning) one day prior to the experiment. The next day cells were gently washed twice with DPBS (PAN Biotech) before cells were growth-factor-depleted and kept in starvation medium (Williams' Medium E (Biochrom F1115), 2 mM L-glutamine (Gibco), 100 U/ml penicillin⁄streptomycin (Gibco)) for three hours prior to the experiment.

4.3 Protein biochemistry

4.3.1 Cell lysis

4.3.1.1 Cellular fractionation

Cellular fractionation was performed to obtain cytoplasmic and nuclear protein lysates. Lysis buffers were freshly supplemented with the protease inhibitors Aprotinin and AEBSF (Sigma). Upon harvesting, cells were lysed in 250 µl cytoplasmic buffer (10 mM Hepes, 10 mM KCl, 0.1 mM EDTA, 0.1 mM EGTA, 1 mM NaF, 1 mM Na_3VO_4, 0.4% NP40) and gently scraped on ice. Lysates were vortexed for 10 sec and centrifugated at 1000 *x g*, at 4 ^{o}C for 5 minutes. Supernatant was transferred (cytoplasmic fraction) and the pellet, representing the nuclear fraction, was washed with 250 µl washing buffer (10 mM Hepes, 10 mM KCl, 0.1 mM EDTA, 0.1 mM EGTA, 1 mM NaF, 1 mM Na_3VO_4,)

and centrifugated at 1000 *x g*, at 4°C for 5 minutes. Supernatant was discarded and 45 µl nuclear lysis buffer was added (20 mM Hepes, 25% Glycerin, 400 mM NaCl, 1 mM EDTA, 1 mM EGTA, 1 mM NaF, 1 mM Na_3VO_4, 0.4% NP40). Lysates were vortexed 10 seconds every two minutes for 15 minutes in total. Nuclear fraction was obtained by collecting the supernatant after 5 min centrifugation at 20817 *x g* at 4 °C.

4.3.1.2 Total cell lysis

Whole cell lysates were prepared by lysing cells in 1x RIPA (PAN-lysis) buffer (1% NP40, 0.5% DOC, 0.1% SDS, 250 mM NaCl, 2.5 mM EDTA, 50 mM Tris pH 7.2). Cells were lysed in 250 µl lysis buffer by scarping and transferred to 1.5 ml tubes, mixed for 20 minutes at 4 °C and subjected to sonication (Sonopuls, Bandelin, for 30 seconds, with 75% amplitude, 0.1s on 0.5s off). Whole cell lysates were collected after 10 minutes centrifugation at 4°C at 20817 *x g.*

4.3.2 Sample processing and immunoprecipitation

The concentration of protein lysates was determined by Pierce™ BCA Protein Assay Kit (Thermo-Fisher) and measured on the InfiniteF200Pro plate reader (Tecan). 10 or 20 µg of cell lysate were prepared for quantitative immunoblotting using 4x Sample buffer (8% SDS, 100mM Tris pH 7.4, 20% glycerol, 10% 2-mercaptoethanol, 200 mM DTT, 0.02% bromophenol blue) and incubated at 98 °C for 2 minutes.

To perform SOCS3 immunoprecipitation, 500 µg of cytoplasmic lysate was supplemented with 4 µl SOCS3 antibody (Merck #04-004), 25 µl protein G sepharose beads (GE Healthcare) and 0.1 ng SBP-SOCS3 (kindly provided by Anja Zeilfelder, Klingmüller lab, DKFZ). Lysates were incubated overnight, and subsequently washed twice with cytoplasmic lysis buffer and once with TNE (10 mM Tris pH 7.4, 100 mM NaCl, 1 mM EDTA pH 8.0, 100 µM Na_3VO_4). SOCS3 was eluted from the beads with 30 µl 2x sample buffer (4% SDS, 50 mM Tris pH 7.4, 10% glycerol, 5% 2-mercaptoethanol, 100 mM DTT, 0.01% bromophenol blue) and samples were incubated at 98 °C for 2 minutes before being processed on SDS-PAGE.

4.3.3 SDS-PAGE and quantitative immunoblotting

4.3.3.1 SDS-PAGE

Protein samples were analysed by 1D sodium dodecyl sulfate polyacrylamide gel electrophoresis (SDS-PAGE). 15% running gels were used to analyse SOCS3, while 10% running gels were used to analyse the other targets (Table 4).

Table 4. Composition of 10% and 15% polyacrylamide gels for SDS-PAGE.

	10% running gel	**15% running gel**	**Stacker**
ddH_2O	8.5 ml	6.42 ml	7.15 ml
10% SDS	200 µl	200 µl	100 µl
1.5 M Tris-HCl, pH 8.8	5.0 ml	5 ml	-
1.5 M Tris-HCl, pH 6.8	-	-	1.25 ml
2% Bis	1.3 ml	0.88 ml	0.5 ml
40% Acrylamide	5.0 ml	7.5 ml	1.0 ml
10% APS	200 µl	200 µl	100 µl
TEMED (99%)	20 µl	20 µl	10 µl

Samples were loaded in randomized order to avoid correlated blotting errors (Schilling et al., 2005).

Gels were run for 2 hours 45 minutes at 40 mAmp per gel in 1x Laemmli buffer (Laemmli, 1970) (192mM glycine, 25mM Tris, 0.1% SDS) and subjected to immunoblotting.

4.3.3.2 Immunoblotting

Proteins from SDS-PAGE gels were transferred to a porous membrane using semi-dry blotting chambers (GE Healthcare). PVDF membranes with 0.45 µm pore size (Millipore) was activated in 98% ethanol (Sigma-Aldrich) for 20 seconds, briefly rinsed with water and transferred to western blot transfer buffer (192 mM glycine, 25 mM Tris, 0.075% SDS, 0.5 mM Na_3VO_4, 15% ethanol). Blotting was performed for one hour at 250 mAmp per blot.

After blotting the proteins were reversible stained by Ponceau S solution (sigma-Aldrich) and blocked with 5% BSA/TBS-T (10 mM Tris pH 7.4, 150 mM NaCl, 0.2% Tween-20) for one hour at room temperature. The membranes were incubated by gently shaking overnight at 4 ^{o}C with primary antibodies dissolved in 5% BSA/TBS-T supplemented with 0.1 % NaN3 (Table 5).

Table 5. Specification of primary antibodies used for immunoblotting and immunoprecipitation.

Protein target	Application	Company	Reference number	Dilution
pTyr(701)	immunoblot	Cell Signaling	9171	1:2500
pTyr(701)	immunoblot	Cell Signaling	9167	1:15 000
pTyr(690)	immunoblot	Cell Signaling	4441	1:3000
STAT1	immunoblot	Merck	06-501	1:5000
STAT2	immunoblot	Merck	06-502	1:3700
USP18	immunoblot	Cell Signaling	4813	1:2000
IRF9	immunoblot	Bectin Dickenson	610285	1:5000
Calnexin	immunoblot	Enzo Life Sciences	Adi-SPA-860	1:5000
β-actin	immunoblot	Sigma-Aldrich	A5441	1:5000
HDAC1	immunoblot	Santa Cruz	sc81598	1:1000
SOCS3	immunoprecipitation	Merck	04-004	4 µl/ 500 µg
SOCS3	immunoblot	Abcam	Ab16030	1:500

Unbound primary antibody was removed by washing three times, gently shaking with TBS-T for 10 minutes at room temperature. Secondary antibodies, coupled to horse-radish peroxidase (HRP), were dissolved in 2.5% BSA/TBS-T and incubated with the membrane for one hour (Table 6) while shaking gently at room temperature.

Table 6. Specification of secondary antibodies used for immunoblotting.

Protein target	Application	Company	Reference number	Dilution
Mouse IgG	immunoblot	Dianova	115-035-146	1:10 000
Rabbit IgG	immunoblot	Dianova	111-035-144	1:10 000
Protein A	immunoblot	BD Biosciences	610438	1:10 000

4.3.3.3 Quantitative immunoblot detection and quantification

Membranes were developed using self-produced ECL solutions (Solution 1: 0.1 M Tris pH 8.5, 2.5 mM Luminol, 0.4 mM p-coumaric acid; Solution 2: 0.1 M Tris pH 8.5, 0.018% H_2O_2) or using ECL Western Blotting Reagents (GE healthcare). Blots were developed on the charge coupled device (CCD)-camera based ImageQuant LAS4000 (GE Healthcare) and bands were quantified using the software ImageQuant TL 1D version 7.0 (GE healthcare). Background subtraction was performed utilizing the rolling ball technique.

4.3.3.4 Reprobing of immunoblots

To remove previous antibody signals, HRP groups were quenched with H2O2, as described previously (Sennepin *et al*, 2009) or antibodies were removed by incubation with stripping buffer (0.063 M Tris

pH6.8, 2% SDS, 0.7% β-mercaptoethanol) at 65 °C. After quenching or stripping of the membrane, the blot was blocked with 5% BSA/TBS-T for one hour at room temperature prior to reprobing with primary antibodies.

4.3.5 Determination of molecules per cell by quantitative immunoblotting

4.3.5.1 Production of recombinant proteins

The amount of molecules per cell was determined based on recombinant proteins.
E.coli BL21-CodonPlus(DE3)-RIL competent bacteria (Agilent) were transformed with 50 ng pGEX-2T-IRF9 and pGEX-2T-USP18 by heat-pulsing the bacteria at 42 °C for 20 seconds (see section 4.1.3.2). Single colonies were picked and a pre-culture of 50 ml was grown in Lysogeny broth (LB) broth containing 100 µg/ml ampicillin and 50 µg/ml chloramphenicol. The next day, the pre-culture was expanded to 500 ml LB and protein expression was induced upon addition of 1 ml 1M Isopropyl β-D-1-thiogalactopyranoside (IPTG). After four hours, bacteria were harvested by centrifugation at 4200 *x g*, for 20 minutes at 4 °C, washed in PBS and the pellet stored at -20 °C overnight.
Bacterial pellets were lysed in lysis buffer (10 mM Tris-HCl pH 8.0, 100 mM NaCl, 1 mM EDTA, 50 mM DTT, 0.233 mg/ml lysozyme) and later supplemented with sarcosyl and sonicated. After centrifugation at 15 180 *x g*, for 15 minutes at 4 °C the supernatant was supplemented with Triton X 100 to a final concentration of 2% and incubated with glutathione-sepharose beads (GE Healthcare) for one hour, mixing at 4 °C to capture the GST-tagged recombinant proteins. Beads were washed four times in PBS-washing buffer (9% PBS, 5mM DTT, 1% NP40) and one time using PBS supplemented with 5 mM DTT. Beads were resuspended in elution buffer (0.75 mM Tris HCl pH8.0, 150 mM NaCl, 0.1% SDS, 5 mM DTT, 20 mM Glutathion) and transferred to 0.45 µm filer column (Millipore) and multiple fractions harvested.
SBP-STAT1ΔN and SBP-STAT2ΔN were established previously in our lab (Maiwald *et al*, 2010) and SBP-SOCS3 calibrator was kindly provided by Anja Zeilfelder (Klingmüller lab, DKFZ, Heidelberg).
The concentration of the calibrators was determined using bovine bovine serum albumin (BSA) protein standards (Pierce) on SDS-PAGE gel stained with Simply Blue Safestain (Invitrogen) according to manufacturer's protocol.

4.3.5.2 Determination of amount of molecules per cell

To determine molecules per cell, the cell number of Huh7.5 was counted with the Neubauer improved counting chamber for each treated condition. For primary human hepatocytes, a calibration curve was established, which was based on protein concentrations derived from different amounts of cells lysed in 250 µl 1x RIPA (PAN-lysis buffer). Different amounts of recombinant proteins were spiked in 10 µg whole cell lysates and quantitative immunoblotting was performed with the indicated antibodies. The linear regions of the calibration curves were fitted with linear regression in R, fixing the offset to the background intensity measured at samples which did not contain spiked in recombinant protein and the amount of endogenous signal was interpolated. Errors represent standard deviations of the different samples.

4.4 RNA Analysis

4.4.1 Isolation of total RNA and production of cDNA

Total RNA was extracted using RNeasy kit (Qiagen) according to manufacturer's instruction. Clearing of the lysates was achieved using QIAshredder spin column (Qiagen). RNA concentrations were determined by absorbance (Nanodrop2000, ThermoFisher Scientific) and reverse transcription was

performed with 1 µg of RNA according to manufacturer's instruction (High Capacity cDNA Reverse Transcription Kit from Applied Biosystems).

4.4.2 Quantitative RT-PCR

Quantitative RT-PCR was performed on the Ligthcycler480 (Roche) using primers and dual hybridization probes in 2x Probes Master (Roche). Samples preparation in 384 well plates was performed using the Microlabstar^{LET} robot (Hamilton). Cycling protocol consisted of 5 minutes pre-incubation at 95 ^{o}C, 50 amplification cycles (95 ^{o}C for 10 sec, 60 ^{o}C for 30 sec and acquisition at 72 ^{o}C for 1 sec) and 2 minutes cooling. Quantification cycles (Cq) were determined by absolute quantification with second derivative maximum method using the LightCycler480SW1.5.1 software. Samples for calibration curve were included in each measurement to assess efficiency of primer hybridization.

Data was normalized with the geometric mean of the reference genes hypoxanthine-guanine phosphoribosyltransferase (HPRT), TATA box binding protein (TBP) and glyceraldehyde-3-phosphate dehydrogenase (GAPDH).

Primers were designed using the Universal Probe Library Assay Design Center (Roche Applied Biosciences) and manufactured by Eurofins. The utilized UPL probes and primers sequences for human genes are listed in Table 7.

Table 7, Primers for quantitative RT-PCR of human genes.

Genes	Accession #	Forward primer 5'-3'	Reverse primer 5'-3'	UPL Probe #
CXCL10	NM_001565.3	gaaagcagttagcaaggaaaggt	gacatatactccatgtagggaagtga	34
CXCL11	NM_005409.3	agtgtgaagggcatggcta	tcttttgaacatggggaagc	76
GAPD	NM_002046	agccacatcgctcagacac	gcccaatacgaccaaatcc	60
HPRT	NM_000194.2	cgagcaagacgttcagtcct	tgaccttgatttattttgcatacc	73
IFI6	NM_002038.3	gggctccgtcactagacctt	aaccgtttactcgctgctgt	40
IFIT2	NM_001547.4	tggtggcagaagaggaagat	gtaggctgctctccaaggaa	27
IFITM3	NM_021034.2	gatgtggatcacggtggac	agatgctcaaggaggagcac	76
IRF1	NM_002198.1	ttggccttccacgtcttg	gagctgggccattcacac	36
IRF2	NM_002199.3	tgaagtggatagtacggtgaaca	cggattggtgacaatctcttg	56
IRF9	NM_006084.4	aactgcccactctccacttg	agcctggacagcaactcag	77
ISG15	NM_005101.3	ggcttgaggccgtactcc	ctgttctggctgaccttcg	24
ISG56	NM_001548.3	gctccagactatccttgacctg	agaacggctgcctaatttacag	9
MxA	NM_30817.1	gagctgttctcctgcacctc	ctcccactccctgaaatctg	42
NMI	NM_004688.2	ttcaggcgctgctgtttt	tgtgtcatctttatcagcttcca	24
PKR	NM_002759.1	cggtatgtattaagttcctccatga	gacaaagcttccaaccagga	62
SOCS1	NM_003745.1	gccccttctgtaggatggta	ctgctgtggagactgcattg	87
SOCS3	NM_003955.3	tctccttcaattcctcagcttc	gttcagcattcccgaagtgt	13
STAT1	NM_007315.3	tgagttgatttctgtgtctgaagtt	acacctcgtcaaactcctcag	32
STAT2	NM_005419.2	ggaacagctggagacatggt	tcctgatagctaaccaggcaac	17
TBP	NM_003194.3	cggctgtttaacttcgcttc	cacacgccaagaaacagtga	3
TRIM21	NM_003141.3	tgagcggaaactgaaagtga	tggagacctttaggggttt	24
USP18	NM_017414.3	tatgtgagccaggcacgat	tcccgacgtggaactcag	75
ZNFX1	NM_021035.2	tcgctggcagctttatagg	tggcgttcatagctgaggat	64

4.5 Transcription factor binding site analysis

Promoter analysis of the human SOCS3 gene was performed of a 3000 bp region consisting of 1250 bp in front and 1750 bp within the SOCS3 gene (>NC_000017.11:78358329-78361329 Homo sapiens chromosome 17, GRCh38.p7 Primary Assembly). The promoter analysis was performed using Findpatterns of the GCG sequence analysis package using W2H (Senger *et al*, 1998). The following consensus sequences were tested: GAS (gamma activated sequence) TTNCNNNAA; ISRE (Interferon

stimulated response element): AGTTTCNNTTTCNC/T (Darnell *et al*, 1994). Gene annotation was based on SOCS3 mRNA (NM_003955.4) and displayed using Geneious v5.3 (Kearse *et al*, 2012).

4.6 Data processing and Mathematical modeling

4.6.1 Conversion of interferon concentrations

For model purposes, IFNα concentrations expressed as units/ml were converted to nM based on information supplied by the datasheet (PBL), or product information on Roferon (Roche 2014).

4.6.2 Normalization of quantitative immunoblot data

Immunoblot data was normalized to housekeepers Calnexin, β-actin or HDAC1 or recombinant SBP-SOCS3 using GelInspector (Schilling *et al*, 2005a). In brief, smoothing splines were fitted both to the housekeeper and to the data of the targets of interest. If division of the data by the smoothened housekeeper reduced the distance between the measured data and the estimated smoothing spline, normalization was valid, otherwise normalized was rejected to prevent adding more noise to the data. Cytoplasmic data was normalized to Calnexin or β-actin, while nuclear data was normalized to HDAC1, while immunoprecipitated SOCS3 was normalized to the spiked in calibrator SBP-SOCS3.

4.6.3 Data scaling and error estimation by blotIt

For each target, data points were scaled together by means of a scaling model using the R package blotIt (Daniel Kaschek (2011) blotIt: Average biological replicates and estimate uncertainties, R package version 0.1). Independent experiments contained more than three overlapping data points of treatment, specifically the 1400 pM IFNα treated samples were used as a reference for scaling.
Data points were assumed to be log-normally distributed and least squares optimization was applied to estimate different scaling factors for each membrane. Uncertainties correspond to 66%-confidence intervals (1σ) of the estimated data points. In total 9946 single data points were scaled by blotIt to obtain 1858 data points with confidence intervals that served for model calibration. In addition the determined amount of molecules per cell of STAT1, STAT2, IRF9 and USP18 protein were utilized for model calibration taking into account errors estimated from the data as standard deviations.

4.6.4 Mathematical modeling

For the modeling process, the R package dMod (Kaschek *et al*, 2016) was used. Model equations (see Supplement) were derived by the law of mass-action and Michaelis-Menten kinetics. Parameters were estimated by the method of Maximum-Likelihood starting from random initial parameter values. In order to test identifiability of the parameters and to calculate confidence levels for the estimated values, the profile likelihood (Raue *et al*, 2009) was calculated for each parameter. In some cases, model simplifications were unraveled that did not affect the likelihood value nor the statistical interpretation of model predictions (Kreutz *et al*, 2012). Unless these could be incorporated by means of a reduced model structure, parameter values were fixed for simplification. In total, 12 initial values, 17 scaling and offset parameters and 56 dynamical parameters were estimated. Profile likelihoods (see appendix) identified finite confidence intervals for 79 out of 84 parameters; no further model reduction was applied due to biological significance of the parameters. Table XX (appendix) summarizes the estimated parameter values and corresponding confidence intervals. Furthermore, analysis of a likelihood waterfall plot displaying multiple rounds of parameter estimation sorted by their objective value (Raue *et al*, 2013), revealed reliable convergence of parameter estimation procedure for our mathematical model (See Appendix 5.1.5).

Different model structures were evaluated by means of Bayesian Information Criterion (Schwarz, 1978).

5 Appendix

5.1 Model analysis

5.1.1 List of observables

pSTAT1_Nuc	log(scale_pSTAT1_Nuc * (ISGF3n + 2 * STAT1Dimn + STAT2STAT1n) + off_pSTAT1_Nuc)
pSTAT1_Cyt	log(scale_pSTAT1_Cyt * (ISGF3c + 2 * STAT1Dimc + STAT2STAT1c) + off_pSTAT1_Cyt)
pSTAT2_Nuc	log(scale_pSTAT2_Nuc * (ISGF3n + STAT2STAT1n) + off_pSTAT2_Nuc)
pSTAT2_Cyt	log(scale_pSTAT2_Cyt * (ISGF3c + STAT2STAT1c) + off_pSTAT2_Cyt)
IRF9_Cyt	log(scale_IRF9_Cyt * (ISGF3c + IRF9c) + off_IRF9_Cyt)
IRF9_Nuc	log(scale_IRF9_Nuc * (ISGF3n + IRF9n) + off_IRF9_Nuc)
USP18_obs	log(scale_USP18 * (USP18) + off_USP18)
STAT1_mRNA_obs	log(STAT1_mRNA)
STAT2_mRNA_obs	log(STAT2_mRNA)
IRF9_mRNA_obs	log(IRF9_mRNA)
IRF2_mRNA_obs	log(IRF2_mRNA)
USP18_mRNA_obs	log(USP18_mRNA)
SOCS1_mRNA_obs	log(SOCS1_mRNA)
SOCS3_mRNA_obs	log(SOCS3_mRNA)
tSTAT1_Nuc	log(scale_tSTAT1_Nuc * (ISGF3n + STAT1n + 2 * STAT1Dimn + STAT2STAT1n) + off_tSTAT1_Nuc)
tSTAT1_Cyt	log(scale_tSTAT1_Cyt * (ISGF3c + STAT1c + 2 * STAT1Dimc + STAT2STAT1c + aSTAT1) + off_tSTAT1_Cyt)
tSTAT2_Nuc	log(scale_tSTAT2_Nuc * (ISGF3n + STAT2n + STAT2STAT1n) + off_tSTAT2_Nuc)
tSTAT2_Cyt	log(scale_tSTAT2_Cyt * (ISGF3c + STAT2c + STAT2STAT1c + aSTAT2) + off_tSTAT2_Cyt)
mc_STAT1	ISGF3n + ISGF3c + STAT1n + STAT1c + 2 * STAT1Dimc + 2 * STAT1Dimn + STAT2STAT1c + STAT2STAT1n + aSTAT1
mc_STAT2	ISGF3n + ISGF3c + STAT2n + STAT2c + STAT2STAT1c + STAT2STAT1n + aSTAT2
mc_IRF9	ISGF3n + ISGF3c + IRF9c + IRF9n
mc_USP18	USP18

5.1.2 Model equations

Educt	→	Product	Rate
Ø	→	Rec	prodRec
Rec	→	Ø	degRec * [Rec]
IFN + Rec	→	aRecIFN	BindIFN * [IFN] * [Rec] / [SOCS1] / [SOCS3]
aRecIFN	→	IFN + Rec	UnbindIFN * [aRecIFN]
aRecIFN	→	Ø	[aRecIFN] * (degBasal + degBySOCSandUSP18 * [SOCS1] * [USP18])
aRecIFNSTAT1c	→	Ø	[aRecIFNSTAT1c] * (degBasal + degBySOCSandUSP18 * [SOCS1] * [USP18])
aRecIFNSTAT2c	→	Ø	[aRecIFNSTAT2c] * (degBasal + degBySOCSandUSP18_STAT2 * [SOCS1] * [USP18])
USP18	→	Ø	degUSP18 * [USP18]
aRecIFN + STAT1c	→	aRecIFNSTAT1c	activateSTAT1 * [aRecIFN] * [STAT1c] / (1 + kinhByUSP18 * [USP18])
aRecIFN + STAT2c	→	aRecIFNSTAT2c	activateSTAT2 * [aRecIFN] * [STAT2c] / (1 + kinhByUSP18 * [USP18])
aRecIFNSTAT2c + STAT1c	→	aRecIFN + pSTAT1pSTAT2c	BindSTAT21 * [aRecIFNSTAT2c] * [STAT1c]
pSTAT1pSTAT2c	→	pSTAT1pSTAT2n	TrLocSTAT2STAT1c * [pSTAT1pSTAT2c]
pSTAT1pSTAT2n	→	STAT1n + STAT2n	decaySTAT2STAT1n * [pSTAT1pSTAT2n]
pSTAT1pSTAT2c + IRF9c	→	ISGF3c	BindIRF9 * [pSTAT1pSTAT2c] * [IRF9c]
ISGF3c	→	ISGF3n	TrLocISGF3c * [ISGF3c]
ISGF3n	→	STAT1n + STAT2n + IRF9n	decayISGF3n * [ISGF3n]
aRecIFNSTAT1c + STAT1c	→	aRecIFN + pSTAT1dimc	STAT1Dimerization * [aRecIFNSTAT1c] * [STAT1c]
pSTAT1dimc	→	pSTAT1dimn	TrLocSTAT1dimc * [pSTAT1dimc]
pSTAT1dimn	→	2*STAT1n	decaySTAT1dimn * [pSTAT1dimn]
Ø	→	OccISREbs	prodOccISREbsByISGF3n * [ISGF3n]
Ø	→	OccISREbs	prodOccISREbsBySTAT1STAT2n * [pSTAT1pSTAT2n]
OccISREbs	→	Ø	hl_OccISREbs * [OccISREbs]
Ø	→	OccGASbs	prodOccGASbsBySTAT1dimn * [pSTAT1dimn]
OccGASbs	→	Ø	hl_OccGASbs * [OccGASbs]
STAT1c	→	Ø	degSTAT1 * [STAT1c]
STAT1n	→	STAT1c	TrLocSTAT1n * [STAT1n]
STAT1c	→	STAT1n	TrLocSTAT1c * [STAT1c]
STAT2c	→	Ø	degSTAT2 * [STAT2c]
STAT2n	→	STAT2c	TrLocSTAT2n * [STAT2n]
STAT2c	→	STAT2n	TrLocSTAT2c * [STAT2c]
IRF9n	→	IRF9c	TrLocIRF9n * [IRF9n]
IRF9c	→	IRF9n	TrLocIRF9c * [IRF9c]
IRF9c	→	Ø	degIRF9 * [IRF9c]
SOCS1	→	Ø	degSOCS1 * [SOCS1]
Ø	→	SOCS3	synthSOCS3 * [SOCS3mRNA]
SOCS3	→	Ø	degSOCS3 * [SOCS3]
Ø	→	STAT1mRNA	synthSTAT1mRNAbasal
Ø	→	STAT1mRNA	synthSTAT1mRNA * [OccISREbs] / (kmSTAT1 + [OccISREbs])
STAT1mRNA	→	Ø	hl_STAT1mRNA * [STAT1mRNA]
Ø	→	STAT2mRNA	synthSTAT2mRNAbasal
Ø	→	STAT2mRNA	synthSTAT2mRNA * [OccISREbs]
STAT2mRNA	→	Ø	hl_STAT2mRNA * [STAT2mRNA]
Ø	→	IRF9mRNA	synthIRF9mRNAbasal
Ø	→	IRF9mRNA	synthIRF9mRNA * [OccISREbs] / (kmIRF9 + [OccISREbs])
IRF9mRNA	→	Ø	hl_IRF9mRNA * [IRF9mRNA]
Ø	→	IRF2mRNA	synthIRF2mRNAbasal
Ø	→	IRF2mRNA	synthIRF2mRNA * [OccISREbs]
IRF2mRNA	→	IRF2	delayIRF2 * [IRF2mRNA]
Ø	→	USP18mRNA	synthUSP18mRNAbasal

∅	→	USP18mRNA	synthUSP18mRNA * [OccISREbs]
USP18mRNA	→	∅	hl_USP18mRNA * [USP18mRNA]
∅	→	SOCS1mRNA	synthSOCS1mRNAbasal
∅	→	SOCS1mRNA	synthSOCS1mRNA * [OccISREbs]
SOCS1mRNA	→	∅	hl_SOCS1mRNA * [SOCS1mRNA] * (1 + [IRF2])
∅	→	SOCS3mRNA	synthSOCS3mRNAbasal
∅	→	SOCS3mRNA	synthSOCS3mRNA * [OccGASbs]
SOCS3mRNA	→	∅	hl_SOCS3mRNA * [SOCS3mRNA]
IRF2	→	∅	degIRF2 * [IRF2]
∅	→	STAT1_LC_1	synthSTAT1 * [STAT1mRNA] / (kmsynthSTAT1 + [STAT1mRNA])
STAT1_LC_1	→	STAT1_LC_2	delaySTAT1 * [STAT1_LC_1]
STAT1_LC_2	→	STAT1_LC_3	delaySTAT1 * [STAT1_LC_2]
STAT1_LC_3	→	STAT1c	delaySTAT1 * [STAT1_LC_3]
∅	→	STAT2_LC_1	synthSTAT2 * [STAT2mRNA]
STAT2_LC_1	→	STAT2_LC_2	delaySTAT2 * [STAT2_LC_1]
STAT2_LC_2	→	STAT2_LC_3	delaySTAT2 * [STAT2_LC_2]
STAT2_LC_3	→	STAT2_LC_4	delaySTAT2 * [STAT2_LC_3]
STAT2_LC_4	→	STAT2_LC_5	delaySTAT2 * [STAT2_LC_4]
STAT2_LC_5	→	STAT2c	delaySTAT2 * [STAT2_LC_5]
∅	→	IRF9_LC_1	synthIRF9 * [IRF9mRNA]
IRF9_LC_1	→	IRF9_LC_2	delayIRF9 * [IRF9_LC_1]
IRF9_LC_2	→	IRF9c	delayIRF9 * [IRF9_LC_2]
∅	→	USP18_LC_1	synthUSP18 * [USP18mRNA]
USP18_LC_1	→	USP18_LC_2	delayUSP18 * [USP18_LC_1]
USP18_LC_2	→	USP18	delayUSP18 * [USP18_LC_2]
∅	→	SOCS1_LC_1	synthSOCS1 * [SOCS1mRNA]
SOCS1_LC_1	→	SOCS1	delaySOCS1 * [SOCS1_LC_1]

5.1.3 Estimated parameter values

Parameter values:

activateSTAT1	0.000993872763956289
activateSTAT2	0.307112377381374
aRec	0
aSTAT1	0
aSTAT2	0
BindIFN	1.40622694076595e-05
BindIRF9	0.0112342373040046
BindSTAT21	74.7633497108704
decayISGF3n	3.82445259353454
decaySTAT1Dimn	10.8481882061649
decaySTAT2STAT1n	1.3985134845049
degBasal	3.69626334858631
degBySOCS	3.40025502285928
degBySOCSandUSP18	0.00209140767747268
degBySOCSandUSP18_STAT2	9.05770375999357
degByUSP18	6.96624865649666e-06
degByUSP18_STAT2	0.0216761724749447
degIRF2	0.800487172723954
degIRF9	0.205236058137056
degRec	0.025470291883322
degSOCS1	0.755307636104949
degSOCS3	1121.48370895196
degSTAT1	0.473426726416077
degSTAT2	0.127129312387179
degUSP18	0.74704730676129
delayIRF2	0.956171575655958
delayIRF9	1.19981321215872
delaySOCS1	0.755127495934233
delaySTAT1	0.515355009684318
delaySTAT2	1.84852017038305
delayUSP18	0.747335237516896
hl_IRF9_mRNA	0.414759065661052
hl_OccGASbs	2.21302134593212
hl_OccISREbs	0.598743912050272
hl_SOCS1_mRNA	0.734392397224882
hl_SOCS3_mRNA	2.22251223835688
hl_STAT1_mRNA	0.223262053039926
hl_STAT2_mRNA	0.222250870221681
hl_USP18_mRNA	0.0872995002351983
ifDegSTAT1	1
ifDegSTAT2	1
IFN	0
iRec	39.3169988491934

IRF2	1.1196649764625
IRF2_mRNA	0.937360484483795
IRF9c	1699.45252084237
IRF9_LC_1	290.702696748293
IRF9_LC_2	290.702696748293
IRF9_mRNA	0.877589265667358
IRF9n	169.945252084237
ISGF3c	0
ISGF3n	0
kinhByUSP18	0.000173489905271306
kmIRF9	0.100416976464999
kmSTAT1	0.724877841790616
kmsynthSTAT1	6.78557053095487
OccGASbs	0
OccISREbs	0
off_IRF9_Cyt	0
off_IRF9_Nuc	0
off_pSTAT1_Cyt	0.169864165581174
off_pSTAT1_Nuc	0.0638957117995784
off_pSTAT2_Cyt	0.897650293730089
off_pSTAT2_Nuc	0.652842739592736
off_tSTAT1_Cyt	1.46975573176963
off_tSTAT1_Nuc	0
off_tSTAT2_Cyt	0.678349899982839
off_tSTAT2_Nuc	0
off_USP18	0
prodOccGASbsBySTAT1Dimn	2.21302134593212
prodOccISREbsByISGF3n	0.000320287057533462
prodOccISREbsBySTAT2STAT1n	0.000236026865832614
prodRec	100.141543666519
Rec	3931.69988491934
reltotSTAT1	1.20453564722414
reltotSTAT2	0.324760358534094
scale_IRF9_Cyt	0.000131963062896893
scale_IRF9_Nuc	0.000861558700988315
scale_pSTAT1_Cyt	0.000178856680200195
scale_pSTAT1_Nuc	0.000859489610323459
scale_pSTAT2_Cyt	0.000222283274555396
scale_pSTAT2_Nuc	0.00108913991022987
scale_tSTAT1_Cyt	1.86330099188799e-06
scale_tSTAT1_Nuc	3.00927465384703e-05
scale_tSTAT2_Cyt	4.33395677962661e-05
scale_tSTAT2_Nuc	0.000386561971203189
scale_USP18	0.000465056159125141
SOCS1	0.865223623612456
SOCS1_LC_1	0.865430027871478
SOCS1_mRNA	0.865223623612456

SOCS3	1.13048863208295
SOCS3_mRNA	1.13048863208295
STAT1c	438012.962626961
STAT1Dimc	0
STAT1Dimerization	3.4217820804707
STAT1Dimn	0
STAT1_LC_1	402377.078184052
STAT1_LC_2	402377.078184052
STAT1_LC_3	402377.078184052
STAT1_mRNA	0.992592384600239
STAT1n	43801.2962626961
STAT2c	30108.189966684
STAT2_LC_1	2070.64740164233
STAT2_LC_2	2070.64740164233
STAT2_LC_3	2070.64740164233
STAT2_LC_4	2070.64740164233
STAT2_LC_5	2070.64740164233
STAT2_mRNA	0.852180088214821
STAT2n	3010.8189966684
STAT2STAT1c	0
STAT2STAT1n	0
synthIRF2_mRNA	0.693031342169068
synthIRF2_mRNAbasal	0.896277451406503
synthIRF9	397.439838901787
synthIRF9_mRNA	18.4757822158466
synthIRF9_mRNAbasal	0.363988103862363
synthSOCS1	0.755307636104949
synthSOCS1_mRNA	9.67327705991996
synthSOCS1_mRNAbasal	1.34686406176118
synthSOCS3	1121.48370895196
synthSOCS3_mRNA	0.0259998710151806
synthSOCS3_mRNAbasal	2.5125248201277
synthSTAT1	1624971.81016501
synthSTAT1_mRNA	3.96542173902869
synthSTAT1_mRNAbasal	0.221608213617645
synthSTAT2	4491.57817768937
synthSTAT2_mRNA	1.70793349614911
synthSTAT2_mRNAbasal	0.189397766191333
synthUSP18	1926.51142983314
synthUSP18_mRNA	3.12004825350251
synthUSP18_mRNAbasal	0.0651011658655035
totIRF9	1869.39777292661
TrLocIRF9c	298.095798704173
TrLocIRF9n	2980.95798704173
TrLocISGF3c	1.0154702333604
TrLocSTAT1c	0.0843439922335831
TrLocSTAT1Dimc	832.093709625105

TrLocSTAT1n	0.843439922335831
TrLocSTAT2c	0.24346909790605
TrLocSTAT2n	2.4346909790605
TrLocSTAT2STAT1c	0.225113042497788
UnbindIFN	0
USP18	1923.0939178005
USP18_LC_1	1922.35299477552
USP18_LC_2	1922.35299477552
USP18_mRNA	0.74572209107854

Parameter values for overexpression:

synthUSP18	1926.51142983314
synthUSP18_mRNA	3.12004825350251
synthUSP18_mRNAbasal	0.790290341984199
USP18	23345.2432035724
USP18_LC_1	23336.2488283871
USP18_LC_2	23336.2488283871
USP18_mRNA	9.05263306038449

Parameter values for USP18siRNA:

synthUSP18	1254.77132585051
synthUSP18_mRNA	0.194540239984718
synthUSP18_mRNAbasal	0.019771789055838
USP18	380.408920134611
USP18_LC_1	380.262357491348
USP18_LC_2	380.262357491348
USP18_mRNA	0.226482270832819

5.1.4 Profiles of estimated parameter values

Profile likelihood analysis of model parameters. 95%. 90% 68% confidence intervals are indicated.

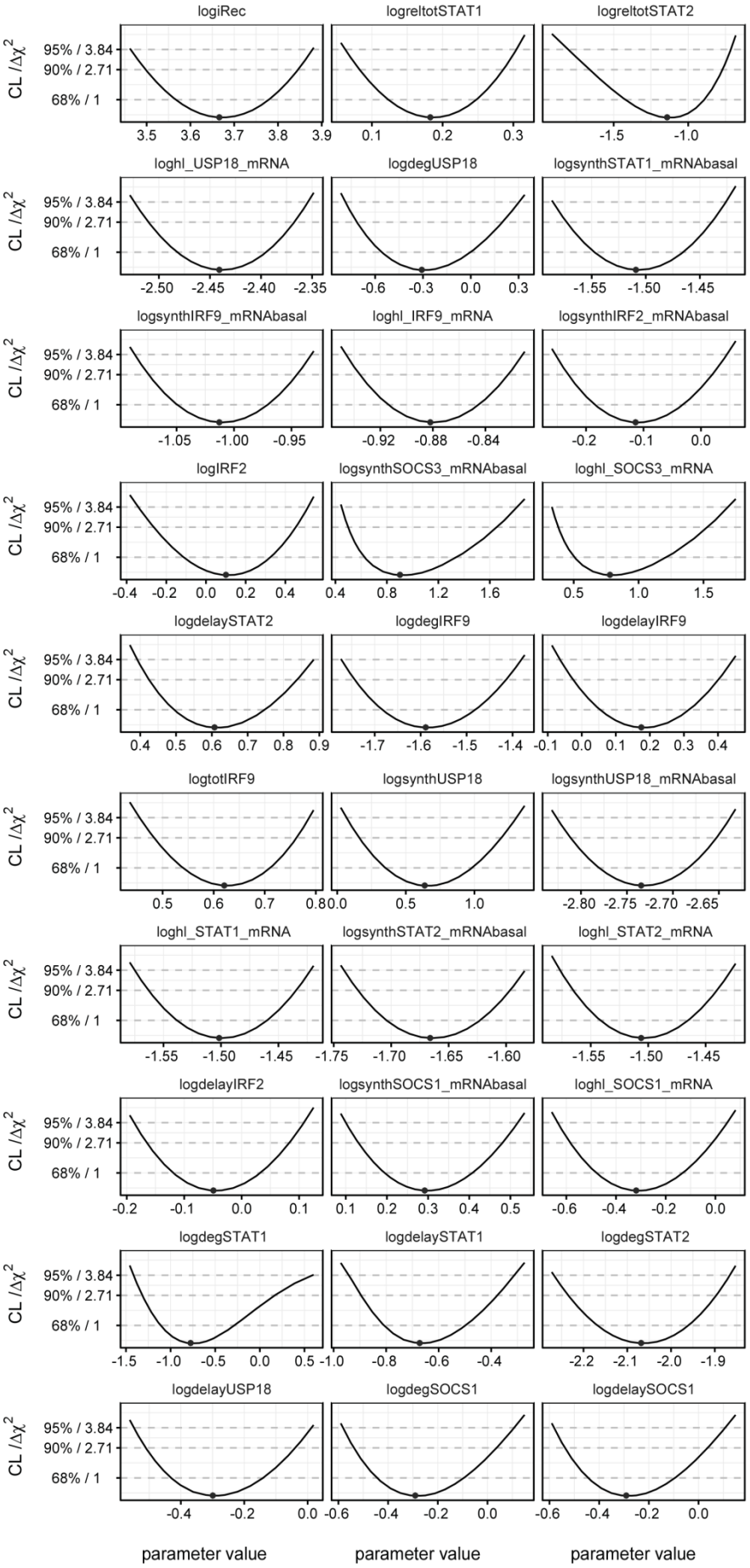
logiRec
logreltotSTAT1
logreltotSTAT2
loghl_USP18_mRNA
logdegUSP18
logsynthSTAT1_mRNAbasal
logsynthIRF9_mRNAbasal
loghl_IRF9_mRNA
logsynthIRF2_mRNAbasal
logIRF2
logsynthSOCS3_mRNAbasal
loghl_SOCS3_mRNA
logdelaySTAT2
logdegIRF9
logdelayIRF9
logtotIRF9
logsynthUSP18
logsynthUSP18_mRNAbasal
loghl_STAT1_mRNA
logsynthSTAT2_mRNAbasal
loghl_STAT2_mRNA
logdelayIRF2
logsynthSOCS1_mRNAbasal
loghl_SOCS1_mRNA
logdegSTAT1
logdelaySTAT1
logdegSTAT2
logdelayUSP18
logdegSOCS1
logdelaySOCS1
CL /Δχ²
95% / 3.84
90% / 2.71
68% / 1
parameter value

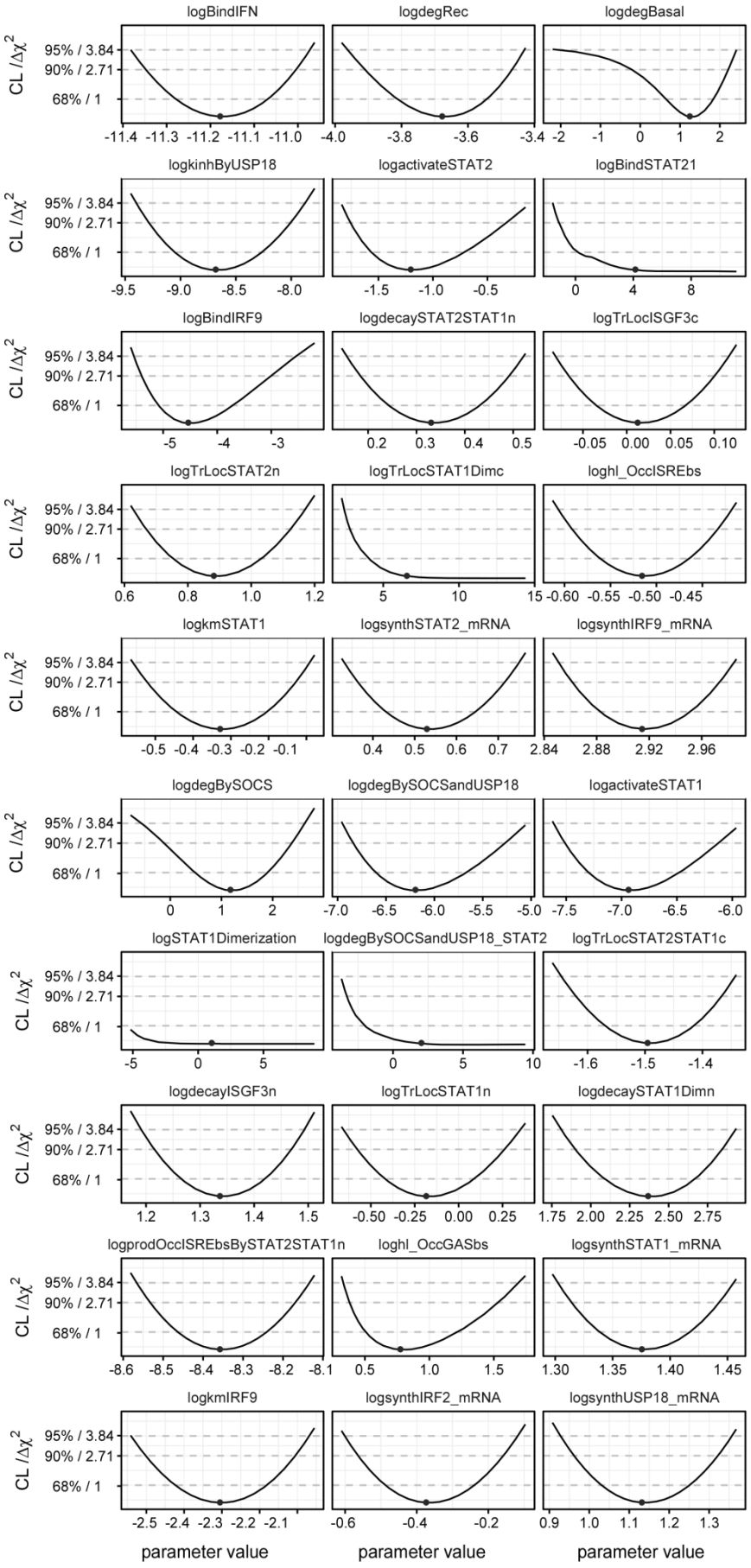
logBindIFN
logdegRec
logdegBasal
logkinhByUSP18
logactivateSTAT2
logBindSTAT21
logBindIRF9
logdecaySTAT2STAT1n
logTrLocISGF3c
logTrLocSTAT2n
logTrLocSTAT1Dimc
loghl_OccISREbs
logkmSTAT1
logsynthSTAT2_mRNA
logsynthIRF9_mRNA
logdegBySOCS
logdegBySOCSandUSP18
logactivateSTAT1
logSTAT1Dimerization
logdegBySOCSandUSP18_STAT2
logTrLocSTAT2STAT1c
logdecayISGF3n
logTrLocSTAT1n
logdecaySTAT1Dimn
logprodOccISREbsBySTAT2STAT1n
loghl_OccGASbs
logsynthSTAT1_mRNA
logkmIRF9
logsynthIRF2_mRNA
logsynthUSP18_mRNA
CL /Δχ²
95% / 3.84
90% / 2.71
68% / 1
parameter value

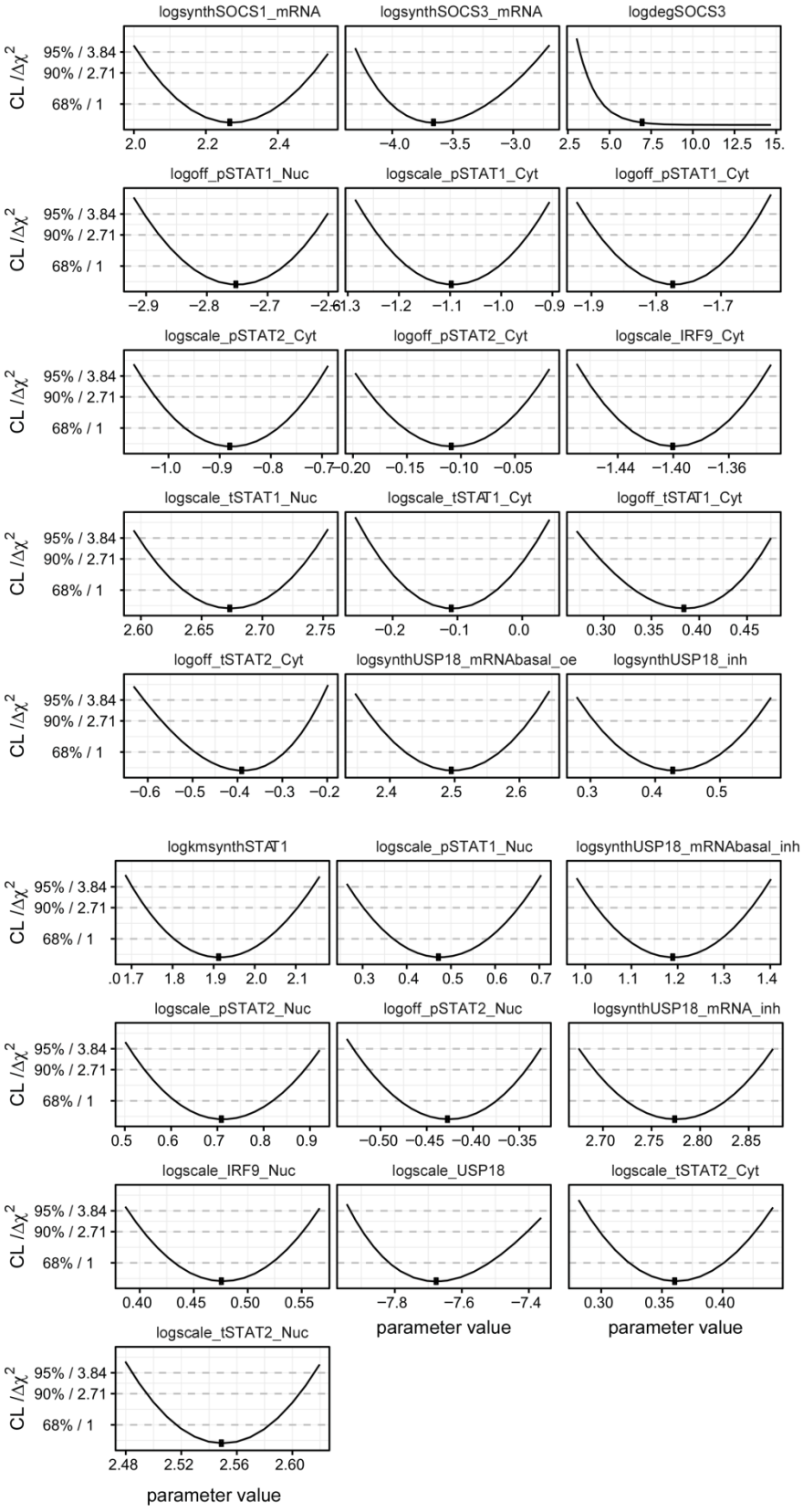
logsynthSOCS1_mRNA
logsynthSOCS3_mRNA
logdegSOCS3
logoff_pSTAT1_Nuc
logscale_pSTAT1_Cyt
logoff_pSTAT1_Cyt
logscale_pSTAT2_Cyt
logoff_pSTAT2_Cyt
logscale_IRF9_Cyt
logscale_tSTAT1_Nuc
logscale_tSTAT1_Cyt
logoff_tSTAT1_Cyt
logoff_tSTAT2_Cyt
logsynthUSP18_mRNAbasal_oe
logsynthUSP18_inh
logkmsynthSTAT1
logscale_pSTAT1_Nuc
logsynthUSP18_mRNAbasal_inh
logscale_pSTAT2_Nuc
logoff_pSTAT2_Nuc
logsynthUSP18_mRNA_inh
logscale_IRF9_Nuc
logscale_USP18
logscale_tSTAT2_Cyt
logscale_tSTAT2_Nuc
CL /Δχ²
95% / 3.84
90% / 2.71
68% / 1
parameter value

5.1.5 Likelihood waterfall plot

Likelihood waterfall plot displaying 100 fits ranked by their objective values.

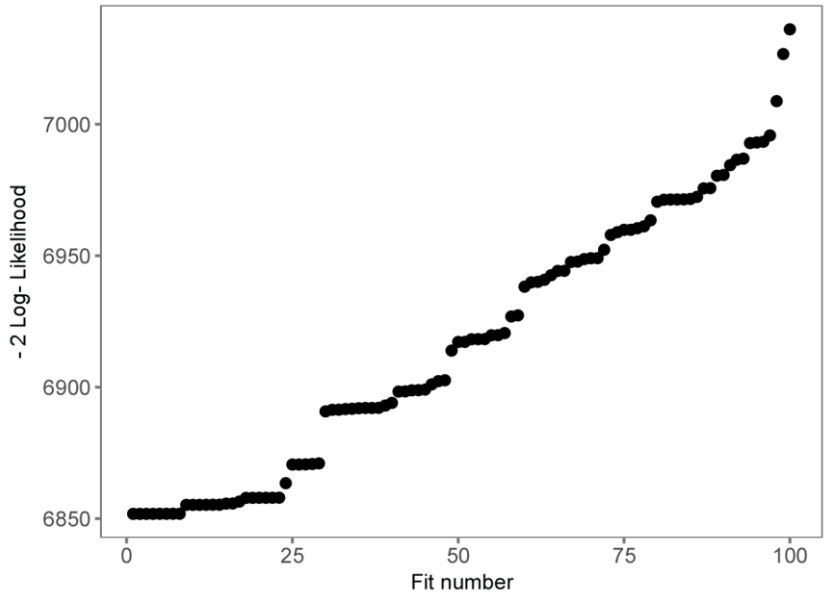

5.2 Additional experimental data belonging to the complete Huh7.5-IFNα dataset

The mathemathical model was calibrated with the complete dataset Huh7.5-IFNα consisting of 1918 scaled data points corresponding to 25 conditions of time- and IFNα-dose-resolved measurements on protein and mRNA level, combined with the number of molecules per cell analysis.

5.2.1 Dose- and time- resolved IFNα-induced signal transduction

Huh7.5 cells were growth-factor depleted and treated with different doses of IFNα. Cytoplasmic and nuclear lysates were subjected to quantitative immunoblotting and protein signals detected with chemoluminescence using a CCD-based camera. Data was normalized to reference proteins Calnexin or HDAC1 and represented by filled circles with errors representing 1σ confidence-interval estimated from biological replicates using an error model. Model trajectories are represented by the line.

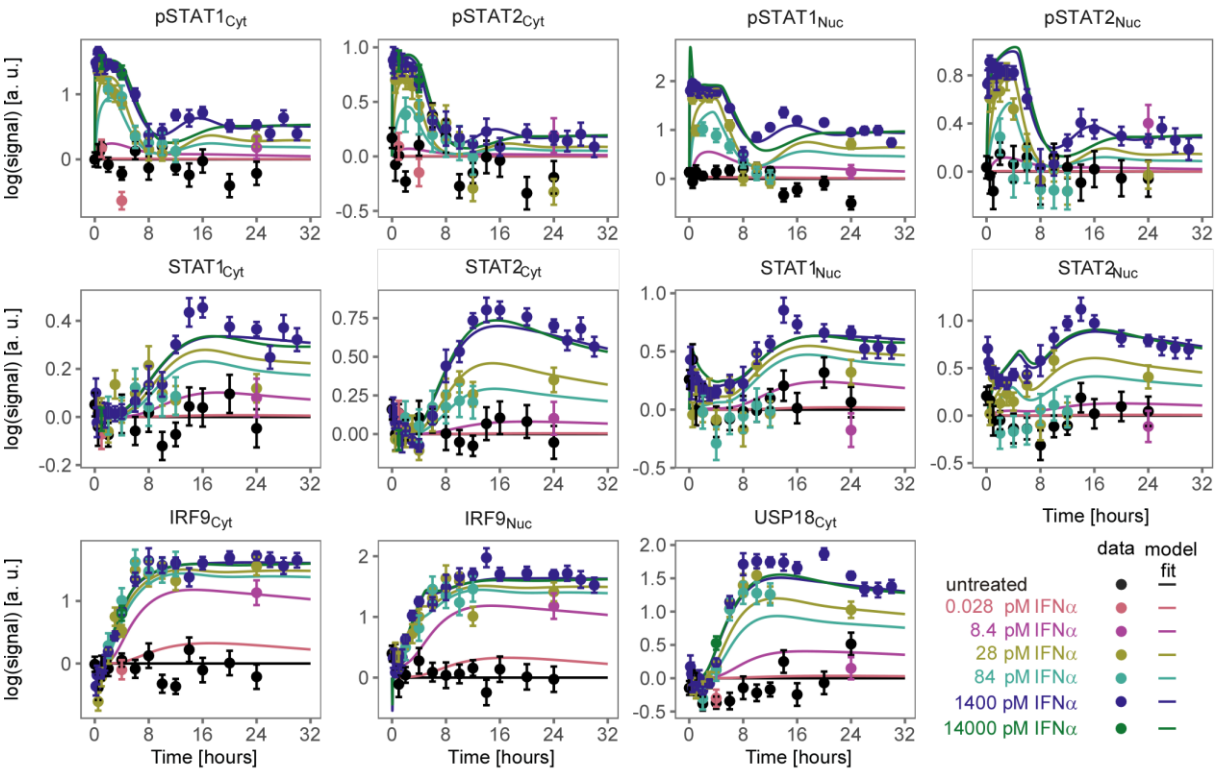

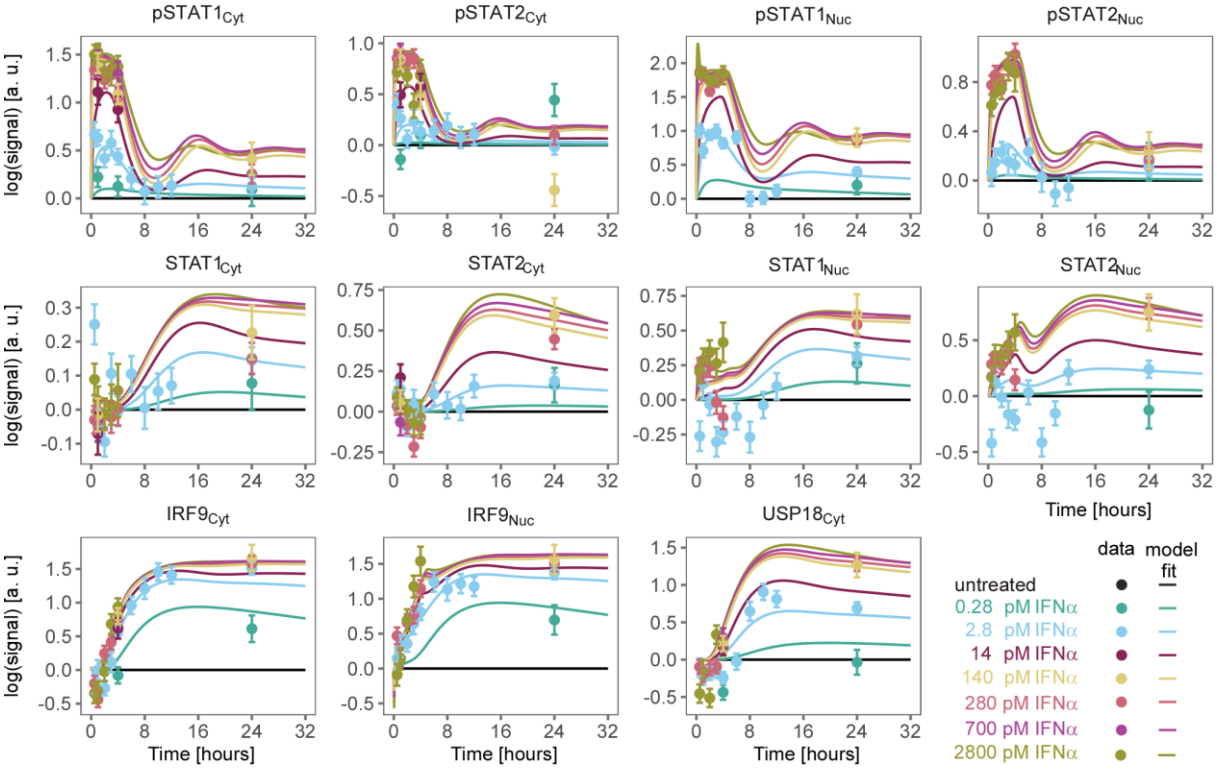

5.2.2 IFNα-induced expression of feedback genes

Growth-factor-depleted Huh7.5 cells were pre-treated with indicated doses IFNα or left untreated, after 24 hours cells were stimulated with 1400 pM IFNα or were left untreated. IFNα-induced expression of feedback genes was analyzed by quantitative RT-PCR. RNA levels were normalized to

the geometric mean of reference genes GAPDH, HPRT and TBP and were displayed as fold change. Experimental data is represented by filled circles with errors representing 1σ confidence-interval estimated from biological replicates (N=3 to N=14) using an error model. Model trajectories are represented by the line

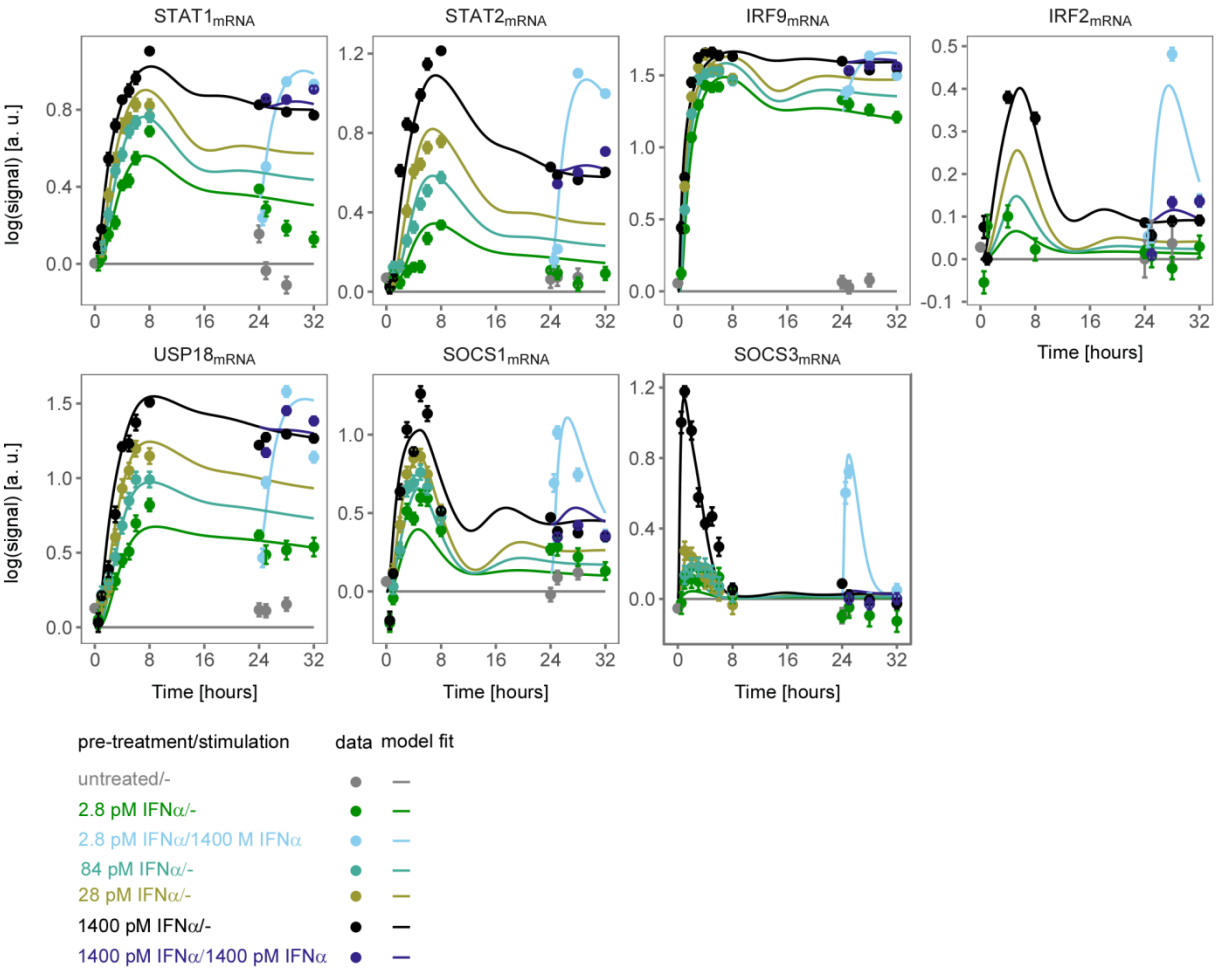

5.2.3 IFNα-induced stimulation in Huh7.5 cells pre-treated with different doses of IFNα

Growth-factor-depleted Huh7.5 were pre-treated with a range of 0.28 pM to 1400 pM IFNα for 24 hours and stimulated with 1400 or 2800 pM IFNα. IFNα-induced phosphorylation of nuclear STAT1 and STAT2 and expression of feedback proteins were analyzed by quantitative immunoblotting. Data was normalized to reference proteins Calnexin or HDAC1 and represented by filled circles with errors representing 1σ confidence-interval estimated from biological replicates A) (N=1 to N=19) using an error model. Model trajectories are represented by the line.

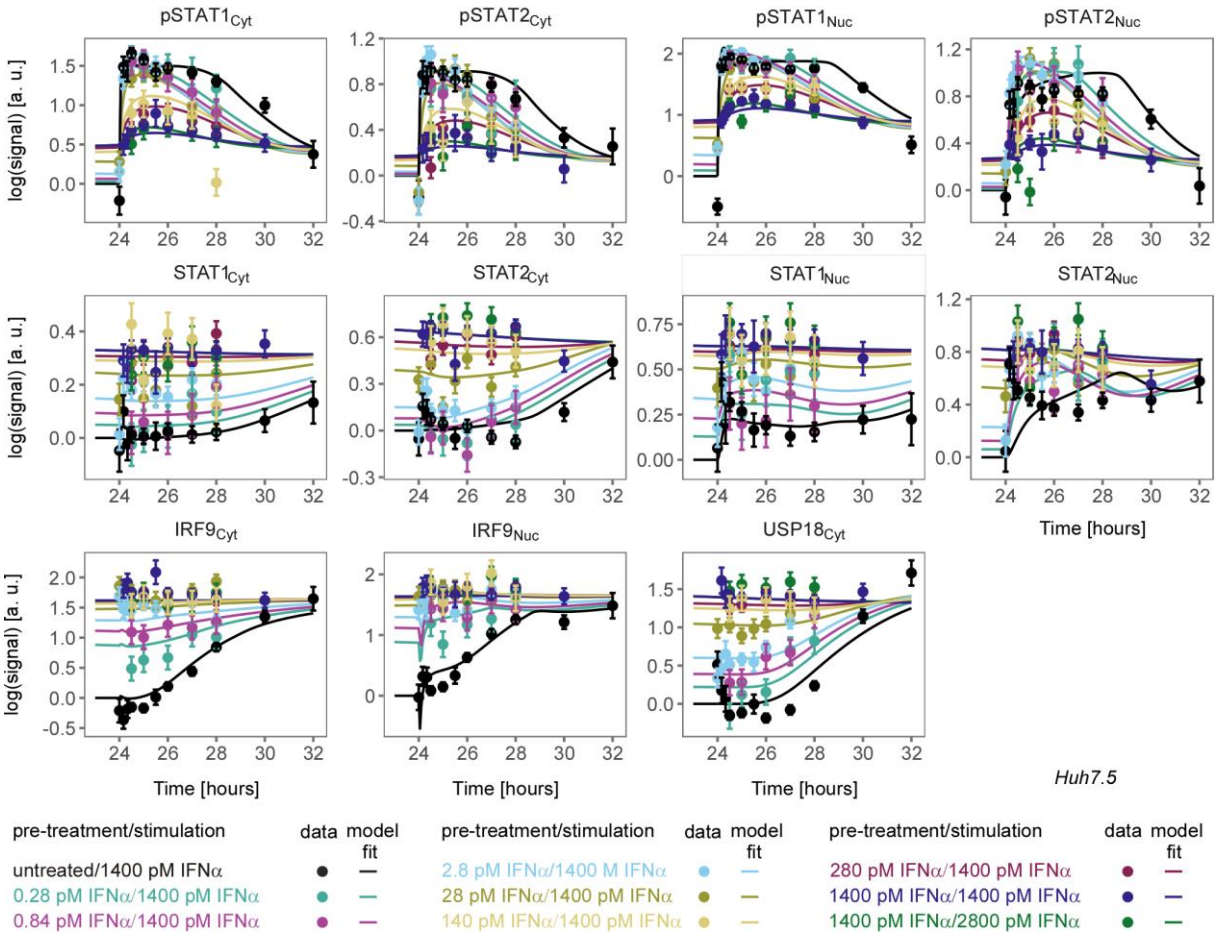

5.2.4 IFNα-induced signalling in USP18 siRNA transfected cells

Model fit and experimental data of Huh7.5 cells transfected with control or USP18 siRNA, growth-factor-depleted and pre-treated with 1400 pM IFNα, stimulated with 1400 PM IFNα or unstimulated. Experimental data of IFNα-induced phosphorylation of STAT1 and STAT2 and expression of STAT1, STAT2, IRF9 and USP18 were analyzed by quantitative immunoblotting using chemoluminescence and a CCD camera device (Imagequant). For model purposes data in control siRNA and untransfected Huh7.5 are combined to one condition. Data from multiple partially overlapping time courses scaled together is displayed as filled circles with errors representing 1σ confidence-interval estimated from biological replicates (N=3) using an error model. Line represents model trajectory.

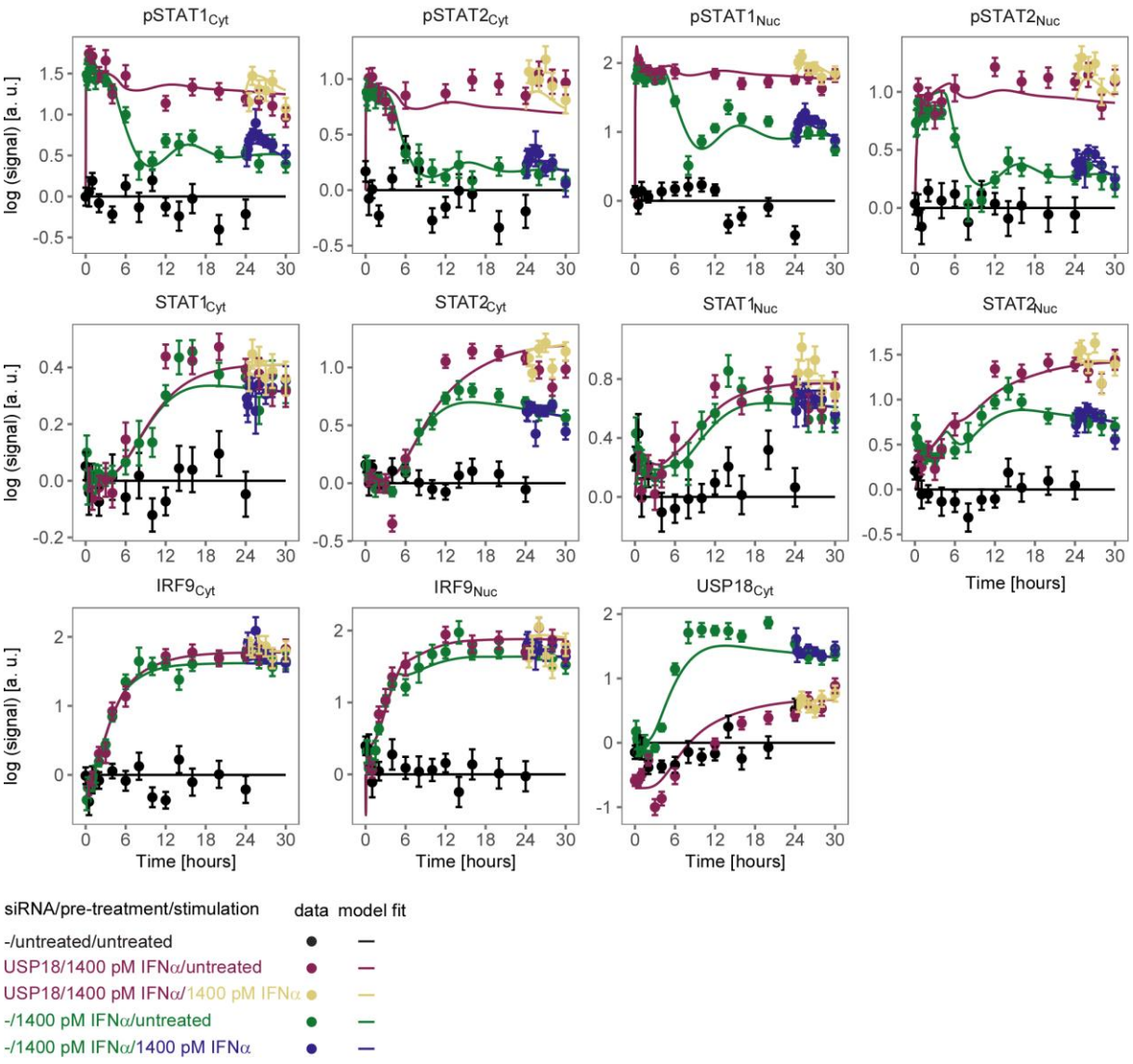

5.2.5 IFNα-induced signal transduction in Huh7.5-TetON-USP18

Model fit and experimental data of IFNα-induced phosphorylation in Huh7.5-TetON-USP18 treated with doxycyclin for 24 hours and stimulated with 1400 pM IFNα or Huh7.5 wildtype cells pre-treated with 0 or 1400 pM IFNα and stimulated with 1400 pM IFNα after 24 hours. Experimental data was obtained by quantitative immunoblotting using chemoluminescence and CCD camera device (Imagequant). For model purposes data Huh7.5-TetON empty vector control and untransduced Huh7.5 are combined to one condition. Data is displayed as filled circles with errors representing 1σ confidence-interval estimated from biological replicates (N=3) using an error model. Line represent model trajectory.

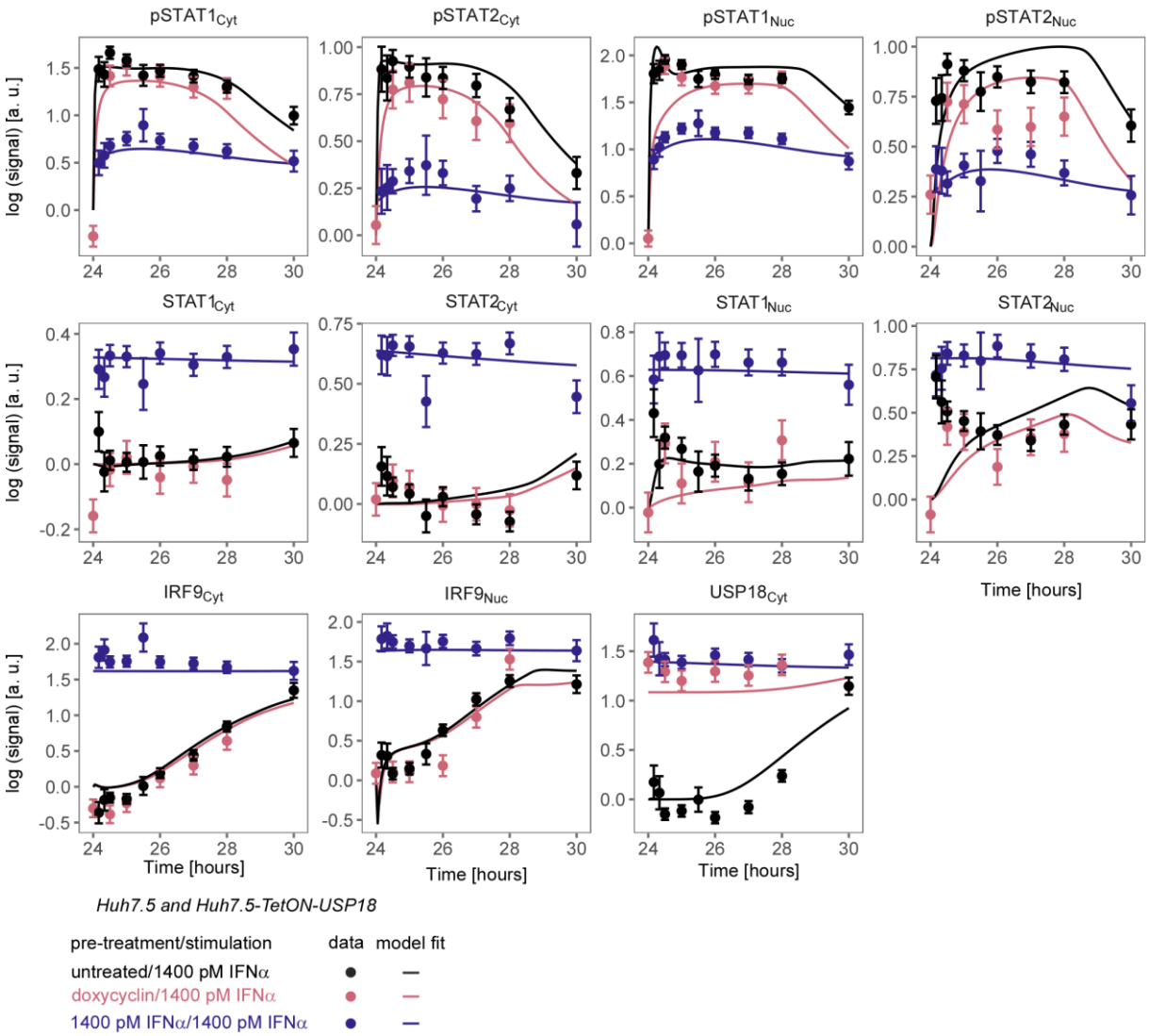

5.3 Complete dataset of Roferon-induced signal transduction in Huh7.5 and HepG2-hNTCP

To analyse Roferon induced signal transduction in Huh7.5 and HepG2-hNTCP, cell line specific synthesis rates and receptor abundances were estimated on 626 data points belonging to 35 conditions generated by Tamar Nizharadze (DKFZ) and Melissa Teusel (DKFZ). Cells were growth-factor depleted and stimulated with indicated amounts of Roferon or IFNα and analysed by quantitative immunoblotting.

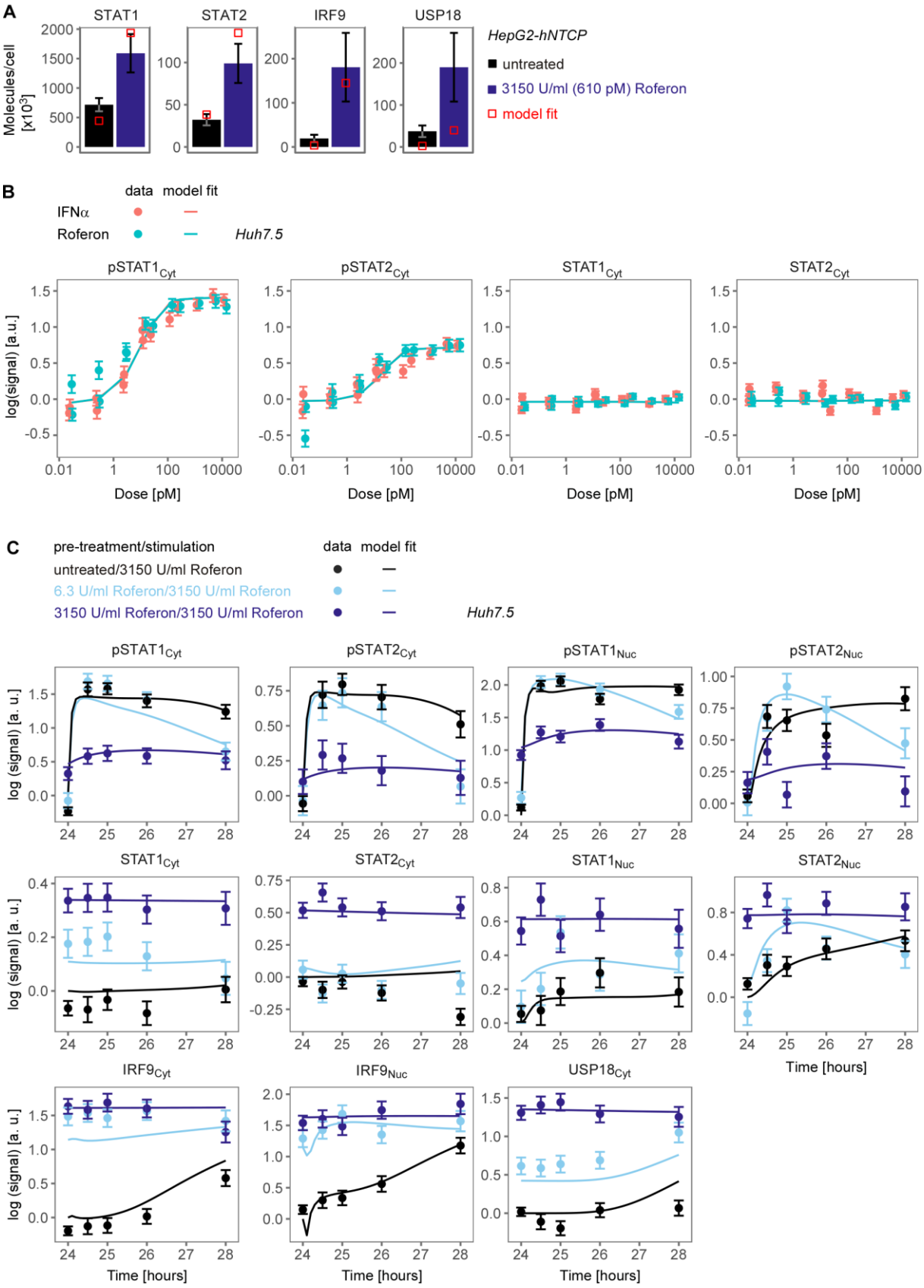
A
STAT1
STAT2
IRF9
USP18
Molecules/cell [x10^3]
HepG2-hNTCP
untreated
3150 U/ml (610 pM) Roferon
model fit
B
data model fit
IFNα
Roferon
Huh7.5
pSTAT1Cyt
pSTAT2Cyt
STAT1Cyt
STAT2Cyt
log(signal) [a.u.]
Dose [pM]
C
pre-treatment/stimulation
data model fit
untreated/3150 U/ml Roferon
6.3 U/ml Roferon/3150 U/ml Roferon
3150 U/ml Roferon/3150 U/ml Roferon
Huh7.5
pSTAT1Cyt
pSTAT2Cyt
pSTAT1Nuc
pSTAT2Nuc
STAT1Cyt
STAT2Cyt
STAT1Nuc
STAT2Nuc
IRF9Cyt
IRF9Nuc
USP18Cyt
log (signal) [a. u.]
Time [hours]

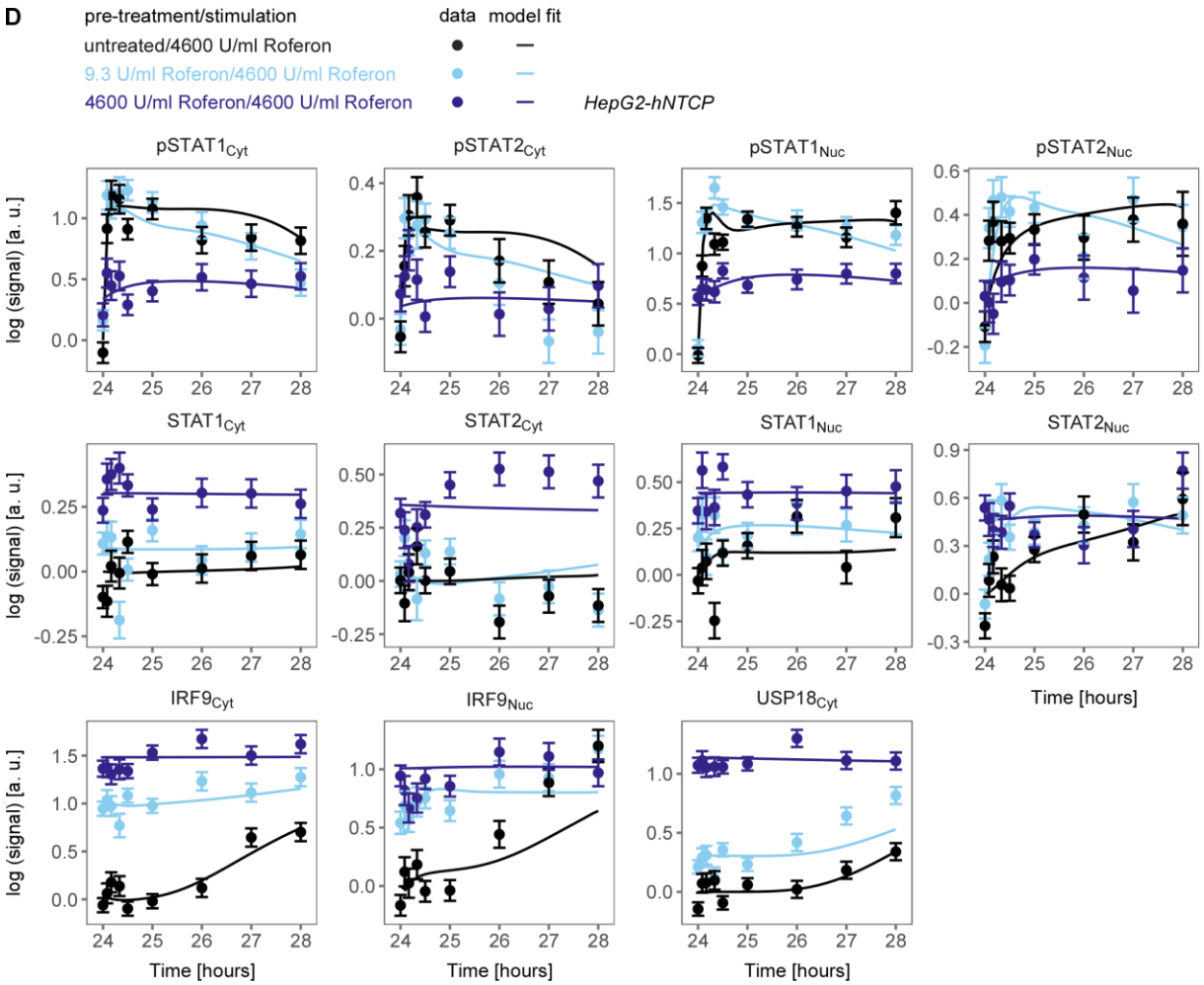
D
pre-treatment/stimulation
data
model fit
untreated/4600 U/ml Roferon
9.3 U/ml Roferon/4600 U/ml Roferon
4600 U/ml Roferon/4600 U/ml Roferon
HepG2-hNTCP
pSTAT1Cyt
pSTAT2Cyt
pSTAT1Nuc
pSTAT2Nuc
STAT1Cyt
STAT2Cyt
STAT1Nuc
STAT2Nuc
IRF9Cyt
IRF9Nuc
USP18Cyt
log (signal) [a. u.]
Time [hours]

5.4 Complete dataset of IFNα-induced signal transduction in primary human hepatocytes

To estimate patient-specific synthesis rates of STAT1, STAT2, IRF9 and USP18 with patient-specific receptor abundance, the following dataset comprising 382 data points belonging to 9 conditions was used.

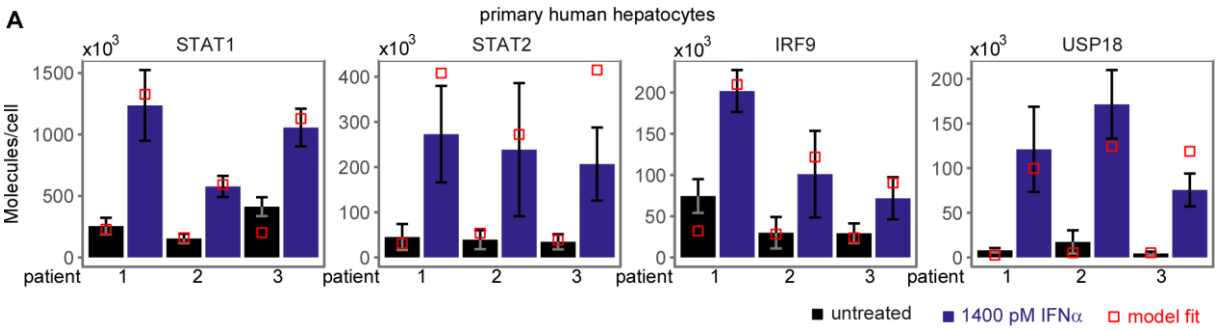

A) The amount of molecules per cell for STAT1, STAT2, IRF9 and USP18 were determined experimentally in primary human hepatocytes from three different patients. Cells were harvested after 24 hours pretreatment with 1400 pM IFNα or without pretreatment, and total cell lysates were spiked in with different amounts of protein calibrators and subjected to immunoblotting. Detection was performed with antibodies specific to STAT1, STAT2, IRF9 or USP18 using chemiluminescence on a CCD camera based device (Imagequant). Average of at least N=3 displayed with standard deviation. Quantitative immunoblotting was performed by Tamar Nizharadze. Red square indicates model fit.

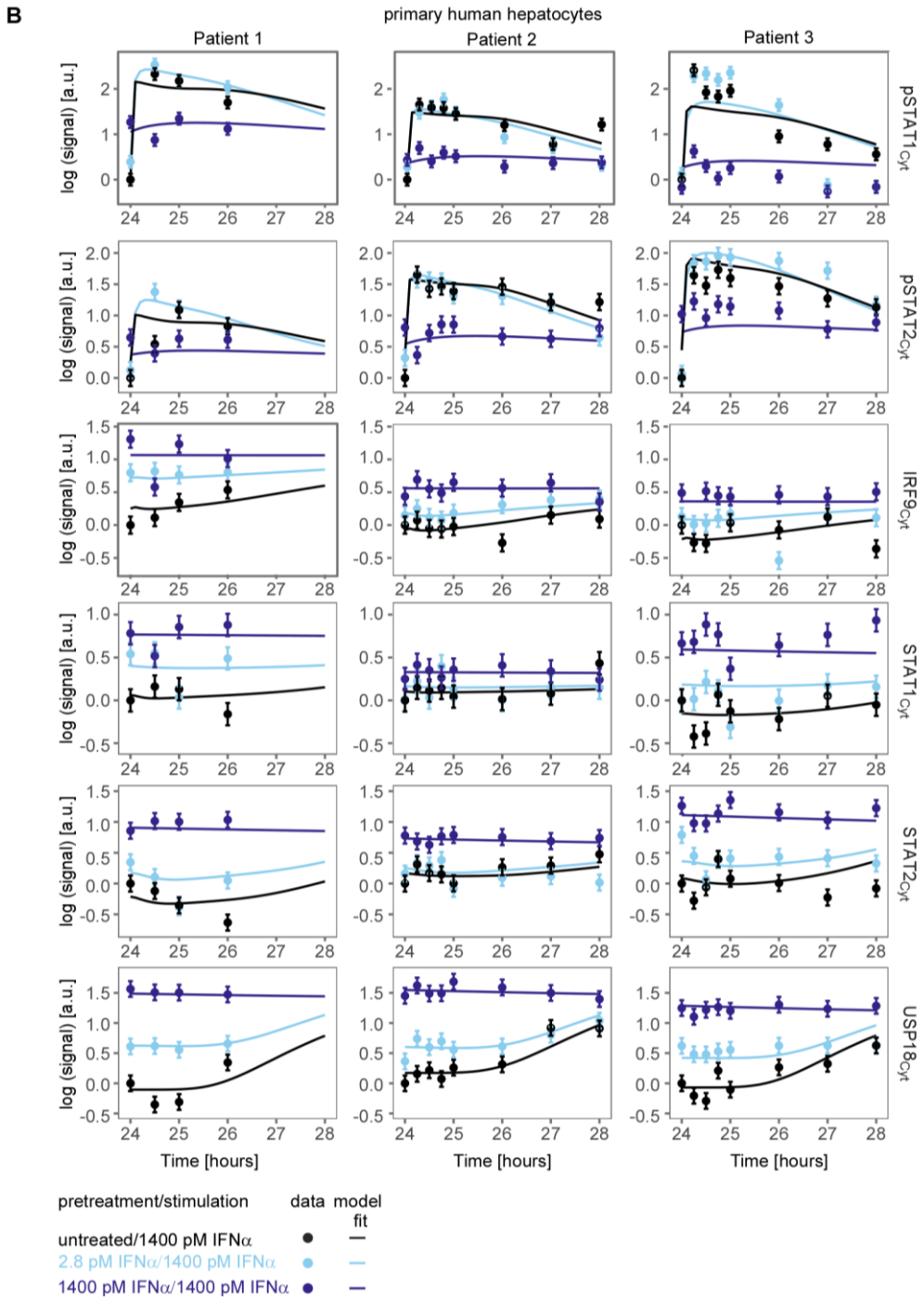

B) Experimental data and model fit of IFNα-induced phosphorylation of cytoplasmic STAT1 and STAT2 in growth-factor depleted primary human hepatocytes pretreated with 0, 2.8 pM or 1400 pM IFNα. Primary human hepatocytes from the same patients 1-3 as in panel B were used. Experimental data is represented by filled circles, per patient N=1. 30% errors were assumed. Lines indicate model fits.

Acknowledgements

First of all, I would like to thank Prof. Dr. Ursula Klingmüller for giving me the opportunity to work on this interdisciplinary project and encouraging me to grow in different fields. I'm very grateful for her support and advice on the project.
I would like to thank Prof. Dr. Ralf Bartenschlager for advice on the project, for acting as TAC member and for being the referee of this PhD thesis. Furthermore, I would like to thank Prof. Dr. Karsten Rippe and Prof. Dr. Jeroen Krijgsveld for acting as examiners, and I would like to thank Prof. Dr. Thomas Höfer for acting as TAC member.
I acknowledge funding from the DFG supported projects FOR1202 and Transregio 179.
This project would not have been possible without the dedication of Marcus Rosenblatt as mathematical modeler of the project. I enjoyed our elaborate discussions on the project and I am very grateful for learning so much from the modeling site! I would also like to thank Dr. Tim Maiwald, who introduced me to mathematical models as my modeling partner at the beginning of my thesis. Furthermore, I would like to thank Dr. Daniel Kaschek for nice discussions whenever I visited Freiburg, and I would like to thank Prof. Dr. Jens Timmer for his input for the project.
Very importantly I would like to thank everyone in the lab for the nice atmosphere. In particular, I would like to start with thanking Marcel for his contributions to the modeling discussions, discussions about technical aspects of experiments, his feedback on many abstracts and reports I wrote and patience for many questions and discussions. Secondly, I would like to thank Lorenza for all the effort she put in proofreading the thesis and TAC reports, for sharing her experience with primary human hepatocytes, for her support, thoughtfulness and always being positive.
Thirdly, I would like to thank Katharina, for helping me to get started at the DKFZ and teaching me the SOPs used in this lab including culturing Huh7.5, time-course experiments, quantitative immunoblotting and quantitative RT-PCR and being my go to person whenever I had question. Furthermore, I would also briefly like to thank her for teaching me to cook risotto! Box dinners started with Katharina, Marie, Florian and Lorenz and by now have expanded to many new box members. I would like to thank my box members for support, discussions, advice and happy memories. Specifically I would like to thank Florian for his advice on cloning and getting me acquainted in the S2 lab. Of course, I would like to thank Agus for sharing the liquid nitrogen duty with me-it definitely made refilling liquid nitrogen fun!- and for his advice about K_Ds.
I would like to thank Melissa and Tamar for contributing with their data to this thesis and the paper. And once more, I would like to thank Ursula as well for giving me the opportunity to supervise a bachelor student. I enjoyed supervising Tamar a lot. Touching upon the therapeutic IFN Roferon, I would like to thank Christopher Dächert for the titration experiments to determine equipotent doses of the different interferons and calibration to the IFNα standard. I would like to thank Dr. Marco Binder for interesting discussions from the viral perspective. Furthermore, I would like to thank Antje Reuter and Silke Bender to get me acquainted in the field of virology.
Of course, I would like to acknowledge Dr. Georg Damm and Prof. Dr. med. Kathrin Hoffmann together with Artyom and Marvin for preparing the primary human hepatocytes used in this study.
And I would like to thank Marvin, Sandra, Susen and Lena + azubis for preparing reagents and buffers in the lab and Martina for her help with traveling arrangements.
Furthermore, I would also like to acknowledge the collaborations of the two projects that were unsuccessful: CRISPR/Cas9 KnockIn cell line of tagged IFNAR1 with Siegfried Hänselmann and quantification of SOCS1 by targeted Mass Spectrometry with Markus Stepath.

I would like to thank my best friend Anne who knows as fellow PhD student and tea-drinking-enthusiast how to create perfect conditions for hanging in there while writing your thesis.
And lastly, but far from least, I am very grateful for the support from my parents and fiancée Sebastiaan, or Seb as most of my colleagues know him. They are always at the ready with their supporting words when things do not go the way I wish them to go. Jullie steun is niet in woorden uit te drukken, jullie drie zijn mijn helden.

Bibliography

Adlung L, Kar S, Wagner M-C, She B, Chakraborty S, Bao J, Lattermann S, Boerries M, Busch H, Wuchter P, Ho AD, Timmer J, Schilling M, Höfer T & Klingmüller U (2017) Protein abundance of AKT and ERK pathway components governs cell type-specific regulation of proliferation. *Mol. Syst. Biol.* **13:** 904

Alon U (2006) An Introduction to Systems Biology: Design Principles of Biological Circuits Chapman and Hall/CRC

Arimoto K, Löchte S, Stoner SA, Burkart C, Zhang Y, Miyauchi S, Wilmes S, Fan J-B, Heinisch JJ, Li Z, Yan M, Pellegrini S, Colland F, Piehler J & Zhang D-E (2017a) STAT2 is an essential adaptor in USP18-mediated suppression of type I interferon signaling. *Nat. Struct. Mol. Biol.***:** 1–7

Arimoto K, Löchte S, Stoner SA, Burkart C, Zhang Y, Miyauchi S, Wilmes S, Fan J-B, Heinisch JJ, Li Z, Yan M, Pellegrini S, Colland F, Piehler J & Zhang D-E (2017b) STAT2 is an essential adaptor in USP18-mediated suppression of type I interferon signaling. *Nat. Struct. Mol. Biol.*

Arora T, Liu B, He H, Kim J, Murphy TL, Murphy KM, Modlin RL & Shuai K (2003) PIASx Is a Transcriptional Co-repressor of Signal Transducer and Activator of Transcription 4. *J. Biol. Chem.* **278:** 21327–21330

Ashour J, Laurent-Rolle M, Shi P-Y & García-Sastre A (2009) NS5 of dengue virus mediates STAT2 binding and degradation. *J. Virol.* **83:** 5408–18

Bachmann J, Raue A, Schilling M, Bohm ME, Kreutz C, Kaschek D, Busch H, Gretz N, Lehmann WD, Timmer J & Klingmuller U (2011) Division of labor by dual feedback regulators controls JAK2/STAT5 signaling over broad ligand range. *Mol. Syst. Biol.* **7:** 516–516

Banninger G & Reich NC (2004) STAT2 nuclear trafficking. *J. Biol. Chem.* **279:** 39199–206

Bartosch B (2010) Hepatitis B and C viruses and hepatocellular carcinoma. *Viruses* **2:** 1504–1509

Bazan JF (1990a) Shared architecture of hormone binding domains in type I and II interferon receptors. *Cell* **61:** 753–4

Bazan JF (1990b) Haemopoietic receptors and helical cytokines. *Immunol. Today* **11:** 350–4

Bellecave P & Sarasin-Filipowicz M (2010) Cleavage of mitochondrial antiviral signaling protein in the liver of patients with chronic hepatitis C correlates with a reduced activation of the endogenous. …

Benno Müller-Hill (1996) The Lac Operon: A Short History of a Genetic Paradigm - Benno Müller-Hill - Google Books Walter de Gruyter, Berlin, Germany

Berke IC & Modis Y (2012) MDA5 cooperatively forms dimers and ATP-sensitive filaments upon binding double-stranded RNA. *EMBO J.* **31:** 1714–26

Berke IC, Yu X, Modis Y & Egelman EH (2012) MDA5 assembles into a polar helical filament on dsRNA. *Proc. Natl. Acad. Sci. U. S. A.* **109:** 18437–41

Biron CA, Nguyen KB, Pien GC, Cousens LP & Salazar-Mather TP (1999) NATURAL KILLER CELLS IN ANTIVIRAL DEFENSE: Function and Regulation by Innate Cytokines. *Annu. Rev. Immunol* **17:** 189–220

Blight KJ, Mckeating JA & Rice CM (2002) Highly Permissive Cell Lines for Subgenomic and Genomic Hepatitis C Virus RNA Replication. *J. Virol.* **76:** 13001–13014

Bluyssen HAR & Levy DE (1997) Stat2 is a transcriptional activator that requires sequence-specific contacts provided by Stat1 and p48 for stable interaction with DNA. *J. Biol. Chem.* **272:** 4600–4605

De Boissieu D, Lebon P, Badoual J, Bompard Y & Dupont C (1993) Rotavirus induces alpha-interferon release in children with gastroenteritis. *J. Pediatr. Gastroenterol. Nutr.* **16:** 29–32

Bolen CR, Ding S, Robek MD & Kleinstein SH (2014) Dynamic expression profiling of type I and type III interferon-stimulated hepatocytes reveals a stable hierarchy of gene expression. *Hepatology* **59:** 1262–1272

Braun D, Caramalho I & Demengeot J (2002) IFN-alpha/beta enhances BCR-dependent B cell responses. *Int. Immunol.* **14:** 411–9

Bruns AM, Leser GP, Lamb RA & Horvath CM (2014) The Innate Immune Sensor LGP2 Activates Antiviral Signaling by Regulating MDA5-RNA Interaction and Filament Assembly. *Mol. Cell* **55:** 771–781

Burkart C, Fan J-B & Zhang D-E (2012) Two independent mechanisms promote expression of an N-terminal truncated USP18 isoform with higher DeISGylation activity in the nucleus. *J. Biol. Chem.* **287:** 4883–93

Burrill DR & Silver PA (2010) Making Cellular Memories. *Cell* **140:** 13–18

Cabibbo G & Craxì A (2010) Epidemiology, risk factors and surveillance of hepatocellular carcinoma. *Eur. Rev. Med. Pharmacol. Sci.* **14:** 352–5

Campos Appel-Da-Silva M, Aparecida S, Miozzo S, De I, Dossin A, Tovo CV, Branco F & Alves De Mattos A (2016) Incidence of hepatocellular carcinoma in outpatients with cirrhosis in Brazil: A 10-year retrospective cohort study Retrospective Study. *World J Gastroenterol* **22:** 10219–10225

Castro F, Dirks WG, Fähnrich S, Hotz-Wagenblatt A, Pawlita M & Schmitt M (2013) High-throughput SNP-based authentication of human cell lines. *Int. J. Cancer* **132:** 308–314

Chandra PK, Bao L, Song K, Aboulnasr FM, Baker DP, Shores N, Wimley WC, Liu S, Hagedorn CH, Fuchs SY, Wu T, Balart L a & Dash S (2014) HCV infection selectively impairs type I but not type III IFN signaling. *Am. J. Pathol.* **184:** 214–29

Chariot A, Leonardi A, Muller J, Bonif M, Brown K & Siebenlist U (2002) Association of the adaptor TANK with the I kappa B kinase (IKK) regulator NEMO connects IKK complexes with IKK epsilon and TBK1 kinases. *J. Biol. Chem.* **277:** 37029–36

Chen L, Borozan I, Feld J, Sun J, Tannis L-L, Coltescu C, Heathcote J, Edwards AM & McGilvray ID (2005) Hepatic Gene Expression Discriminates Responders and Nonresponders in Treatment of Chronic Hepatitis C Viral Infection. *Gastroenterology* **128:** 1437–1444

Chen WW, Niepel M & Sorger PK (2010) Classic and contemporary approaches to modeling biochemical reactions. *Genes Dev.* **24:** 1861–1875

Chen XP, Losman JA & Rothman P (2000) SOCS proteins, regulators of intracellular signaling. *Immunity* **13:** 287–290

Cheon H, Holvey-Bates EG, Schoggins JW, Forster S, Hertzog P, Imanaka N, Rice CM, Jackson MW, Junk DJ & Stark GR (2013) IFNβ-dependent increases in STAT1, STAT2, and IRF9 mediate resistance to viruses and DNA damage. *EMBO J.* **32:** 2751–63

Cheon H & Stark GR (2009) Unphosphorylated STAT1 prolongs the expression of interferon-induced immune regulatory genes. *Proc. Natl. Acad. Sci. U. S. A.* **106:** 9373–8

Chmiest D, Sharma N, Zanin N, Viaris de Lesegno C, Shafaq-Zadah M, Sibut V, Dingli F, Hupé P, Wilmes S, Piehler J, Loew D, Johannes L, Schreiber G & Lamaze C (2016) Spatiotemporal control of interferon-induced JAK/STAT signalling and gene transcription by the retromer complex. *Nat. Commun.* **7:** 13476

Chung CD, Liao J, Liu B, Rao X, Jay P, Berta P & Shuai K (1997) Specific inhibition of Stat3 signal transduction by PIAS3. *Science* **278:** 1803–5

Cohen B, Novick D, Barak S & Rubinstein M (1995) Ligand-induced association of the type I interferon receptor components. *Mol. Cell. Biol.* **15:** 4208–14

Cohen HT & McGovern FJ (2005) Renal-Cell Carcinoma. *N. Engl. J. Med.* **353:** 2477–2490

Colonna M, Cella M, Jarrossay D, Facchetti F, Alebardi O, Nakajima H & Lanzavecchia A (1999) Plasmacytoid monocytes migrate to inflamed lymph nodes and produce large amounts of type I interferon. *Nat. Med.* **5:** 919–923

Conrady CD, Zheng M, Mandal NA, van Rooijen N & Carr DJJ (2013) IFN-α-driven CCL2 production recruits inflammatory monocytes to infection site in mice. *Mucosal Immunol.* **6:** 45–55

Cowan AE, Moraru II, Schaff JC, Slepchenko BM & Loew LM (2012) Spatial modeling of cell signaling networks. *Methods Cell Biol.* **110:** 195–221

Crow YJ, Hayward BE, Parmar R, Robins P, Leitch A, Ali M, Black DN, van Bokhoven H, Brunner HG, Hamel BC, Corry PC, Cowan FM, Frints SG, Klepper J, Livingston JH, Lynch SA, Massey RF, Meritet JF, Michaud JL, Ponsot G, et al (2006a) Mutations in the gene encoding the 3'-5' DNA exonuclease TREX1 cause Aicardi-Goutières syndrome at the AGS1 locus. *Nat. Genet.* **38:** 917–920

Crow YJ, Leitch A, Hayward BE, Garner A, Parmar R, Griffith E, Ali M, Semple C, Aicardi J, Babul-Hirji R, Baumann C, Baxter P, Bertini E, Chandler KE, Chitayat D, Cau D, Déry C, Fazzi E, Goizet C, King MD, et al (2006b) Mutations in genes encoding ribonuclease H2 subunits cause Aicardi-Goutières syndrome and mimic congenital viral brain infection. *Nat. Genet.* **38:** 910–916

Crow YJ & Manel N (2015) Aicardi–Goutières syndrome and the type I interferonopathies. *Nat. Rev. Immunol.* **15:** 429–440

Dabo S & Meurs EF (2012) dsRNA-dependent protein kinase PKR and its role in stress, signaling and HCV infection. *Viruses* **4:** 2598–635

Darnell JE, Kerr IM & Stark GR (1994) Jak-STAT pathways and transcriptional activation in response to IFNs and other extracellular signaling proteins. *Science* **264:** 1415–21

Decker T, Lew DJ & Darnell JE (1991) Two Distinct Alpha-Interferon-Dependent Signal Transduction Pathways May Contribute to Activation of Transcription of the Guanylate-Binding Protein Gene. *EMBO J. Mol. Cell. Biol* **11:** 182–191

Der SD, Zhou A, Williams BRG & Silverman RH (1998) Identification of genes differentially regulated by interferon alpha, beta, or gamma using oligonucleotide arrays. *Proc. Natl. Acad. Sci.* **95:** 15623–8

Dérijard B, Hibi M, Wu IH, Barrett T, Su B, Deng T, Karin M & Davis RJ (1994) JNK1: a protein kinase stimulated by UV light and Ha-Ras that binds and phosphorylates the c-Jun activation domain. *Cell* **76:** 1025–37

Dhalluin C, Ross A, Huber W, Gerber P, Brugger D, Gsell B & Senn H (2005) Structural, Kinetic, and

Thermodynamic Analysis of the Binding of the 40 kDa PEG−Interferon-α 2 a and Its Individual Positional Isomers to the Extracellular Domain of the Receptor IFNAR2. *Bioconjug. Chem.* **16:** 518–527

Díaz MO, Pomykala HM, Bohlander SK, Maltepe E, Malik K, Brownstein B & Olopade OI (1994) Structure of the Human Type-I Interferon Gene Cluster Determined from a YAC Clone Contig. *Genomics* **22:** 540–552

Domanski P, Witte M, Kellum M, Rubinstein M, Hackett R, Pitha P & Colamonici OR (1995) Cloning and expression of a long form of the beta subunit of the interferon alpha beta receptor that is required for signaling. *J. Biol. Chem.* **270:** 21606–11

Dragan AI, Hargreaves V V, Makeyeva EN & Privalov PL (2007) Mechanisms of activation of interferon regulator factor 3: the role of C-terminal domain phosphorylation in IRF-3 dimerization and DNA binding. *Nucleic Acids Res.* **35:** 3525–34

Eisen H, Brachet P, Pereira Da Silva L & Jacobt F (1970) Regulation of Repressor Expression in lambda. *Proc. Natl. Acad. Sci.* **66:** 855–862

Elena SF SR (2005) Adaptive Value of High Mutation Rates of RNA Viruses: Separating Causes from Consequences. *J. Virol.* **79:** 11555–11558

Ellis MJ & Goodbourn S (1994) NF-kappa B-independent activation of beta-interferon expression in mouse F9 embryonal carcinoma cells. *Nucleic Acids Res.* **22:** 4489–96

Endo TA, Masuhara M, Yokouchi M, Suzuki R, Sakamoto H, Mitsui K, Matsumoto A, Tanimura S, Ohtsubo M, Misawa H, Miyazaki T, Leonor N, Taniguchi T, Fujita T, Kanakura Y, Komiya S & Yoshimura A (1997) A new protein containing an SH2 domain that inhibits JAK kinases. *Nature* **387:** 921–924

Erlandsson L, Blumenthal R, Eloranta M-L, Engel H, Alm G, Weiss S & Leanderson T (1998) Interferon-b is required for interferon-a production in mouse fibroblasts. *Curr. Biol.* **8:** 223–226

Fagerlund R, Mélen K, Kinnunen L & Julkunen I (2002) Arginine/lysine-rich nuclear localization signals mediate interactions between dimeric STATs and importin alpha 5. *J. Biol. Chem.* **277:** 30072–8

Ferrell JE (2002) Self-perpetuating states in signal transduction: Positive feedback, double-negative feedback and bistability. *Curr. Opin. Cell Biol.* **14:** 140–148

Ferreon JC, Ferreon ACM, Li K & Lemon SM (2005) Molecular Determinants of TRIF Proteolysis Mediated by the Hepatitis C Virus NS3/4A Protease. *J. Biol. Chem.* **280:** 20483–20492

Filippakopoulos P, Müller S & Knapp S (2009) SH2 domains: modulators of nonreceptor tyrosine kinase activity. *Curr. Opin. Struct. Biol.* **19:** 643–9

Fitzgerald KA, McWhirter SM, Faia KL, Rowe DC, Latz E, Golenbock DT, Coyle AJ, Liao S-M & Maniatis T (2003) IKKε and TBK1 are essential components of the IRF3 signaling pathway. *Nat. Immunol.* **4:** 491–496

Ford E & Thanos D (2010) The transcriptional code of human IFN-Beta gene expression. *Biochim. Biophys. Acta - Gene Regul. Mech.* **1799:** 328–336

Francois-Newton V, Livingstone M, Payelle-Brogard B, Uzé G & Pellegrini S (2012) USP18 establishes the transcriptional and anti-proliferative interferon α/β differential. *Biochem. J.* **446:** 509–516

François-Newton V, Magno de Freitas Almeida G, Payelle-Brogard B, Monneron D, Pichard-Garcia L, Piehler J, Pellegrini S & Uzé G (2011) USP18-based negative feedback control is induced by type I and type III interferons and specifically inactivates interferon α response. *PLoS One* **6:** e22200

Fried MW (2002) Side effects of therapy of hepatitis C and their management. *Hepatology* **36:** 237–244

Friedman RM (2008) Clinical uses of interferons. *Br. J. Clin. Pharmacol.* **65:** 158–62

Gao B, Wang H, Lafdil F & Feng D (2012) STAT proteins - Key regulators of anti-viral responses, inflammation, and tumorigenesis in the liver. *J. Hepatol.* **57:** 430–441

García-Sastre A (2017) Ten Strategies of Interferon Evasion by Viruses. *Cell Host Microbe* **22:** 176–184

García MA, Gil J, Ventoso I, Guerra S, Domingo E, Rivas C & Esteban M (2006) Impact of protein kinase PKR in cell biology: from antiviral to antiproliferative action. *Microbiol. Mol. Biol. Rev.* **70:** 1032–60

García MA, Meurs EF & Esteban M (2007) The dsRNA protein kinase PKR: Virus and cell control. *Biochimie* **89:** 799–811

Gerein V, Rastorguev E, Gerein J, Jecker P & Pfister H (2005) Use of Interferon-Alpha in Recurrent Respiratory Papillomatosis: 20-Year Follow-up. *Ann. Otol. Rhinol. Laryngol.* **114:** 463–471

Ghosh JK & Samanta T (2001) Model selection – An overview. *Curr. Sci.* **80:**

Goubau D, Deddouche S & Reis e Sousa C (2013a) Cytosolic Sensing of Viruses. *Immunity* **38:** 855–869

Goubau D, Deddouche S & Reis e Sousa C (2013b) Cytosolic Sensing of Viruses. *Immunity* **38:** 855–869

Gupta S, Campbell D, Dérijard B & Davis RJ (1995) Transcription factor ATF2 regulation by the JNK signal transduction pathway. *Science* **267:** 389–93

Hancock EJ, Ang J, Papachristodoulou A & Stan GB (2017) The Interplay between Feedback and Buffering in Cellular Homeostasis. *Cell Syst.* **5:** 498–508.e23

Haque SJ & Sharma P (2006) Interleukins and STAT signaling. *Vitam. Horm.* **74:** 165–206

Harada H, Fujita T, Miyamoto M, Kimura Y, Maruyama M, Furia A, Miyata T & Taniguchi T (1989) Structurally similar but functionally distinct factors, IRF-1 and IRF-2, bind to the same regulatory elements of IFN and IFN-inducible genes. *Cell* **58:** 729–39

Harada H, Takahashi E, Itoh S, Harada K, Hori TA & Taniguchi T (1994) Structure and regulation of the human interferon regulatory factor 1 (IRF-1) and IRF-2 genes: implications for a gene network in the interferon system. *Mol. Cell. Biol.* **14:** 1500–9

Hardy MP, Owczarek CM, Jermiin LS, Ejdebäck M & Hertzog PJ (2004) Characterization of the type I interferon locus and identification of novel genes☆. *Genomics* **84:** 331–345

Hoeve J ten (2002) Identification of a nuclear Stat1 protein tyrosine phosphatase. *… Cell. Biol.* **22:** 5662–5668

Honda K, Takaoka A & Taniguchi T (2006) Type I Inteferon Gene Induction by the Interferon Regulatory Factor Family of Transcription Factors. *Immunity* **25:** 349–360

Hoofnagle JH & Seeff LB (2006) Peginterferon and ribavirin for chronic hepatitis C. *N. Engl. J. Med.* **355:** 2444–2451

Hornung G & Barkai N (2008) Noise propagation and signaling sensitivity in biological networks: a role for positive feedback. *PLoS Comput. Biol.* **4:** e8

Hou F, Sun L, Zheng H, Skaug B, Jiang QX & Chen ZJ (2011) MAVS forms functional prion-like aggregates to activate and propagate antiviral innate immune response. *Cell* **146:** 448–461

Hu X, Herrero C, Li W-P, Antoniv TT, Falck-Pedersen E, Koch AE, Woods JM, Haines GK & Ivashkiv LB (2002) Sensitization of IFN-gamma Jak-STAT signaling during macrophage activation. *Nat. Immunol.* **3:** 859–866

Isaacs, A. and Lindenmann J (1957) Virus interference. I. The interferon.

Ishikawa H & Barber GN (2008) STING is an endoplasmic reticulum adaptor that facilitates innate immune signalling. *Nature* **455:** 674–678

Iwanami M, Hiromi Y & Okabe M (2005) Cell-type specific utilization of multiple negative feedback loops generates developmental constancy. *Genes to Cells* **10:** 743–752

Izaguirre A, Barnes BJ, Amrute S, Yeow W, Megjugorac N, Dai J, Feng D, Chung E & Pitha PM (2003) Comparative analysis of IRF and IFN-alpha expression in human plasmacytoid and monocyte-derived dendritic cells. *J. Leukoc. Biol.* **74:** 1125–1138

Jacobs MD & Harrison SC (1998) Structure of an IkBalpha/NF-kB Complex. *Cell* **95:** 749–758

Jacobson IM, Davis GL, El–Serag H, Negro F & Trépo C (2010) Prevalence and Challenges of Liver Diseases in Patients With Chronic Hepatitis C Virus Infection. *Clin. Gastroenterol. Hepatol.* **8:** 924–933

Jang MA, Kim EK, Now H, Nguyen NTH, Kim WJ, Yoo JY, Lee J, Jeong YM, Kim CH, Kim OH, Sohn S, Nam SH, Hong Y, Lee YS, Chang SA, Jang SY, Kim JW, Lee MS, Lim SY, Sung KS, et al (2015) Mutations in DDX58, which encodes RIG-I, Cause atypical singleton-merten syndrome. *Am. J. Hum. Genet.* **96:** 266–274

Jensen S & Thomsen AR (2012) Sensing of RNA Viruses: a Review of Innate Immune Receptors Involved in Recognizing RNA Virus Invasion. *J. Virol.* **86:** 2900–2910

Jeremiah N, Neven B, Gentili M, Callebaut I, Maschalidi S, Stolzenberg M, Goudin N, Frémond M, Nitschke P, Molina TJ, Blanche S, Picard C, Rice GI, Crow YJ, Manel N, Fischer A, Bader-meunier B & Rieux-laucat F (2014) Inherited STING-activating mutation underlies a familial inflammatory syndrome with lupus-like manifestations. *J. Clin. Invest.* **124:** 5516–5520

Jin L, Waterman PM, Jonscher KR, Short CM, Reisdorph NA & Cambier JC (2008) MPYS, a Novel Membrane Tetraspanner, Is Associated with Major Histocompatibility Complex Class II and Mediates Transduction of Apoptotic Signals. *Mol. Cell. Biol.* **28:** 5014–5026

Johnson ES (2004) Protein Modification by SUMO. *Annu. Rev. Biochem.* **73:** 355–382

Jolliffe IT & Cadima J (2016) Principal component analysis: a review and recent developments. *Philos. Trans. A. Math. Phys. Eng. Sci.* **374:** 20150202

Kamura T, Maenaka K, Kotoshiba S, Matsumoto M, Kohda D, Conaway RC, Conaway JW & Nakayama KI (2004) VHL-box and SOCS-box domains determine binding specificity for Cul2-Rbx1 and Cul5-Rbx2 modules of ubiquitin ligases. *Genes Dev.* **18:** 3055–3065

Kaschek D, Mader W, Rosenblatt M & Timmer J (2016) Dynamic Modeling , Parameter Estimation and Uncertainty Analysis in R.

Kauffman SA (1969) Metabolic stability and epigenesis in randomly constructed genetic nets. *J. Theor. Biol.* **22:** 437–467

Kearse M, Moir R, Wilson A, Stones-Havas S, Cheung M, Sturrock S, Buxton S, Cooper A, Markowitz S, Duran C, Thierer T, Ashton B, Meintjes P & Drummond A (2012) Geneious Basic: An integrated and extendable desktop software platform for the organization and analysis of sequence data. *Bioinformatics* **28:** 1647–1649

Kegel V, Deharde D, Pfeiffer E, Zeilinger K, Seehofer D & Damm G (2016) Protocol for Isolation of Primary

Human Hepatocytes and Corresponding Major Populations of Non-parenchymal Liver Cells. *J. Vis. Exp.***:** 1–10

Keskinen P, Ronni T, Matikainen S, Lehtonen A & Julkunen I (1997) Regulation of HLA class I and II expression by interferons and influenza A virus in human peripheral blood mononuclear cells. *Immunology* **91:** 421–9

King P & Goodbourn S (1994) The B-Interferon Promoter Responds to Priming Through Multiple Independent Regulatory Elements. *J. Biol. Chem.* **269:** 30609–30615

Kitano H (2002) Systems biology: a brief overview. *Science* **295:** 1662–4

Kitano H (2007) Towards a theory of biological robustness. *Mol. Syst. Biol.* **3:** 137

Klipp E, Liebermeister W, Wierling C, Kowald A, Lehrach H & Herwig R (2009) Systems Biology: A Textbook 1st editio. Wiley-Blackwell

Komyod W, Bauer UM, Heinrich PC, Haan S & Behrmann I (2005) Are STATS arginine-methylated? *J. Biol. Chem.* **280:** 21700–21705

Kotenko S V., Gallagher G, Baurin V V., Lewis-Antes A, Shen M, Shah NK, Langer JA, Sheikh F, Dickensheets H & Donnelly RP (2003) IFN-λs mediate antiviral protection through a distinct class II cytokine receptor complex. *Nat. Immunol.* **4:** 69–77

Kreutz C, Raue A & Timmer J (2012) Likelihood based observability analysis and confidence intervals for predictions of dynamic models. *BMC Syst. Biol.* **6:** 120

Kumthip K, Chusri P, Jilg N, Zhao L, Fusco DN, Zhao H, Goto K, Cheng D, Schaefer EA, Zhang L, Pantip C, Thongsawat S, O'Brien A, Peng LF, Maneekarn N, Chung RT & Lin W (2012) Hepatitis C virus NS5A disrupts STAT1 phosphorylation and suppresses type I interferon signaling. *J. Virol.* **86:** 8581–91

Laemmli UK (1970): (1970) Cleavage of Structural Proteins during Assembly of Head of Bacteriophage-T4. *Nature* **227:** 680–685

Larner AC, Chaudhuri A & Darnell JE (1986) Transcriptional Induction by Interferon. *J. Biol. Chem.* **2:** 453–459

Larnerl AC & Chaudhuri A (1986) Transcriptional Induction by Interferon. **2:**

Lavoie TB, Kalie E, Crisafulli-Cabatu S, Abramovich R, DiGioia G, Moolchan K, Pestka S & Schreiber G (2011) Binding and activity of all human alpha interferon subtypes. *Cytokine* **56:** 282–9

Lebon P, Meritet JF, Krivine A & Rozenberg F (2002) Interferon and Aicardi-Goutières syndrome. *Eur. J. Paediatr. Neurol.* **6:**

Lefèvre F, Guillomot M, D'Andréa S, Battegay S & La Bonnardière C Interferon-delta: the first member of a novel type I interferon family. *Biochimie* **80:** 779–88

Lehtonen a, Matikainen S & Julkunen I (1997) Interferons up-regulate STAT1, STAT2, and IRF family transcription factor gene expression in human peripheral blood mononuclear cells and macrophages. *J. Immunol.* **159:** 794–803

Lester SN & Li K (2014) Toll-like receptors in antiviral innate immunity. *J. Mol. Biol.* **426:** 1246–1264

Li K, Foy E, Ferreon JC, Nakamura M, Ferreon ACM, Ikeda M, Ray SC, Gale M & Lemon SM (2005) Immune evasion by hepatitis C virus NS3/4A protease-mediated cleavage of the Toll-like receptor 3 adaptor protein TRIF. *Proc. Natl. Acad. Sci.* **102:** 2992–2997

Li X, Leung S, Qureshi S, Darnell JE & Stark GR (1996) Formation of STAT1-STAT2 heterodimers and their role in the activation of IRF-1 gene transcription by interferon-α. *J. Biol. Chem.* **271:** 5790–5794

Li Y, Li S, Duan X, Liu B, Yang C, Zeng P, Mcgilvray I & Chen L (2014) Activation of endogenous type I IFN signaling contributes to persistent HCV infection.

Liao J, Fu Y & Shuai K (2000) Distinct roles of the NH2- and COOH-terminal domains of the protein inhibitor of activated signal transducer and activator of transcription (STAT) 1 (PIAS1) in cytokine-induced PIAS1-Stat1 interaction. *Proc. Natl. Acad. Sci. U. S. A.* **97:** 5267–72

Lin R, Heylbroeck C, Pitha PM & Hiscott J (1998) Virus-dependent phosphorylation of the IRF-3 transcription factor regulates nuclear translocation, transactivation potential, and proteasome-mediated degradation. *Mol. Cell. Biol.* **18:** 2986–96

Lin R, Lacoste J, Nakhaei P, Sun Q, Yang L, Paz S, Wilkinson P, Julkunen I, Vitour D, Meurs E & Hiscott J (2006) Dissociation of a MAVS/IPS-1/VISA/Cardif-IKK Molecular Complex from the Mitochondrial Outer Membrane by Hepatitis C Virus NS3-4A Proteolytic Cleavage. *J. Virol.* **80:** 6072–6083

Lin W, Choe WH, Hiasa Y, Kamegaya Y, Blackard JT, Schmidt E V. & Chung RT (2005) Hepatitis C virus expression suppresses interferon signaling by degrading STAT1. *Gastroenterology* **128:** 1034–1041

Liu B, Gross M, ten Hoeve J & Shuai K (2001) A transcriptional corepressor of Stat1 with an essential LXXLL signature motif. *Proc. Natl. Acad. Sci. U. S. A.* **98:** 3203–7

Liu B, Liao J, Rao X, Kushner SA, Chung CD, Chang DD & Shuai K (1998) Inhibition of Stat1-mediated gene activation by PIAS1. *Proc. Natl. Acad. Sci. U. S. A.* **95:** 10626–31

Liu B, Mink S, Wong KA, Stein N, Getman C, Dempsey PW, Wu H & Shuai K (2004) PIAS1 selectively inhibits

interferon-inducible genes and is important in innate immunity. *Nat. Immunol.* **5:** 891–898

Liu Y, Jesus AA, Marrero B, Yang D, Ramsey SE, Montealegre Sanchez GA, Tenbrock K, Wittkowski H, Jones OY, Kuehn HS, Lee C-CR, DiMattia MA, Cowen EW, Gonzalez B, Palmer I, DiGiovanna JJ, Biancotto A, Kim H, Tsai WL, Trier AM, et al (2014) Activated STING in a Vascular and Pulmonary Syndrome. *N. Engl. J. Med.* **371:** 507–518

Lucarelli P, Schilling M, Kreutz C, Vlasov A, Boehm ME, Iwamoto N, Steiert B, Lattermann S, Wäsch M, Stepath M, Matter MS, Heikenwälder M, Hoffmann K, Deharde D, Damm G, Seehofer D, Muciek M, Gretz N, Lehmann WD, Timmer J, et al (2017) Resolving the Combinatorial Complexity of Smad Protein Complex Formation and the Link to Gene Expression. *Cell Syst.* **in press:**

Lutfalla G, Holland SJ, Cinato E, Monneron D, Reboul J, Rogers NC, Smith JM, Stark GR, Gardiner K & Mogensen KE (1995) Mutant U5A cells are complemented by an interferon-alpha beta receptor subunit generated by alternative processing of a new member of a cytokine receptor gene cluster. *EMBO J.* **14:** 5100–8

Lyashenko E, Niepel M, Dixit P, Lim SK, Sorger PK & Vitkup D (2017) Receptor-Based Mechanism of Relative Sensing in Mammalian Signaling Networks. **:** 1–14

Maarifi G, Maroui MA, Dutrieux J, Dianoux L, Nisole S & Chelbi-Alix MK (2015) Small Ubiquitin-like Modifier Alters IFN Response. *J. Immunol.* **195:** 2312–24

Maarleveld TR, Khandelwal RA, Olivier BG, Teusink B & Bruggeman FJ (2013) Basic concepts and principles of stoichiometric modeling of metabolic networks. *Biotechnol. J.* **8:** 997–1008

MacDonald N (1976) Time delay in simple chemostat models. *Biotechnol. Bioeng.* **18:** 805–812

Machado D, Costa RS, Rocha M, Ferreira EC, Tidor B & Rocha I (2011) Modeling formalisms in systems biology. *AMB Express* **1:** 1–14

MacParland SA, Ma X-Z, Chen L, Khattar R, Cherepanov V, Selzner M, Feld JJ, Selzner N & McGilvray ID (2016) Lps and Tnf-A Inhibit Interferon-Signaling in Hepatocytes By Increasing Usp18 Expression. *J. Virol.***:** JVI.02557-15

Maiwald T, Schneider A, Busch H, Sahle S, Gretz N, Weiss TS, Kummer U & Klingmüller U (2010) Combining theoretical analysis and experimental data generation reveals IRF9 as a crucial factor for accelerating interferon α-induced early antiviral signalling. *FEBS J.* **277:** 4741–54

Makowska Z, Duong FHT, Trincucci G, Tough DF & Heim MH (2011) Interferon-β and interferon-λ signaling is not affected by interferon-induced refractoriness to interferon-α in vivo. *Hepatology* **53:** 1154–63

Malakhov MP, Malakhova O a, Kim K Il, Ritchie KJ & Zhang D-E (2002) UBP43 (USP18) specifically removes ISG15 from conjugated proteins. *J. Biol. Chem.* **277:** 9976–81

Malakhova O a, Kim K Il, Luo J-K, Zou W, Kumar KGS, Fuchs SY, Shuai K & Zhang D-E (2006) UBP43 is a novel regulator of interferon signaling independent of its ISG15 isopeptidase activity. *EMBO J.* **25:** 2358–67

Malathi K, Dong B, Gale M & Silverman RH (2007) Small self-RNA generated by RNase L amplifies antiviral innate immunity. *Nature* **448:** 816–819

Mannion NM, Greenwood SM, Young R, Cox S, Brindle J, Read D, Nellåker C, Vesely C, Ponting CP, McLaughlin PJ, Jantsch MF, Dorin J, Adams IR, Scadden ADJ, Ohman M, Keegan LP & O'Connell MA (2014) The RNA-editing enzyme ADAR1 controls innate immune responses to RNA. *Cell Rep.* **9:** 1482–94

Marcellin P, Lau GKK, Bonino F, Farci P, Hadziyannis S, Jin R, Lu Z-M, Piratvisuth T, Germanidis G, Yurdaydin C, Diago M, Gurel S, Lai M-Y, Button P, Pluck N & Peginterferon Alfa-2a HBeAg-Negative Chronic Hepatitis B Study Group (2004) Peginterferon Alfa-2a Alone, Lamivudine Alone, and the Two in Combination in Patients with HBeAg-Negative Chronic Hepatitis B. *N. Engl. J. Med.* **351:** 1206–1217

Marie I, Durbin JE & Levy DE (1998) Differential viral induction of distinct interferon-alpha genes by positive feedback through interferon regulatory factor-7. *EMBO J.* **17:** 6660–6669

Marks F, Klingmüller U & Müller-Decker K (2017) Cellular Signal Processing: An Introduction to the Molecular Mechanisms of Signal Transduction 2nd editio. Taylor and Francis Ltd.

Matsumoto K, Okano J-I & Murawaki Y (2005) Differential effects of interferon alpha-2b and beta on the signaling pathways in human liver cancer cells. *J Gastroenterol* **40:** 722–732

McBride KM, Banninger G, McDonald C & Reich NC (2002) Regulated nuclear import of the STAT1 transcription factor by direct binding of importin-alpha. *EMBO J.* **21:** 1754–63

Melén K, Fagerlund R, Nyqvist M, Keskinen P & Julkunen I (2004) Expression of hepatitis C virus core protein inhibits interferon-induced nuclear import of STATs. *J. Med. Virol.* **73:** 536–547

Mertens C, Zhong M, Krishnaraj R, Zou W, Chen X & Darnell JE (2006) Dephosphorylation of phosphotyrosine on STAT1 dimers requires extensive spatial reorientation of the monomers facilitated by the N-terminal domain. *Genes Dev.* **20:** 3372–3381

Meyer T, Begitt A, Lödige I, van Rossum M & Vinkemeier U (2002) Constitutive and IFN-gamma-induced nuclear import of STAT1 proceed through independent pathways. *EMBO J.* **21:** 344–54

Milo R (2013) What is the total number of protein molecules per cell volume? A call to rethink some published values. *Bioessays* **35:** 1050–5

Miyamoto M, Fujita T, Kimura Y, Maruyama M, Harada H, Sudo Y, Miyata T & Taniguchi T (1988) Regulated expression of a gene encoding a nuclear factor, IRF-1, that specifically binds to IFN-beta gene regulatory elements. *Cell* **54:** 903–13

Miyoshi K, Cui Y, Riedlinger G, Robinson P, Lehoczky J, Zon L, Oka T, Dewar K & Hennighausen L (2001) Structure of the Mouse Stat 3/5 Locus: Evolution from Drosophila to Zebrafish to Mouse. *Genomics* **71:** 150–155

Morrison J, Laurent-Rolle M, Maestre AM, Rajsbaum R, Pisanelli G, Simon V, Mulder LCF, Fernandez-Sesma A & García-Sastre A (2013) Dengue Virus Co-opts UBR4 to Degrade STAT2 and Antagonize Type I Interferon Signaling. *PLoS Pathog.* **9:** e1003265

Mowen KA, Tang J, Zhu W, Schurter BT, Shuai K, Herschman HR & David M (2001) Arginine Methylation of STAT1 Modulates IFNα/β-Induced Transcription. *Cell* **104:** 731–741

Muzio M, Bosisio D, Polentarutti N, D'amico G, Stoppacciaro A, Mancinelli R, van't Veer C, Penton-Rol G, Ruco LP, Allavena P & Mantovani A (2000) Differential expression and regulation of toll-like receptors (TLR) in human leukocytes: selective expression of TLR3 in dendritic cells. *J. Immunol.* **164:** 5998–6004

Myers MP, Andersen JN, Cheng a, Tremblay ML, Horvath CM, Parisien JP, Salmeen a, Barford D & Tonks NK (2001) TYK2 and JAR2 are substrates of protein-tyrosine phosphatase 1B. *J. Biol. Chem.* **276:** 47771–47774

Nishiya T & DeFranco AL (2004) Ligand-regulated Chimeric Receptor Approach Reveals Distinctive Subcellular Localization and Signaling Properties of the Toll-like Receptors. *J. Biol. Chem.* **279:** 19008–19017

Le Novere N, Hucka M & Mi H (2009) The systems biology graphical notation. *Nat. Comput. Biol.* **27:** 735–41

Novick D, Cohen B & Rubinstein M (1994) The human interferon alpha/beta receptor: characterization and molecular cloning. *Cell* **77:** 391–400

Okabe Y, Sano T & Nagata S (2009) Regulation of the innate immune response by threonine-phosphatase of Eyes absent. *Nature* **460:** 520–4

Oshiumi H, Sakai K, Matsumoto M & Seya T (2010) DEAD/H BOX 3 (DDX3) helicase binds the RIG-I adaptor IPS-1 to up-regulate IFN-β-inducing potential. *Eur. J. Immunol.* **40:** 940–948

Paludan SR & Bowie AG (2013) Immune Sensing of DNA. *Immunity* **38:** 870–880

Paz S, Vilasco M, Werden SJ, Arguello M, Joseph-Pillai D, Zhao T, Nguyen TL-A, Sun Q, Meurs EF, Lin R & Hiscott J (2011) A functional C-terminal TRAF3-binding site in MAVS participates in positive and negative regulation of the IFN antiviral response. *Cell Res.* **21:** 895–910

Pestka S, Krause CD & Walter MR (2004) Interferons, interferon-like cytokines, and their receptors. *Immunol. Rev.* **202:** 8–32

Peters KL, Smith HL, Stark GR & Sen GC (2002) IRF-3-dependent, NFkappa B- and JNK-independent activation of the 561 and IFN-beta genes in response to double-stranded RNA. *Proc. Natl. Acad. Sci. U. S. A.* **99:** 6322–6327

Pfeifer AC, Kaschek D, Bachmann J, Klingmüller U & Timmer J (2010) Model-based extension of high-throughput to high-content data. *BMC Syst. Biol.* **4:** 106

Piehler J, Thomas C, Christopher Garcia K & Schreiber G (2012) Structural and dynamic determinants of type I interferon receptor assembly and their functional interpretation. *Immunol. Rev.* **250:** 317–334

Piganis R a R, De Weerd N a, Gould J a, Schindler CW, Mansell A, Nicholson SE & Hertzog PJ (2011) Suppressor of cytokine signaling (SOCS) 1 inhibits type I interferon (IFN) signaling via the interferon alpha receptor (IFNAR1)-associated tyrosine kinase Tyk2. *J. Biol. Chem.* **286:** 33811–8

Platanias LC, Uddin S & Colamonici OR (1994) Tyrosine phosphorylation of the alpha and beta subunits of the type I interferon receptor. Interferon-beta selectively induces tyrosine phosphorylation of an alpha subunit-associated protein. *J. Biol. Chem.* **269:** 17761–4

Porritt RA & Hertzog PJ (2015) Dynamic control of type I IFN signalling by an integrated network of negative regulators. *Trends Immunol.* **36:** 150–160

Prokunina-Olsson L, Muchmore B, Tang W, Pfeiffer RM, Park H, Dickensheets H, Hergott D, Porter-Gill P, Mumy A, Kohaar I, Chen S, Brand N, Tarway M, Liu L, Sheikh F, Astemborski J, Bonkovsky HL, Edlin BR, Howell CD, Morgan TR, et al (2013) A variant upstream of IFNL3 (IL28B) creating a new interferon gene IFNL4 is associated with impaired clearance of hepatitis C virus. *Nat. Genet.* **45:** 164–171

Ptashne M (2006) Lambda's Switch: Lessons from a Module Swap. *Curr. Biol.* **16:**

Quesada JR, Reuben J, Manning JT, Hersh EM & Gutterman JU (1984) Alpha Interferon for Induction of Remission in Hairy-Cell Leukemia. *N. Engl. J. Med.* **310:** 15–18

Qureshi S & Salditt-Georgieff M (1995) Tyrosine-phosphorylated Stat1 and Stat2 plus a 48-kDa protein all

contact DNA in forming interferon-stimulated-gene factor 3. *Proc. Natl. Acad. Sci.* **92:** 3829–3833

Ragimbeau J, Dondi E, Alcover A, Eid P, Uzé G & Pellegrini S (2003) The tyrosine kinase Tyk2 controls IFNAR1 cell surface expression. *EMBO J.* **22:** 537–547

Rand U, Rinas M, Schwerk J, Nöhren G, Linnes M, Kröger A, Flossdorf M, Kály-Kullai K, Hauser H, Höfer T & Köster M (2012) Multi-layered stochasticity and paracrine signal propagation shape the type-I interferon response. *Mol. Syst. Biol.* **8:** 1–13

Randall RE & Goodbourn S (2008) Interferons and viruses: An interplay between induction, signalling, antiviral responses and virus countermeasures. *J. Gen. Virol.* **89:** 1–47

Raue A, Kreutz C, Maiwald T, Bachmann J, Schilling M, Klingmüller U & Timmer J (2009) Structural and practical identifiability analysis of partially observed dynamical models by exploiting the profile likelihood. *Bioinformatics* **25:** 1923–1929

Raue A, Schilling M, Bachmann J, Matteson A, Schelker M, Schelke M, Kaschek D, Hug S, Kreutz C, Harms BD, Theis FJ, Klingmüller U & Timmer J (2013) Lessons learned from quantitative dynamical modeling in systems biology. *PLoS One* **8:** e74335

Reis LF, Ho Lee T & Vilcek J (1989) Tumor necrosis factor acts synergistically with autocrine interferon-beta and increases interferon-beta mRNA levels in human fibroblasts. *J. Biol. Chem.* **264:** 16351–4

Rice GI, Kasher PR, Forte GMA, Mannion NM, Greenwood SM, Szynkiewicz M, Dickerson JE, Bhaskar SS, Zampini M, Briggs TA, Jenkinson EM, Bacino CA, Battini R, Bertini E, Brogan PA, Brueton LA, Carpanelli M, De Laet C, de Lonlay P, del Toro M, et al (2012) Mutations in ADAR1 cause Aicardi-Goutières syndrome associated with a type I interferon signature. *Nat. Genet.* **44:** 1243–1248

Rice GI, del Toro Duany Y, Jenkinson EM, Forte GMA, Anderson BH, Ariaudo G, Bader-Meunier B, Baildam EM, Battini R, Beresford MW, Casarano M, Chouchane M, Cimaz R, Collins AE, Cordeiro NJ V, Dale RC, Davidson JE, De Waele L, Desguerre I, Faivre L, et al (2014) Gain-of-function mutations in IFIH1 cause a spectrum of human disease phenotypes associated with upregulated type I interferon signaling. *Nat. Genet.* **46:** 503–509

Roberts RM (2007) Interferon-tau, a Type 1 interferon involved in maternal recognition of pregnancy. *Cytokine Growth Factor Rev.* **18:** 403–8

Robichon K (2015) Disentangling the intracellular and extracellular feedbacks regulating IFNα-induced expression of antiviral genes.

Rothenfusser S, Goutagny N, DiPerna G, Gong M, Monks BG, Schoenemeyer A, Yamamoto M, Akira S & Fitzgerald KA (2005) The RNA Helicase Lgp2 Inhibits TLR-Independent Sensing of Viral Replication by Retinoic Acid-Inducible Gene-I. *J. Immunol.* **175:** 5260–5268

Rytinki MM, Kaikkonen S, Pehkonen P, Jääskeläinen T & Palvimo JJ (2009) PIAS proteins: pleiotropic interactors associated with SUMO. *Cell. Mol. Life Sci.* **66:** 3029–41

Samarajiwa SA, Forster S, Auchettl K & Hertzog PJ (2009) INTERFEROME: The database of interferon regulated genes. *Nucleic Acids Res.* **37:**

Sarasin-Filipowicz M (2008) Interferon signaling and treatment outcome in chronic hepatitis C. *Proc. …*

Sarasin-Filipowicz M, Krol J, Markiewicz I, Heim MH & Filipowicz W (2009a) Decreased levels of microRNA miR-122 in individuals with hepatitis C responding poorly to interferon therapy. *Nat. Med.* **15:** 31–3

Sarasin-filipowicz M, Oakeley EJ, Duong FHT, Christen V, Terracciano L, Filipowicz W & Heim MH (2008) Interferon signaling and treatment outcome in chronic hepatitis C.

Sarasin-Filipowicz M, Wang X, Yan M, Duong FHT, Poli V, Hilton DJ, Zhang D-E & Heim MH (2009b) Alpha interferon induces long-lasting refractoriness of JAK-STAT signaling in the mouse liver through induction of USP18/UBP43. *Mol. Cell. Biol.* **29:** 4841–51

Sato M, Hata N, Asagiri M, Nakaya T, Taniguchi T & Tanaka N (1998) Positive feedback regulation of type I IFN genes by the IFN-inducible transcription factor IRF-7. *FEBS Lett.* **441:** 106–110

Scheinfeld N & Lehman DS (2006) An evidence-based review of medical and surgical treatments of genital warts. *Dermatol. Online J.* **12:** 5

Schilling M, Maiwald T, Bohl S, Kollmann M, Kreutz C, Timmer J & Klingmüller U (2005a) Computational processing and error reduction strategies for standardized quantitative data in biological networks. *FEBS J.* **272:** 6400–6411

Schilling M, Maiwald T, Bohl S, Kollmann M, Kreutz C, Timmer J & Klingmüller U (2005b) Quantitative data generation for systems biology: the impact of randomisation, calibrators and normalisers. *Syst. Biol. (Stevenage).* **152:** 193–200

Schindler C & Plumlee C (2008) Inteferons pen the JAK-STAT pathway. *Semin. Cell Dev. Biol.* **19:** 311–8

Schindler C, Shuai K, Prezioso VR & Darnell JE (1992a) Interferon-Dependent Tyrosine Phosphorylation of. **257:** 809–814

Schindler CC, Fu XYXY, Improta TT, Aebersold RR & Darnell JEJE (1992b) Proteins of transcription factor ISGF-3: one gene encodes the 91-and 84-kDa ISGF-3 proteins that are activated by interferon alpha. *Proc. Natl. Acad. Sci.* **89:** 7836–7839

Schmitt M & Pawlita M (2009) High-throughput detection and multiplex identification of cell contaminations. *Nucleic Acids Res.* **37:**

Schneider A (2011) Analysis of dynamic properties of interferon alpha signaling and implications for the antiviral response.

Schoenborn JR & Wilson CB (2007) Regulation of Interferon-γ During Innate and Adaptive Immune Responses. *Adv. Immunol.* **96:** 41–101

Schoggins JW & Rice CM (2011) Interferon-stimulated genes and their antiviral effector functions. *Curr. Opin. Virol.* **1:** 519–525

Schoggins JW, Wilson SJ, Panis M, Murphy MY, Jones CT, Bieniasz P & Rice CM (2011a) A diverse range of gene products are effectors of the type I interferon antiviral response. *Nature* **472:** 481–485

Schoggins JW, Wilson SJ, Panis M, Murphy MY, Jones CT, Bieniasz P & Rice CM (2011b) A diverse range of gene products are effectors of the type I interferon antiviral response. *Nature* **472:** 481–5

Schoggins JW, Wilson SJ, Panis M, Murphy MY, Jones CT, Bieniasz P & Rice CM (2011c) A diverse range of gene products are effectors of the type I interferon antiviral response. *Nature* **472:** 481–5

Schwarz G (1978) Estimating the Dimension of a Model. *Ann. Stat.* **6:** 461–464

Sekimoto T, Imamoto N, Nakajima K, Hirano T & Yoneda Y (1997) Extracellular signal-dependent nuclear import of Stat1 is mediated by nuclear pore-targeting complex formation with NPI-1 , but not Rch1. **16:** 7067–7077

Senger M, Flores T, Glatting K, Ernst P, Hotz-Wagenblatt a & Suhai S (1998) W2H: WWW interface to the GCG sequence analysis package. *Bioinformatics* **14:** 452–7

Sennepin AD, Charpentier S, Normand T, Sarr?? C, Legrand A & Mollet LM (2009) Multiple reprobing of Western blots after inactivation of peroxidase activity by its substrate, hydrogen peroxide. *Anal. Biochem.* **393:** 129–131

Sharma S, tenOever BR, Grandvaux N, Zhou G-P, Lin R & Hiscott J (2003) Triggering the Interferon Antiviral Response Through an IKK-Related Pathway. *Science (80-.).* **300:** 1148–1151

Shuai K (2006) Regulation of cytokine signaling pathways by PIAS proteins. *Cell Res.* **16:** 196–202

Siegal FP, Kadowaki N, Shodell M, Fitzgerald-Bocarsly PA, Shah K, Ho S, Antonenko S & Liu YJ (1999) The nature of the principal type 1 interferon-producing cells in human blood. *Science* **284:** 1835–7

Simmons DP, Wearsch PA, Canaday DH, Meyerson HJ, Liu YC, Wang Y, Boom WH & Harding C V. (2012) Type I IFN Drives a Distinctive Dendritic Cell Maturation Phenotype That Allows Continued Class II MHC Synthesis and Antigen Processing. *J. Immunol.* **188:** 3116–3126

Sirén J, Pirhonen J, Julkunen I & Matikainen S (2005) IFN-alpha regulates TLR-dependent gene expression of IFN-alpha, IFN-beta, IL-28, and IL-29. *J. Immunol.* **174:** 1932–7

Sobotta S, Raue A, Huang X, Vanlier J, Jünger A, Bohl S, Albrecht U, Hahnel MJ, Wolf S, Mueller NS, D'Alessandro LA, Mueller-Bohl S, Boehm ME, Lucarelli P, Bonefas S, Damm G, Seehofer D, Lehmann WD, Rose-John S, van der Hoeven F, et al (2017) Model Based Targeting of IL-6-Induced Inflammatory Responses in Cultured Primary Hepatocytes to Improve Application of the JAK Inhibitor Ruxolitinib. *Front. Physiol.* **8:** 775

Song MM & Shuai K (1998) The suppressor of cytokine signaling (SOCS) 1 and SOCS3 but not SOCS2 proteins inhibit interferon-mediated antiviral and antiproliferative activities. *J. Biol. Chem.* **273:** 35056–35062

Souma Y, Nishida T, Serada S, Iwahori K, Takahashi T, Fujimoto M, Ripley B, Nakajima K, Miyazaki Y, Mori M, Doki Y, Sawa Y & Naka T (2012) Antiproliferative effect of SOCS-1 through the suppression of STAT3 and p38 MAPK activation in gastric cancer cells. *Int. J. Cancer* **131:** 1287–1296

Stark GR, Kerr IM, Williams BR, Silverman RH & Schreiber RD (1998) How cells respond to interferons. *Annu. Rev. Biochem.* **67:** 227–64

Sumpter Jr. R, Loo YM, Foy E, Li K, Yoneyama M, Fujita T, Lemon SM & Gale Jr. M (2005) Regulating intracellular antiviral defense and permissiveness to hepatitis C virus RNA replication through a cellular RNA helicase, RIG-I. *J Virol* **79:** 2689–2699

Sun B, Li N & Sun B (2016) IFN-λ4 desensitizes the response to IFN-α treatment in chronic hepatitis C through. *J. Gen. Virol.*

Sun W, Li Y, Chen L, Chen H, You F, Zhou X, Zhou Y, Zhai Z, Chen D & Jiang Z (2009) ERIS, an endoplasmic reticulum IFN stimulator, activates innate immune signaling through dimerization. *Proc Natl Acad Sci U S A* **106:** 8653–8658

Sung PS, Hong S-H, Chung J-H, Kim S, Park S-H, Kim HM, Yoon SK & Shin E-C (2017) IFN-lambda4 potently blocks

IFN-alpha signalling by ISG15 and USP18 in hepatitis C virus infection. *Sci. Rep.* **7:** 3821

Talpaz M, McCredie KB, Mavligit GM & Gutterman JU (1983) Leukocyte interferon-induced myeloid cytoreduction in chronic myelogenous leukemia. *Blood* **62:** 689–92

Tanaka Y & Chen ZJ (2012) STING Specifies IRF3 Phosphorylation by TBK1 in the Cytosolic DNA Signaling Pathway. *Sci. Signal.* **5:** ra20-ra20

Tough DF (2012) Modulation of T-cell function by type I interferon. *Immunol. Cell Biol.* **90:** 492–497

Trengove MC & Ward AC (2013) SOCS proteins in development and disease. *Am J Clin Exp Immunol* **2:** 1–29

Tsao H, Atkins MB & Sober AJ (2004) Management of Cutaneous Melanoma. *N. Engl. J. Med.* **351:** 998–1012

Tur E & Brenner S (1998) Classic Kaposi's sarcoma: low-dose interferon alfa treatment. *Dermatology* **197:** 37–42

Uzé G, Lutfalla G & Gresser I (1990) Genetic transfer of a functional human interferon alpha receptor into mouse cells: cloning and expression of its cDNA. *Cell* **60:** 225–234

Veals S & et al. (1992) Subunit of an alpha-interferon-responsive transcription factor is related to interferon regulatory factor and myb families of DNA binding-proteins. *Mol. Cell. Biol. 12, 3315-3324* **12:** 3315

de Veer MJ, Holko M, Frevel M, Walker E, Der S, Paranjape JM, Silverman RH & Williams BR (2001) Functional classification of interferon-stimulated genes identified using microarrays. *J. Leukoc. Biol.* **69:** 912–20

Vizán P, Miller DSJ, Gori I, Das D, Schmierer B & Hill CS (2013) Controlling long-term signaling: receptor dynamics determine attenuation and refractory behavior of the TGF-β pathway. *Sci. Signal.* **6:** ra106

De Weerd NA & Nguyen T (2012) The interferons and their receptors—distribution and regulation. *Immunol. Cell Biol.* **90:** 483–491

Wenta N, Strauss H, Meyer S & Vinkemeier U (2008) Tyrosine phosphorylation regulates the partitioning of STAT1 between different dimer conformations. *Proc. Natl. Acad. Sci. U. S. A.* **105:** 9238–9243

Wilkinson DJ (2009) Stochastic modelling for quantitative description of heterogeneous biological systems. *Nat. Rev. Genet.* **10:** 122–133

Wilmes S, Beutel O, Li Z, Francois-Newton V, Richter CP, Janning D, Kroll C, Hanhart P, Hötte K, You C, Uzé G, Pellegrini S & Piehler J (2015) Receptor dimerization dynamics as a regulatory valve for plasticity of type I interferon signaling. *J. Cell Biol.* **209:** 579–593

Wu B, Peisley A, Richards C, Yao H, Zeng X, Lin C, Chu F, Walz T & Hur S (2013) Structural basis for dsRNA recognition, filament formation, and antiviral signal activation by MDA5. *Cell* **152:** 276–289

Wu TR, Hong YK, Wang X-D, Ling MY, Dragoi AM, Chung AS, Campbell AG, Han Z-Y, Feng G-S & Chin YE (2002) SHP-2 is a dual-specificity phosphatase involved in Stat1 dephosphorylation at both tyrosine and serine residues in nuclei. *J. Biol. Chem.* **277:** 47572–80

Wullaert A, Heyninck K, Janssens S & Beyaert R (2006) Ubiquitin: tool and target for intracellular NF-κB inhibitors. *Trends Immunol.* **27:** 533–540

Yasukawa H, Misawa H, Sakamoto H, Masuhara M, Sasaki A, Wakioka T, Ohtsuka S, Imaizumi T, Matsuda T, Ihle JN & Yoshimura A (1999) The JAK-binding protein JAB inhibits Janus tyrosine kinase activity through binding in the activation loop. *EMBO J.* **18:** 1309–1320

Yoshimura A, Naka T & Kubo M (2007) SOCS proteins, cytokine signalling and immune regulation. *Nat. Rev. Immunol.* **7:** 454–465

You C, Marquez-Lago TT, Richter CP, Wilmes S, Moraga I, Garcia KC, Leier A & Piehler J (2016) Receptor dimer stabilization by hierarchical plasma membrane microcompartments regulates cytokine signaling. *Sci. Adv.* **2:** 1–13

You M, Yu DH & Feng GS (1999) Shp-2 tyrosine phosphatase functions as a negative regulator of the interferon-stimulated Jak/STAT pathway. *Mol. Cell. Biol.* **19:** 2416–24

Zhang JG, Farley A, Nicholson SE, Willson TA, Zugaro LM, Simpson RJ, Moritz RL, Cary D, Richardson R, Hausmann G, Kile BT, Kile BJ, Kent SB, Alexander WS, Metcalf D, Hilton DJ, Nicola NA & Baca M (1999) The conserved SOCS box motif in suppressors of cytokine signaling binds to elongins B and C and may couple bound proteins to proteasomal degradation. *Proc. Natl. Acad. Sci. U. S. A.* **96:** 2071–6

Zhang X, Bogunovic D, Payelle-Brogard B, Francois-Newton V, Speer SD, Yuan C, Volpi S, Li Z, Sanal O, Mansouri D, Tezcan I, Rice GI, Chen C, Mansouri N, Mahdaviani SA, Itan Y, Boisson B, Okada S, Zeng L, Wang X, et al (2014) Human intracellular ISG15 prevents interferon-α/β over-amplification and auto-inflammation. *Nature* **517:** 89–93

Zhang Z, Yuan B, Lu N, Facchinetti V & Liu Y-J (2011) DHX9 Pairs with IPS-1 To Sense Double-Stranded RNA in Myeloid Dendritic Cells. *J. Immunol.* **187:** 4501–4508

Zhao T, Yang L, Sun Q, Arguello M, Ballard DW, Hiscott J & Lin R (2007) The NEMO adaptor bridges the nuclear factor-kappaB and interferon regulatory factor signaling pathways. *Nat. Immunol.* **8:** 592–600

Zhong B, Yang Y, Li S, Wang YY, Li Y, Diao F, Lei C, He X, Zhang L, Tien P & Shu HB (2008) The Adaptor Protein

MITA Links Virus-Sensing Receptors to IRF3 Transcription Factor Activation. *Immunity* **29:** 538–550

Zhong M, Henriksen MA, Takeuchi K, Schaefer O, Liu B, ten Hoeve J, Ren Z, Mao X, Chen X, Shuai K & Darnell JE (2005) Implications of an antiparallel dimeric structure of nonphosphorylated STAT1 for the activation-inactivation cycle. *Proc. Natl. Acad. Sci. U. S. A.* **102:** 3966–71

Zhu B & Reinberg D (2011) Epigenetic inheritance: Uncontested? *Cell Res.* **21:** 435–441

Zhu Y, Qin B, Xiao C, Lu X & Chen L (2012) Cell-Type Specific Interferon Stimulated Gene Staining in Liver Underlies Response to Interferon Therapy in Chronic HBV Infected Patients. *Dig. Dis. Sci.* **57:** 2355–2361

Zimnik S, Gaestel M & Niedenthal R (2009) Mutually exclusive STAT1 modifications identified by Ubc9/substrate dimerization-dependent SUMOylation. *Nucleic Acids Res.* **37:**

Zurney J, Howard KE & Sherry B (2007) Basal expression levels of IFNAR and Jak-STAT components are determinants of cell-type-specific differences in cardiac antiviral responses. *J. Virol.* **81:** 13668–13680